# FAILURE ANALYSIS OF ULTRA-HIGH MOLECULAR WEIGHT POLYETHYELENE ACETABULAR CUPS

by

NICOLAAS DANIEL LOMBARD BURGER

Submitted in partial fulfilment of the requirements for the degree

**DOCTOR PHILOSOPHIAE (PhD)**

In Mechanical Engineering

In the

FACULTY OF ENGINEERING, THE BUILT ENVIRONMENT AND INFORMATION TECHNOLOGY

UNIVERSITY OF PRETORIA

PRETORIA

DECEMBER 2005

Supervisors: Prof. PL de Vaal and Prof. J Meyer

## ACKNOWLEDGEMENTS

I would like to thank the following people and companies for their support which made this study possible:

1. My Creator for giving me the ability to do this study
2. My wife Estelle and children for their support
3. Prof. E Fourie for his guidance
4. Prof. PL de Vaal for his assistance and guidance
5. Prof. J Meyer for his assistance and guidance
6. Mr At von Wielligh for his assistance in building the simulator
7. Mr F Bader, Department of Material Science, for his assistance with the microscopic work
8. Mr B Mans, Department of Biochemistry, for his assistance with the electrophoresis work
9. Dr F Weber, Sandton Clinic, for providing me with the samples
10. Messrs A Steynberg, T Opperman, T Wilcocks and A Hohls, postgraduate students for assistance with the test work
11. Gammatron (Pty) Ltd for the crosslinking and sterilisation of test pieces
12. CMTI Developments (Pty) Ltd for their financial assistance.

# THESIS SUMMARY

## Failure analysis of ultra-high molecular weight polyethylene acetabular cups

**Student:** Nicolaas Daniel Lombard Burger
**Supervisors:** Prof. PL de Vaal and Prof. J Meyer
**Department:** Mechanical and Aeronautical Engineering
University of Pretoria
**Degree:** PhD (Mechanical Engineering)
**Keywords:** Ultra-high molecular weight polyethylene, acetabular cup, wear, lubrication, poor heat conduction

Owing to the crippling nature of arthritis, surgeons have been trying for well over a century to successfully treat this debilitating disease particularly when attacking the hip joint. In the early 1970s, Sir John Charnley started with total hip replacement as a solution to this ever-increasing problem. Many different designs were developed but all the designs revolved around a femoral stem, femoral head and acetabular component. Independent of the design, longevity of the implant remains a problem. The major cause of replacements, according to various hip registers, is due to aseptic loosening resulting from osteolysis. According to these registers, the average in-vivo life of a hip replacement is approximately 12 years.

The main aim of this study was to determine the root cause of mechanical failure of the acetabular cups and to determine the origin of the excessive amount of ultra-high molecular weight polyethylene (UHMWPE) wear debris floating in the joint resulting in osteolysis.

During the study, various techniques were used to investigate the acetabular components to try to establish the root cause of mechanical failure. These techniques included:

1. Visual inspection
2. Investigation making use of dye penetrant spray
3. Investigation under stereo microscope
4. Investigation making use of a scanning electron microscope
5. Electrophoresis
6. Mass-spectrometric analysis
7. Analysis of the synovial fluid on high-frequency linear-oscillation machine (SRV).

The wear debris retrieved from the scar tissue surrounding the joints of a number of patients was also analysed.

Apart from the obvious defects such as mechanical damage due to impingement, the main defect on which this study focuses is the wear patches found on the inside of the acetabular components.

The wear areas were presented as areas where the surface layer of the UHMWPE was ripped off by adhering to the rotating femoral head. This type of failure is possible if localised overheating takes place resulting in the material either adhering to the rotating femoral head or the material being squeezed out under the prevailing pressure. Both these mechanisms were confirmed by the wear debris retrieved from the scar tissue, being either droplets of UHMWPE or whisker-like wear products.

To confirm the existence of elevated temperatures the brown discolouring on the inside of the acetabular cups was analysed, making use of electrophoresis, mass-spectrometric analysis and scanning electron microscope recordings. In this part of the study, it was confirmed that

localised temperatures on the bearing surface had reached at least 60°C during in-vivo service. This temperature was confirmed by inserting a thermocouple just under the surface of an acetabular cup and then measuring the temperature while in-vitro testing was taking place on a hip simulator.

The wear debris as retrieved was also duplicated in laboratory experiments while the temperature on the surface of an acetabular cup was monitored. It was established that wear particles similar in shape and size were formed at temperatures in excess of 90°C. At temperatures above 50°C the UHMWPE had visually shown extensive increase in creep, indicating that at these temperatures the material softens sufficiently for this type of debris to be generated

The overheating as described can also only occur if there is a lack of lubrication in the bearing couple. The synovial fluid from 12 patients was retrieved during revision surgery. This synovial fluid was then tested on a high-frequency linear-oscillation machine (Optimol SRV test machine) to determine the lubricity characteristics of the synovial fluid as retrieved. It was discovered that the load-carrying capability of the synovial fluid did not comply with the minimum requirements for a fluid to function as a lubricant.

The final conclusion of this study is that excessive amounts of wear debris are generated due to the localised overheating of the bearing couple as a result of insufficient lubrication. The localised heat build-up results in excessive amounts of wear debris being generated and deposited in the joint area resulting in osteolysis.

# TABLE OF CONTENTS


| | | | DESCRIPTION | PAGE |
|---|---|---|---|---|
| **CHAPTER** | **1** | | **INTRODUCTION** | **1** |
| | 1.1 | | Development history of total hip replacement | 1 |
| | 1.2 | | Current concepts | 4 |
| | 1.3 | | Principal clinical diagnosis – total hip replacement | 4 |
| | 1.4 | | Clinical diagnosis resulting in revision hip replacement | 6 |
| | 1.5 | | Aim of study | 10 |
| **CHAPTER** | **2** | | **LITERATURE REVIEW** | **12** |
| | 2.1 | | Introduction | 12 |
| | 2.2 | | Review of existing designs | 13 |
| | | 2.2.1 | Femoral component | 14 |
| | | 2.2.2 | Femoral head | 15 |
| | | 2.2.3 | Acetabular cup | 16 |
| | 2.3 | | Biomechanics of the hip joint | 17 |
| | 2.4 | | Material properties of ultra-high molecular weight polyethylene (UHMWPE) | 23 |
| | 2.5 | | Wear and wear modes in acetabular components | 28 |
| | 2.6 | | Summary of previous retrieval and wear studies | 35 |
| | | 2.6.1 | Summary of retrieval studies – excluding crosslinked components | 35 |
| | | 2.6.2 | Summary of follow-up study on crosslinked components (see paragraph 2.9 for the effects of crosslinking on the properties of UHMWPE.) | 45 |
| | 2.7 | | Results from simulator studies – in-vitro testing found in literature | 46 |

| | | | | |
|---|---|---|---|---|
| | 2.8 | | Effects of gamma-irradiated sterilisation on wear characteristics | 49 |
| | 2.9 | | Effects of crosslinking on characteristics of UHMWPE | 52 |
| | 2.10 | | Hip simulators for in-vitro testing | 55 |
| | 2.11 | | Summary of literature review | 62 |
| **CHAPTER** | **3** | | **CREEP ANALYSIS FOR UHMWPE** | **63** |
| | 3.1 | | Introduction | 63 |
| | | 3.1.1 | Test protocol | 63 |
| | 3.2 | | Clamping effects | 64 |
| | | 3.2.1 | Purpose of test | 64 |
| | | 3.2.2 | Test procedure | 66 |
| | | 3.2.3 | Results | 68 |
| | 3.3 | | Investigation of anisotropic effects | 70 |
| | | 3.3.1 | Purpose of test | 70 |
| | | 3.3.2 | Test procedure | 70 |
| | | 3.3.3 | Test results | 72 |
| | 3.4 | | Effect of elevated temperature on the creep properties of UHMWPE | 74 |
| | | 3.4.1 | Purpose of test | 74 |
| | | 3.4.2 | Test procedure | 75 |
| | 3.5 | | Effect of sterilisation on the creep properties of UHMWPE | 77 |
| | | 3.5.1 | Purpose of test | 77 |
| | | 3.5.2 | Test procedure | 78 |
| | | 3.5.3 | Test results | 78 |
| | 3.6 | | Effect of crosslinking on the creep characteristics of UHMWPE | 81 |
| | | 3.6.1 | Purpose of test | 81 |
| | | 3.6.2 | Test procedure | 82 |

| | | | | |
|---|---|---|---|---|
| | | 3.6.3 | Test results | 82 |
| | 3.7 | | Proposed use of creep data in cup design | 85 |
| **CHAPTER** | **4** | | **PRELIMINARY INVESTIGATION OF RETRIEVED ACETABULAR CUPS** | **86** |
| | 4.1 | | Introduction | 86 |
| | 4.2 | | Proposed failure criteria | 88 |
| | 4.3 | | Descriptive explanation of defects in acetabular cups | 88 |
| | | 4.3.1 | Mechanical damage | 89 |
| | | 4.3.2 | Cracks in material | 90 |
| | | 4.3.3 | Plastic flow | 92 |
| | | 4.3.4 | Scratches | 94 |
| | | 4.3.5 | Adhesion wear | 94 |
| | | 4.3.6 | Wear particles embedded in base material | 96 |
| | | 4.3.7 | Flaking | 96 |
| | 4.4 | | Statistical analysis of retrieved acetabular cups | 98 |
| | 4.5 | | Conclusion | 100 |
| **CHAPTER** | **5** | | **RETRIEVAL STUDY** | **101** |
| | 5.1 | | Introduction | 101 |
| | 5.2 | | Summary of retrieved components | 102 |
| | 5.3 | | Visual inspection of retrieved acetabular cups | 103 |
| | 5.4 | | Inspection making use of dye penetrant | 109 |
| | 5.5 | | Investigation making use of stereoscope | 113 |
| | 5.6 | | Electron microscope investigation | 119 |
| | 5.7 | | Electrophoresis | 128 |
| | | 5.7.1 | Method | 128 |
| | | 5.7.2 | Results | 128 |
| | 5.8 | | Mass-spectrometric analysis | 130 |

| | | | | |
|---|---|---|---|---|
| | | 5.8.1 | Method | 130 |
| | | 5.8.2 | Results | 131 |
| | 5.9 | | Analysis of wear particles from human tissue | 132 |
| | | 5.9.1 | Method used | 132 |
| | | 5.9.2 | Results | 133 |
| **CHAPTER** | **6** | | **FAILURE ANALYSIS OF RETRIEVED ACETABULAR COMPONENTS** | **137** |
| | 6.1 | | Introduction | 137 |
| | 6.2 | | Cracks in acetabular components | 137 |
| | | 6.2.1 | Cracks on the rim of the cup | 137 |
| | | 6.2.2 | Cracks inside the bearing area | 140 |
| | 6.3 | | Scratches | 143 |
| | | 6.3.1 | Scratches caused by third-body wear | 143 |
| | | 6.3.2 | Scratches formed by normal UHMWPE wear products | 144 |
| | 6.4 | | Plastic flow | 150 |
| | 6.5 | | Adhesion wear | 152 |
| | 6.6 | | Postulate for mechanical failure of acetabular cups | 156 |
| **CHAPTER** | **7** | | **EXPERIMENTAL VERIFICATION** | **159** |
| | 7.1 | | Simulator studies | 159 |
| | | 7.1.1 | Introduction | 159 |
| | | 7.1.2 | Design of the simulator | 161 |
| | 7.2 | | Overview of test work to be carried out | 169 |
| | 7.3 | | Test with lubrication – test 1(a) | 170 |
| | | 7.3.1 | Test protocol | 170 |
| | | 7.3.2 | Test results | 171 |
| | 7.4 | | Test without lubricant – test 1 (b) | 173 |
| | | 7.4.1 | Test protocol | 173 |
| | | 7.4.2 | Test results | 173 |

| | | | |
|---|---|---|---|
| 7.5 | | Test to generate wear particles by generating frictional heat on the bearing surface – test 2 (a) | 176 |
| | 7.5.1 | Purpose of the test | 176 |
| | 7.5.2 | Test protocol | 176 |
| | 7.5.3 | Test results | 178 |
| 7.6 | | Test to generate wear particles by externally heating up a femoral head – test 2 (b) | 181 |
| | 7.6.1 | Purpose of the test | 181 |
| | 7.6.2 | Test protocol | 181 |
| | 7.6.3 | Test results | 182 |
| 7.7 | | Test to determine the coefficient of friction on the inside of an acetabular cup – test 3 | 185 |
| | 7.7.1 | Purpose of the test | 185 |
| | 7.7.2 | Test protocol | 185 |
| | 7.7.3 | Test results | 187 |
| 7.8 | | Conclusion of experimental results | 189 |
| | 7.8.1 | Simulator study | 189 |
| | 7.8.1.1 | Temperature in acetabular cup | 190 |
| | 7.8.1.2 | Wear debris retrieved from simulator | 190 |
| | 7.8.2 | Simulating of wear debris formation in laboratory | 194 |
| 7.9 | | Lubrication of the hip joint | 197 |
| **CHAPTER 8** | | **LUBRICATION OF THE HIP JOINT** | **198** |
| 8.1 | | Introduction | 198 |
| 8.2 | | Apparatus used | 201 |
| 8.3 | | Test method | 203 |
| 8.4 | | Test outcome | 205 |
| 8.5 | | Lubricity properties of patients | 208 |
| 8.6 | | Discussion | 209 |

| | | | |
|---|---|---|---|
| **CHAPTER** | **9** | **CONCLUSION AND RECOMMENDATIONS** | **212** |
| | 9.1 | Conclusion | 212 |
| | 9.2 | Recommendations | 214 |
| | | **REFERENCES** | 217 |

## LIST OF APPENDICES


| ANNEXURE | DESCRIPTION |
|---|---|
| **A** | Retrieval analysis of 20 acetabular cups |
| **B** | Electron microscope analysis of white deposits in acetabular cups |
| **C** | Electron microscope investigation into brown discolouring in acetabular cups |
| **D** | Electron microscope investigation into brown discolouring in acetabular cups |
| **E** | Electron microscope investigation into micro wear |
| **F** | Electrophoresis analysis of particles retrieved from brown deposit in acetabular cups and synovial fluid |
| **G** | Mass spectrometric analysis of particles retrieved from brown deposit in acetabular cups and synovial fluid |
| **H** | Lubricity analysis of retrieved synovial fluid |

## LIST OF TABLES


| Table | | Page |
|---|---|---|
| Table 2.1 | The maximum joint forces present in the hip joint, for a range of activities (Paul 1976) | 21 |
| Table 2.2 | Mechanical properties of UHMWPE (Charnley, 1979; Material data sheet, Poli HiSolidur 1999 ; Lewis 2001) | 27 |
| Table 2.3 | Summary of in-vivo wear rates as per literature from Jasty et al. (1997) | 36 |
| Table 2.4 | Wear rates of metal -on- polyethylene total hip implants as summarised from bulk literature data (Buford & Goswani, 2004) | 37 |
| Table 2.5 | Wear rates of ceramic -on- polyethylene total hip implants as summarised from bulk literature data (Buford & Goswani, 2004) | 37 |
| Table 2.6 | Mean (mm or $mm^3$), standard deviation and range of wear measurements from retrieved acetabular components at revision surgery (Kesteris et al., 2003) | 38 |
| Table 2.7 | Results of retrieval studies where wear was determined volumetrically (Sychterz et al., 1996; Jasty et al., 1997) | 40 |
| Table 2.8 | Summary of sizes of wear particles as determined by Schmalzried et al. (1997) and Maloney et al. (1995) | 44 |
| Table 2.9 | Summary of contemporary hip simulators (Calonius & Saikko, 2002) | 57 |
| Table 2.10 | Variation with time of angular movement to be applied to the femoral test specimen (ISO 14242-1, 2002) | 61 |
| Table 3.1 | Creep value differences for various test pieces | 72 |
| Table 3.2 | Summary of creep values after 2 hours | 77 |
| Table 3.3 | Summary of creep after gamma irradiation | 81 |
| Table 3.4 | Summary of creep values after 2 hours | 84 |
| Table 4.1 | The most common defects noticed on inside of retrieved cups | 88 |

| | | |
|---|---|---|
| Table 4.2 | Common defects present in acetabular cups with possible effect on useful life | 97 |
| Table 4.3 | Statistical analysis of 47 retrieved cups, with in total 125 defects | 99 |
| Table 7.1 | Values for masses needed to cause movement | 187 |
| Table 7.2 | Values for estimated coefficient of friction under various conditions | 189 |
| Table 8.1 | The test parameters used to determine the lubricity characteristics of the joint fluid | 205 |
| Table 8.2 | Tests results to determine lubricity characteristics for 12 patients | 208 |

## LIST OF FIGURES


| Figure | | Page |
|---|---|---|
| Figure 1.1: | Austin Moore prosthesis | 2 |
| Figure 1.2: | The early prosthesis as designed by Sir John Charnley. Note the migration of the femoral head into the Teflon | 3 |
| Figure 1.3: | Principle diagnosis - primary total hip replacements (Davidson et al., 2002; Davidson et al., 2003) | 5 |
| Figure 1.4: | Schematic presentation of mechanism resulting in osteolysis (http://www.geocities.com/hip_replacements/history) | 7 |
| Figure 1.5: | Wear debris-mediated osteolytic lesion superior (above) loose press-fit modular acetabular component. Note eccentricity of liner; mechanical failure ensued 5 years postoperatively (Dumbleton et al., 2002) | 7 |
| Figure 1.6: | Polyethylene from an acetabular liner that has been attacked by the body, resulting in giant cells that eat away the bone resulting in component loosening (Manley et al., 2002) | 7 |
| Figure 1.7: | Diagnosis - Revision surgery hip replacement (Davidson et al., 2002; Davidson et al., 2003) | 8 |
| Figure 1.8: | Survival rate for different models of cemented and uncemented prostheses (Havelin et al., 2003) | 9 |
| Figure 2.1 | Basic modular design of total hip replacement | 13 |
| Figure 2.2 | Femoral osteolysis with signs of bone resorption below collar (Dumbleton et al., 2002). | 15 |
| Figure 2.3 | Polyethylene liner with hydroxy-apatite-coated metal back (http://www.aesculap.de/) | 17 |
| Figure 2.4 | Polyethylene liner in metal back with holes for fixation (http://www.depuy.com/) | 17 |
| Figure 2.5 | Man standing on his right leg. The gravity vertical line from $S_6$ falls in the supporting area of the right foot. The | 18 |

| | | |
|---|---|---|
| | weight $G_5$ is to be balanced in the right hip joint. M - abductor muscles of the right hip, R - hip resultant, $S_5$ - centre of gravity of the body mass to be borne in the right hip joint (Kummer, 1976) | |
| Figure 2.6 | Side (lateral) and back (posterior) view of abductor muscles (http://www.geocities.com/hip_replacements/history) | 19 |
| Figure 2.7 | Side and back view of abductor forces acting on hip joint (http://www.geocities.com/hip_replacements/history) | 19 |
| Figure 2.8 | Stress distribution on the normal hip joint (Kummer 1976) | 20 |
| Figure 2.9 | Graphical presentation of the loading on the acetabular cup (Paul, 1976; Kummer, 1976; Sychterz et al., 1996; Zupanc et al., 2001) | 20 |
| Figure 2.10 | Variation with time of hip joint forces for slow, normal and fast walking (Paul, 1976). The scale of the x axes is percentage time | 21 |
| Figure 2.11 | Resultant force on hip joint for patient jogging on treadmill at 6 km/h (Bergmann et al. 1993; Bergmann et al. 1995). HS: heel strike, TO: hoe off; MLR: measured load profile | 22 |
| Figure 2.12 | PV values for UHMWPE at 20°C (Engineering Materials Handbook, 1987) | 24 |
| Figure 2.13 | Izod impact strength against temperature with 15° double V notched (Engineering Materials Handbook, 1987) | 25 |
| Figure 2.14 | Compression creep for various loads at 20°C (Engineering Materials Handbook, 1987) | 26 |
| Figure 2.15 | The origins of the friction associated with the sliding of a hard, smooth surface over a polymer surface (Hutchings, 1992) | 30 |
| Figure 2.16 | Wear rate of UHMWPE sliding against a steel counter face, as a function of the roughness of the steel surface (Hutchings, 1992) | 33 |

| | | |
|---|---|---|
| Figure 2.17 | Illustration of the asperities on the surface of a component after manufacturing (Hutchings, 1992) | 33 |
| Figure 2.18 | Reduced contact area with increase in non-conformity between femoral head and acetabular cup | 35 |
| Figure 2.19 | Linear wear in the cup and stem group (Kesteris et al., 2003) | 38 |
| Figure 2.20 | Position of maximum wear in cups according to Sychterz et al. (1996) | 40 |
| Figure 2.21 | Photograph of a polyethylene acetabular component (Jasty et al., 1997) retrieved during a revision that was performed because of osteolysis six years post-operatively. There is an eccentric pattern of wear. The superior worn area is highly polished and is separated from the inferior, less worn area by a ridge (small arrows). Note the evidence of impingement anteriorly (a large arrow). Discolouration and flaking are seen in the less worn area | 42 |
| Figure 2.22 | Scanning electron micrograph showing the highly worn area with numerous multidirectional fine scratches in a well-fixed acetabular component that was retrieved at autopsy ten years after implantation (original magnification, x 79.5) | 42 |
| Figure 2.23 | Scanning electron micrograph showing striations (arrows) perpendicular to the direction of the scratches, indicating tearing of the material during abrasive wear (original magnification, x 3900) | 42 |
| Figure 2.24 | High-power scanning electron micrographs of a component retrieved six years after an arthroplasty. Reorganisation of the material has occurred during the wear process | 43 |
| Figure 2.25 | X-ray that shows 2.5 mm wear in cup as indicated by | 46 |

| | | |
|---|---|---|
| | arrows as an eccentricity. No scale was shown in reference (Grobbelaar et al., 1999). | |
| Figure 2.26 | Particles of non-irradiated, ethylene oxide sterilised UHMWPE against chrome cobalt femoral head (x 10 000) (Ries et al., 2001) | 49 |
| Figure 2.27 | Wear particles of inert gas gamma-irradiated UHMWPE against chrome cobalt (x 10 000) (Ries et al., 2001) | 51 |
| Figure 2.28 | Average wear rate for acetabular components sterilised with gamma (Orishimo et al., 2003) | 51 |
| Figure 2.29 | Average wear rate for acetabular components sterilised with ethylene oxide (Orishimo et al., 2003) | 52 |
| Figure 2.30 | Tensile strength of crosslinked UHMWPE (Du Plessis et al., 1977) | 53 |
| Figure 2.31 | Surface hardness of crosslinked UHMWPE (Du Plessis et al., 1977) | 53 |
| Figure 2.32 | Impact energy of crosslinked UHMWPE (Du Plessis et al., 1977) | 54 |
| Figure 2.33 | Wear particles of highly crosslinked UHMWPE subjected to 5 Mrad of gamma irradiation (x 10 000) (Ries et al., 2001) | 55 |
| Figure 2.34 | Wear particles of highly crosslinked UHMWPE subjected to 10 Mrad of gamma irradiation (x 10 000) (Ries et al., 2001) | 55 |
| Figure 2.35 | Boston hip simulator (http://www.geocities.com/hip_replacements/ history) | 56 |
| Figure 2.36 | Motion waveforms used in computation of slide tracks for hip simulators | 57 |
| Figure 2.37 | Schematic illustration of the loading/motion configuration of the Bi-axial rocking motion (BRM) hip simulator (Wang et al., 1996) | 58 |
| Figure 2.38 | Three-station, statically loaded bi-axial rocking motion | 59 |

| | | |
|---|---|---|
| | (BRM) hip wear simulator (Saikko et al., 2001) | |
| Figure 2.39 | Loading profile for hip simulator according to ISO standard (ISO 14242-1, 2002) | 60 |
| Figure 3.1 | Illustration of clamping effect | 65 |
| Figure 3.2 | Size of an ASTM test piece according to ASTM D2990 (1990) | 65 |
| Figure 3.3 | Orientation of test pieces in virgin material | 66 |
| Figure 3.4a | Test set-up in Schenk testing machine | 68 |
| Figure 3.4b | Clip-on extensometer | 68 |
| Figure 3.5 | Results for the test to determine clamping effect | 69 |
| Figure 3.6 | Position and orientation of test piece 1 to 5 | 70 |
| Figure 3.7 | Position and orientation of test pieces 6 to 8 | 71 |
| Figure 3.8 | Creep in virgin material at different orientations | 73 |
| Figure 3.9 | Orientation of test pieces machined from bar stock for tests at elevated temperatures | 75 |
| Figure 3.10 | Test set-up for tests at elevated temperatures | 76 |
| Figure 3.11 | Summary of creep results at elevated temperatures | 76 |
| Figure 3.12 | Creep properties of material irradiated in air | 79 |
| Figure 3.13 | Creep properties of material irradiated in nitrogen atmosphere | 79 |
| Figure 3.14 | Creep properties of material radiated in air and heat treated at 80°C and tested at room temperature | 80 |
| Figure 3.15 | Creep properties of crosslinked UHMWPE at room temperature | 83 |
| Figure 3.16 | Creep properties of crosslinked UHMWPE tested at 50°C | 83 |
| Figure 3.17 | Creep properties of crosslinked UHMWPE tested at 60°C | 84 |
| Figure 4.1 | Mechanical damage on rim of cup | 89 |
| Figure 4.2 | Schematic presentation of mechanical damage on rim of cup | 89 |
| Figure 4.3a | Metal-backed acetabular cup with cracks on rim | 91 |
| Figure 4.3b | Separation within material | 91 |

| | | |
|---|---|---|
| Figure 4.4 | Schematic layout of areas where cracks can be expected | 92 |
| Figure 4.5 | Cup treated with dye penetrant showing “orange peel” effect indicating plastic flow of material | 93 |
| Figure 4.6 | Schematic layout of expected plastic flow in acetabular cups | 93 |
| Figure 4.7 | Scratches visible on inside of cup | 94 |
| Figure 4.8 | Adhesion wear on inside made visible with dye penetrant treatment | 95 |
| Figure 4.9 | Schematic layout of areas where cracks can be expected in the area under tensile stress | 95 |
| Figure 4.10 | Acetabular cup with embedded PMMA particles | 96 |
| Figure 4.11 | Acetabular cup with serious delamination visible | 97 |
| Figure 5.1 | Fractured cup | 102 |
| Figure 5.2 | A cup with delamination | 103 |
| Figure 5.3 | Cross section of cups showing an amount of wear/creep | 104 |
| Figure 5.4 | Deposited debris – coloured with liquid dye penetrant to make it more visible | 104 |
| Figure 5.5 | Wear pattern in retrieved cups with area of debris deposits indicated | 105 |
| Figure 5.6 | Crater in fractured cup | 105 |
| Figure 5.7 | Cracking in fractured cup | 106 |
| Figure 5.8 | A cup with evidence of interference and subsequent damage | 106 |
| Figure 5.9 | Piece of steel embedded in polyethylene (magnification x 40) | 107 |
| Figure 5.10 | Plastic flow on the rim of cup | 108 |
| Figure 5.11 | Amount of plastic flow | 108 |
| Figure 5.12 | White deposits on inside of cup and brown discolouring | 109 |
| Figure 5.13 | Deposited debris, resulting flow pattern and adhesion wear | 110 |
| Figure 5.14 | The rim of cup showing plastic flow on circumference of | 110 |

| | | |
|---|---|---|
| | rim | |
| Figure 5.15 | A cup with areas of higher concentration of debris | 111 |
| Figure 5.16 | Close-up of the area of adhesion wear | 112 |
| Figure 5.17 | Schematic lay-out to indicate position of fretting mark | 112 |
| Figure 5.18 | Magnification (x 10) of defect before treatment with dye penetrant | 113 |
| Figure 5.19 | Magnification (x 20) of defect before treatment with dye penetrant | 113 |
| Figure 5.20 | Magnification(x 20) of defect after treatment with dye penetrant | 114 |
| Figure 5.21 | Magnification (x 40) of second crater after treatment with dye penetrant | 114 |
| Figure 5.22 | Magnification (x 10) of defect on rim of cup | 115 |
| Figure 5.23 | Magnification (x 20) of defect on rim of cup | 115 |
| Figure 5.24 | Magnification (x 10). From this photograph the white irregular shape of material deposited is clearly visible | 116 |
| Figure 5.25 | Magnification (x 20). The arrow points to a droplet of material which was either extruded from the bearing surface or was flattened after being ripped out of the surface | 116 |
| Figure 5.26 | Magnification (x 20). The photograph shows softened/extruded debris with what looks like craters in between. Note the irregular shape of the deposit after being flattened by the ball | 117 |
| Figure 5.27a | Magnification (x 40): The results from Figure 5.25 are investigated further. It can be seen that the white piece of material appears not to have been totally removed from the base material, as there are no sharp edges on one side | 117 |
| Figure 5.27b | Schematic of material extruded from the bearing surface | 117 |
| Figure 5.28 | Magnification (x 20) of wear area on bearing surface | 118 |

| | | |
|---|---|---|
| Figure 5.29 | Magnification (x 40) of wear on bearing surface area | 118 |
| Figure 5.30 | Electron microscope investigation of a brown layer on inside of cup (magnification x 50) | 119 |
| Figure 5.31 | Electron microscope investigation of the brown layer on inside of the cup (magnification x 250) | 120 |
| Figure 5.32 | Electron microscope image of virgin UHMWPE sample (magnification x 10 000) | 120 |
| Figure 5.33 | An electron microscope image of deformed UHMWPE (magnification x 10 000) | 120 |
| Figure 5.34 | Anatomical cup orientation with position of worn area | 121 |
| Figure 5.35 | Machining marks visible in acetabular cup | 122 |
| Figure 5.36 | Machining marks on inside of cup (magnification x 500) | 122 |
| Figure 5.37 | Wear particle entrapped in cup (magnification x 3700) | 122 |
| Figure 5.38 | Surface of acetabular cup with scratches due to third-body wear (magnification x 1500) | 123 |
| Figure 5.39 | Abrasion wear on acetabular cup (magnification x 1300) | 123 |
| Figure 5.40 | Back scatter analysis on wear particle lodged at end of abrasion wear in acetabular cup (magnification x 1500) | 124 |
| Figure 5.41 | Adhesion wear area in acetabular cup | 125 |
| Figure 5.42 | Electron microscope photograph of adhesion wear in acetabular cup (magnification x 23) | 125 |
| Figure 5.43 | Adhesion wear area under higher magnification (magnification x 5000) | 125 |
| Figure 5.44 | Adhesion wear defect under electron microscope (magnification x 22) | 126 |
| Figure 5.45 | Adhesion wear under higher magnification (magnification x 190) | 126 |
| Figure 5.46 | Acetabular cup with visible plastic flow on bearing area (magnification x 180) | 127 |
| Figure 5.47 | Plastic flow on bearing area under higher magnification (magnification x 1300) | 127 |

| | | |
|---|---|---|
| Figure 5.48 | Electrophoresis analysis of synovial fluid and retrieved proteins from acetabular cups | 129 |
| Figure 5.49 | Mass-spectrometric analysis of a synovial fluid sample | 132 |
| Figure 5.50 | Schematic explanation of formation of jagged/wavy edges during extrusion | 134 |
| Figure 5.51 | Particles retrieved from tissue (magnification x 40) | 134 |
| Figure 5.52 | Retrieved particle (magnification x 100) | 134 |
| Figure 5.53 | Retrieved particle (magnification x 40) | 135 |
| Figure 5.54 | Retrieved particle (magnification x 100) | 135 |
| Figure 6.1 | Metal-back acetabular cup with cracks and delamination on rim of cup | 138 |
| Figure 6.2 | Cross section of acetabular cup showing delamination on the rim of the cup (magnification x 20) | 138 |
| Figure 6.3 | Schematic layout of UHMWPE liner not fitting snugly into metal backing | 139 |
| Figure 6.4 | Acetabular component after catastrophic failure | 140 |
| Figure 6.5 | Crack on inside of acetabular cup | 141 |
| Figure 6.6 | Electron microscope analysis of adhesion wear area (magnification x 110) | 141 |
| Figure 6.7 | Crater under the surface after adhesion wear (magnification x 450) | 142 |
| Figure 6.8 | Acetabular cup with severe scratches on inside | 143 |
| Figure 6.9 | Acetabular cup with multidirectional fine scratches and with machining marks still visible (magnification x 20) | 144 |
| Figure 6.10 | Bearing area with signs of big scratches and area with adhesion wear | 145 |
| Figure 6.11 | Scratches on bearing surface with white particles visible (magnification x 35) | 146 |
| Figure 6.12 | Scratch mark on bearing surface (magnification x 250) | 146 |
| Figure 6.13 | Final position of particle causing damage to bearing surface (magnification x 1500) | 147 |

| | | |
|---|---|---|
| Figure 6.14 | Electron microscope back scatter analysis of scratch (magnification x 1500) | 147 |
| Figure 6.15 | Scratch on bearing surface (magnification x 33) | 148 |
| Figure 6.16 | End of scratch on bearing surface (magnification x 1300) | 148 |
| Figure 6.17 | Whisker-like debris retrieved from patient (magnification x 20) | 149 |
| Figure 6.18 | Debris retrieved from patient (magnification x 40) | 149 |
| Figure 6.19 | Plastic flow of material visible in cup (magnification x 10) | 151 |
| Figure 6.20 | Plastic flow in acetabular cup (magnification x 1300) | 152 |
| Figure 6.21 | Area with plastic flow lines visible (magnification x 75) | 152 |
| Figure 6.22 | Visible adhesion wear in acetabular cup | 153 |
| Figure 6.23 | Butterfly wear pattern on inside of acetabular cup | 153 |
| Figure 6.24 | Area with adhesion wear (magnification x 40) | 153 |
| Figure 6.25 | Area with adhesion wear exposing the base material of the acetabular cup (magnification x 5000) | 154 |
| Figure 6.26 | Wear particle with smaller particles attached to it (magnification x 3700) | 155 |
| Figure 6.27 | Area with adhesion wear (magnification x 60) | 155 |
| Figure 6.28 | Adhesion particle about to be broken out (magnification x 200) | 156 |
| Figure 6.29 | Steps in wear debris formation in acetabular cup | 158 |
| Figure 7.1 | Concept for simulator movement | 162 |
| Figure 7.2a | Schematic layout of the simulator | 163 |
| Figure 7.2b | Schematic layout of the simulator: Side view | 163 |
| Figure 7.3 | Hip movement as measured by Bergman et al. (1993) | 164 |
| Figure 7.4 | Recorded force/time graph of the simulator | 164 |
| Figure 7.5 | Loading spring with adjusting plate | 165 |
| Figure 7.6 | Assembly of stabilising springs | 165 |
| Figure 7.7 | Graphical presentation of the forces on the connecting pin | 166 |
| Figure 7.8 | Mechanical stops to achieve ±5º abduction/adduction | 167 |

| | | |
|---|---|---|
| | rotation | |
| Figure 7.9 | Two cups in position showing the thermocouples and strain gages | 168 |
| Figure 7.10 | Detail of the acetabular cup in the test station | 168 |
| Figure 7.11 | Test-recording equipment | 171 |
| Figure 7.12 | Wear particles on filter material (magnification x 40) | 172 |
| Figure 7.13 | Wear particle retrieved from simulator (magnification x 100) | 172 |
| Figure 7.14 | Retrieved wear particle from simulator (magnification x 900) | 173 |
| Figure 7.15 | Wear surface on the inside of the cup (magnification x 10) | 174 |
| Figure 7.16 | Wear on inside of a cup (magnification x 20) | 174 |
| Figure 7.17 | Wear debris retrieved from an acetabular cup on simulator (magnification x 20) | 175 |
| Figure 7.18 | Wear debris retrieved from an unlubricated acetabular cup in a hip simulator (magnification x 40) | 175 |
| Figure 7.19 | Wear debris retrieved from an unlubricated acetabular cup in a hip simulator (magnification x 40) | 176 |
| Figure 7.20 | Test layout to manufacture wear particles with frictional heat | 177 |
| Figure 7.21 | Area of damage on a test piece | 178 |
| Figure 7.22 | Surface damage on UHMWPE test piece (magnification x 20) | 178 |
| Figure 7.23 | Wear debris adhering to femoral ball - indicated with an arrow | 179 |
| Figure 7.24 | Wear debris generated by frictional heat at a measured temperature of 105°C (magnification x 40) | 179 |
| Figure 7.25 | Wear particle at higher magnification (magnification x 100). | 180 |
| Figure 7.26 | Schematic layout of surface roughness | 181 |
| Figure 7.27 | Surface of a test piece after damage by preheated | 182 |

| | | |
|---|---|---|
| | femoral head (magnification x 10) | |
| Figure 7.28 | Damage surface of UHMWPE test piece (magnification x 20) | 182 |
| Figure 7.29 | Wear particles adhering to femoral ball —indicated with an arrow | 183 |
| Figure 7.30 | Retrieved wear debris from preheated ball test. Ball temperature 100°C (magnification x 20) | 183 |
| Figure 7.31 | Wear particles retrieved from externally heated femoral head at temperature of 100°C (magnification x 40) | 184 |
| Figure 7.32 | Wear particles retrieved from externally heated femoral head at a temperature of 100°C (magnification x 40) | 184 |
| Figure 7.33 | Test set up for determining coefficient of friction between ceramic femoral head and UHMWPE acetabular cup | 186 |
| Figure 7.34 | Data used for the calculation of coefficient of friction | 188 |
| Figure 7.35 | Wear debris retrieved from simulator (magnification x 100) | 191 |
| Figure 7.36 | UHMWPE wear debris retrieved from scar tissue (magnification x 100) | 192 |
| Figure 7.37 | UHMWPE wear particle still attached to base material (magnification x 3700) | 192 |
| Figure 7.38 | UHMWPE wear debris retrieved from simulator running without lubrication (magnification x 20) | 193 |
| Figure 7.39 | UHMWPE wear debris retrieved from scar tissue (magnification x 100) | 193 |
| Figure 7.40 | UHMWPE wear particle generated by means of frictional heating (magnification x 100) | 195 |
| Figure 7.41 | UHMWPE wear debris generated by preheating the femoral head (magnification x 40) | 195 |
| Figure 7.42 | UHMWPE wear debris retrieved from scar tissue (magnification x 100) | 196 |
| Figure 8.1 | A schematic drawing of the human hip joint | 198 |

| | | |
|---|---|---|
| | (http://www.healthsystem.virginia.edu/UVAHealth/adult_arthritis/anatomy.cfm) | |
| Figure 8.2 | Areolar tissue (magnification x 400) (http://science.nhmccd.edu/biol/tissue/areolar.html) | 199 |
| Figure 8.3 | Schematic layout of surface roughness. | 201 |
| Figure 8.4 | Schematic layout of the Optimol SRV machine | 202 |
| Figure 8.5 | Fixed specimen in Optimol SRV machine | 203 |
| Figure 8.6 | Moving specimen in Optimol SRV machine | 203 |
| Figure 8.7 | An example of a typical lubricity test result. The loads at failure are indicated on the graph | 206 |
| Figure 8.8 | Wear scar on moving specimen (ball) | 207 |
| Figure 8.9 | Wear scar on fixed specimen (disk) (magnification x 60) | 207 |
| Figure 8.10 | Combined lubricity data for 12 patients as tested with averages as indicated | 209 |
| Figure 8.11 | Adhesion wear on bearing surface of retrieved acetabular cup | 210 |
| Figure 8.12 | Wear particle still attached to UHMWPE acetabular cup | 210 |
| Figure 8.13 | Wear debris retrieved from patient no. 5 (magnification x 200) | 211 |

**List of symbols**

| | |
|---|---|
| σ | Principal stress – either tension or compression |
| r | Radius |
| E | Young's modulus of elasticity |
| H | Hardness of material |
| v | Poisson's ratio |

**Glossary**

| | |
|---|---|
| Abduction | Act of turning outward. |
| Acetal | Acetal, also known as polyacetal, polyoxymethylene (POM), or polyformaldehyde, is a high-performance engineering polymer. |
| Adduction | Act of turning inward. |
| Arthritis | Arthritis is inflammation of one or more joints. When joints are inflamed they can develop stiffness, warmth, swelling, redness and pain. There are over 100 types of arthritis, including osteoarthritis, rheumatoid arthritis, ankylosing spondylitis, psoriatic arthritis, lupus, gout, and pseudogout. Earlier and accurate diagnosis can help to prevent irreversible damage and disability. |
| Arthrodesis | Athrodesis is the surgical fixation of a joint. It is also called artificial ankylosis. |
| Avascular necrosis | Condition in which poor blood supply to an area of bone leads to bone death. This is called avascular necrosis and osteonecrosis. |
| Cortical bone | Main construction of the shaft of the femur. |
| Dislocation, congenital hip | The abnormal formation of the hip joint in which the ball at the top of the thigh bone (the femoral head) is not stable within the socket (the acetabulum). The ligaments of the hip joint may also be loose and stretched. |
| Dysplasia | Abnormal in form. Dysplasia is derived from the Greek *dys*- (bad, disordered, abnormal) and *plassein* (to form). For example, retinal dysplasia is the abnormal formation of the retina during embryonic development. |

| | |
|---|---|
| Electrophoresis | Gel electrophoresis is a method that separates macromolecules — either nucleic acids or proteins — on the basis of size, electric charge, and other physical properties. |
| Ethylene oxide | Ethylene oxide is a colourless liquefied gas with a sweet odour used for the sterilisation of implants and equipment within a steriliser/autoclave. |
| Extension | Movement that increases the angle at a joint. |
| Fixation, internal | A surgical procedure that stabilises and joins the ends of fractured (broken) bones by mechanical devices, such as metal plates, pins, rods, wires or screws. |
| Flexion | Movement that decreases the angle at a joint. |
| Fracture | A fracture is a break in the bone or cartilage. It usually is a result of trauma. A fracture can, however, be the result of an acquired bone disease such as osteoporosis or the result of abnormal formation of bone in a congenital bone disease such as osteogenesis imperfecta ("brittle bone disease"). |
| Hydroxy-apatite | Plasma-sprayed calcium phosphate coating that is bio-active. |
| Izod impact strength | Material test that provides toughness data under dynamic rather than static conditions (Shigley & Mischke, 2003). |
| Lateral | Side of the patient. |
| Lysis | Destruction. Haemolysis (*haemo-lysis*) is the destruction of red blood cells with the release of haemoglobin; bacteriolysis (*bacterio-lysis*) is the destruction of bacteria; and so on. Lysis can also refer to the subsidence of one or |

more symptoms of an acute disease as, for example, the fever of pneumonia.

Osteoarthritis

A type of arthritis caused by inflammation, breakdown, and eventual loss of cartilage in the joints. Osteoarthritis is also known as degenerative arthritis. Osteoarthritis can be caused by ageing, heredity, and injury from trauma or disease. The most common symptom of osteoarthritis is pain in the affected joint(s) after repetitive use.

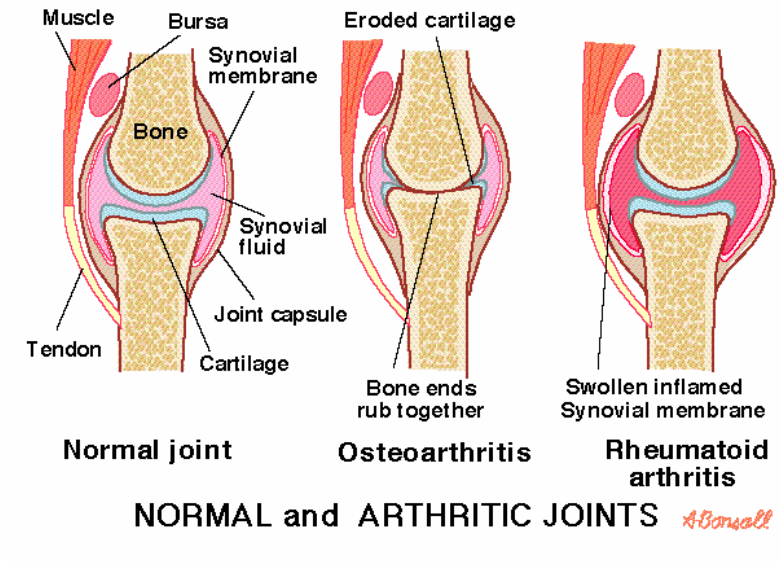


Osteolastic

A pathological condition resulting from accumulation of acid or a loss of base in the body; characterised by an increase in hydrogen ion concentration (decrease in pH). Has various causes including several states that produce excesses in various acids; included are diabetes mellitus (keotone bodies), renal insufficiency (phosphorus, sulfuric and hydrochloric acids), respiratory disease (carbonic acid), and prolonged strenuous exercise (lactic acid).

| | |
|---|---|
| Osteolysis | Also called particle disease, aggressive granulomatosis. Particulate debris from wear of arthroplasty components, most commonly polyethylene component (Schmalzried et al.,1997). Large pieces sequestered in fibrous tissue. |
| Osteotomy | Osteotomy is an operation in which a bone is cut, enabling a surgeon to reposition it. An osteotomy may be performed to lengthen or shorten a leg, to correct bowed or bent legs, or to reset a fracture. |
| PMMA | Polymethyl methacrylate — a thermoplastic polymer synthesised from methyl methacrylate and used as bone cement for the fixation of implant. |
| Smaller trochanter | 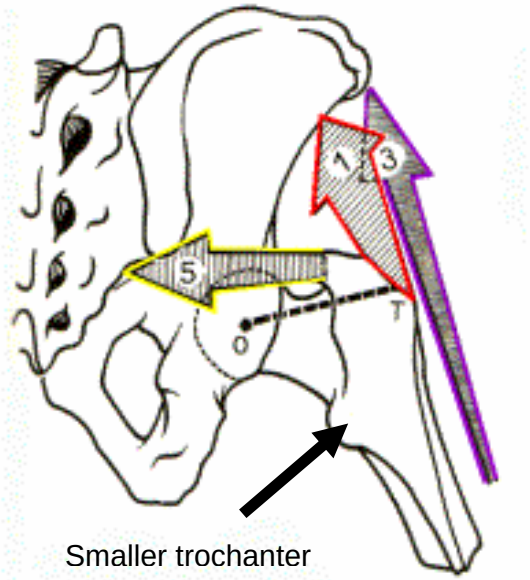 Smaller trochanter |
| Posterior | Back of the patient. |
| Rheumatoid arthritis | An auto-immune disease that causes chronic inflammation of the joints, the tissue around |

the joints, as well as other organs in the body. Auto-immune diseases occur when the body tissues are mistakenly attacked by its own immune system. The immune system is a complex organisation of cells and antibodies designed normally to "seek and destroy" invaders of the body, particularly infections. Patients with these diseases have antibodies in their blood which target their own body tissues, where they can be associated with inflammation. Because it can affect multiple other organs of the body, rheumatoid arthritis is referred to as a systemic illness and is sometimes called rheumatoid disease. While rheumatoid arthritis is a chronic illness (meaning it can last for years), patients may experience long periods without symptoms.

# CHAPTER 1

# INTRODUCTION

## 1.1 Development history of total hip replacement

Owing to the crippling nature of arthritis, the medical profession has been trying for well over a century to successfully treat this debilitating disease especially when it attacks the hip joints (Charnley, 1979; Schaldach & Hohmann, 1976). It was clear that many people required surgery to relieve the terrible pain and keep their joints mobile. Initial attempts to treat arthritic hips included arthrodesis (fusion), osteotomy, nerve division and joint debridements. The goal of these early debridements was to remove arthritic spurs, calcium deposits and irregular cartilage in an attempt to smooth the surface of the joint.

During this period, there was a concerted search for some material that could be used to resurface or even replace the hip. Several proposals and trials were made including the use of muscles, fat, chromatised pig bladder, gold, magnesium and zinc. All met with failure. Surgeons and scientists were unable to find a material which was biocompatible with the body, and yet strong enough to withstand the tremendous forces placed on the hip. (http://www.utahhipandknee.com/history.htm; http://www.geocities.com/ hip_ replacements/history)

In 1925, a Boston surgeon, MN Smith-Peterson (M.D.), moulded a piece of glass into the shape of a hollow hemisphere which could fit over the ball of the hip joint and provide a new smooth surface for movement. Although the glass proved to be biocompatible, it was not able to withstand the forces acting across the hip joint and resulting stresses from walking. Dr Smith-Peterson then tried other materials including plastic and stainless steel without any major success (http://www.geocities. com/hip_replacements/history).

An improvement was made in 1936 when scientists manufactured a cobalt-chromium alloy which was almost immediately applied to orthopaedics. This alloy is very strong and corrosion-resistant and is still used in orthopaedics today. Although the material proved to be successful, the technique of resurfacing the femoral head was found to be less than adequate. Pain relief was not as predictable as had been anticipated and hip movement remained limited for many patients.

The mould technique did not allow surgeons to treat the numerous and varied arthritic deformities of the hip.

In the 1950s Thompson and Moore (http://www.utahhipandknee.com/history.htm) separately developed replacements for the entire ball of the hip. These could be used to treat hip fractures and also certain arthritic cases. This type of hip replacement, called hemi-arthroplasty, only solved the problem of the arthritic femoral head (ball). The diseased acetabulum (hip socket) was not replaced. The prosthesis consisted of a metal stem which was placed into the marrow cavity of the femur, fitted with a metal ball (one-piece construction) which fitted into the hip socket (see Figure 1.1).

Although very popular in the early 1950s, results remained unpredictable and arthritic destruction of the acetabulum persisted and was not solved. A further problem was that there was no known method for properly securing the implant to the bone. After the development of good cementing techniques, this prosthesis is still used today for the treatment of fractured femurs (Robinson & Adams, 2002). Large numbers of patients, however, developed pain because of loosening of the implant with subsequent loss of mobility.

Figure 1.1: Austin-Moore prosthesis

As early as 1938, Dr Jean Judet and his brother, Dr Robert Judet of Paris, (http://www.utahhipandknee.com/history.htm), attempted to use an acrylic material to replace arthritic hip surfaces. The design of the prosthesis was very similar to the Austin-Moore model except for the material. The acrylic provided a smooth surface but unfortunately tended to work loose. This idea did lead Dr Edward J Haboush from the Hospital for Joint Diseases in New York City to utilise "fast-setting dental acrylic" to glue the prosthesis to the bone. This started a new era of implant-fixation techniques.

In England, an innovative surgeon, Sir John Charnley, was also attempting to solve these ongoing problems. Some of his ideas were so bold and creative that he was seriously questioned by many of his colleagues. Charnley aggressively pursued effective methods of replacing both the femoral head and the acetabulum of the hip. In 1958, he dealt with the problem of an eroded arthritic socket by replacing it with a Teflon implant (see Figure 1.2). He hoped that this would allow for a smooth joint surface to articulate with the metal ball of the femoral component. When Teflon did not achieve this goal he went on to try polyethylene (Charnley, 1979; Mendenhall, 2000). This worked well. In order to obtain fixation of this polyethylene socket, as well as the femoral implant to the bone, Charnley borrowed poly(methyl methacrylate) (PMMA) from dental supplies. This substance, known as bone cement, was mixed during the operation, then used as a strong grouting agent to firmly secure the artificial joint to the bone. This was the birth of low-friction arthroplasty.

Figure 1.2: The early prosthesis as designed by Sir John Charnley. Note the migration of the femoral head into the Teflon.

By 1961, Charnley was performing this type of surgery on a regular basis with good results (McCoy et al., 1988; Schulte et al., 1993; Klapach et al., 2001). He further improved the techniques and component designs. Thousands of people were successfully relieved of their hip pain and the long-term results became predictable. (Schulte et al., 1993; Klapach et al., 2001)

## 1.2 Current concepts

Total hip arthroplasty has been offered to younger and more active patients with increasing frequency over the last decade as the clinical success of this operation continues to be validated. The general concept of prosthesis used for total hip arthroplasty is a modular system consisting of an acetabular component, a femoral component and a femoral ball fitted between the acetabulum and femoral component to establish the articulating effect (Mallchau et al., 2000; Huo and Cook, 2001; Davidson et al., 2002).

The materials commonly used for the various components are as follows:

**Acetabulum**

Ultra-high molecular weight polyethylene (UHMWPE)

Metal alloy (chrome-cobalt, 316L stainless steel)

Ceramics (alumina)

**Femoral head**

Metal alloy (chrome-cobalt, 316L stainless steel, vitalium)

Ceramics (alumina, zirconia)

**Femoral Stem**

Chrome-cobalt

316L stainless steel

Orthron 90

Titanium (90-6Al-4Va)

## 1.3 Principal clinical diagnosis — total hip replacement

Only a small number of countries are keeping records of the state of hip surgeries performed. The leading hip replacement registers are the “Swedish National Hip Arthroplasty Register” (Mallchau et al., 2000), the “Norwegian

Arthroplasty register" (Havelin et al., 2003) and the Report by the "Australian Orthopaedic Association" (Davidson et al., 2002; Davidson et al., 2003). According to these reports, the number of primary procedures performed per year is 17 378 in Australia for the period 1/7/2001 to 30/6/2002, just over 11000 in Sweden for the year 2000, and 6 108 in Norway for the period 2002. These numbers equate to approximately 110 - 120 total hip replacements (THR) per 100 000 inhabitants per year. It is estimated that the total number of primary replacements in the United States of America amounts to approximately 200 000 per year (Huo & Cook, 2001). The average age for receiving a total hip replacement in Australia for female patients is 69.6 years and for male patients it is 66.1 years. Female patients account for 52.6% of all THR procedures and male patients for 47.4% of all procedures performed.

According to the report by the Australian Orthopaedic Association, the primary diagnosis resulting in primary total hip replacement is osteoarthritis as can be seen in Figure 1.3. Of all the reasons total hip replacements were performed in Australia, osteoarthritis is the main cause of hip joint degeneration in 87.7% of the cases.

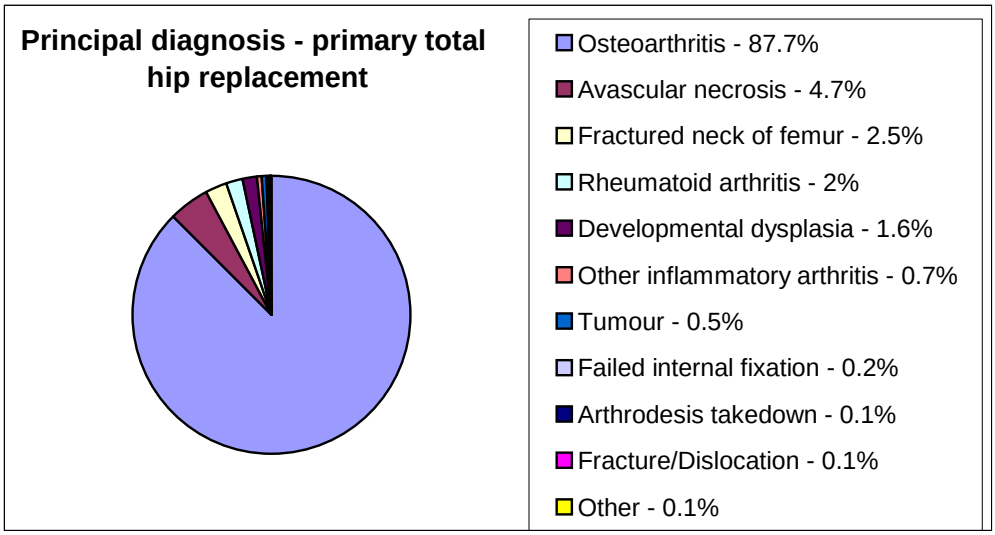


Figure 1.3: Principal diagnosis - primary total hip replacements (Davidson et al., 2002; Davidson et al., 2003)

Osteoarthritis is responsible for 75% of all the total hip replacements performed in Sweden and for 70% of replacements in Norway.

## 1.4 Clinical diagnosis resulting in revision hip replacement

Revision hip replacement is the exchange or removal of one or both components (Mallchau et al., 2000).

According to the Swedish, Australian and Norwegian hip registers endorced by the literature reviewed, the major cause for revision hip replacement is a phenomenon known as aseptic loosening, resulting from osteolysis. (Claus et al., 2001; Dumbleton et al., 2002; Manley et al., 2002; Foguet et al., 2003; Oakley et al., 2003; Wilkinson et al., 2003). Osteolysis occurs as a response to implant-derived particulate debris, and possibly other stimuli, resulting in increased local osteolastic bone resorption. Therefore the major cause of osteolysis is polyethylene wear debris generated during activity (Davidson et al., 2002; Davidson et al., 2003).

The clinical presentation of aseptic loosening can be explained as an attack on the bone tissue by the immune system as a result of the polyethylene wear debris present in the area. The schematic presentation of the mechanism is presented in Figure 1.4 with a clinical case shown on X-ray in Figure 1.5. The osteolastic bone resorption is shown in Figure 1.6.

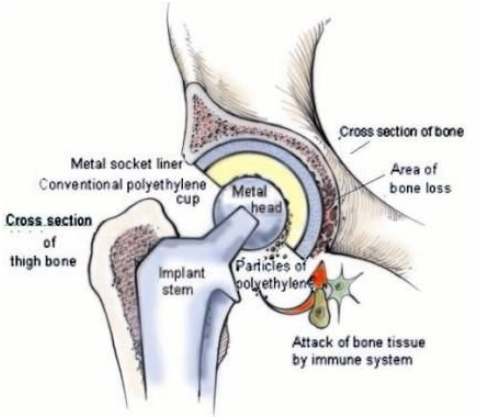


Figure 1.4: Schematic presentation of mechanism resulting in osteolysis (http://www.geocities.com/hip_replacements/history)

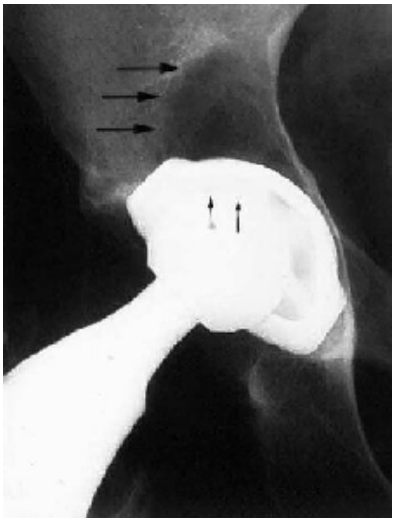

Figure 1.5: Wear debris-mediated osteolytic lesion superior (above) loose press-fit modular acetabular component. Note eccentricity of liner; mechanical failure ensued 5 years post-operatively. (Dumbleton et al., 2002)

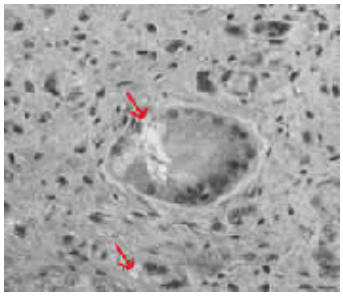

Figure 1.6: Polyethylene from an acetabular liner that has been attacked by the body, resulting in giant cells that eat away the bone resulting in component loosening (Manley et al., 2002)

Aseptic loosening resulting from osteolysis induced by excessive wear is therefore a major problem in total hip replacement (see Figure 1.7). From the Australian hip register, it is seen that during the period 1/7/2001 to 30/6/2002 a total number of 3 710 revision procedures were performed. The total number of revisions attributed to aseptic loosening resulting from osteolysis-induced wear amounts to 63%, while in the Swedish register, the total number of revisions attributed to aseptic loosening is 75%, and in Norway it amounts to 68%. Revision total hip replacements amount to approximately 22% of the primary total hip replacements done during the same period in Australia. Female patients account for 1 664 of the procedures done and the male patients account for 1 422.

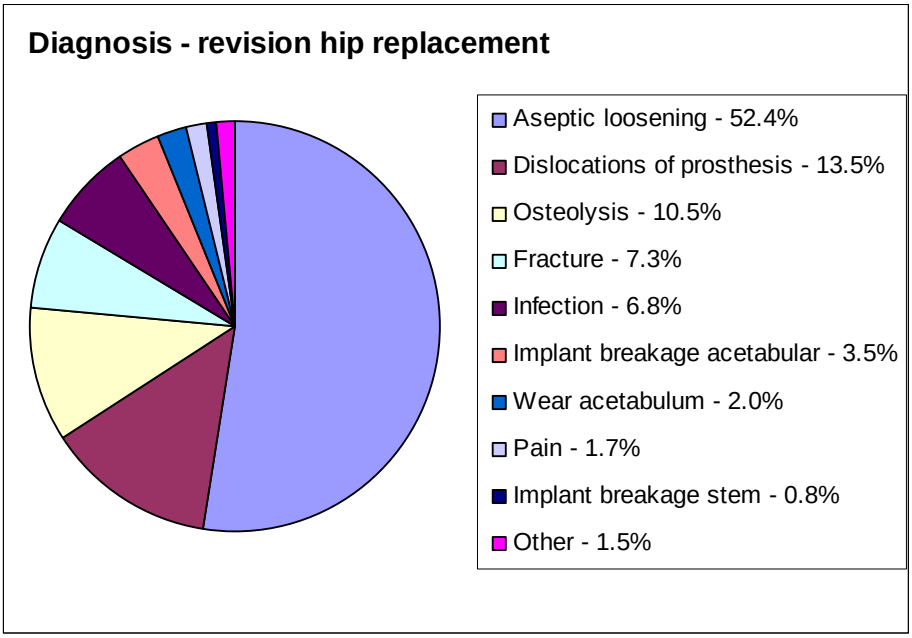


Figure 1.7: Diagnosis — revision surgery hip replacement (Davidson et al., 2002, Davidson et al., 2003)

The average survival rate for the various designs varies dramatically (Davidson et al., 2002, Davidson et al., 2003). The Charnley prosthesis still has a survival rate of approximately 85% after 15 years (McCoy et al., 1988; Schulte et al., 1993; Mallchau et al., 2000; Klapach et al., 2001; Davidson et

al., 2002; Davidson et al., 2003). If other designs are included the statistics are quite different. For the elite plus prosthesis with an acetabular component manufactured from hylamer together with a zirconia femoral head, the survival rate after six years is a catastrophic 36% (Norton et al., 2002). A summary of the survival rates for different models of cemented and uncemented prostheses can be seen in Figure 1.8. (Havelin et al., 2003) These failures are mainly attributed to osteolysis due to excessive wear. In those hips that had already failed, the acetabular component wear at 36 months was on average 2.04 mm.

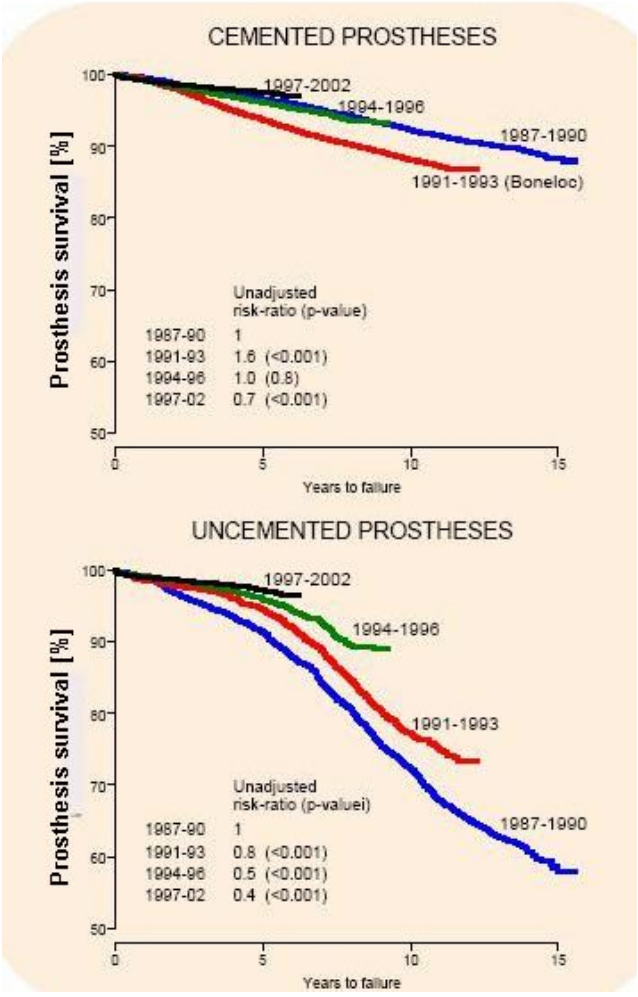


Figure 1.8: Survival rate for different models of cemented and uncemented prostheses (Havelin et al., 2003)

## 1.5 Aim of study

Local osteolastic bone resorption as a direct result of polyethylene wear debris generated during activity is a major factor causing component loosening, resulting in total hip replacement.

The aim of this study is to obtain a better understanding of the mechanical failure mechanism when the femoral head rotates in the UHMWPE acetabular socket.

This investigation begins with a comprehensive literature survey to establish the current state of affairs regarding the design, materials, failure analysis and life expectancy of implants used during hip replacement surgery. The literature survey is followed by a chapter in which the criteria are set to enable a detailed failure analysis of the retrieved components.

The next phase in the research is a failure analysis on retrieved components by making use of:

- Visual inspection
- Liquid dye penetrant
- Stereoscope
- Electron microscope
- Electrophoresis
- Mass-spectrometric analysis
- Analysis of the wear particles retrieved

This failure analysis was performed to gain a clear understanding of the mode of failure on the bearing surface in the retrieved components.

A study is also undertaken to obtain an indication of the creep behaviour of UHMWPE test pieces manufactured with different manufacturing techniques. This is necessary in order to arrive at a better understanding of the behaviour of the material at high contact stress values and at localised high operating temperatures. The various manufacturing techniques also include

crosslinking of the material in a hydrogen atmosphere. Making use of the data gathered during the previous phases, an experimental verification was made possible making use of a hip simulator and various other experimental techniques to verify the formation of the wear debris as well as the heat generated in the joint. This verification enables a better understanding of the failure mode in the bearing.

The last part of the study is the determination of the lubricating capabilities of retrieved synovial fluid to allow an evaluation of the lubrication available in the joint after the implantation of the various components.

# CHAPTER 2
# LITERATURE REVIEW

## 2.1 Introduction

The literature survey presented below first covers a review of the current designs for total hip replacements prostheses/implants being used throughout the world. To fully understand the function of the hip, it is necessary to obtain a good understanding of the biomechanics of the joint. It is also necessary to have an understanding of the materials that are being used for the manufacture of these implants.

The rest of the chapter is devoted to an overview of the current research in retrieval studies; wear mechanisms; the effects of different sterilisation techniques on service; the effect of crosslinking on the characteristics of the material and an overview of the current hip simulators being used for in-vitro testing. Another area that is discussed in this thesis is the lack of lubrication in the joint and the consequences of insufficient or inadequate lubrication. A literature review of research into the lubricating capabilities of synovial fluid is also presented.

In this thesis a different set of criteria from an engineering base is proposed to be used to evaluate the retrievals for the different wear mechanisms active in-vivo. To be able to make this proposal, it is important to understand the set of criteria currently in use, as well as its shortcomings.

As crosslinking of UHMWPE is seen as a short-term solution to the problem, the effect of crosslinking on the material characteristics needs to be understood. In this thesis, results are presented, indicating the influence of crosslinking on the creep behaviour of UHMWPE. As crosslinking is achieved by means of gamma irradiation, it is also necessary to look into the effect of the different sterilisation techniques on in-vivo life as well as the effect of the

different sterilisation techniques on the mechanical properties of the materials involved. Again, the influence of the different sterilisation techniques on the creep behaviour of the base material is investigated.

As the new ISO standard for the testing of hip implants came into effect in 2002 (ISO 14242-1, 2002), the standard of current simulators must be investigated. The simulator used for in-vitro testing in this investigation differs from the simulators proposed in the ISO standard. The reason for using a simulator that does not conform to the ISO standard is explained in Chapter 7.

## 2.2 Review of existing designs

Various companies are currently manufacturing components for total hip replacements. Although their designs differ slightly in the smaller detail or in the approach to total hip replacement, for example, cemented or uncemented implants, the basic modular design of all these designs is the same, as can be seen from the respective data sheets (http://www.aesculap.de/; http://www.centerpulse-orthopedics.com/uk/en/Home/Home; http://www.depuy. com/; http://www.ceraver.fr/anglais/sommaireang.htm). A basic modular design is shown in Figure 2.1.

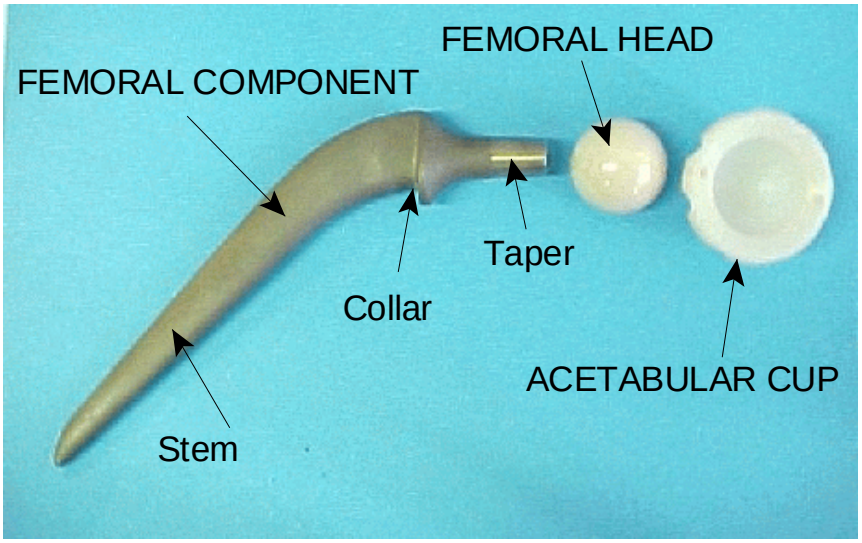


Figure 2.1: Basic modular design of total hip replacement

### 2.2.1 Femoral component

The design of the femoral component can be divided into three regions namely the design of the stem, the design of the collar area and the taper for the fitment of the femoral head (see Figure 2.1).

The design of the stem can vary according to the following concepts:

a. Taper or straight stem
b. Length of stem, anything between 160 mm (primary total hip arthroplasty) to 240 mm for revision total hip arthroplasty
c. Smooth or highly polished surface finish
d. Surface with or without flutes
e. Sharp or round corners
f. Cemented or uncemented, where there are a number of surface coatings available to establish bone in growth (Engh & Bobyn, 1985), namely sintered bead or a bio-active coating such as hydroxyl-apatite.

The use of a collar determines the design of the collar. The principal reason for the use of the collar is to transmit the load via the smaller trochanter area into the cortical bone of the femur. These designs tend to cause bone resorption (degeneration of the bone in the area under compression) just below the collar in the cortical bone. (See illustration of bone resorption below collar in Figure 2.2.)

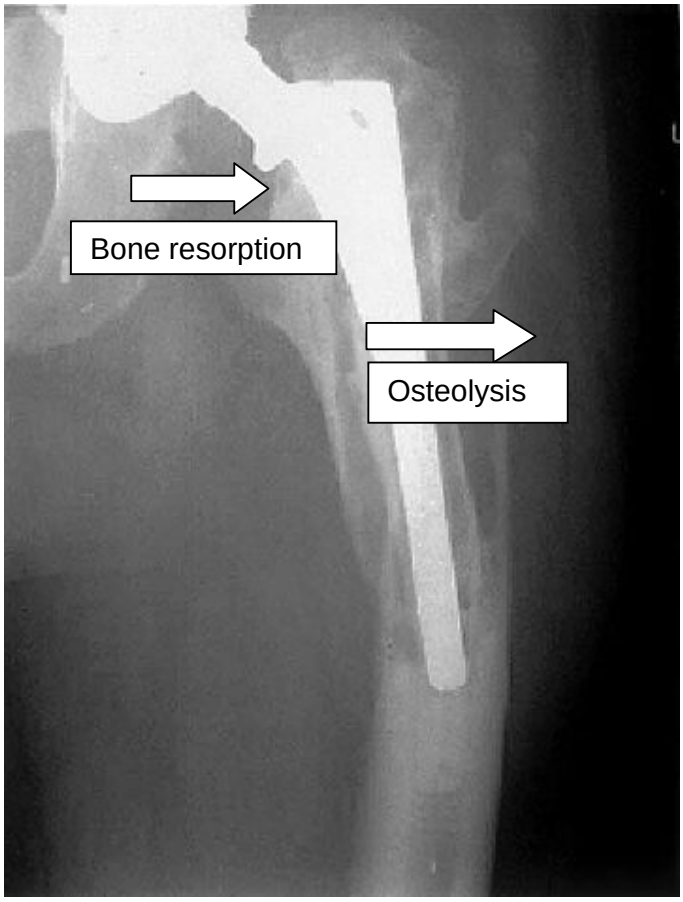


Figure 2.2: Femoral osteolysis with signs of bone resorption below collar (Dumbleton et al., 2002)

The taper on the femoral stem is used for the fitment of a modular femoral head. The whole design philosophy behind a loose femoral head is that with variation in taper depth the length of the implant can be changed to accommodate and rectify differences in leg lengths (http://www.aesculap.de/; http://www.centerpulse-orthopedics.com/uk/en/Home/Home; http://www.ceraver.fr/anglais/sommaireang.htm; http://www.depuy.com/). The standard tapers being used are 10/12 or 12/14 tapers both with a 6º included angle.

### 2.2.2 Femoral head

The femoral head acts as the male part of the bearing interface in the

replacement of the joint. The major design change in the design of the femoral ball, apart from the material changes, is the change in diameter. The diameters used are 22, 26, 28, and 32 mm.

The taper depth on the femoral ball also varies to enable the surgeon to compensate for changes in patient leg length. The options available are -5, 0, +5 and + 10 mm. All the tapers are 10/12 or 12/14 with a 6° included angle.

### 2.2.3 Acetabular cup

The acetabular cup acts as the female part of the bearing interface in total hip arthroplasty. The design of the acetabular component can vary according to the following concepts:

a. Cemented or cementless components, where the cementless components have a bearing liner mounted inside a metal backing and the metal backing is coated either with sintered beads or hydroxy-apatite to promote bone in growth into or onto the implant. (See Figure 2.3.)

b. The metal back acetabular cup can be kept in position with cortical bone screws, especially during revision total hip arthroplasty (see Figure 2.4), or with spikes, if the back of the cup is equipped with spikes to stabilise the cup.

c. The liner can either be factory-fitted or be fitted during the procedure. Where the liner is fitted during the procedure, it clips into the metal backing to keep it in position.

d. Material used — UHMWPE, ceramic or metal alloy

e. The use of a retaining ring is also becoming more popular, especially in patients where the risk of dislocation is high.

f. The back of the acetabular cup, in cemented implants, can also vary in design to establish compression of the cement mantle and to ensure an even distribution of the cement.

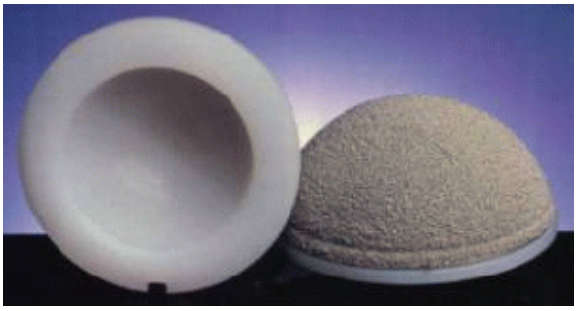

Figure 2.3: Polyethylene liner with hydroxy-apatite coated metal back (http://www.aesculap.de/)

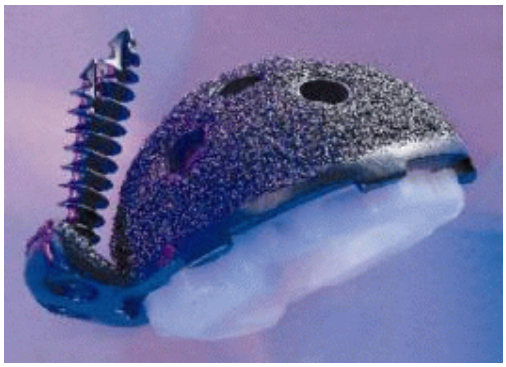

Figure 2.4: Polyethylene liner in metal back with holes for fixation (http://www.depuy.com/)

If the statistics of the existing hip registers are taken into account the most common system used for total hip arthroplasty is a cemented polyethylene acetabular component in conjunction with either Cr-Co or ceramic femoral heads (Mallchau et al., 2000; Davidson et al., 2002; Davidson et al., 2003). A comparison of the in-vivo wear rates between Cr-Co and UHMWPE; and ceramics and UHMWPE is discussed in paragraph 2.6.1.

## 2.3 Biomechanics of the hip joint

When the body is supported on only one leg, its centre of gravity $S_6$ has to be balanced vertically above the bearing area of the foot. (See Figure 2.5.) This determines the posture as a whole, including the posture of the leg and joint

position (Kummer, 1976).

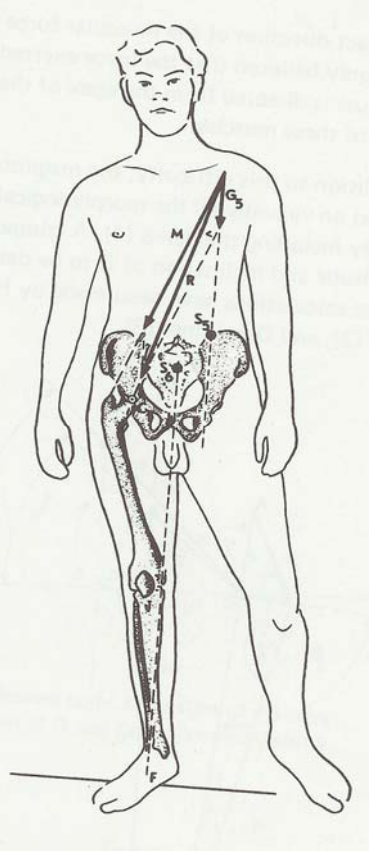


Figure 2.5: Man standing on his right leg. The gravity vertical line from $S_6$ falls in the supporting area of the right foot. The weight $G_5$ is to be balanced in the right hip joint. M - abductor muscles of the right hip, R - hip resultant, $S_5$ - centre of gravity of the body mass must be borne in the right hip joint (Kummer, 1976).

With regard to the hip joint of the supporting leg, the centre of gravity $S_5$ has to be considered; and the moment of the mass $G_5$ must be balanced in the joints by means of the abductor muscles. The magnitude and direction of the joint-resultant load then depend on the

- Direction and tension of the hip abductors – (see Figures 2.6, and 2.7.)
- Posture of the pelvis
- Length and posture of the leg.

The direction and tension of the abductor muscles are related to the lever arm

of the load (depending, among other things, on the width of the pelvis), to the length of the femoral neck and trochanter, and to the angle between the neck and shaft. Furthermore, it must be remembered that the posture of the leg is strictly determined by the position of $S_6$, on account of the equilibrium conditions.

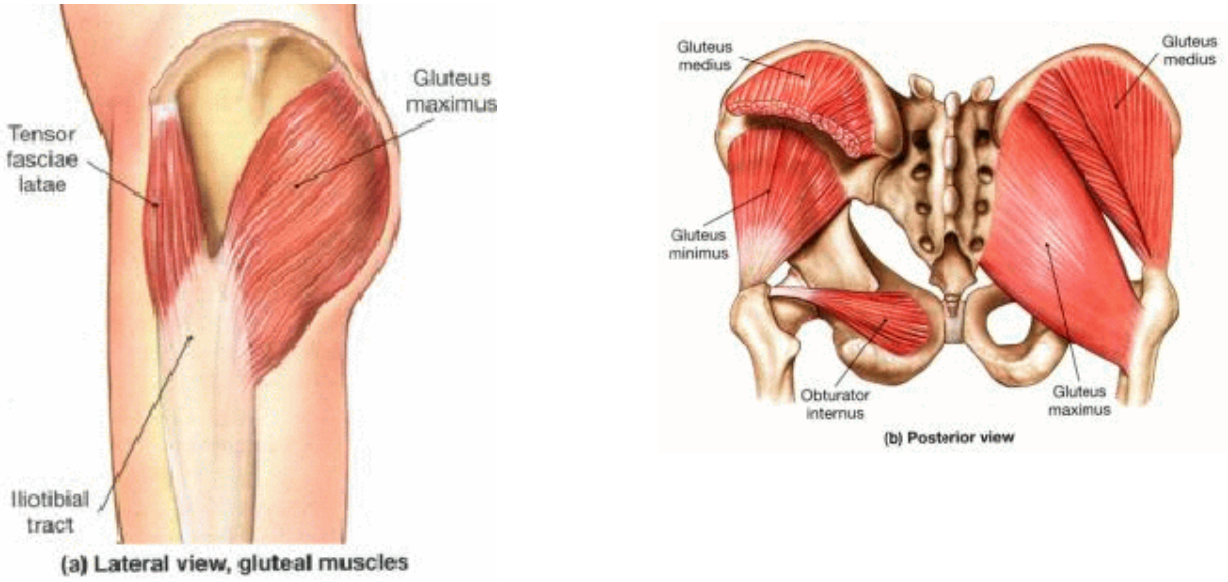


Figure 2.6: Side (lateral) and back (posterior) view of abductor muscles (http://www.geocities.com/hip_replacements/history)

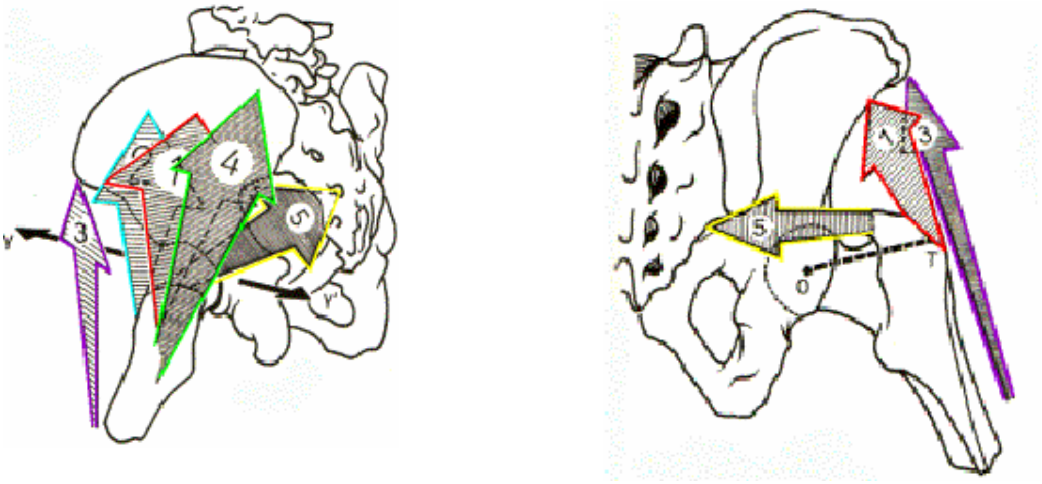

Figure 2.7: Side and back view of abductor forces acting on hip joint (http://www.geocities.com/hip_replacements/history)

The resultant force resulting from the various abductor muscles acting on the hip joint works in on an angle of 13.7° away from the most posterior point of the face towards the posterior side (Kummer, 1976). (See Figure 2.8.)

The resultant force acting on the hip, as described, generates an in-vivo resultant force on the acetabular cup. Measured from the anteroposterior view of the liner, this vector is orientated at a mean of 19.3° away from the face of the liner towards the apex as shown in Figure 2.9 (Sychterz et al., 1996).

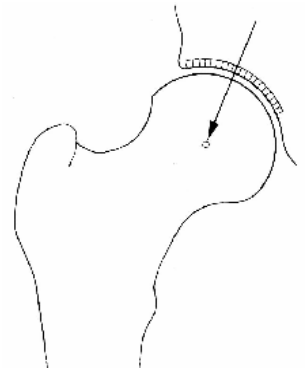

Figure 2.8: Stress distribution to the normal hip joint (Kummer, 1976)

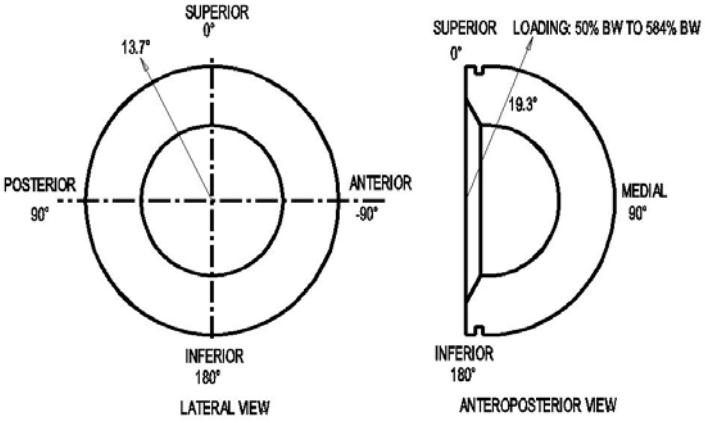


Figure 2.9: Graphical presentation of the loading on the acetabular cup (Paul, 1976; Kummer, 1976; Sychterz et al., 1996; Zupanc et al., 2001)

An exact analysis of the resultant load, acting on the hip joint, is difficult since the precise load in the relevant muscles has not yet be determined nor can the force transmitted by the ligaments at any instant be inferred from external measurements. By making reasonable assumptions for the position of the resultant force transmitted by certain groups of muscles, Paul (1976) was able to establish a basic loading pattern for the hip joint. The graphical presentation of these forces can be seen in Figure 2.10 and a summary of the results obtained in Table 2.1.

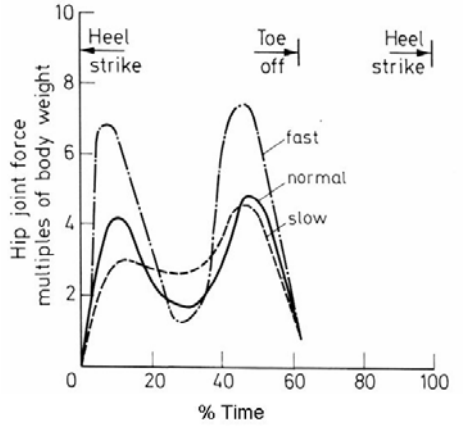


Figure 2.10: Variation with time of hip joint forces for slow, normal and fast walking (Paul, 1976). The scale of the x axis is percentage time

Table 2.1: The maximum joint forces present in the hip joint, for a range of activities (Paul 1976)

| **Activity** | **Maximum joint force — Multiples of body weight** |
|---|---|
| Level walking | |
| - slow | 4.9 |
| - normal | 4.9 |
| - fast | 7.6 |
| Up stairs | 7.2 |
| Down stairs | 7.1 |
| Up ramp | 5.9 |
| Down ramp | 5.1 |

The work done by Paul was verified by Bergmann (1985; 1993). Two femoral components were instrumented with strain gauges and transmitters. The two prostheses were then implanted into two patients. After the recovery period, strain measurements were taken while the patients were walking at different speeds on a treadmill. The data were analysed and plotted as a resultant force acting on the hip joint during the walking cycle. The plotted data can be seen in Figure 2.11.

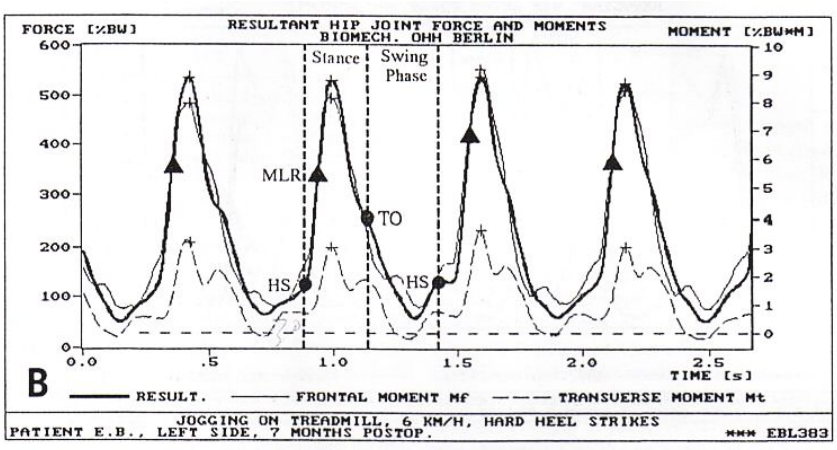


Figure 2.11: Resultant force on hip joint for patient jogging on treadmill at 6 km/h (Bergmann et al., 1993, Bergmann et al., 1995). HS: heel strike, TO: toe off; MLR: measured load profile

The maximum loading on the hip joint during fast walking, according to Bergmann et al., is 580% times the body weight of the patient, with the minimum loading, to prevent dislocation, 50% of the body weight. The increase of 530% is a result of the abductor muscles active across the joint.

As these actual measured values are deemed to be more accurate (by this researcher), than the calculated values of Paul (1976) or ISO 14242-1 (2002), this load profile is simulated in the University of Pretoria hip simulator which was designed and built for this study.

## 2.4 Material properties of ultra-high molecular weight polyethylene (UHMWPE)

From previous studies (Mallchau et al., 2000; Claus et al., 2001; Davidson et al., 2002; Dumbleton et al., 2002; Manley et al., 2002; Norton et al., 2002; Davidson et al., 2003; Foguet et al., 2003; Oakley et al., 2003; Wilkinson et al., 2003) it is evident that the unacceptably short, life achieved with hip implants mainly occurs from aseptic loosening of the acetabular cup. These authors also reveal that osteolysis, as a result of the UHMWPE wear debris, is the major cause of this aseptic loosening. In the work done by Dumbleton et al. (2002), it was shown that osteolysis is rarely observed if the wear rate is smaller than 0.1mm per year. Ultra-high molecular weight polyethylene has become the industry standard material for the manufacturing of acetabular components (Mallchau et al., 2000; Davidson et al., 2002; Davidson et al., 2003). The focus of this study is therefore on the wear and the wear mechanisms of UHMWPE as used in acetabular cups.

UHMWPE is a tough, durable material with a low coefficient of friction. The density (Lewis, 2001; Engineering materials handbook, 1987) of this material varies between 9 260 and 9 340 kg/m$^3$ and a typical value for the coefficient of friction (lubricated) is 0.05 to 0.1, depending on the type of lubrication.

A frequently used guide to the capacity of marginally lubricated or dry bearings (Hutchings, 1992) is the value of the product PV, where P is the mean bearing pressure in MPa (load divided by projected bearing area) and V is the sliding velocity in ms$^{-1}$. A typical dry PV value for this material is 4 N/mm$^2$.m/s, as shown in Figure 2.12, with a maximum compression strength of 10 MPa determined at room temperature.

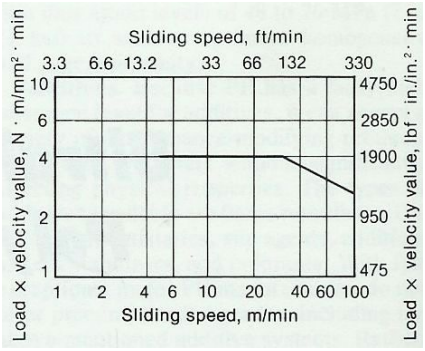


Figure 2.12: PV values for UHMWPE at 20°C (Engineering Materials Handbook, 1987)

The molecular mass of UHMWPE is almost ten times that of high-density polyethylene. UHMPWE has the highest abrasion resistance and impact strength of any plastic (Engineering Materials Handbook, 1987). Combined with a low coefficient of friction, UHMWPE yields a self-lubricating, non-stick surface. Its static and dynamic coefficients of friction are significantly lower than those of steel and most other plastic materials. The basic chemical unit of UHMWPE is $-CH_2-$. Thus, a $4 \times 10^6$ molecular weight resin contains approximately $285 \times 10^3$ carbon atoms or units in the polymer chain (Engineering Materials Handbook, 1987).

Because of its self-lubricating, non-stick, lightweight and wear-resistant characteristics, UHMWPE is widely used as bearing material in joint replacements. Although the material can maintain its properties at high temperatures only for a very short time, **"**it is recommended that in journal bearings temperatures above 40°C should be avoided at all times**"** **(**Engineering Materials Handbook, 1987). From Figure 2.13, it is clear that the izod impact value of this material decreases dramatically if the material is heated above 40°C as the material becomes more ductile, suggesting that, for a given geometry and loading condition plastic flow is more likely to occur.

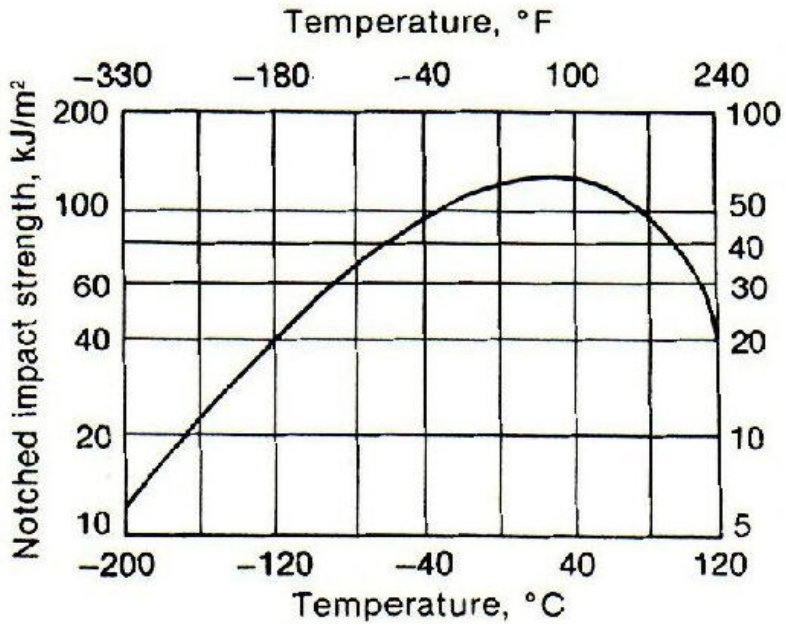


Figure 2.13: Izod impact strength against temperature with 15° double V notched (Engineering Materials Handbook, 1987)

UHMWPE is a material that is susceptible to plastic flow under constant pressure applications. From Figure 2.14, an increase in creep (% compression) of almost 12.5% at 56 days under a pressure of 12 MPa, and at a temperature of 20°C, is visible. In the designed life of a prosthesis of 20 years (Malchau et al., 2000; Davidson et al., 2002; Davidson et al., 2003), 56 days represent in the order of 0.78% of the expected lifespan of an acetabular cup. It must, however, be noted that in the cup the material is more constrained against creep than in the case of a test piece. (It will be shown that 12 MPa is the typical pressure inside an acetabular cup.) This data correlates with the data published by Sun et al. (1996); Lee and Pienkowski (1998); and Meng Deng et al. (1998). From Figure 2.13, it can be seen that the material softens at temperatures above 40 °C. The softening leads to an increase in plastic creep. From the material specifications, the maximum short time operating temperature (seconds) is 80°C with the melting point 135 - 138°C (Material data sheet, UHMWPE, Poli HiSolidur, 1999). Note, however, that the creep flattens off, especially in a confined space, and that the almost

linear graph of Figure 2.14 cannot simply be extrapolated. This aspect is discussed further in this thesis in the discussions of the experimental phase.

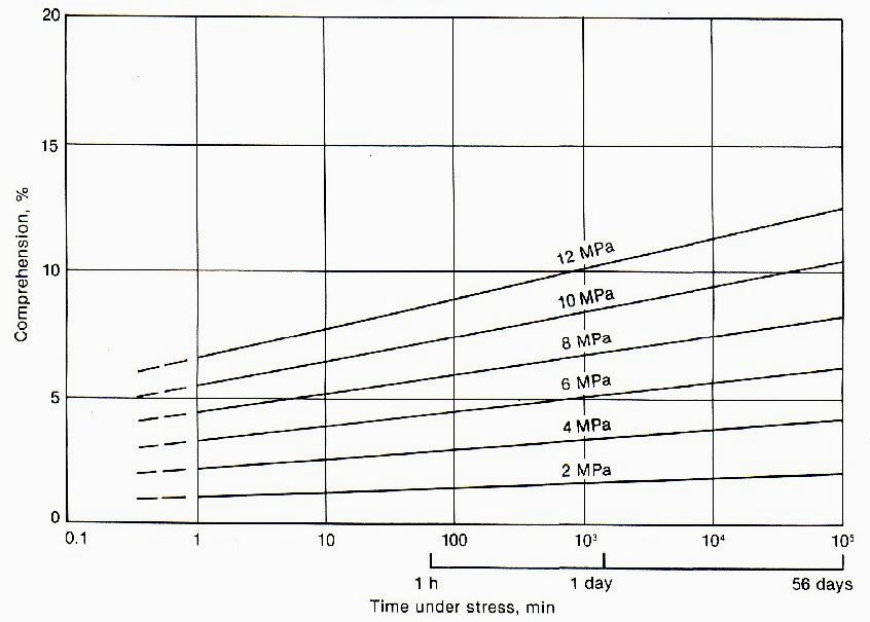


Figure 2.14: Compression creep for various loads at 20°C (Engineering Materials Handbook, 1987)

Chemical crosslinking with 0.3 to 0.5% organic peroxides (an active ingredient) has been found to improve wear resistance by as much as 30% over a non-modified resin, while reducing deformation under a load (Du Plessis et al., 1977; Sun and Wang, 1996; Oonishi and Kuno, 1997; Wang et al., 1998). Thin film transparency improves, and density is lowered by a reduction in crystallinity. Crosslinking can also be accomplished by beta or gamma irradiation.

The mechanical properties for UHMWPE can differ taking into account the various manufacturing methods (Lewis 2001), whether moulded or extruded and the amount of annealing. A summary of the average mechanical properties of UHMWPE is shown in Table 2.2.

Table 2.2: Mechanical properties of UHMWPE (Charnley, 1979; Material data sheet, Poli HiSolidur, 1999; Lewis, 2001)

| **Property** | **Typical value** | **ASTM test method** |
|---|---|---|
| Density (kg/m$^3$) | 9260 - 9340 | D792 |
| Tensile strength at yield (MPa) | 21 | D638 |
| Tensile strength at break (MPa) | 48 | D638 |
| Elongation at break (%) | 350 | D638 |
| **Young's modulus (GPa)** | | |
| At 23 °C | 1.6 | D638 |
| At -269 °C | 2.97 | D638 |
| **Izod impact strength (kJ/m)** | | |
| At 23 °C | 1.6 | D256(a) |
| At -269 °C | 1.1 | D256(a) |
| Hardness, shore D | 62-66 | D2240 |
| Water absorption (%) | 0 | D570 |
| Poisson's ratio | 0.28 | |
| **Dynamic coefficient of friction on polished steel** | | |
| Dry | 0.1 - 0.22 | |
| Water | 0.05 - 0.1 | |
| Oil | 0.05 - 0.08 | |
| **PV values (N/mm$^2$.m/s)** | | |
| Dry | 4 | See figure 2.12 |
| Wet | 6 - 7 | |
| Maximum load (MPa) - compression | 10 | |
| Maximum contact speed | 120 m/min | |

The values for yield and izod impact strength are given at room temperature and at sub-zero temperatures where this material performs excellently. However, at elevated temperatures, as can be seen from Figure 2.13 above,

there is a decrease in performance.

Various tensile creep studies have been conducted on UHMWPE by different authors (Sun and Wang, 1996; Lee and Pienkowski, 1998; Material data sheet, Poli HiSolidur, 1999). The results of these studies appear similar to the data presented in figure 2.14 given earlier. The major gap in this data and within these studies is that they either did not consider creep at elevated temperatures, or they only investigated the virgin material and did not consider the effect of sterilisation by irradiation or the effect of the crosslinking of the material. An indication of the behaviour of the material under these conditions and with different sterilisation techniques is discussed in Chapter 3 of this thesis.

It is also important to note that the PV values specified in Table 2.2 above apply to ventilated bearings with a specific geometry. If the temperature inside the bearing rises above the permissible value the PV values must decrease to compensate for the lack of heat dissipation from the bearing surface, because the heat generated cannot be dissipated. Although the Engineering Materials Handbook (1987) specifies an operating temperature below 40°C, the manufacturers of UHMWPE specify 80°C as the maximum short term service temperature while the melting point of the material is 135 - 138°C (Material Data Sheet, Poli HiSolidur, 1999). It must be noted that the allowable PV data is not available for crosslinked material.

## 2.5 Wear and wear modes in acetabular components

Whenever surfaces move over relative to each other, wear will occur, with damage to one or both of the surfaces, generally involving progressive loss of material. In most cases, wear is detrimental, leading to increased clearances between the moving components, unwanted freedom of movement and loss of precision with a resulting increase in mechanical loading and yet more rapid wear. This rapid wear can also result in fatigue failure (Sun & Wang, 1996).

Contact between polymers, or between a polymer and a metal, is

predominantly elastic; therefore the friction and wear behaviour of polymers differs fundamentally from that of metals. In the plasticity index (ψ) equation (Hutchings, 1992):

$$\psi = \frac{E}{H}\left(\frac{\sigma}{r}\right)^{1/2} \qquad (2.1)$$

The ratio E/H, where E is Young's modulus and H is the hardness of the material, determines the extent of plasticity in the contact region. The surface topography is also important. For metals the ratio E/H is typically 100 or more, while for many of the polymers E/H is only about 10. The plasticity index for a polymer thus has only one tenth of the value for metal, and the contact is therefore almost completely elastic, except against very rough surfaces.

A second factor that plays an important role in the friction of polymers is the strong time dependence of their mechanical properties. Most polymers are visco-elastic (Engineering Materials Handbook, 1987; Sun & Wang, 1996) and also show a marked increase of flow stress with strain rate.

The friction and, therefore, the wear of polymers, such as metals, can be attributed to two sources: a deformation term, involving the dissipation of energy in quite a large volume around the local area of contact, and an adhesion term originating from the interface between the slider and the counterface. The regions where these two sources of friction and wear originate are illustrated in Figure 2.15, for the sliding of a hard asperity over a polymer surface. As for metals, the distinction between the deformation and adhesion components of friction is somewhat artificial, and under many circumstances no clear demarcation can be made. However, in some experiments, and in some practical applications, one term dominates and can then be examined in isolation (Hutchings, 1992).

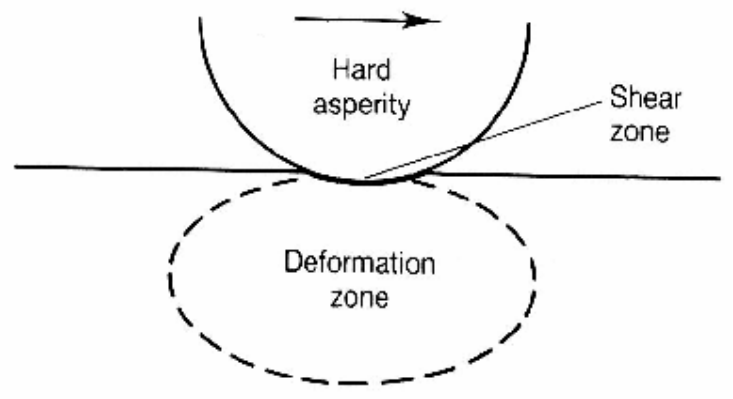


Figure 2.15: The origins of the friction associated with the sliding of a hard, smooth surface over a polymer surface (Hutchings, 1992)

Wear modes for acetabular cups have been defined in literature as an aid to orthopaedic surgeons to enable them to classify the hip joint failures of their patients. This classification is not really intended to be used in an engineering examination of the failed components.

As this classification is open to interpretation, a different classification is proposed in Chapter 4, which will help researchers in identifying the applicable wear mode. This proposed classification is based on engineering principles to aid in the determination of the root cause of mechanical failure of the components. The existing wear modes, as described in literature, for intended use by the medical profession are (Schmalzried et al., 1999):

Mode 1 wear: Results from the motion that is intended to occur between the two primary bearing surfaces, such as the motion of the prosthetic femoral head against the polyethylene acetabular bearing surface

Mode 2 wear: Refers to the condition of a primary bearing surface that moves against a secondary surface it is not intended to slide against. For example, Mode 2 wear occurs when a femoral component penetrates through a modular polyethylene bearing liner and then moves against the metallic shell of the acetabular, in the case of a metal

backing. At this point the implant has long exceeded its useful life.

Mode 3 wear: Refers to the condition of the primary surfaces as they move against each other but with the interposition of third-body particles. In Mode 3 wear, the origin of the contaminant particles is unknown. They directly abrade one or both of the primary bearing surfaces.

Mode 4 wear: Refers to two secondary (non-primary) surfaces sliding against each other. An example of this mode of failure is the neck of the femoral part sliding against the rim of the acetabular component. This wear mode is normally a direct result of misalignment and leads directly to third-body wear and early loosening of the cup.

Mode 1 wear is natural for a well-functioning transplant while Modes 2, 3 and 4 are unacceptable and will lead directly to early failure. The above classification is used by the medical profession to report on their patients. It does not attempt to qualify or quantify adhesion or abrasion or any other factor as already mentioned.

Unless the surgeon can clearly see third-body wear (any particle entering the bearing surface), for example, from bone deposits or cement particles, he/she is unable to identify the basic cause of failure stemming from third-body wear. *Failure*, as used in this context, means the point where the bearing is unable to perform its intended function without causing the patient discomfort. There are a number of variables that can affect the wear of the polyethylene bearing in-vivo, including the wear resistance of the material as well as the loads, sliding speed, motion pattern, manufacturing processes for the polyethylene component, implantation technique, use of the joint including frequency of use (Charnley & Halley, 1975), design specifics, such as conformity between the femoral head and the cup, lubrication, heat conduction, etc. (Fourie & Burger, 1999). The wear resistance of the polyethylene component is a function of the

base resin, the manufacturing process, the method of sterilisation and the extent of crosslinking (Du Plessis et al., 1977; Fisher et al., 1995; Wang et al., 1995; Sun and Wang, 1996;).

Polyethylene wear is also a function of the motion pattern (Wang et al., 1997; Charnley & Halley, 1975). In wear tests like reciprocating pin-on-disk tests, the quoted rate of polyethylene wear for a given set of parameters is 10 to 100 times lower than in wear tests that use crossing motion paths as found in a hip joint. Wear tests with a crossing motion path more closely simulate the wear occurring in-vivo. A problem that is found in most of the wear literature is based on either reciprocating pin-on-disk or circular pin-on-disk tests although a lot of work is done on simulators that will be discussed later in Chapter 7 (Wang et al., 1997).

Increased roughness of the femoral counter surface may dramatically accelerate wear of the polyethylene component. Experimental studies have indicated that a threefold increase in the roughness of the femoral counter surface can cause at least a tenfold increase in the rate of polyethylene wear (Dowson et al., 1987; Livermore et al., 1990; Li & Burstein, 1994). See Figure 2.16 for the results of the wear coefficient for steel on UHMWPE. From Figure 2.16 it is clear that there is an optimum surface finish for mating material in a bearing couple.

The explanation for the shape of the data in Figure 2.16 is given when one examines the function of the asperities on the surface of a bearing as indicated in Figure 2.17. The main functions of the irregular shape of the asperities are to transport lubricant into the bearing surface area (Hutchings, 1992) and to keep the two bearing surfaces apart. If the surface roughness ($R_a$ value) is increased, the asperities increase in size to the extent where the asperities start functioning as a rasp. On the other hand, if the surface roughness is decreased ($R_a$ value), the surface is too smooth to aid in the transport of the lubricant into the bearing surface area leading to lubrication starvation and subsequent seizure of the bearing. The crossover point for

surface roughness ($R_a$) for steel sliding on UHMWPE is 0.06 µm.

.

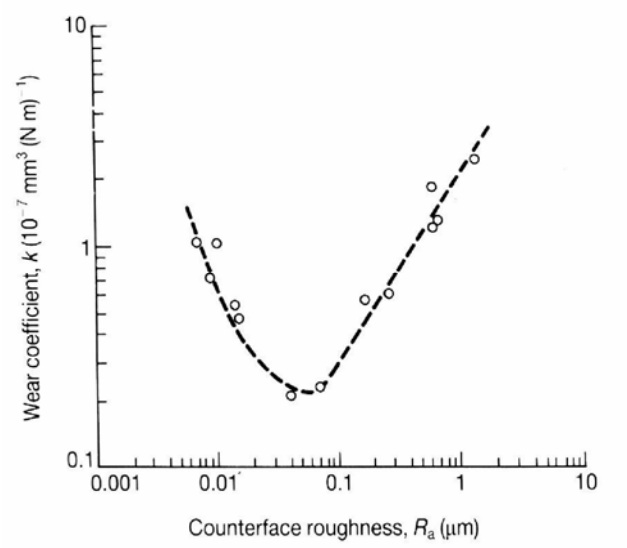


Figure 2.16: Wear rate of UHMWPE dry sliding against a steel counter face, as a function of the roughness of the steel surface (Hutchings, 1992)

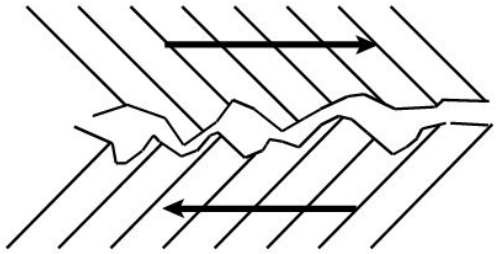

Figure 2.17: Illustration of the asperities on the surface of a component after manufacturing (Hutchings, 1992)

The polyethylene wear rate is also sensitive to the specific type of surface damage that exist in a contact pair or that occurs during service. However, in clinical comparisons in which the operating environment of the articulation is

more variable, ceramic heads are reported to have demonstrated rates of wear that are lower than those of metallic heads (Schmalzried et al., 1999). This derivation is not totally true as indicated by Buford and Goswani (2004). In this study, cases are reported where the wear rate (mm/yr) for UHMWPE against alumina (0.1 mm/yr) is larger than for UHMWPE against stainless steel (0.08 mm/yr), both for 28 mm femoral heads. There are also reported cases where the wear rate is 0.04 mm/yr for UHMWPE against cobalt-chromium, as well as cases with a wear rate of 0.03 mm/yr for UHMWPE against alumina (Buford & Goswani, 2004). If one looks at the distribution of these results statistically it is clear that the bearing couple cannot be evaluated alone, but the patient conditions, that is activity levels and quality of synovial fluid, must be taken into account. Apart from comparing the results of this study to the work done by Buford and Goswani (2004), the results of the current investigation were also compared to the work done by Jasty et al. (1997) and Sychterz et al. (1996).

As an important part of this study the variation in wear rate is explained by the theory that the lack of lubrication in the joint plays a major role in the wear mechanism active in the bearing couple.

Decreased geometric conformity between the femoral head and the acetabular component can lead to a drastic increase in the contact stresses resulting in plastic flow or creep. Apart from being dependent on the Young's modulus (E) and the Poisson's ratio ($\nu$) of the material, the biggest single influence on the contact stress is the size of the contact on the bearing interface as illustrated in Figure 2.18 (Boresi & Sidebottom, 1985).

In total hip replacements the dominant wear mechanisms appear to be micro-adhesion and micro-abrasion with wear particles less than 1 μm in length (Barbour et al., 1995; Maloney et al., 1995; Scmalzried et al. 1997). Osteolysis is mostly attributed to these sub-micron wear particles (Clauset al., 2001; Dumbleton et al., 2002; Manley et al., 2002; Foguet et al., 2003; Oakley et al.,

2003; Wilkinson et al., 2003). Subsurface delamination, pitting and fatigue cracking with the release of much larger wear particles have also been identified as important mechanisms of wear (Maloney et al., 1995; Scmalzried et al., 1997). This study shows that wear particles as big as 0.5 mm were retrieved from patients. A detailed analysis of retrieved cups will be presented in Chapter 5.

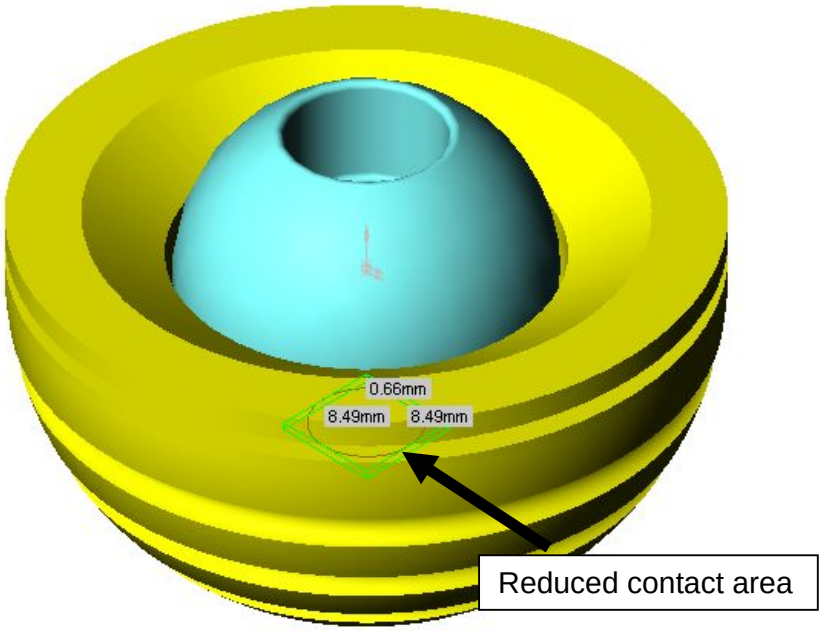


Figure 2.18: Graphical presentation of the effect of reduction in conformity on reduction in contact area – contact area becomes much smaller

## 2.6 Summary of previous retrieval and wear studies

### 2.6.1 Summary of retrieval studies — excluding crosslinked components

Various wear studies, based on X-ray analyses, have been published over the years (Charnley & Halley, 1975; Bragdon et al., 1997; Jasty et al., 1997; Wang et al., 1997; Bajaria & Bellare, 1998; Pietrabissa et al., 1998; Kesteris et al., 2003; Orishimo et al., 2003; Buford & Goswani, 2004). When this data is carefully analysed it is evident that the main aim was to try and determine the average linear wear over a period of time and not as much to determine the exact cause of mechanical failure. Doing a study by means of X-rays as detail failure analysis is problematic. Table 2.3 gives a summary of the available

results. The big scatter in the amount of linear wear per year is also not explained.

These studies were done by means of X-rays and the magnification factor of the X-rays is not consistent. It can be argued that the data as shown is of very limited value because it is not possible to measure accurately to one tenth of a millimetre on X-ray plates. X-rays are printed in shades of grey with not always a clear distinction between the edges. (See Figure 2.2 for an example.) Another effect is that some of the metals tend to create a halo effect around the material which makes measuring the component exactly very difficult. The only conclusion possible from these studies is an approximate wear rate over a period of time.

Table 2.3: Summary of in-vivo wear rates as per literature from Jasty et al. (1997)

| Study | Number of samples | Average linear wear/year mm/year | Range mm/year |
|---|---|---|---|
| Charnley and Halley, 1975 | 72 | 0.15 | 0 - 0.6 |
| Griffith et al., 1978 | 493 | 0.07 | 0 - 0.24 |
| Wroblewski, 1985 | 21 | 0.21 | 0 - 0.41 |
| Wroblewski, 1986 | 103 | 0.1 | 0 - 0.43 |
| Livermore et al., 1990 | 227 | 0.13 | 0 - 0.39 |
| Wroblewski et al., 1992 | 57 | 0.07 | 0.01 - 0.2 |
| Cates et al., 1993 | 99 | 0.08 | 0 - 0.37 |
| Cates et al., 1993 | 134 | 0.11 | 0 - 0.31 |
| Hernandez et al., 1994 | 97 | 0.14 | 0 - 0.92 |
| Hernandez et al., 1994 | 134 | 0.22 | 0 - 1.41 |
| Woolsen and Murphy, 1995 | 80 | 0.14 | 0 - 0.35 |
| Wroblewski et al., 1996 | 19 | 0.06 | 0.024 - 0.32 |
| Sychterz et al., 1997 | 96 | 0.17 | 0.02 - 0.45 |

In the work done by Buford and Goswani (2004), existing data from the literature was summarised to determine the extent of the range of linear wear rates (mm/yr) taking into account the materials of the mating couples that are metal on polyethylene hip replacements and ceramic-on-polyethylene replacements (see Tables 2.4 and 2.5).

Table 2.4: Wear rates of metal -on- polyethylene total hip implants as summarised from existing literature data (Buford & Goswani, 2004)

| **Acetabular bearing** | **Femoral bearing** | **Femoral head diameter [mm]** | **Average liner wear rate [mm/yr]** |
|---|---|---|---|
| Polyethylene | Cobalt-chromium | 28 | 0.14 |
| Polyethylene | Stainless steel | 22 | 0.14 |
| Polyethylene | Stainless steel | 22 | 0.13 |
| Polyethylene | Cobalt-chromium | 32 | 0.1 |
| Polyethylene | Stainless steel | 28 | 0.08 |
| Polyethylene | Stainless steel | 22 | 0.09 |
| Polyethylene | Cobalt-chromium | 28 | 0.05 |
| Polyethylene | Cobalt-chromium | 32 | 0.04 |
| Polyethylene | Stainless steel | 28 | 0.04 |

Table 2.5: Wear rates of ceramic-on-polyethylene total hip implants as summarised fromexisting literature data (Buford & Goswani, 2004)

| **Acetabular bearing** | **Femoral bearing** | **Femoral head diameter [mm]** | **Average liner wear rate [mm/yr]** |
|---|---|---|---|
| Polyethylene | Alumina | 28 | 0.1 |
| Polyethylene | Alumina | 28 | 0.1 |
| Polyethylene | Alumina | 28 | 0.08 |
| Polyethylene | Alumina | 32 | 0.03 |
| Polyethylene | Alumina | 28 | 0.03 |
| Cross-linked Polyethylene | Alumina | 22 | 0.03 |

From the study by Buford and Goswani (2004), it again became clear that there is a significant spread in the amount of linear wear for the different bearing couples as well as for bearing couples from the same material. The study by Buford and Goswani (2004), however, does not try to explain this difference in linear wear rates.

In a similar study done by Kesteris et al. (2003) the data of 42 total hip replacements due to loose acetabular components was compared to the data of 41 total hip replacements due to loose femoral components all because of aseptic loosening due to osteolysis. The summary of the data can be seen in Table 2.6 and the graphical presentation of the data is provided in Figure 2.19.

Table 2.6: Mean (mm or $mm^3$), standard deviation and range of wear measurements from retrieved acetabular components at revision surgery (Kesteris et al., 2003)

| | **Linear wear [mm]** | **Linear wear rate [mm/yr]** | **Volumetric wear [$mm^3$]** | **Volumetric wear rate [$mm^3$/yr]** |
|---|---|---|---|---|
| Cup group<br>cup replacement | 3.4 ± 1.4 (1.2-7.4) | 0.3 ± 0.1 (0.1-0.6) | 1086 ± 454 (397 – 2215) | 84 ± 37 (26-173) |
| Stem group<br>Stem replacement | 1.5 ± 0.9 (0-4.3) | 0.1 ± 0.1 (0-0.3) | 531 ± 332 (109-1506) | 40 ± 23 (6-106) |

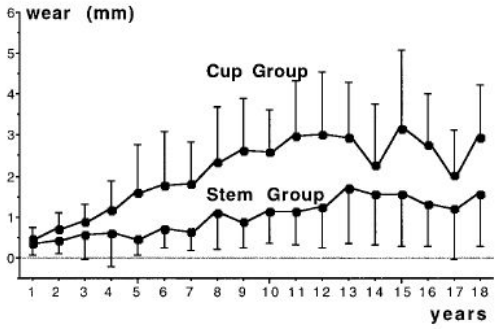


Figure 2.19: Linear wear in the cup replacement and stem replacement group (Kesteris et al., 2003)

If one brings the data as presented by Kesteris et al. (2003) and Buford and Goswani (2004) into the context of the work done by Dumbleton et al. (2002), it is clear that if the wear rate exceeds 0.1 mm/yr a loose acetabular component can be expected. The practical wear rate threshold of 0.05 mm/yr, as suggested by Dumbleton et al. (2002), to prevent osteolysis seems not to be acceptable if one looks at the data as presented by Buford and Goswani (2004) and Kesteris et al. (2003).

**It must again be emphasised that in all of these studies the actual wear mechanism was not identified and the scatter in the wear data was not explained. This thesis shows that the dominant wear mechanism is localised overheating and that the scatter in the wear data is influenced by the difference in the lubricating capabilities of the synovial fluid present**.

A different approach was followed by Sychterz et al. (1996) and by Jasty et al. (1997) in two separate studies. Wear of retrievals was measured volumetrically. A summary of their results is given in Table 2.7. In these studies, no attention was given to the mechanism of failure, but again only to the extent of wear. However, very useful information was gathered, regarding the location of the maximum wear in these cups (see Figure 2.20). These studies, however, do not distinguish between wear, plastic creep, plastic flow, extrusion, delamination, pitting and the like. The main aim of these studies was to establish the amount of material loss over a period of time.

Table 2.7: Results of retrieval studies where wear was determined volumetrically (Sychterz et al., 1996; Jasty et al., 1997)

| | **Mean Rate linear wear per year** | **Range mm/year** | **Mean volumetric wear per year** | **Range $mm^3$/year** |
|---|---|---|---|---|
| Sychterz et al. (1996) | 0.07 | 0.02 - 0.18 | 245 $mm^3$ | 1.0 - 131.3 |
| Jasty et al. (1997) | | | | 8 - 284 |

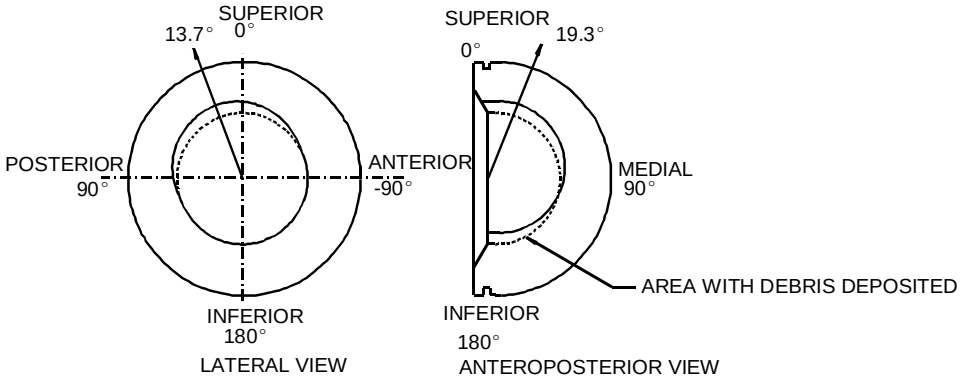


Figure 2.20: Position of maximum wear in cups according to Sychterz et al. (1996)

From Figure 2.20, it can be seen that the wear in the lateral view was orientated at 13.7 ° away from the most posterior point of the face towards the posterior side. From the anteroposterior view of the liner, this vector was orientated at a mean of 19.3° away from the face of the liner towards the apex.

According to these studies, 'burnishing' was the most common type of polyethylene wear. (Note: The use of the word *burnishing*, in this context, is a misnomer when considered in terms of the commonly understood meaning of the word *burnishing* as used in engineering terms. *Burnishing* is a process whereby a smooth hard tool (using sufficient pressure) is rubbed on the material surface. This process flattens the high spots by causing plastic flow of the material. Roller burnishing improves the finish and size of a part and is not a wear mechanism. Plastic flow or creep or perhaps polishing would have been more appropriate.) Scratching and pitting also occurred in all the liners studied by Sychterz et al. (1996), but were less severe. Permanent plastic deformation, embedded particles and abrasion were also seen. Another interesting finding by Sychterz et al. (1996) was that the wear rate was higher in the metal backed cups (average 10.9 years in-vivo) than in the all polyethylene cemented cups (average 12.4 years in-vivo), contrary to what would have been expected. No engineering explanation was given for this observation.

Jasty et al. (1997) investigated the influence of head diameter. In this study, it was found that the wear rates were higher with 32 mm diameter heads, intermediate with 28 and 26 mm heads and the lowest with 22 mm heads. These conclusions regarding femoral head size are not supported by the work done by Buford and Goswani (2004). (See Tables 2.4 and 2.5.) Once again, the study did not distinguish between wear and creep and no engineering explanation was given for these failures.

The most common types of damage reported by Jasty et al. (1997) were polishing of the running surface (see Figure 2.21), fine scratches (55 μm or less in width), see Figure 2.21, flaking (delamination of the surface), pitting, cracking, coarse abrasive wear (scratches 100 μm or more in width), embedded particles of metal or cement and dislocation. Additional findings by Jasty et al. (1997) are shown in Figures 2.21 to 2.24.

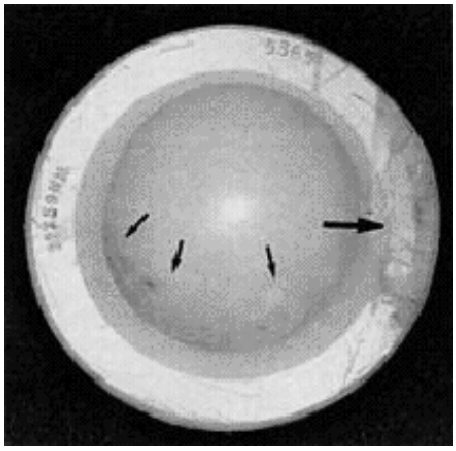

Figure 2.21: Photograph of a polyethylene acetabular component (Jasty et al., (1997) retrieved during a revision that was performed because of osteolysis six years post-operatively. There is an eccentric pattern of wear. The superior worn area is highly polished and is separated from the inferior, less worn area by a ridge (small arrows). Note the evidence of impingement anteriorly (a large arrow). Discolouration and flaking are seen in the less worn area

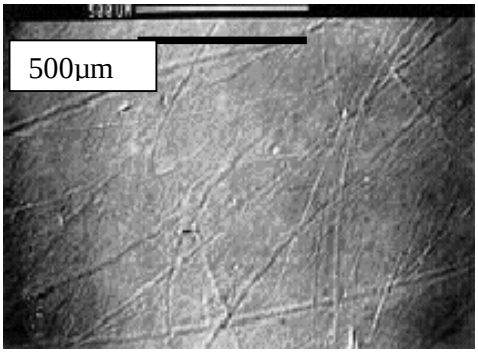


Figure 2.22: Scanning electron micrograph showing the highly worn area with numerous multidirectional fine scratches in a well-fixed acetabular component that was retrieved at autopsy ten years after implantation (original magnification, x 79.5)

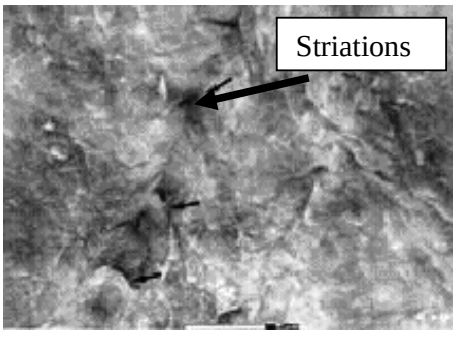


Figure 2.23: Scanning electron micrograph showing striations (arrows) perpendicular to the direction of the scratches, indicating tearing of the material during abrasive wear (original magnification, x 3900)

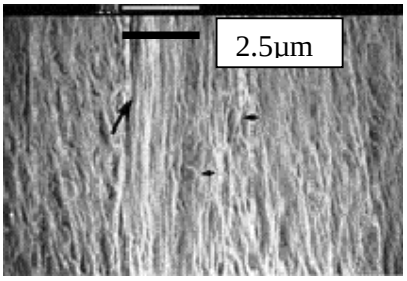


Figure 2.24: High-power scanning electron micrographs of a component retrieved six years after an arthroplasty. Reorganisation of the material has occurred during the wear process

In Figure 2.24 the scratch that formed much earlier is still visible. Within the scratch, the polyethylene is drawn into fine fibrils oriented parallel to the scratch (a large arrow). Scratches are not visible in adjacent areas, but fine fibrils, one micrometer or less in diameter, are present over the entire area. These fibrils are the major source of sub-micrometer wear particles. There are tears in the fibres in some areas and curled fibres (small arrows) (original magnification, x 10 400).

According to Jasty et al. (1997), McKellop et al. (1997) and Wang et al. (1997), the dominant mechanisms of failure are abrasion and adhesion at the surface.

If the test results between the studies of Jasty et al. (1997) and Sychterz et al. (1996) are compared, it is evident that a certain correlation between the different types of wear is observed, but no engineering explanation is given.

Various studies were undertaken by Schmalzried et al. (1997) and Maloney et al. (1995) to determine the size and distribution of wear particles found in tissue surrounding the joint at failure. A summary of the results can be seen in Table 2.8. From the results, it can be seen that the majority of wear particles (90%) is smaller than 0.7µm. (It will again be shown during the discussion in this study that particles as big as 0.5 mm were retrieved from tissue surrounding the joints of the samples retrieved during revision surgery.)

In a further study done by Young-Hoo and Kim (2001), the mean and annual linear wear and mean and annual volumetric wear between UHMWPE

acetabular cups working together with zirconia and chrome cobalt femoral heads were investigated in 70 patients with a mean of 6.4 years post-operatively. The mean linear wear in the zirconia femoral heads, of diameter 22 mm, was the highest — 1.25 mm compared to the 0.7 mm of the chrome cobalt femoral heads. The annual wear rate was 0.21 mm for the zirconia femoral heads compared to the 0.12 mm for the chrome cobalt femoral heads. The mean volumetric wear was again the highest for the zirconia femoral heads, — 730.79 $mm^3$ compared to the 264.67 $mm^3$ for the chrome cobalt femoral heads.

Table 2.8: Summary of sizes of wear particles as determined by Schmalzried et al. (1997) and Maloney et al. (1995)

| **Design of cup** | **Shape of particles** | **Mean size of particles (μm)** | **Size of 90% of particles (μm)** | **Mean total no. of particles per gram of tissue(in millions) (Range is given in parentheses)** |
|---|---|---|---|---|
| Fixed | Spherical or globular | 0.4 | < 0.7 | 1 443 ± 1 496<br>(92 – 4 286) |
| Bipolar | Spherical, needle or flake-like | 0.7 | <1.1 | 2 935 ± 1 489<br>(725 - 4 698) |

In a comparative study by Eggli et al. ( 2002), between chrome cobalt femoral heads of different sizes, 22 and 32 mm, the volumetric wear for the 22 femoral heads, at an average follow-up time of 71.4 months was 41.5 $mm^3$/year compared to the 120.3 $mm^3$/year for the 32 mm femoral heads.

### 2.6.2 Summary of follow-up study on crosslinked components (see paragraph 2.9 for the effects of crosslinking on the properties of UHMWPE.)

Crosslinked cups were implanted in almost 1 000 cases during the years 1978 to 1982 in Pretoria and Johannesburg by Grobbelaar and Weber (Grobbelaar et al., 1999). These cups were manufactured from UHMWPE and then crosslinked in an acetylene atmosphere. A follow-up study was done in 1999, where a review protocol was drawn up and all patients fitting this protocol were examined; and the hip joints were evaluated by means of X-rays. The average follow-up of the patients was 15.5 years. In all, 103 patients were examined and investigated during the course of this study. After the publication of the results of various studies by Oonishi et al. (1997) and Muratoglu et al. (2001) on techniques to improve the crosslinking quality of the UHMWPE as well as published results on various in vitro wear studies on simulators by Mckellop et al. (1997) and Mckellop et al. (2000), in conjunction with the publication of clinical results by Grobbelaar et al. (1999) and Muratoglu et al. (2004) the use of crosslinked acetabular components has become popular again.

The results of the Grobbelaar et al. (1999) study are as follows: In 86 of these patients, no wear could be measured and the rest of the wear varied between 0.7 and 1.5 mm. In Figure 2.25, an example of an X-ray is shown of the worst case in this follow-up. The total wear is given as 2.5 mm. No engineering explanation is given to explain the wear mechanism. Again the problem remains that, owing to magnification of the X-ray, it is very difficult to measure on X-rays.

The results of this study look very promising, but the practice of crosslinking was discontinued internationally in 1983 after a number of fractures, presumably caused by the reduction in izod impact strength values, occurred (Oonishi & Kuno 1997). The use of crosslinked acetabular cups has since been resumed and is on the increase (Mallchau et al., 2000; Davidson et al.,

2002; Davidson et al., 2003).

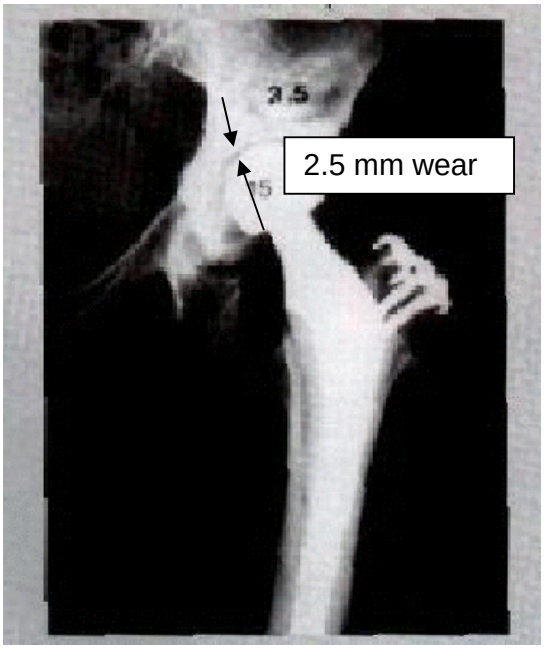


Figure 2.25: X-ray that shows 2.5 mm wear in cup as indicated by arrows as an eccentricity. No scale was shown in the reference but 30 mm femoral head serve as scale (Grobbelaar et al., 1999).

## 2.7 Results from simulator studies — in-vitro testing found in literature

Results of a number of simulator studies were found in the literature (Davidson et al., 1988; Kukureka et al., 1995; Wang et al., 1995; Wang et al., 1998; Clarke et al., 1996; Lu and McKellop, 1999; Wang et al., 1999; McKellop et al., 2000; Ries and Scott, 2001). Most of the simulator studies were done with bovine calf serum (BSA) as lubricant, while the average operating speed for these simulators was 1.5 to 2 Hz according to the ISO specification 14242-1 and ISO TR 9325 specification for simulator testing.

The materials tested during these in-vitro tests varied from metal alloy on metal alloy (stainless steel on stainless steel and chrome cobalt on chrome cobalt) to various femoral heads (alumina, zirconium, stainless steel and chrome cobalt) on UHMWPE, whether crosslinked or tests performed on the virgin material.

These studies reported that proteins precipitated as thin sheet-like deposits on the bearing surfaces, as well as in the simulator. In the study done by Lu and McKellop (1999), the temperatures were monitored by drilling holes in the ceramic femoral balls and mounting thermocouples 0.5 mm below the surface. The measured temperatures were extrapolated by means of a finite element analysis (FEA) to the bearing surface. The surface temperature was estimated to be between 60 and 99°C. The precipitation of proteins was regarded as an artefact of the simulators (Lu & McKellop, 1999). During the same study by Lu and McKellop (1999), the BSA (Bovine serum albumen) was heated up in a test tube and it was found that the proteins in the BSA started to precipitate at 60°C. After1 hour at 90°C, 40% of the proteins had precipitated (Lu & McKellop 1999). The studies investigated frictional heating and protein precipitation in a hip simulator as a function of the material of the femoral head, the rotation of the component (inverted or anatomically), the cycling speed and the volume of the lubricating chamber. The volume of fluid used varied between 45 and 135 ml. Although it is not stated as such, a very important conclusion can be drawn from the temperature at which precipitation of the proteins occurred. The high temperature calculated by the FEA was confirmed by the protein deposits inside the cups during the actual testing.

Friction was measured by making use of a custom-designed 3-axes strain gauge torque transducer mounted on a load axis above the test chamber. During these studies, it became evident that there was an increase in torque applied as the test progressed. This finding confirmed the work done by Wang et al. (1998), namely that solid protein is not a good lubricant.-depending the concentration of protein present During the testing phase of this thesis, it has also been shown, that the denaturated solid proteins perform even worse (apart from the fact that BSA is not a good lubricant.)

During these simulator studies, two major observations were made, namely:

a. The importance of multidirectional motion in the wear mechanism and wear testing of UHMWPE
b. Solid proteins are found not to be effective in boundary layer lubrication

applications.

A common observation of all these investigations was that all cups examined, exhibited the characteristic appearance of surface stretching in the form of fibril formation or fibrillation. McKellop et al. (1997) believe that this fibril morphology was a result of micro-adhesive wear or just third-body abrasive wear. Wang et al. (1997) proposed that fibril appearance simply reflected the occurrence of molecular orientation on a worn surface, which could be the result of either adhesion or abrasive wear.

The Wang et al. (1999), examinations of simulated tests on acetabular cups revealed the following four types of surface features:

a. Regular and irregular arrays or surface rip-off and bumps
b. Oriented and non-oriented loose fibrils
c. Oriented fibrils with no loose ends
d. Multidirectional scratches within which loose fibrils are sometimes seen.

According to Wang et al. (1999) features b, c and d are associated with high rate of wear, while feature (a) is associated with low wear rates. No reference was made to the effect of temperature and no engineering explanation was provided for these failures.

The importance of measuring temperature as accurately as possible to the bearing surface is indirectly borne out by the work of Davidson et al. (1988). A heat transfer analysis was compiled for femoral implants in simulator studies. During these studies, temperature rises of only a maximum of 10°C were recorded. What is not clear from this study is the size of thermocouples used in the simulators. It would seem that only bulk temperatures were recorded and the local hot spots were ignored.

In a study done by Ries and Scott (2001), wear particles retrieved from a simulator were measured and examined under a scanning electron

microscope at 10 000 times magnification. The wear debris was generated in a simulator with bovine serum as a lubricant, where the acetabular cup is submerged under 130 mm of lubricant, and running against a chrome cobalt femoral head at 1 Hz, according to the Bergmann et al., (Figure 2.11) and ISO 14242-1 (Figure 2.39) load profiles. The volume of lubricant is not known as the size of the reservoir was not specified. The wear particles for the non-irradiated, ethylene-oxide sterilised acetabular cup can be seen in Figure 2.26.

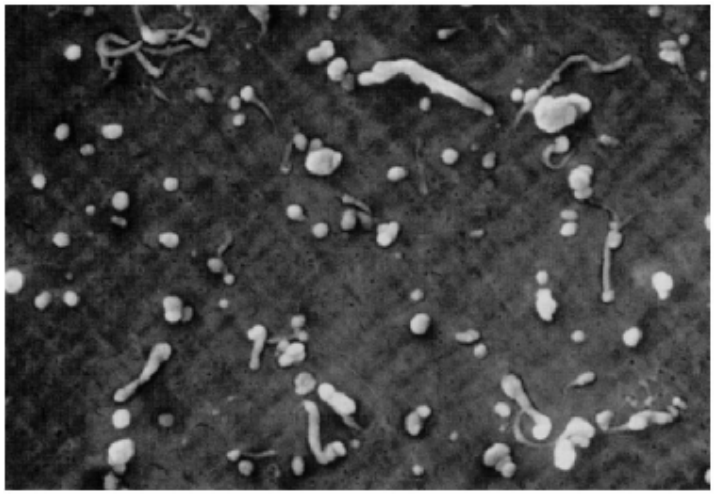

Figure 2.26: Particles of non-irradiated, ethylene oxide sterilised UHMWPE against chrome cobalt femoral head (x 10 000) (Ries & Scott, 2001)

## 2.8 Effects of gamma-irradiated sterilisation on wear characteristics

Sterilisation and crosslinking of polyethylene affect its wear rate (Rimnac et al., 1994; Fischer et al., 1995; Parr and Jack, 1995; McKellop et al., 1997; Wang et al., 1997; Orishimo et al., 2003). A time-dependent increase in the extent of oxidation can result from gamma sterilisation in air. The gamma irradiation breaks molecular bonds in the long polyethylene chains, giving rise to free radicals. Oxygen can combine with these free radicals. Saum (1994) and Parr and Jack (1995) reported subsurface oxidation which remains significant up to 2 mm below the surface. Oxidation as deep as 3 mm into test samples was also found by Rimnac et al. (1994). Trieu and Paxson (1995) demonstrated an oxidised surface layer as thick as 6 mm in UHMWPE components.

The common understanding of the oxidation process is as follows (Lewis, 2001; Parr & Jack, 1995): UHMWPE initially consists of extremely long molecular chains which provide excellent abrasion resistance. Sterilisation by gamma irradiation causes chain scission by breaking of chemical bonds and creating reactive free radicals. Oxygen diffuses into the material and reacts with the free radicals to cause oxidation, which leads to much shorter molecular chains. As a result, the original properties of polyethylene, including abrasion resistance, change significantly. Preliminary data indicates that long-term oxidative degradation can alter the performance of the polyethylene in total joint replacement, especially its resistance to fatigue wear, which can cause pitting and delamination.

An appreciable difference in hardness between the surface layer and the core results from gamma sterilisation. Extensive reduction in toughness was also found in the case of gamma sterilisation. Similar to elongation, the reduction in toughness of the surface layer is more severe upon ageing of the component. This indicates an increase in surface embrittlement that is caused by oxidation.

Research has shown that most of the oxidation occurs during post-radiation ageing and not during the sterilisation process, because long life free radicals exist in the UHMWPE as a result of reduced mobility within crystalline regions (Rimnac et al., 1994; Trieu & Paxson, 1995).

In simulator studies Ries and Scott (2001) had shown that the particle morphology of non-irradiated, ethylene-oxide sterilised components (Figure 2.26) is almost the same as for inert gas gamma-irradiated components (see Figure 2.27).

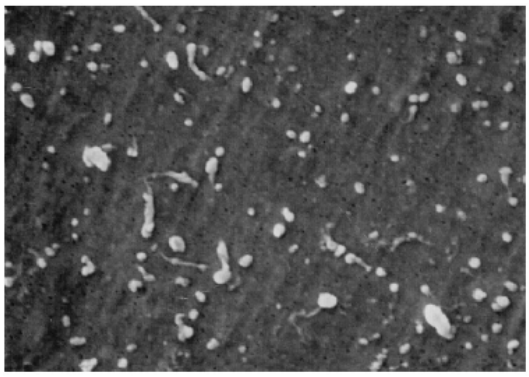

Figure 2.27: Wear particles of inert gas gamma-irradiated UHMWPE against chrome cobalt (x 10 000) (Ries & Scott, 2001)

In a study done by Orishimo et al. (2003), the long-term in-vivo wear performance of two groups of well-functioning cementless acetabular cups sterilised by two different methods, namely gamma irradiation and ethylene-oxide were compared. The first group consisted of 31 acetabular cups sterilised by means of gamma irradiation while the second group consisted of 28 acetabular cups sterilised with ethylene oxide. The linear wear rate follow-up data for the gamma-sterilised acetabular cups can be seen in Figure 2.28 while the follow-up data for the ethylene oxide acetabular cups can be seen in Figure 2.29. On average, it can be seen that the linear wear rate in mm/year for the gamma-sterilised cups is slightly better than for the ethylene oxide cups.

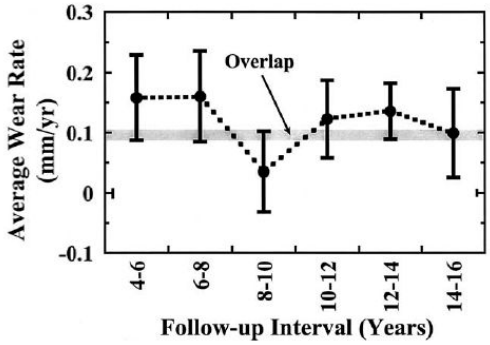


Figure 2.28: Average wear rate for acetabular components sterilised with gamma radiation (Orishimo et al., 2003)

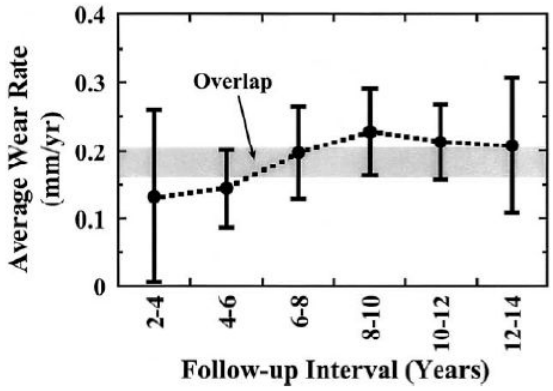


Figure 2.29: Average wear rate for acetabular components sterilised with ethylene oxide (Orishimo et al., 2003)

## 2.9 Effects of crosslinking on characteristics of UHMWPE

Crosslinking, as a method to improve the properties of UHMWPE, has been tried and used over the years with limited success. The success was limited despite an almost 30% improvement in abrasion resistance (Sun and Wang, 1996; Oonishi & Kuno, 1997). The major factor preventing crosslinked material from being the industry standard for acetabular cups is the reduction in the izod impact strength. According to the various hip registers, crosslinked UHMWPE is again becoming more popular (Mallchau et al., 2000; Davidson et al., 2002; Davidson et al., 2003). This material, however, also showed better wear resistance and, as such, it is important to review the research in this field. An extensive study into crosslinking of UHMWPE was done by Du Plessis et al. (1977), which yielded excellent results. UHMWPE was used and crosslinked with irradiation in the presence of acetylene and chlorotrifluoroethylene (CTFE) as well as nitrogen, which was used as an inert atmosphere. All the gases used were of an analytical grade. The material was irradiated at different dosages. Tensile and impact strength tests were carried out at temperatures of 37°C. The tensile strength (Figure 2.30) showed a decrease in strength with an increase in radiation, the surface hardness (Figure 2.31) increased markedly, while the izod impact strength (Figure 2.32) values decreased dramatically. It must be pointed out that the effect of elevated temperatures above 37°C, on the properties of crosslinked

UHMWPE is not known.

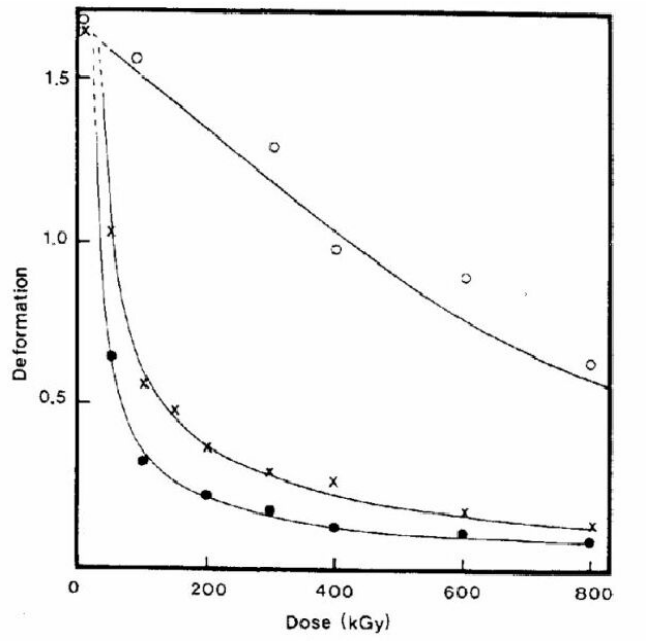


- Acetylene and CTFE, ○ Nitrogen, x Acetylene

Figure 2.30: Deformation of crosslinked UHMWPE (Du Plessis et al., 1977).

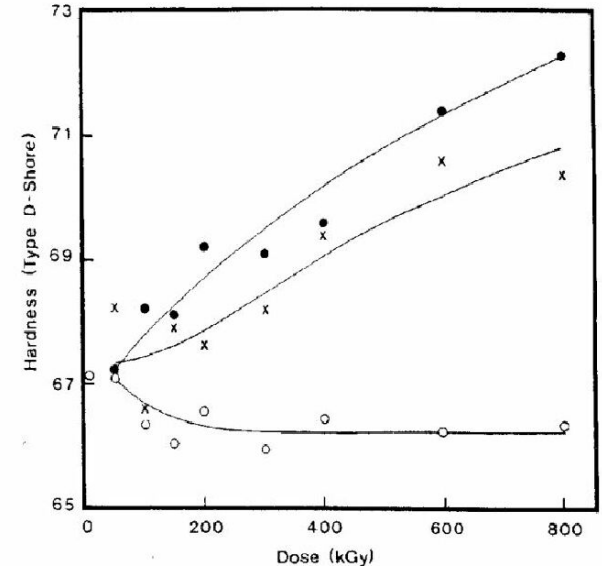


- Acetylene and CTFE, ○ Nitrogen, x Acetylene

Figure 2.31: Surface hardness of crosslinked UHMWPE (Du Plessis et al., 1977)

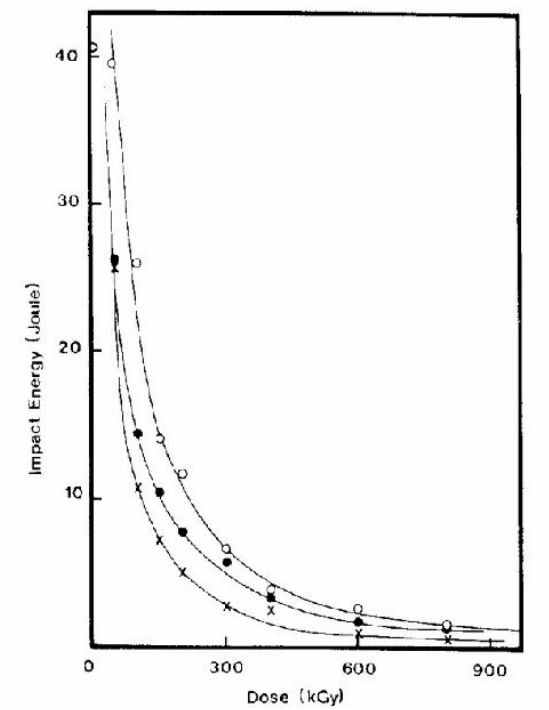


- Acetylene and CTFE, ○ Nitrogen, x Acetylene

Figure 2.32: Impact energy of crosslinked UHMWPE (Du Plessis et al., 1977)

In the simulator study done by Ries & Scott (2001), the wear debris formed when running crosslinked UHMWPE against a chrome-cobalt femoral head showed a significant decrease in quantity and size (Figures 2.33 and 2.34) if compared to the debris formed with non-irradiated UHMWPE running against a chrome cobalt femoral head. The tests were done with UHMWPE acetabular cups crosslinked at different levels of irradiation, namely 5 Mrad (Figure 2.33) and 10 Mrad (Figure 2.34), and then compared to the wear found in non-crosslinked components.

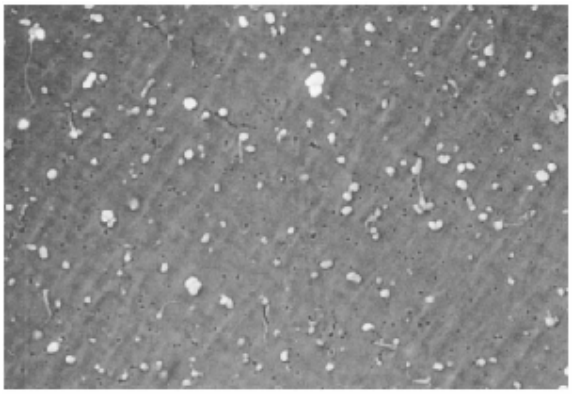

Figure 2.33: Wear particles of highly crosslinked UHMWPE subjected to 5 Mrad of gamma irradiation (x 10 000) (Ries & Scott, 2001)

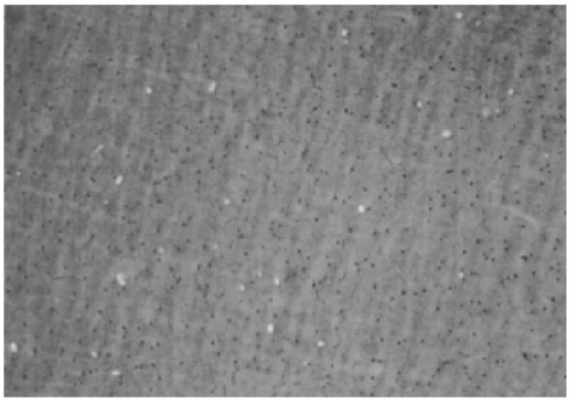

Figure 2.34: Wear particles of highly crosslinked UHMWPE subjected to 10 Mrad of gamma irradiation (x 10 000) (Ries & Scott, 2001)

## 2.10 Hip simulators for in-vitro testing

Various studies employing hip simulators are used to evaluate the performance of acetabular cups of various designs, materials and material combinations for longevity (Davidson et al., 1988; Kukureka et al., 1995; Wang et al., 1995; Clarke et al., 1996; Wang et al., 1998; Lu and McKellop, 1999; Wang et al., 1999; Mckellop et al., 2000; Smith and Unsworth, 2000; Ries & Scott, 2001; Saiko et al., 2001; Tipper et al., 2001; Calonius and Saiko, 2002; Masaoka et al., 2003). In all of these tests, wear is either measured as linear wear or as volumetric wear with some of the studies analysing the

retrieved wear debris.

A number of designs for simulators are used of which the Boston simulator, (see Figure 2.35) is the most common. These simulators are all described in literature and are using either/or both the Paul load profile (Paul, 1976) (Figure 2.10) or the Bergmann profile (Bergmann et al., 1993; Bergmann et al., 1995) (Figure 2.11) or a combination of the two. The biggest difference between the two profiles is that the Paul profile was calculated where the Bergmann was measured. A summary of eight contemporary hip simulators is given in Table 2.9 with a summary of the various motion waveforms shown in Figure 2.36.

Figure 2.35: Boston hip simulator
(http://www.geocities.com/hip_replacements/ history)

A major disadvantage of these simulators is the high capital cost, as well as the expensive operating cost owing to the fact that the load is applied via a computer-controlled servo hydraulic system. The result of this is that simulators were, until now, inaccessible for primary research, owing to the fact that they were mainly positioned at major manufacturing companies.

Table 2.9: Summary of contemporary hip simulators (Calonius & Saikko, 2002)

| Design | Euler sequence and partition of rotations, and classification of axes | Direction of load, and component relative to which it is fixed | | Assumed position or neutral position in computation | | Reference |
|---|---|---|---|---|---|---|
| | | | | Head axis | Cup | |
| BRM offset lever | $FE_{h,s} \rightarrow AA_{h,m} \rightarrow IER_{h,m}$ | V | c | V | H | Present study, see Fig. 5 |
| AMTI | $AA_{c,m} \rightarrow FE_{c,s} \rightarrow IER_{h,s}$ | V | h | V | H | Bragdon et al. (1996) |
| Munich | $FE_{c,m} \rightarrow AA_{c,m} \rightarrow IER_{c,s}$ | V | h | 45° | 45° | Ungethüm (1976) |
| Leeds Mk I | $IER_{c,s} \rightarrow FE_{h,s} \rightarrow AA_{h,m}$ | Changing | Neither | 45° | 45° | Dowson and Jobbins (1988) |
| ISO/DIS 14242-1 | Not specified | V | c | 30° | 30° | Draft ISO/DIS 14242-1 (2001) |
| Durham Mk II | $IER_{c,s} \rightarrow FE_{h,s}$ | V[a] | h | 45° | 45° | Smith and Unsworth (2001) |
| Leeds Mk II | $IER_{c,s} \rightarrow FE_{h,s}$ | V | c | 45° | 45° | Barbour et al. (1999) |
| ProSim | $IER_{c,s} \rightarrow FE_{h,s}$ | V[a] | h | V | 35° | Goldsmith and Dowson (1999) |
| HUT-3[b] | $IER_{c,s} \rightarrow AA_{h,s} \rightarrow FE_{h,m}$ | 12° to V | c | 45° | 45° | Saikko (1996) |
| BRM zero-offset lever[b] | $FE_{h,s} \rightarrow AA_{h,m}$ | V | c | V | H | Saikko and Ahlroos (1999) |

*Note*: h, head; c, cup; s, stationary axis; m, moving axis; V, vertical; H, horizontal.
[a] In neutral position of FE cradle.
[b] Included here for comparison; their slide tracks were computed earlier, Saikko and Calonius (2002).

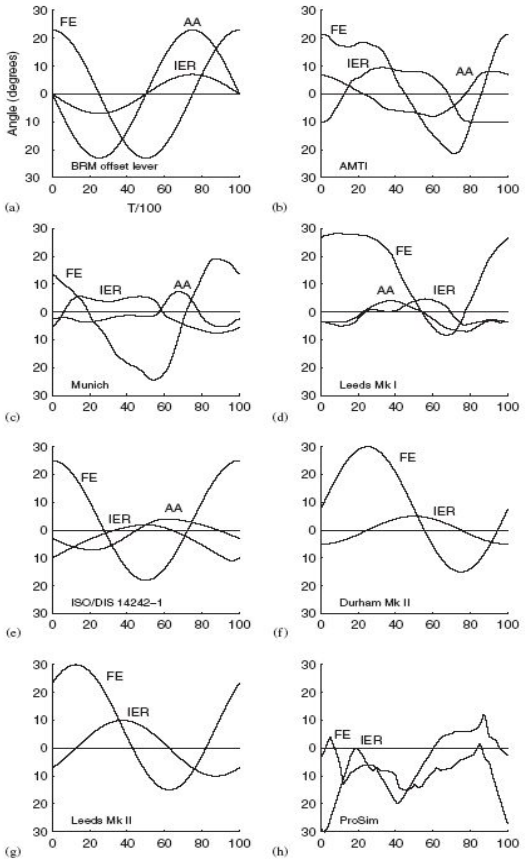


Figure 2.36: Motion waveforms used in computation of slide tracks for hip simulators

a BRM with offset lever
b AMTI
c Munich
d Leeds Mk I
e ISO 14242-1
f Durham Mk II
g Leeds MK II
h ProSim

Positive angle represents flexion, abduction and internal rotation, and negative angle represents extension, adduction, and external rotation.

The above simulators all used various concentrations of bovine serum as lubricant. The lubricant was stabilised with 0.1% sodium azide to retard bacterial growth (Davidson et al., 1988; Kukureka et al., 1995; Wang et al., 1995; Clarke et al., 1996; Wang et al., 1998; Lu and McKellop, 1999; Wang et al., 1999; Mckellop et al., 2000; Smith and Unsworth, 2000; Ries & Scott, 2001; Saiko et al., 2001; Tipper et al., 2001; Calonius and Saiko, 2002; Masaoka et al., 2003). The cups were mounted inverted with the acetabular component pointing upwards. A typical design of such a simulator is shown in Figure 2.37 with a close-up photograph of such a simulator shown in Figure 2.38. In the literature the volume of lubricant in the receptacles is not always specified but in the articles where the lubricant volume is specified the volume of lubricant varied from 100 ml/receptacle (Saikko et al., 2001) to 350 ml/receptacle (Wang et al., 1996). In all the cases, where specified, the fluid was replenished twice daily with distilled water and the total amount of fluid was changed at each wear measurement which is every 250 000 cycles (Masaoka et al., 2003).

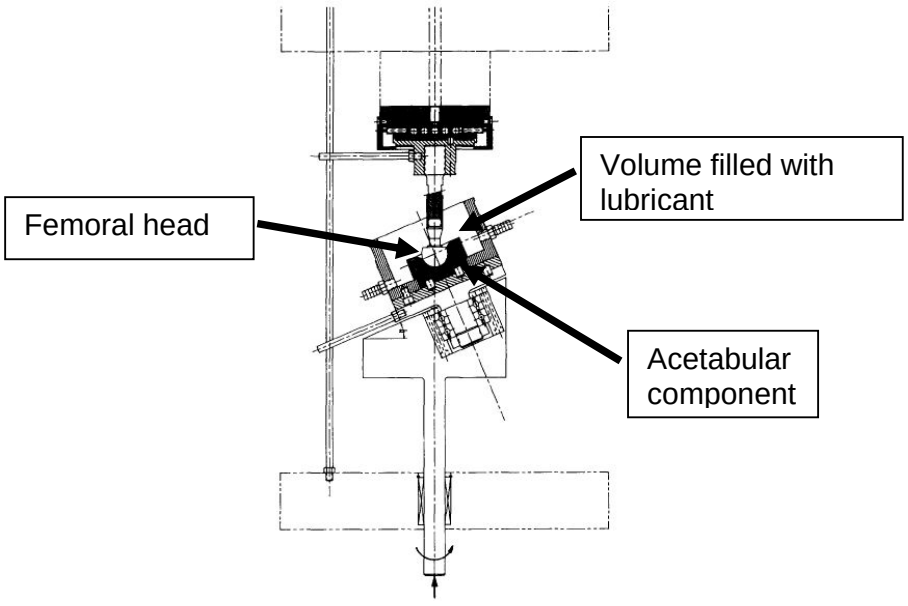


Figure 2.37: Schematic illustration of the loading/motion configuration of the Bi-axial rocking motion (BRM) hip simulator. (Wang et al., 1996)

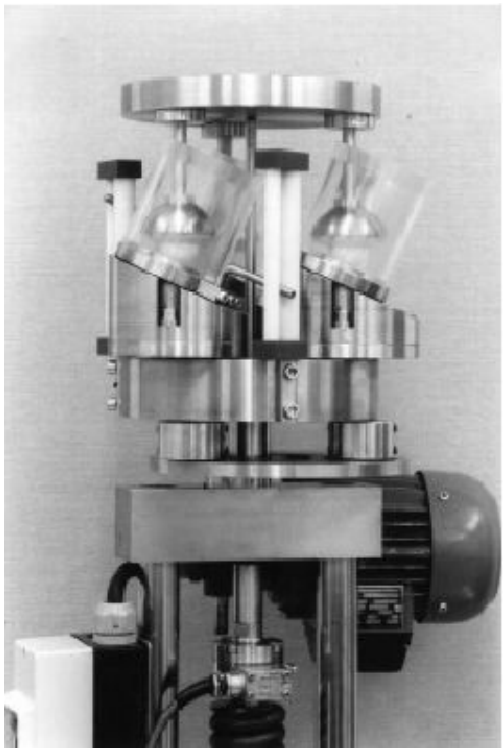

Figure 2.38: Three-station, statically loaded bi-axial rocking motion (BRM) hip wear simulator (Saikko et al., 2001)

If the design of the existing simulators, as shown in Figure 2.37, is analysed it is seen that the cup is continuously rotated in one direction resulting in an elliptical wear pattern inside the cup. Although the load is applied according to the load waveforms shown in Figure 2.36, the wear pattern is still elliptical and the asperities on the surface are continuously loaded in one direction, making it extremely unlikely that surface fatigue will occur.

A major problem common to these designs is retrieving of the wear debris and the concentration of bovine serum in the lubricant during testing. As mentioned, the wear debris is retrieved every 250 000 cycles when the simulator is stopped, the acetabular cup is removed and the retrieved lubricant

is passed through filters (0.2µm) to retrieve the wear debris (Smith & Unsworth, 2000; Saikko et al., 2001; Masaoka et al., 2003). The machines are then again assembled, the receptacles filled with the lubricant and the test started. The problems with this method are the following:

- The concentration of the lubricant is not constant throughout the test
- The accumulative effect of the wear debris of 20 million cycles is not achieved
- The removal of the test specimen from the machine destroys the wear pattern with the effect that a new test is effectively started on re-starting.

In 2002, an ISO standard (ISO 14242-1, 2002) was published specifying the hip simulators to be used in future testing. The load profile is a combination of the work done by Paul (1975), Bergmann et al. (1993) and Bergmann et al. (1995) with the following major exceptions:

- The maximum load is specified as 3 kN where Bergmann and Paul had taken the maximum load as up to 580% of body weight. (See Figure 2.39.) For the European male lying on the 50% percentile (ergonomic data) this is 4.9 kN.
- The load profile is for 40% of the loading cycle kept at a minimum of 0.3 kN.

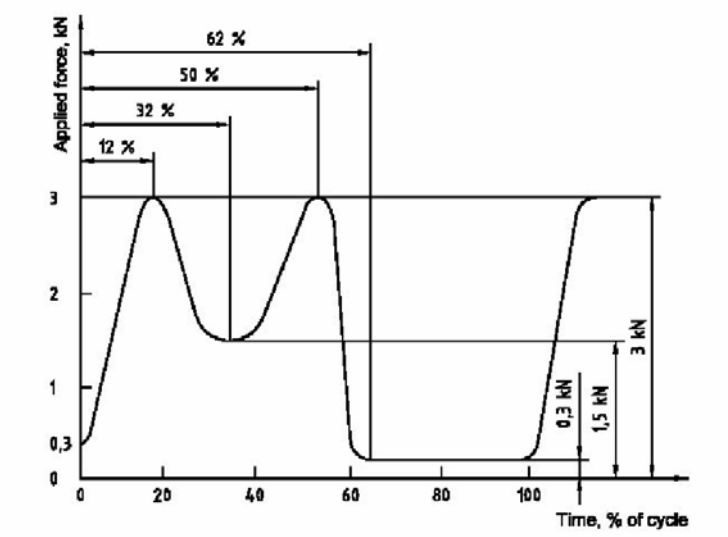


Figure 2.39: Loading profile for hip simulator according to ISO standard (ISO 14242-1, 2002)

The lubricant to be used is also specified as calf serum (25% ± 2%) diluted with de-ionized water (balance). An anti-microbial reagent such as sodium azide, may be added. The amount of lubricant per test station is not specified.

Apart from the specification regarding lubrication, extension/flexion, adduction/abduction and inward/outward rotation (see Table 2.10), the following general specifications apply:

- Operate the simulator at 1 Hz ± 0.1 Hz
- Replace the fluid lost by evaporation during the test at least daily, by adding de-ionized water. Replace the fluid test medium completely at least every 500 000 cycles.
- Stop the test for measurements atleast after 500 000 cycles, one million cycles and at least every one million cycles thereafter until the test is terminated.
- Remove the test specimen and control specimen from the testing machine and take wear measurements

Table 2.10: Variation with time of angular movement to be applied to the femoral test specimen (ISO 14242-1, 2002)

| Time, % of cycle ± 1 % | 0 | 21 | 50 | 62 | 100 |
|---|---|---|---|---|---|
| Angle of flexion (+) or extension (–) ° ± 3 ° | 25 | | – 18 | | 25 |
| Angle of adduction (+) or abduction (–) ± 3 ° | 3 | 7 | | – 4 | 3 |
| Angle of inward (+) or outward (–) rotation ± 3 ° | – 10 | | 2 | | – 10 |

The general specification has the same problem regarding the removal of the test specimen for wear measurements as discussed earlier. This is a very serious problem, because the biggest drawback of all simulators is currently the lack in correlation of in-vivo wear mechanism and in-vitro results, as stated by Harris (http://www.centerpulse-orthopedics.com/uk/en/Home/Home). The simulator wear studies predict unrealistically long life, which is not attained as can be seen by various retrieval studies, as discussed in paragraph 2.6.

## 2.11 Summary of literature review

After examining the vast amount of available literature on the relevant topics, the following shortcomings were identified:

- Insufficient data on the creep characteristics of UHMWPE at elevated temperatures, after gamma irradiation and after crosslinking.
- A look at a well-defined set of failure criteria that will allow the researcher to objectively analyse retrieved acetabular components.
- A complete engineering failure analysis on retrieved acetabular components to establish the reason for mechanical, not clinical, failure of acetabular components.
- The failure to develop an inexpensive hip joint simulator that is physiologically more representative and that will yield more accurate in-vitro results.
- Difficulties in obtaining an indication of the lubricating capabilities of synovial fluid and explaining the scatter in the wear results as found in the literature.

# CHAPTER 3

# CREEP ANALYSIS FOR UHMWPE

## 3.1 Introduction

As noted, the literature review in Chapter 2 revealed that the creep properties of UHMWPE under different conditions have not been clearly established. Creep data for UHMWPE is found (Engineering Materials Handbook, 1987; Lee & Pienkowski, 1998; Meng Deng & Latour, 1998), but all these tests were done at room temperature. Tests at elevated temperatures were performed by Meng Deng and Latour (1998) but this study did not include tests on crosslinked or gamma-irradiated material. Therefore, the effect of sterilisation and crosslinking on the creep properties of UHMWPE could not be found in the literature.

The purpose of this part of the study is not to undertake an in-depth study of the creep properties for UHMWPE under various conditions, but rather to show that the effect of elevated temperatures, gamma sterilisation and crosslinking on creep properties of UHMWPE is substantial and has a pronounced effect on wear characteristics. If the data is to be used for design purposes, more tests will have to be done to enable statistical analysis of the data.

### 3.1.1 Test protocol

The investigation into the creep properties of UHMWPE was broken down into various stages to obtain the data required within available cost constraints. The following investigations were performed:

a. Clamping effects
b. Investigation of anisotropic effects
c. The effect of temperature on virgin material

d. The effect of temperature on sterilised material

e. The effect of temperature on crosslinked material.

## 3.2 Clamping effects

This investigation was done to establish the effect of the clamping force between the test piece and platen (see Figure 3.1). The expected effect is that with the test piece being too short the lateral restraining force from the platen is going to restrain the material from plastically flowing sideways at the interface between the platen and the test piece.

### 3.2.1 Purpose of test

The purpose of this test was to establish the influence of the clamping effects, due to test piece length, on the creep values for UHMWPE. The effect is illustrated in Figure 3.1. The lateral restraining force between the platen and the test piece limits the amount of plastic flow at the interface between the platen and the test piece. The shorter the test piece, the more dominant this effect is in influencing the achieved results. From the literature survey, there is an indication that the material is anisotropic and visco-elastic (Engineering Materials Handbook, 1987).

According to the Engineering Materials Handbook (1987), *anisotropic behaviour* can be defined as: “The material exhibits different properties when tested along axes in different directions.” The material is therefore non-isotropic.

*Visco-elasticity* (Engineering Materials Handbook, 1987) can be defined as a property involving a combination of elastic and viscous behaviour. A material having this property is considered to combine the features of a perfect elastic

solid and a perfect fluid. Visco-elasticity is a phenomenon of time-dependence, in addition to elastic deformation (or recovery) in response to load.

According to ASTM D2990 (1990), to enable tensile, compressive and flexural creep and creep rupture of plastics to be tested, the creep test piece must be 12.56 mm square with a slenderness ratio between 11 and 14. This means that the ratio of length to a minimum radius of gyration must be between 11 and 14. The radius of gyration is defined as 0.2887 x the width of the specimen (ASTM D2990, 1990). The test piece dimensions, as required by ASTM D2990 (1990), are shown in Figure 3.2. Based on these parameters, the test piece must have a minimum length of 40 mm.

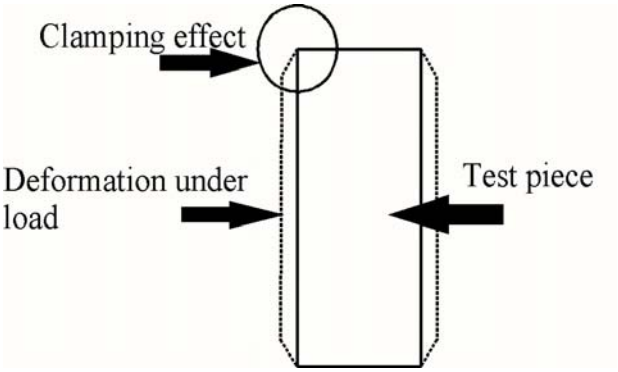


Figure 3.1: Illustration of clamping effect

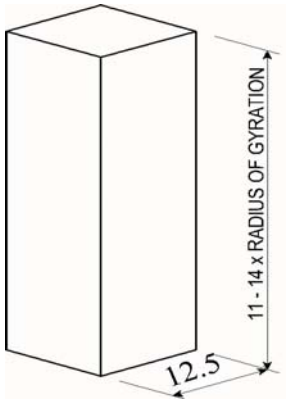


Figure 3.2: Size of an ASTM test piece according to ASTM D2990 (1990)

The stock material from which acetabular cups are manufactured is Φ65 mm as manufactured and imported from Poli Hi Solidur. A 40 mm test piece cannot be cut out at different orientations when testing the anisotropic behaviour of the material. The aim of this test was therefore to find the shortest test piece that

would still give reliable results.

### 3.2.2 Test procedure

Test pieces were manufactured from a bar of Chirulen® (lot nr. B15331081) material manufactured and imported from Poli Hi Solidur. The test blocks were 12.5 mm square and the lengths were 10, 20 and 40 mm. The orientation of the test pieces in the virgin material before machining is shown in Figure 3.3.

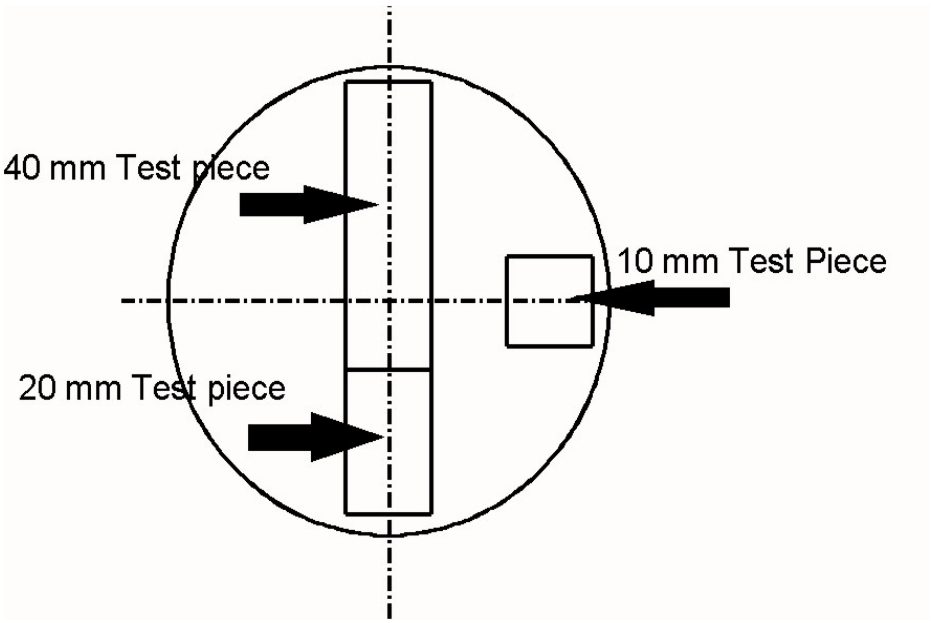


Figure 3.3: Orientation of test pieces in virgin material

The test pieces were placed, individually, in a Schenk testing machine (100 kN) and loaded to the equivalent of 8 MPa in compression. (See Figure 3.4 for the test configuration in the Schenk Hydro-pulse testing machine.) With this machine, it is possible to load a test piece in tensile and compression under computerised control. The load applied to the test piece was determined as follows: the most common size femoral head that is used is 28 mm in diameter. The maximum projected area in the

acetabular bearing will then be:

$$Area = \frac{\pi . D^2}{4} = 0.000616 m^2$$

The maximum load applied to the bearing is on average six times the body weight (Paul, 1976), and if the weight of an average person is taken as 70 kg (95% percentile) (Adult data, 1988), the maximum load on the bearing is 4 800 N resulting in a compressive stress of:

$$\sigma = \frac{force}{area} = 8 MPa$$

This compressive stress of 8 MPa also correlates with load case as applied by Meng Deng and Latour (1998) and Lee and Pienkowski (1998). The load to be applied on the 12.5 mm square test piece can then be calculated as follows:

$$Load = \sigma . area = 8.(12.5)^2 = 1250 N$$

The displacement was measured by making use of a calibrated clip-on extensometer, while the load was measured with a calibrated 500 kg load cell. According to the ASTM standard (ASTM D2990, 1990), the load was applied within three seconds and kept on the test piece for one hour. The displacement data was recorded and plotted. The data was sampled at a rate of 50 Hz resulting in 1.8 x $10^5$ data points over a one-hour period.

Figure 3.4a: Test set-up in Schenk testing machine

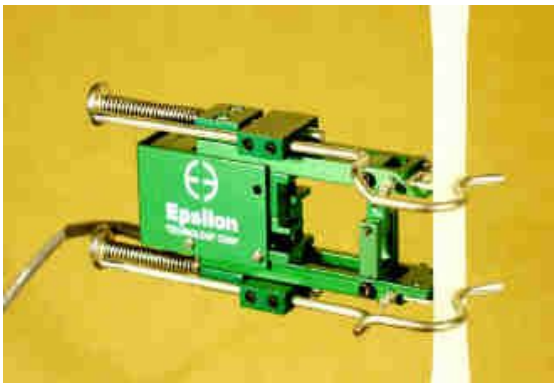


Figure 3.4b: Clip-on extensometer

### 3.2.3 Results

The data presented in Figure 3.5 represents the strain plotted against time for the three different lengths, 10, 20 and 40mm as shown in Figure 3.3. An increase in the creep rate of the 10mm test piece is visible if compared to the plotted data of the 20 and 40mm test pieces. This difference can be attributed to the restraint to lateral movement caused by the platen faces, namely the barrel shape effect. Another reason for this deviation can be explained by looking at Figure 3.3. The 10 mm test piece was machined from the bar right at the edge of the material. If there is any non-homogeneity, across the material, as was later proved to be the case the material will behave differently during these tests. This effect will have to be investigated further.

From the data presented in Figure 3.5, the strain plotted against time for creep in the 20 and 40mm test pieces is very similar. The two plots actually meet as the test progresses. The conclusion that can be drawn from these tests is that the clamping or restraint effect on a test piece of 20 mm long is almost negligible. If test data is compared with the work of Lee and Pienkowski (1998) and Meng Deng and Latour (1998), the trend of the plots is the same for testing at room temperature with a loading of 8MPa.

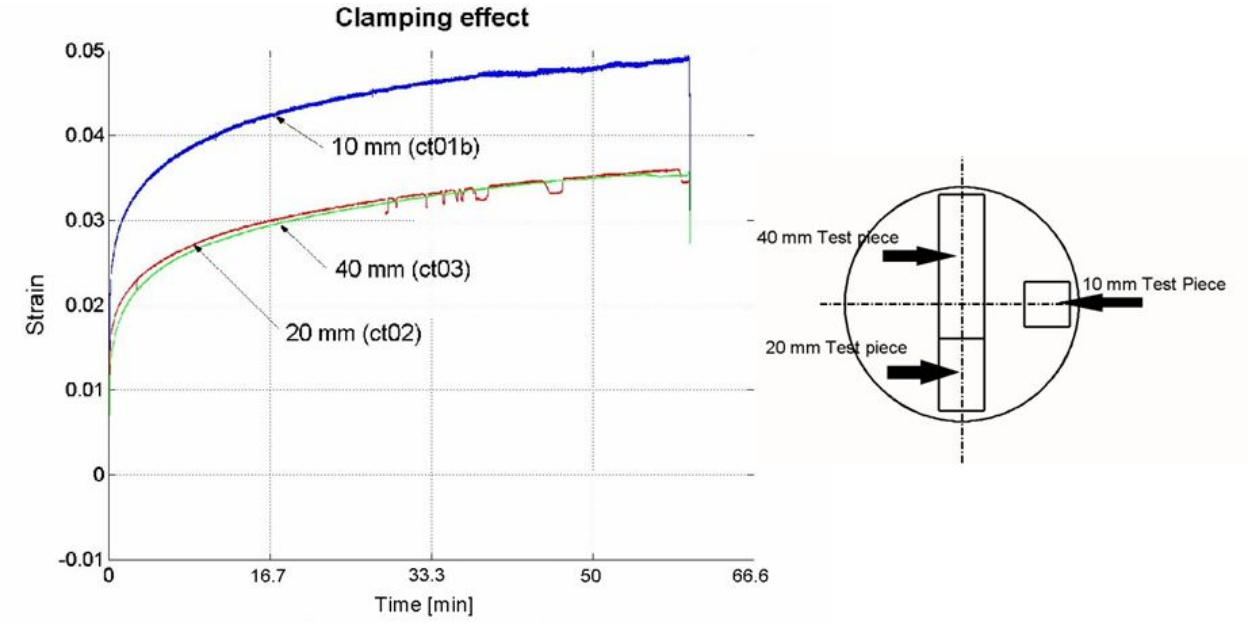


Figure 3.5: Results for the test to determine clamping effect

The conclusion from this part of the investigation is that a 20 mm test piece will be used for the rest of the investigation regarding the influence of various factors on the creep behaviour of UHMWPE. The effect of non-homogeneity or anisotropic properties, as well as the effect of elevated temperatures together with sterilisation and crosslinking on the material is

investigated further.

## 3.3 Investigation of anisotropic effects

### 3.3.1 Purpose of test

The creep data, as presented in paragraph 3.2.3, for a test piece cut out from the edge of the material (see Figure 3.3) differed significantly from the other results. As explained, this can be due to the clamping effects or due to anisotropic properties caused either by the extrusion process or by heat treatment of the bar. The aim is to determine the effect of test piece orientation on the creep properties of the material.

### 3.3.2 Test procedure

Test pieces were machined from a standard Φ65 mm stock bar at various orientations. In all, eight test pieces were manufactured. (See Figures 3.6 and 3.7 for the position and orientation of the different test pieces.)

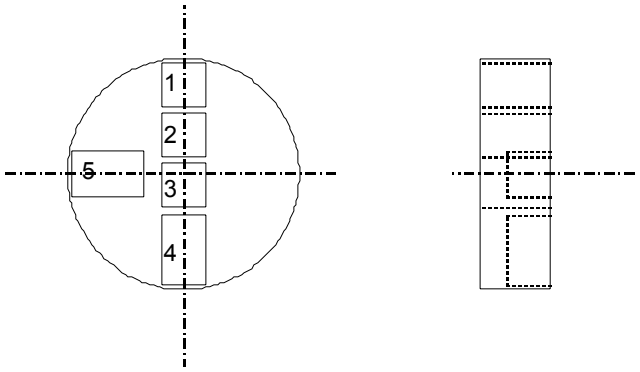


Figure 3.6: Position and orientation of test pieces 1 to 5

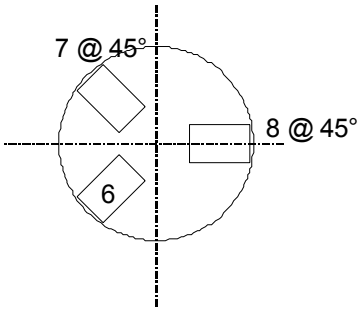


Figure 3.7: Position and orientation of test pieces 6 to 8

A slice of material, 20 mm thick, was cut from the bar stock and test pieces 1 to 5 were machined as shown in Figure 3.6. Test pieces 1 to 3 were cut out in the axial direction while 4 and 5 were cut out radially, perpendicular to the axial direction.

A second slice of material was used to manufacture test pieces 6 to 8. Test piece 6 is also perpendicular to the axial direction, but midway between test pieces 4 and 5 while test pieces 7 and 8 are cut at an angle of 45° to the axial plane.

The testing procedure was the same as that used to determine the clamping effects. The data sampling was again done at a frequency of 50 Hz. However, for test number 3, running for 18 hours, the sampling rate was brought down to 25 Hz. The test was done to ascertain the amount of creep that can be expected over a longer period. As a result of the amount of data that is gathered, the sampling was paused after one hour, keeping the load in place. The sampling was resumed after 16 hours to observe

the long-term effect.

### 3.3.3 Test results

The results, plotted in Figure 3.8, show a substantial difference in creep between the outside and the inside of the raw material in the axial direction (tests 1 and 3). The difference in the creep values between these two tests is 32.43% or 0.24 mm. From this data, it appears that the centre of the virgin bar is the most creep-sensitive and that it is less creep-sensitive towards the outside.

The orientation of the test piece in the stock material is crucial. As can be seen from Figure 3.6, test pieces 3 and 4 were at different orientations. The difference in the creep values between these two test pieces is 25% or 0.18 mm. The differences between the test pieces cut out radially (4, 5, and 6) are given in Table 3.1

Table 3.1: Creep value differences for various test pieces

| Test pieces | Percentage difference | Difference in mm |
|---|---|---|
| 4 – 5 | 7% | 0.05 mm |
| 4 – 6 | 14% | 0.1 mm |

.

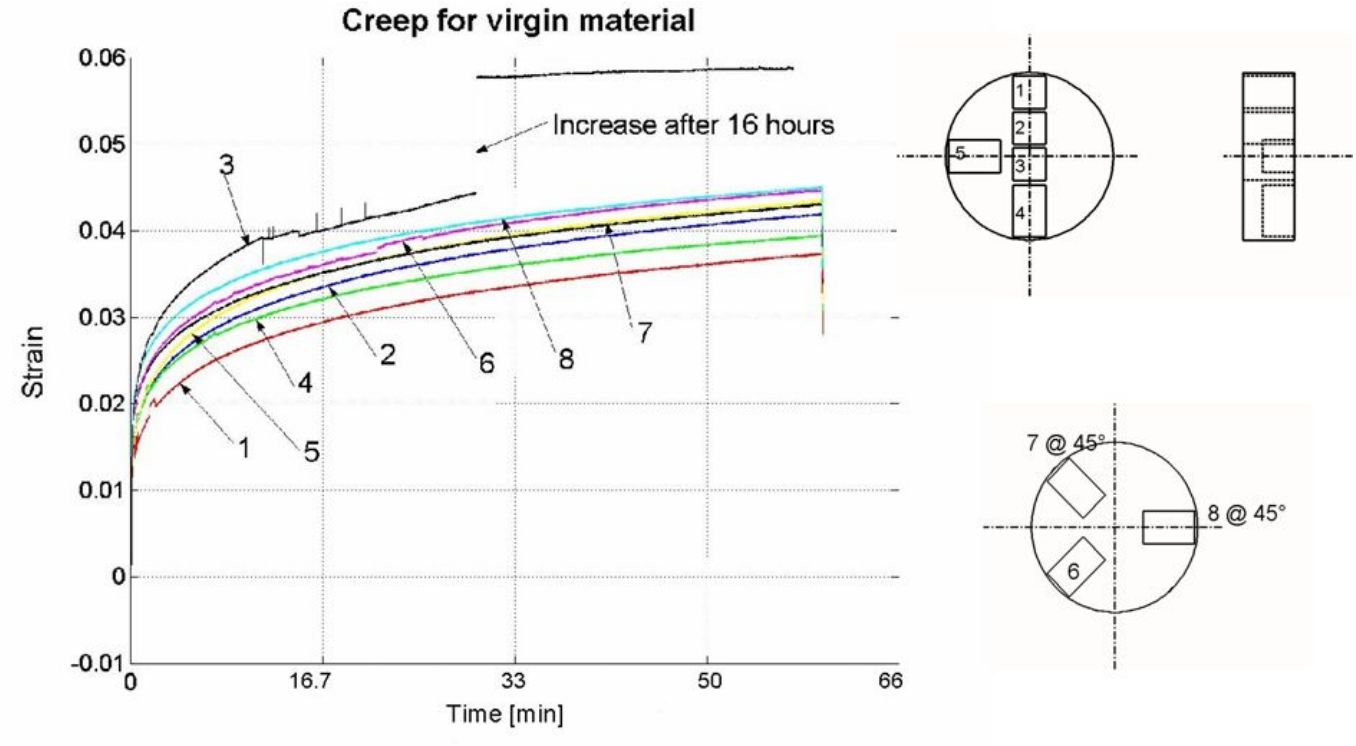


Figure 3.8: Creep in virgin material at different orientations

The creep values of the two test pieces cut out at an angle of 45°, test pieces 7 and 8, only differ 5% or 0.044 mm. What is, however, important namely is again the difference between the test piece cut out radially (4) and the rest of the test pieces that were cut out at 45° (7). The difference is 16% or 0.11 mm.

The maximum creep measured during the experiment was 1.18 mm and was measured after 18 hours of continuous loading.

The most important conclusion that can be drawn from this test is that the

material shows anisotropic behaviour. The anisotropic properties could have been a result of the extrusion process or could be caused by insufficient or incorrect procedures used during the heat treatment afterwards.

It is, however, important that designers take note of this anisotropic behaviour during the design and manufacturing process of an acetabular cup as this anisotropic behaviour of the extruded UHMWPE could lead to severe distortion of the acetabular cup under load.

## 3.4 Effect of elevated temperature on the creep properties of UHMWPE

Localised elevated temperature is a severe risk in acetabular cups during motion as a direct result of friction between the two counter-bearing surfaces. The behaviour of the UHMWPE under these conditions together with gamma sterilisation and/or crosslinking is unknown.

### 3.4.1 Purpose of test

The purpose of the test is to determine an estimated effect of elevated temperature on the creep properties of UHMWPE. Creep tests at elevated temperatures were done by Meng Deng and Latour (1998), but these tests did not incorporate the effect of gamma irradiation and/or crosslinking as already stated. Therefore, tests on the virgin material had to be carried out to establish a baseline. It is important to note that all the creep data must be used with caution. The temperature in a cup is not homogeneous. Only small localised areas on the bearing surface will operate at elevated temperatures and the complete cup will not be subjected to the total creep effect.

### 3.4.2 Test procedure

Test pieces were manufactured from a standard bar, Φ65 mm, cut out radially as shown in Figure 3.9. The test pieces were cut out and marked to enable correlation with the creep tests done at room temperature. Tests were then performed at temperatures of 40, 50 and 60°C respectively.

The temperature was monitored by placing a thermocouple down the centre of the test piece, measuring the core temperature of the test piece. This was done to ensure that the complete test piece was at the specified temperature and not only the outside. The test piece was heated up by circulating hot water around the test piece until the core had reached the desired temperature. The test set-up is shown in Figure 3.10. The rest of the test procedure remains as described earlier.

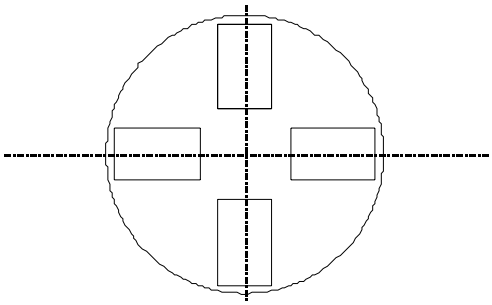

Figure 3.9: Orientation of test pieces machined from bar stock for tests at elevated temperatures

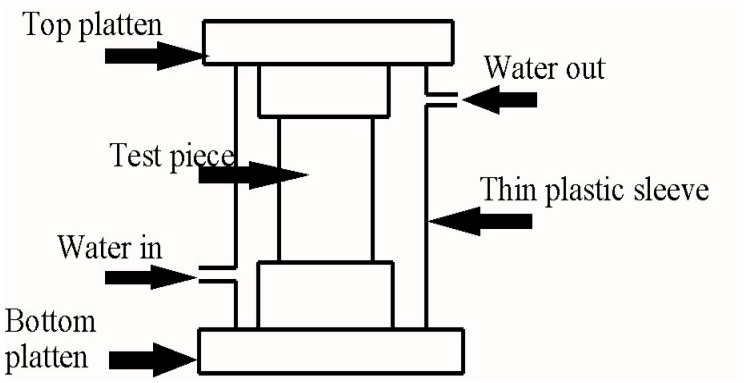


Figure 3.10: Test set-up for tests at elevated temperatures

The summary of the results of the tests at elevated temperatures are shown in Figure 3.11

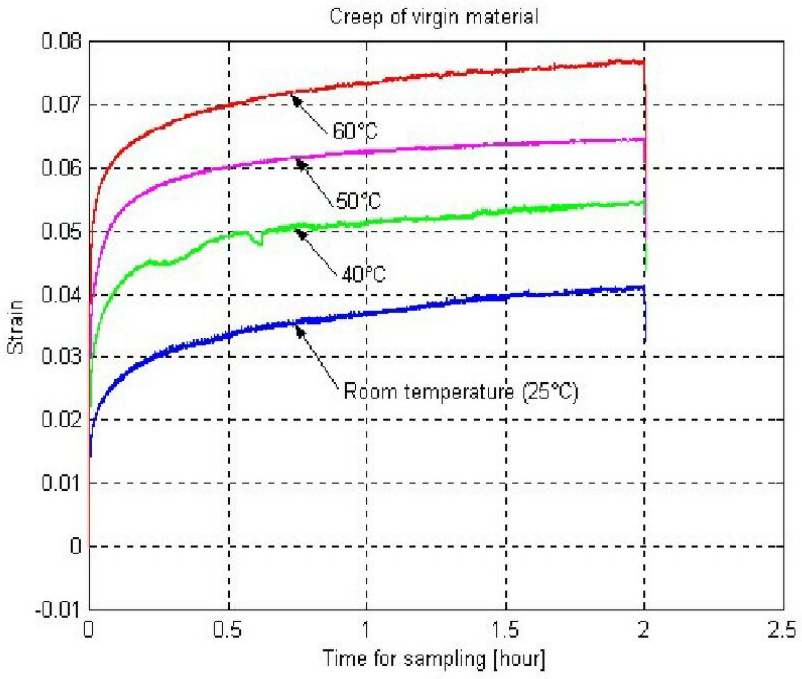


Figure 3.11: Summary of creep results at elevated temperatures

Table 3.2: Summary of creep values after 2 hours

| Test | Virgin material creep after 2 hours |
|---|---|
| Creep at room temperature | 0.79 mm |
| Creep at 40°C | 1.08 mm |
| Creep at 50°C | 1.26 mm |
| Creep at 60°C | 1.536 mm |

From the data as presented in Figure 3.11 and Table 3.2, it can be seen that there is a substantial difference in the creep properties of UHMWPE at room temperature and at 60°C. The difference in the creep values done at room temperature and at 60°C is 87% or 0.716 mm as measured over a two-hour period. The total amount of creep, at 60°C, after two hours was 1.5 mm.

The test data as presented above correlates with the data presented by Meng Deng and Latour (1998). Although Meng Deng and Latour (1998) do not present actual data values they report an increase in the creep values of 80% if the temperature is taken from 37ºC to 62ºC. The creep test data illustrates that at elevated temperature the material softens to such an extent that extrusion of material in the local hot spot areas will be possible.

## 3.5 Effect of sterilisation on the creep properties of UHMWPE

### 3.5.1 Purpose of test

Gamma sterilisation is the industry standard used for the sterilisation of medical components. From the relevant literature (Saum, 1994; Rimnac et al., 1994; Trieu & Paxson, 1995), it can be seen that the gamma

sterilization causes free radicals to form. These free radicals can cause an increase in oxidation that can have a negative effect on the mechanical properties of UHMWPE. The purpose of this test was to determine the effect of gamma sterilisation on the creep behaviour of UHMWPE.

### 3.5.2 Test procedure

Test pieces were manufactured, as described in paragraph 3.4.2. The test pieces were gamma-irradiated using three different methods to simulate sterilisation:

a. Irradiated with 25 kGy in air
b. Irradiated with 25 kGy in a nitrogen atmosphere
c. Irradiated with 25 kGy in air and heat-treated at 80°C to get an annealing effect.

The gamma irradiation and crosslinking were done by Gammatron CC using commercially available processes.

The tests were performed at room temperature to enable a comparison with data available in this study as well as with data available in the literature.

### 3.5.3 Test results

The test results to determine the effect of gamma irradiation are shown in Figure 3.12 (irradiation in air), Figure 3.13 (irradiation in nitrogen) and Figure 3.14 (irradiation in air and heat-treated to achieve annealing).

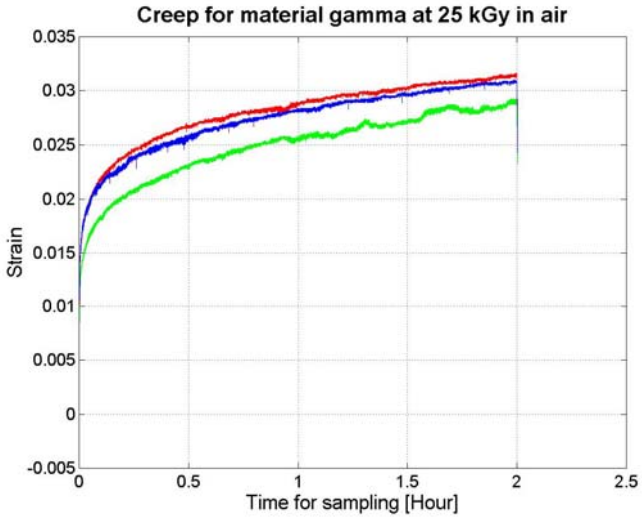


Figure 3.12: Creep properties of material irradiated in air

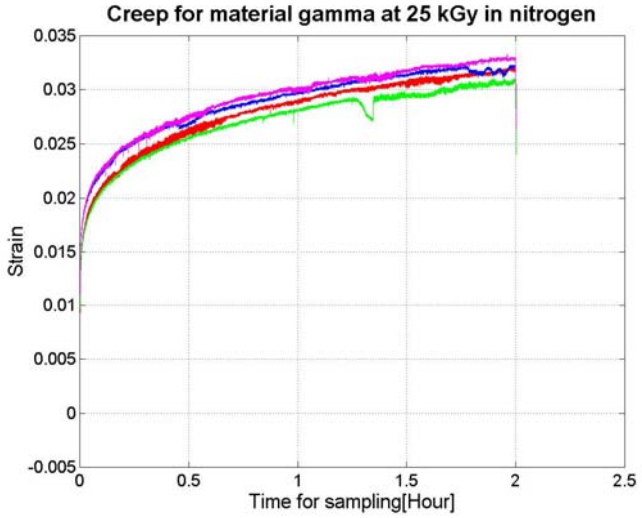


Figure 3.13: Creep properties of material irradiated in nitrogen atmosphere

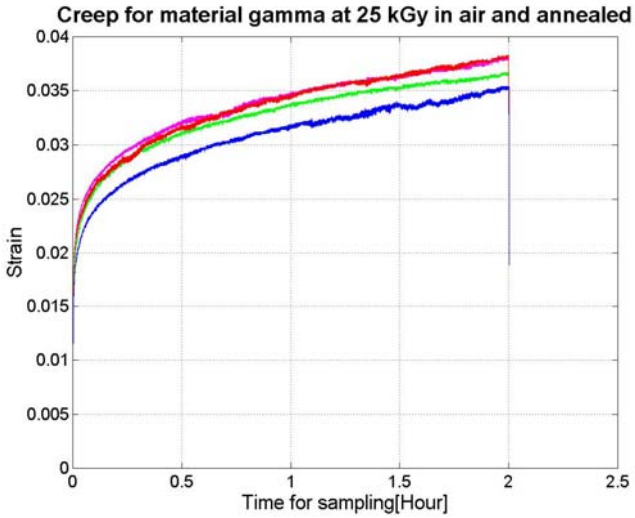


Figure 3.14: Creep properties of material radiated in air and heat-treated at 80°C and tested at room temperature

If the data as presented in Figures 3.12 to 3.14 is compared to the creep property data in the literature (Lee & Pienkowski, 1998; Meng Deng & Latour, 1998) and taking the data from paragraphs 3.2 and 3.4 into account, it can be seen that there is a slight decrease in the creep values for UHMWPE. However, the annealed material showed a substantial increase in the amount of creep (see Table 3.3).

Table 3.3: Summary of creep after gamma irradiation

| **Test (average)** | **Gamma-irradiated creep after 2 hours** |
|---|---|
| Test 4 (paragraph 3.2 and 3.4): Creep at room temperature (virgin material) | 0.79 mm |
| Material radiated in air | 0.6 mm |
| Material radiated in nitrogen | 0.65 mm |
| Material radiated in air and then heat-treated at 80°C to achieve annealing | 0.75 mm |

From the data presented in Table 3.3, it can be concluded that the effect of gamma irradiation on the creep properties of UHMWPE is negligible. In this test, the biggest contributing factor to excessive creep was the annealing of the material after manufacturing, which is an indication that this is not a good manufacturing practice although the intention is to create a material with less anisotropic behaviour.

## 3.6 Effect of crosslinking on the creep characteristics of UHMWPE

### 3.6.1 Purpose of test

The latest tendency, in the manufacturing, is to crosslink the UHMWPE to achieve better wear characteristics, although there is a reported decrease in fracture toughness (Du Plessis et al., 1977). This was discussed in Chapter 2. The purpose of this test is to determine the effect of crosslinking in an acetylene atmosphere on the creep properties of

UHMWPE at an elevated temperature.

### 3.6.2 Test procedure

Test pieces were manufactured from a standard Φ65 mm bar as described in paragraph 3.4.2. The test pieces were then crosslinked in an acetylene atmosphere with gamma irradiation at 125 kGy. Three different tests were performed, namely:

a. Creep at room temperature
b. Creep at 50°C
c. Creep at 60°C.

The same test procedure was used as described earlier. Again, the crosslinking was done by Gammatron CC with commercially available processes.

### 3.6.3 Test results

The test results of the gamma crosslinked test pieces are shown in Figure 3.15 (room temperature), Figure 3.16 (creep at 50°C) and Figure 3.17 (creep at 60°C).

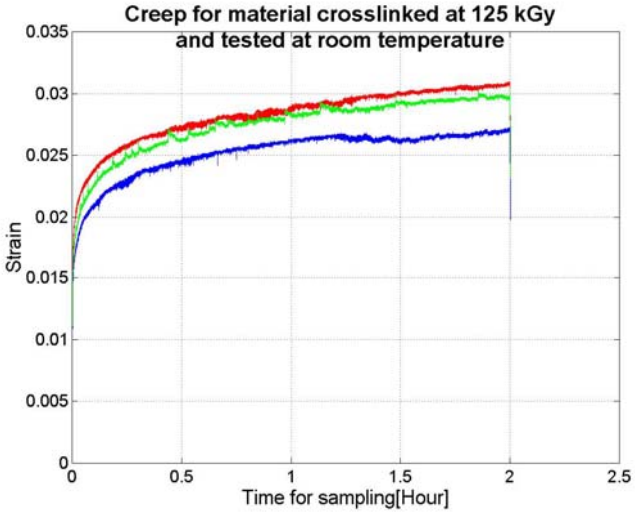


Figure 3.15: Creep properties of crosslinked UHMWPE at room temperature

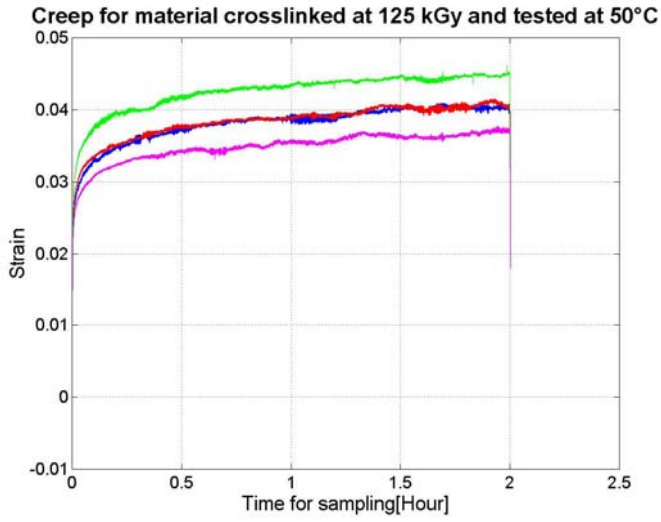


Figure 3.16: Creep properties of crosslinked UHMWPE tested at 50°C

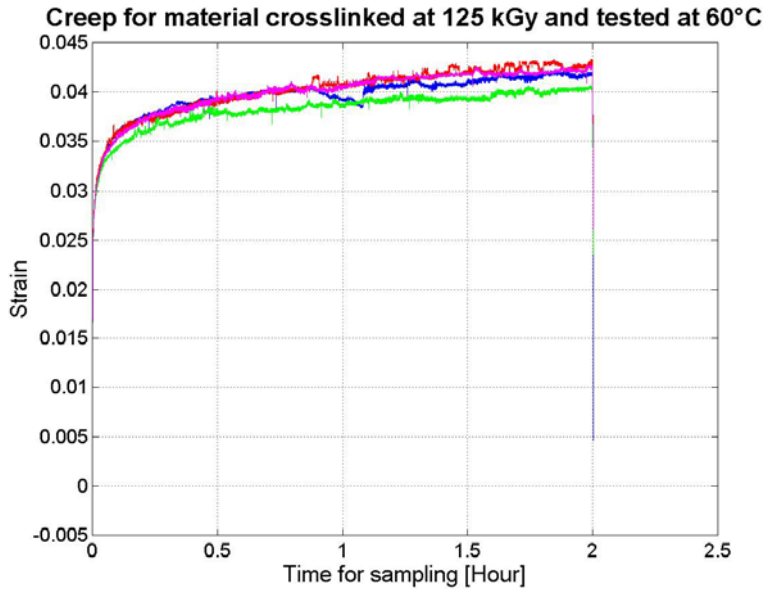


Figure 3.17: Creep properties of crosslinked UHMWPE tested at 60°C

The summary of the test data compared to the data of virgin material can be seen in Table 3.4. The creep data is average values.

Table 3.4: Summary of creep values after 2 hours

| **Test** | **Virgin material**<br>**Creep after 2 hours** | **Crosslinked**<br>**Creep after 2 hours** | **Difference** |
|---|---|---|---|
| Creep at room temperature | 0.79 mm | 0.58 mm | -36% |
| Creep at 50°C | 1.26 mm | 0.8 mm | -58% |
| Creep at 60°C | 1.536 mm | 0.84 mm | -83% |

From the data presented in Table 3.4, it can be concluded that there is a

significant decrease in the amount of creep after crosslinking. This is to be expected if the decrease in impact strength, as explained in Chapter 2, is taken into account. This decrease in the creep properties will result in a lower tendency for plastic flow to occur in the local hot spots, on the bearing surface, in the acetabular cups.

## 3.7 Proposed use of creep data in cup design

The tests show that the manufacturing process, material heat treatment, orientation and temperature all play a part in the creep characteristics. If this creep tendency is to be incorporated into future designs, more tests will have to be done to enable statistical determination of the creep properties to be used in the design process.

# CHAPTER 4

# PRELIMINARY INVESTIGATION OF RETRIEVED ACETABULAR CUPS

## 4.1 Introduction

Product failure represents one of the most persistent and expensive problems in the cost structure of any company. In the case of hip implants, the cost of these failures is carried by the health care sector and the patient. Therefore, with aseptic loosening due to wear-induced osteolysis as the principal cause of product failure (Claus et al., 2001; Dumbleton et al., 2002; Manley et al., 2002; Foguet et al., 2003; Oakley et al., 2003; Wilkinson et al., 2003), it is essential that the root cause for mechanical failure in UHMWPE acetabular cups is properly understood, especially in view of the fact that UHMWPE acetabular cups are the most commonly used in the industry (Mallchau et al., 2000; Davidson et al., 2002; Davidson et al., 2003).

The information obtained from acetabular cups retrieved during revision surgery is invaluable. The purpose of this preliminary investigation was to try and obtain a broader perspective on the defects seen in retrieved acetabular cups in order to formulate the possible failure criteria and the methodology to be used during the detail investigation of this study.

In engineering failure analysis, all possible analytical tools are used to conduct a scientific investigation to provide a better understanding into the root cause of mechanical failure. However, the classification found in some of the literature (Schmalzried et al., 1999), namely mode 1 to mode 4 wear, is vague and inadequate for a root cause failure analysis. A more comprehensive classification will have to be established to enable an engineering failure

analysis.

In ISO 12891-3 (2000), a guideline of defects for polymeric retrievals is provided. This section was not included in the literature survey in Chapter 2 of this study as it is most suited here where the new proposed criteria are presented. The ISO 12891-3 guideline, is applicable in general to all polymeric retrievals and include the following:

a. Wear
b. Discolouration
c. Material transfer
d. Scratching or pitting
e. Embedded particles
f. Cracking
g. Warping
h. Change of shape
i. Burnishing
j. Mechanical damage
k. Tissue attachment
l. Macro porosity
m. Dimensions.

All the abovementioned defects are listed in the ISO specification, as a guideline, but no detailed description of the various defects is provided and these defects are therefore, open to interpretation by the user.

The methodology used to establish a set of failure criteria, applicable to acetabular cups, was arrived at by studying more than 100 retrieved components and by observing the defects present in these cups. The defects found were then categorised enabling the formulation of a set of failure criteria for an engineering failure analysis. The retrievals studied were all received from one

centre. The retrievals were not clearly identified and therefore an accurate assessment of in-vivo service could not be made. Nonetheless these retrievals provided research material for an initial assessment of the failure mechanism. A detailed engineering failure analysis on retrievals for which all data is available is presented in Chapter 5.

## 4.2 Proposed failure criteria

After investigating the mechanical failures in more than 100 retrieved components and categorising these failures, the most common defects are listed in Table 4.1.

Table 4.1: The most common defects noticed on inside of retrieved cups

| | **Defect noticed** | **ISO 12891-3 Items** |
|---|---|---|
| 1 | Mechanical damage | j |
| 2 | Cracks in the material | f, l |
| 3 | Plastic flow | a, g, h |
| 4 | Scratches | a, d, j |
| 5 | Adhesion wear | a |
| 6 | Wear particles embedded in base material | a, c, e, |
| 7 | Flaking | a |

The visible defects, as set out in Table 4.1, are used as a classification tool to identify defects in the detailed failure analysis in this study. Scientific analytic tools, some of them suggested in ISO 12891-3 (2000), are used to establish the cause of defect formation.

## 4.3 Descriptive explanation of defects in acetabular cups

The defects, as listed in ISO 12891-3 (2000), are not described in detail in the specification and are therefore open to interpretation by the user. In this part of the study, the different defects, as listed in Table 4.1, are described in detail.

This is done to ensure a clear set of criteria, which can be followed in a root cause analysis into the mechanical failure of acetabular cups.

### 4.3.1 Mechanical damage

Mechanical damage, predominantly caused by impingement, is normally the result of an acetabular cup not properly aligned in vivo, whether during implantation or during rotation after aseptic loosening. The mechanical damage is normally a result of the neck of the femoral stem making contact with the rim of the acetabular component. Impingement can also occur after excessive wear when the neck of the femoral component is making contact with the acetabular component. Impingement normally results in pieces of material (UHMWPE or cement) being ripped from the edge of the cup as seen in Figure 4.1. A schematic presentation of the defect is shown in Figure 4.2

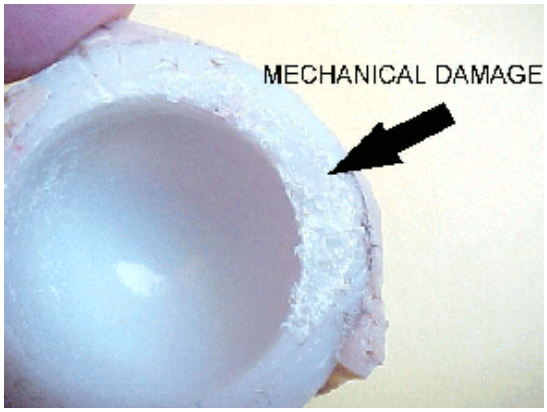


Figure 4.1: Mechanical damage on rim of cup

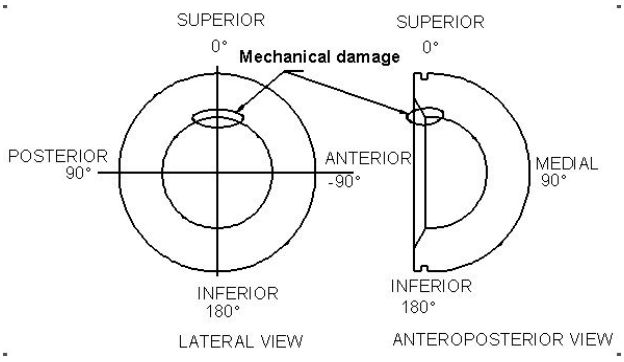


Figure 4.2: Schematic presentation of mechanical damage on rim of cup

An initial assessment of the problem is that the pieces of material forcefully removed by the neck of the femoral component will cause large floating particles and possible loosening of the cup due to impact loading. If rotation of the cup with resulting impingement is a result of aseptic loosening, impingement will cause further rotation and discomfort to the patient.

### 4.3.2 Cracks in material

Cracks in the material can be caused by stress raisers and are normally expected in the high-stress or contact stress areas or on the rim of the cup as occasionally seen in the case of cups with metal backing. A typical defect is shown in Figure 4.3a and schematic presentation of the defect is shown in Figure 4.4.

Fracturing of metal backed liners can conceivably also occur as follows: If the polyethylene liner is not machine-pressed into the metal backing, but only clipped into position, the possible lack of conformity between the cup and metal backing can cause higher stresses on the rim of the cup. The resulting alternating stress can cause fatigue cracks (Figure 4.3a) and separation within the material on the rim (Figure 4.3b).

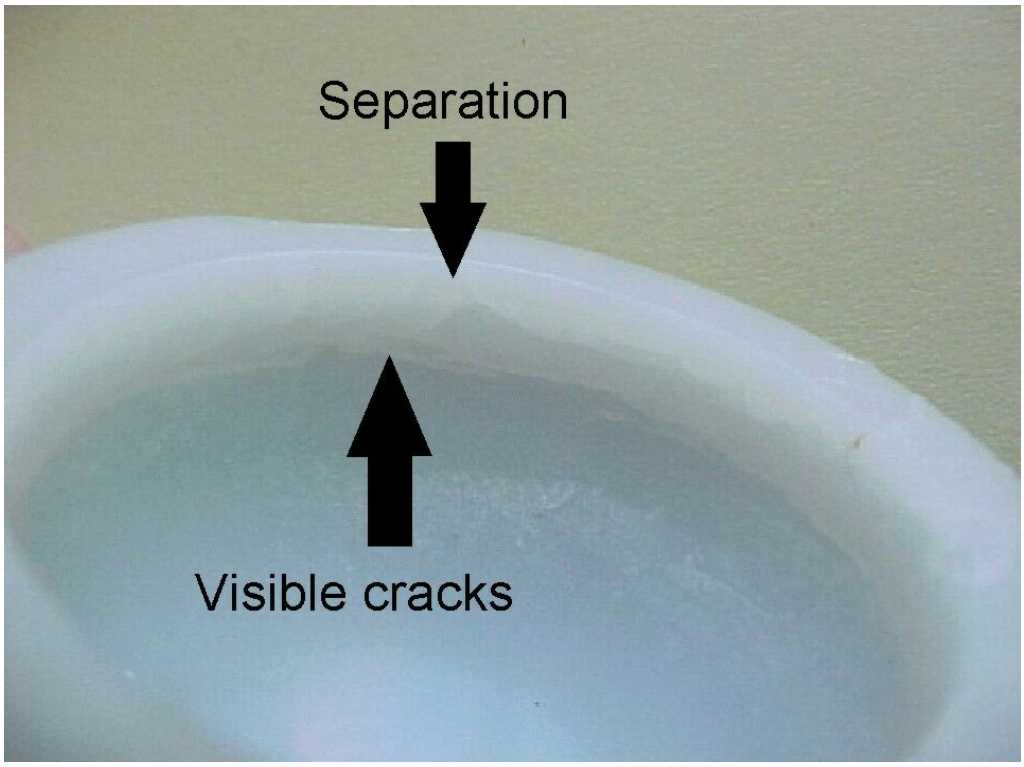


Figure 4.3a: Metal backed acetabular cup with cracks on rim

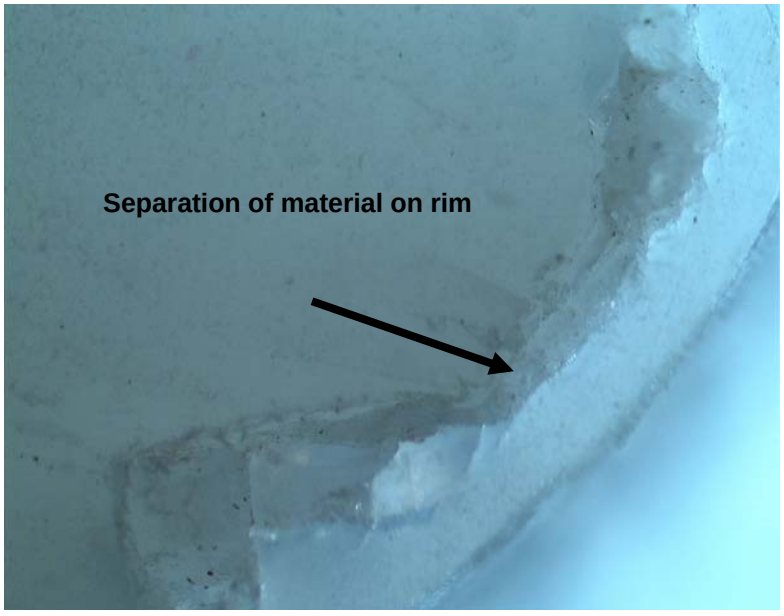


Figure 4.3b: Separation within material

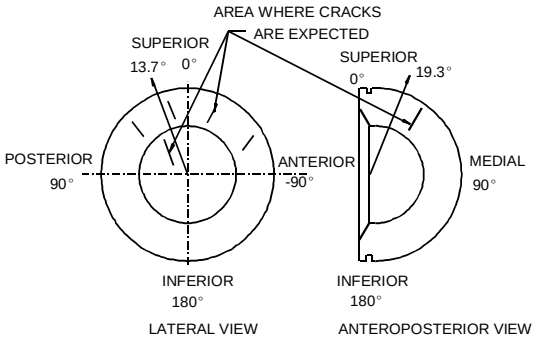


Figure 4.4: Schematic layout of areas where cracks can be expected in the area under tensile stress

### 4.3.3 Plastic flow

When the acetabular cups are investigated by means of a magnifying glass, areas of plastic flow are visible. These areas can have different appearances. The first is the orange peel effect. The term "*orange peel*" is used to describe the surface texture and should not be related to the surface roughening encountered in forming products from metal stock that has a coarse grain size as is commonly referred to in metallurgy and in injection moulding of plastics (Gold Technology, 1990; Engineering Materials Handbook, 1987; http://www.principalmetals.com /glossary/odoc.htm). This area normally occurs just outside the area of high contact stress on the bearing surface. Visually, it seems as if "molten" material or material sufficiently softened to be extruded was expelled from the area of high contact stress and transferred to an area where the contact stress is less intense. A typical defect is shown in Figure 4.5 with a schematic presentation of the defect shown in Figure 4.6.

A further example of this defect is plastic flow on the rim of the cup. An example of this defect can be seen in Figure 4.3b. This defect presents as if the compressive stress, on the bearing surface in the cup, exceeded the maximum

limits resulting in an outward flow and/or creep of the material.

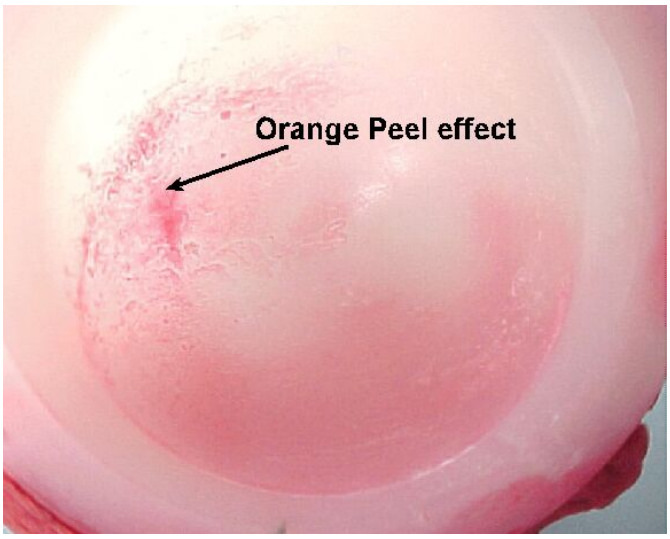


Figure 4.5: Cup treated with dye penetrant showing “orange peel” effect indicating plastic flow of material

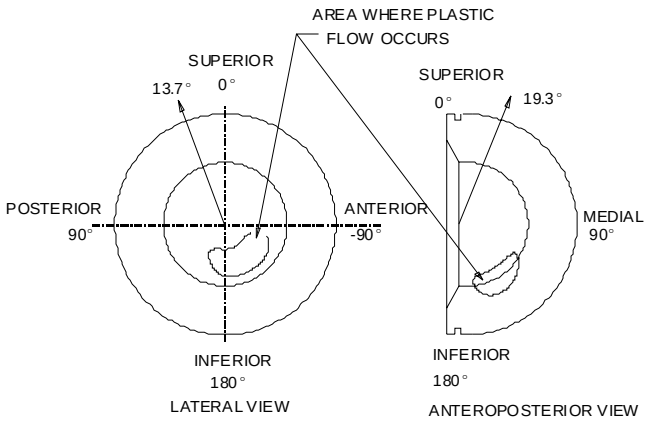


Figure 4.6: Schematic layout of expected plastic flow in acetabular cups

The defect, classified as plastic flow, in the acetabular cups appears similar to the defects found in the work of Kukureka et al. (1995), where acetal was tested in unlubricated rolling-sliding contact. At this early stage of the investigation, it

would appear that there is an underlying problem with the available lubrication in the acetabular joint.

### 4.3.4 Scratches

During examination of the retrieved cups, scratches were found in some of them. Although scratches on a micro scale have been reported in the literature (see Chapter 2), scratches visible with the naked eye are also present. These large scratches will be synonymous with third-body wear, independent of what caused the wear particles or the type of particles. The appearance of these scratches is not limited to the final wear area, but can also be created during the initial stages shortly after implantation. An example of a cup with this defect is shown in Figure 4.7.

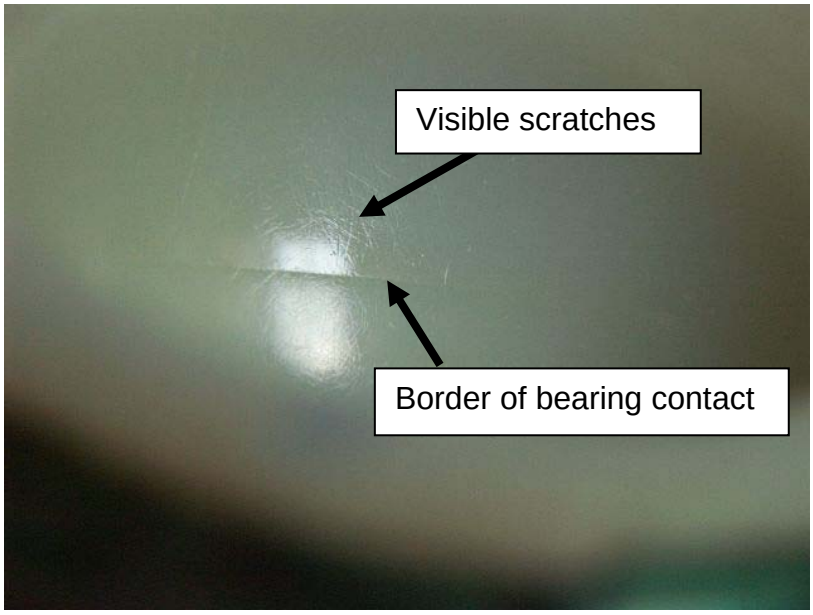


Figure 4.7: Scratches visible on inside of cup

### 4.3.5 Adhesion wear

*Adhesion wear* can be described as areas where adhesion wear, probably due to overheating and/or lack of lubrication, has taken place. This normally occurs under conditions of high frequency, short stroke, small movement (Hutchings, 1992). When bonding between asperities on the two surfaces in contact occurs

and subsequent movement causes the asperities of the softer surface to be torn out, rather than breaking the bond between the asperities, the process is called *adhesion wear,* typically the areas present as rough patches and are seen in the high contact stress areas where lubrication is the poorest. An example of an acetabular cup with signs of adhesion wear is shown in Figure 4.8 and a schematic presentation of the defect is shown in Figure 4.9.


Figure 4.8: Adhesion wear on inside made visible with dye penetrant treatment

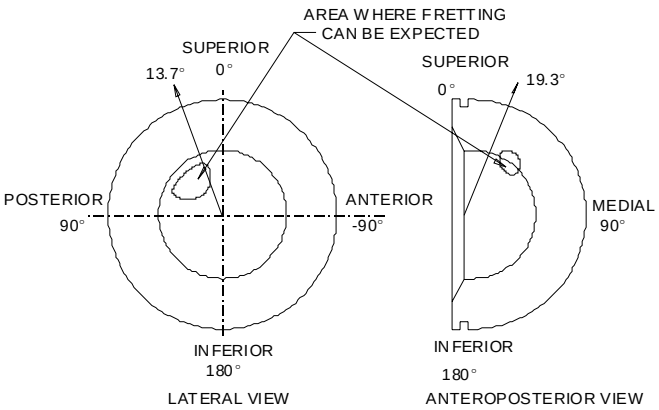


Figure 4.9: Schematic presentation of expected adhesion wear marks

### 4.3.6 Wear particles embedded in base material

During the examination of some of the acetabular cups, wear particles were found embedded in the base material. Although wear products from the base material are also embedded in the base material, the most common particle found embedded was poly methacrylate (PMMA) cement used for the fixation of the implant as well as UHMWPE wear particles. An acetabular cup with PMMA particles embedded is shown in Figure 4.10.

Figure 4.10: Acetabular cup with embedded PMMA particles

### 4.3.7 Flaking

*Flaking* (delamination) can be defined as areas where pieces of material separate from the base material. This defect presents either as craters or areas of delamination. A cup with serious delamination is shown in Figure 4.11. This type of defect, although not common, is normally associated with a defect within the material and occurs in the high stress or contact stress areas.

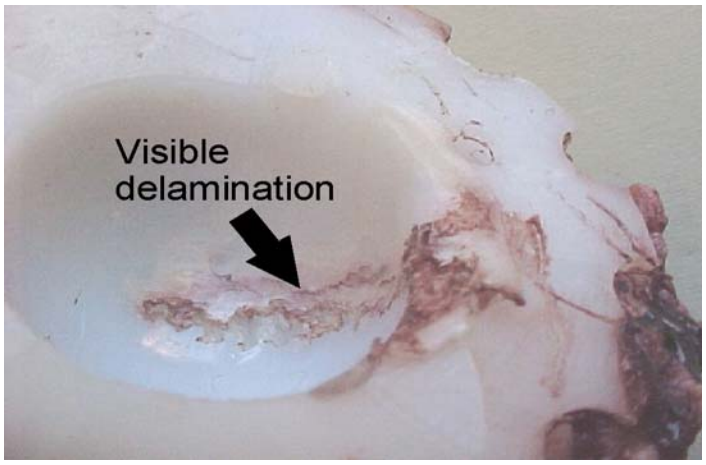


Figure 4.11: Acetabular cup with serious delamination visible.

The following question can now be raised: Can the defect present in the acetabular cup in itself cause the end of useful life? The influence of the most common defects as listed in Table 4.1 on the functional life of the acetabular cups can be seen in Table 4.2.

Table 4.2: Common defects present in acetabular cups with possible effect on useful life

| | **Defect** | **Question: Could the defect in itself cause the end of useful life** |
|---|---|---|
| 1 | Mechanical damage | Yes |
| 2 | Cracks in the material | Yes |
| 3 | Plastic flow | Yes |
| 4 | Scratches | Possible — dependent on the severity |
| 5 | Adhesion wear | Yes |
| 6 | Wear particles embedded in base material | Possible — dependent on severity |
| 7 | Flaking | Yes |

## 4.4 Statistical analysis of retrieved acetabular cups

After the completion of the preliminary study, a more detailed set of defects, as given in Table 4.1, was compiled, compared to the defects as listed in ISO 12891-3 (2000). Making use of this proposed set of defects, a controlled retrieval study was done on 47 acetabular cups retrieved during revision surgery. All of these acetabular cups were obtained from one centre and procedures were performed by the same surgeon. All the details of the patients, duration in service and the type of femoral head were recorded as suggested by ISO 12891-3 (2000). The full failure analysis is discussed in Chapter 6 and the detail analysis of 20 cups is attached in Annexure A.

The results of the analysis, according to the proposed defects, can be seen in Table 4.3. The analysis is based on the number of occurrences per defect. Some of the acetabular cups had more than one defect present in the cup. (See Annexure A.)

Table 4.3: Statistical analysis of 47 retrieved cups, with in total 125 defects

*The percentage is based on the number of occurrences per defect in 47 cups

| **Defect** | **Number** | **Percentage*** | **Comments** |
|---|---|---|---|
| Mechanical damage | 18 | 38.3% | Caused by misalignment or movement after aseptic loosening |
| Cracks | 11 | 23.4% | Cups with metal backing in specific series prone to cracks on rim |
| Plastic flow | 29 | 61.7% | More prominent when ceramic femoral head is used |
| Scratches (Visual) | 21 | 44.6% | Caused by third-body wear |
| Adhesion wear | 23 | 48.9% | More prominent when ceramic femoral head was used |
| Wear particles embedded in base material | 22 | 46.8% | Secondary effect or particles that originate outside the bearing |
| Flaking | 1 | 2.1% | Most likely a material defect |

.

From the data presented in Table 4.3, the major defects resulting in 'end of useful life' are:

a. Plastic flow: present in 61.7% of the acetabular cups retrieved. Plastic flow is more prominent in the UHMWPE/ceramic bearing couples than in UHMWPE/steel couples. The severity of the amount of plastic flow in the UHMWPE/steel bearing couples is also less.

b. Adhesion wear: present in 48.9% of the retrieved acetabular cups. Adhesion wear is also more prominent in the UHMWPE/ceramic bearing couples than in the UHMWPE/steel bearing couples. Adhesion wear was

only found in 2 components running with UHMWPE/steel bearing couples.

The fact that plastic flow and adhesion wear are both influenced by the amount of heat generated on the bearing surface, the less frequent occurrence and severity in the UHMWPE/steel bearing couples are already an indication that there is better cooling in these bearing couples if compared to UHMWPE/ceramic bearing couples.

## 4.5 Conclusion

From the data presented in Table 4.3 and taking into account the results of the creep characteristics of UHMWPE at elevated temperatures (Chapter 3) it would seem that there is an underlying problem of localised excessive heat build-up on the bearing surface of the polyethylene acetabular cups. This heat build-up might at this stage be attributed to either a lack of sufficient lubrication and/or the difference in the ability of the various materials to conduct the generated heat away from the surface. This is supported by the difference in the thermal conductivity of steel (k=1.35 W/mK) (Engineering Materials Handbook, 1987) compared to the very low thermal conductivity value for ceramic (k= 0.0158 W/mK) (Engineering Materials Handbook, 1987) resulting in the generated heat being trapped between the mating surfaces.

# CHAPTER 5
# RETRIEVAL STUDY

## 5.1 Introduction

Retrievals obtained after revision surgery provided valuable information with respect to the causes of wear that take place in-vivo.

*Note: For better clarity, please view all photographs (jpg format) on the CD enclosed.*

The components investigated were randomly retrieved from one centre, properly marked and the details of the patients were noted for further reference. In all, 57 components were retrieved. Forty-seven (47) components were brought to the laboratory for an engineering investigation into the causes of failure. The ISO standard for the removal and handling of retrievals was followed (ISO 12891-3, 2000). The bearing couples varied between steel on UHMWPE and ceramic on UHMWPE

A second investigation was conducted making use of a further 5 components retrieved during revision surgery. During this second study all the freshly retrieved components were analysed in a biochemistry laboratory within one hour after removal from the patient. The purpose of this investigation was to try and determine if any proteins were deposited inside the cup. These components were not cleaned in theatre but were supplied as retrieved. The findings of this investigation are discussed in paragraph 5.4.

A third investigation was conducted also making use of 10 freshly retrieved components. These retrievals also included tissue removed from the patients. The purpose of this investigation was to try to find wear debris on either the retrieved components or in the tissue surrounding the prosthesis in-vivo to enable the qualification of the mechanism creating this debris. The detail of this investigation will be discussed in paragraph 5.8.

During this investigation, the following techniques were used to inspect and analyse the retrieved components:

a. Visual inspection
b. Investigation making use of a colour dye penetrant
c. Investigation under a stereo microscope
d. Investigation making use of a scanning electron microscope
e. Electrophoresis
f. Mass-spectrometric analysis

## 5.2 Summary of retrieved components

The 47 components used in the initial study were retrieved from 24 male and 23 female patients. All of the components had reached the end of their usable life, in-vivo, after an average of eight years and three months in service and were manufactured from UHMWPE. Of the 47 components 9 were polyethylene liners implanted with metal-backing and the rest (38) were implanted only with PMMA cement. The service life in these cases varied from 1 year to 23 years and 5 months in-vivo. The retrieved acetabular cups were from various manufacturers. In all cases, the reason for revision surgery was a loose acetabular cup causing severe pain and discomfort to the patient.

All the retrieved cups showed signs of excessive wear and/or creep. In four cases, there were catastrophic failures. For an example of these catastrophic failures, see Figure 5.1. In the second cup, something was wrong with the material (Figure 5.2), as the material started delaminating within a year after implantation. These details are discussed later.

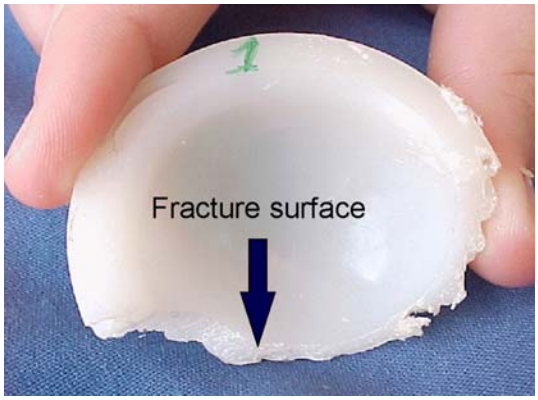


Figure 5.1: Fractured cup


Figure 5.2: A cup with delamination

## 5.3 Visual inspection of retrieved acetabular cups

The cups were visually inspected to try to identify any obvious defects in the retrieved components. The findings of the visual inspection are as follows:

All the cups showed some form of wear and/or creep. It is difficult to distinguish exactly between wear and creep. It was therefore assumed that a combination of both occurred. The extent of wear/creep varies depending on the number of years in-vivo. The position of the maximum wear/creep correlated with data found in literature (Sychterz et al., 1996; Jasty et al., 1997; Schmalzried et al., 1999). Figure 5.3 shows a cross section of an acetabular cup showing the amount of wear/creep and Figure 5.5 provides a schematic presentation of the wear area.

Visible in all of the cups was some form of debris deposited outside the high load area (see Figures 5.4 and 5.5). The debris was attached to the base material and could not be removed. When viewed under a magnifying glass, this debris appeared like “molten” material deposited on a cold surface. Also visible under the magnifying glass were craters and pieces of material with an irregular pattern similar to the surface of an orange. (See paragraph 4.3.3.) At this stage of the investigation, it was felt that this debris holds the key to what is actually happening on the running surface and therefore warranted an in-depth investigation.


Figure 5.3: Cross section of cups showing an amount of wear/creep


Figure 5.4: Deposited debris – coloured with liquid dye penetrant to make it more visible

As mentioned in paragraph 5.2, four of the retrieved cups showed catastrophic failures. The first cup had fractured and it also showed some signs of cracking in other areas. It appears that the fatal crack started from a crater caused by material being extruded from the base material in the main adhesion wear area (See Figures 5.6 and 5.7).

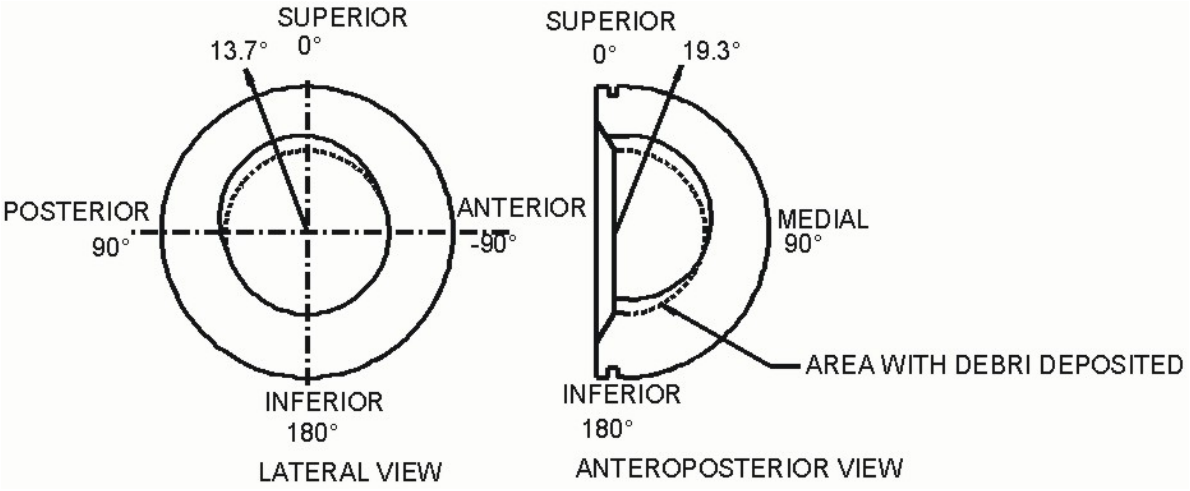


Figure 5.5: Wear pattern in retrieved cups with area of debris deposits indicated

The cups were treated with dye penetrant to make the defects more visible. The cup, shown in Figure 5.2, failed after only one year in-vivo. When inspected, using a magnifying glass, it appeared that the material was defective and that it had delaminated as can be seen in Figure 5.2. A possible explanation for this delamination is that during the manufacturing process a harder layer on the surface had formed, similar to case hardening in steel. This can be a result of incorrect cooling, incorrect cutting speed or a blunt cutting tool. When the acetabular cup is in service, contact stresses are generated at a distance below the surface (Boresi & Sidebottom, 1985). Repetitive loading may then result in fatigue failure at the depth below the surface where the contact stresses are maximised, causing the top layer of material to delaminate.

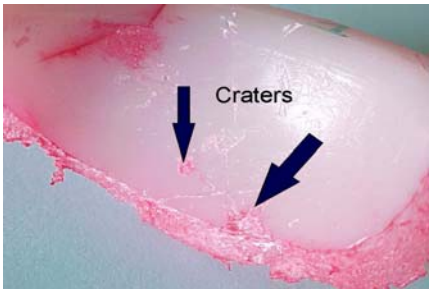


Figure 5.6: Crater in fractured cup

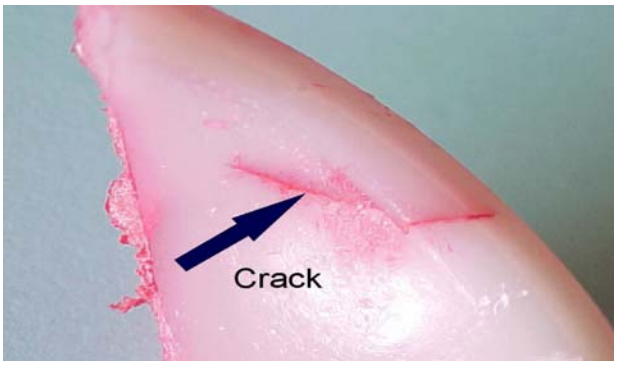


Figure 5.7: Cracking in fractured cup

Apart from the wear/creep and the catastrophic failures, a number of other types of failure were identified in the retrieved acetabular components. The first is interference between the acetabular cup and the neck of the femoral component as shown in Figure 5.8. This was caused by misalignment in-vivo. This misalignment may be a result of problems during surgery or, more often, the impingement damage is secondary to a cup loosened due to osteolysis with the resulting movement of the cup causing misalignment. The result is that the neck of the femoral component interferes with the acetabular cup removing pieces of material (UHMWPE and PMMA cement). This debris can find its way into the bearing area where it can cause third-body wear, as discussed earlier. The larger pieces of UHMWPE removed from the rim of the cup, can also cause further osteolysis.

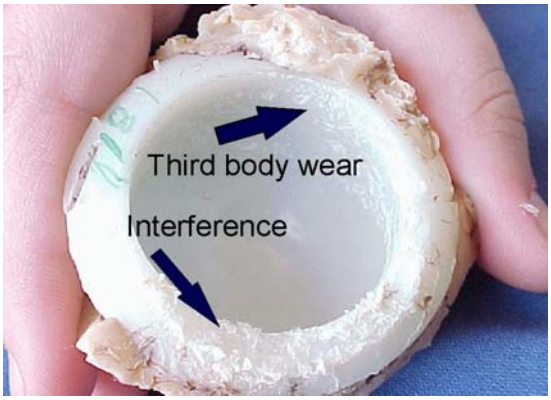


Figure 5.8: A cup with evidence of interference and subsequent damage

Foreign particles can find their way onto the bearing surface area. In one of the cups, a steel chip or shaving was trapped on the bearing surface and subsequently pressed into the softer polyethylene by the zirconium femoral head as shown in Figure 5.9. The origin of the steel particle is not known, but it can only be from the surgical tools because the femoral head was not manufactured from steel but zirconium and the femoral stem was manufactured from titanium. The piece of steel was embedded in the cup and did not cause the failure. Defects originating from surgical procedures will not be investigated further in this study.

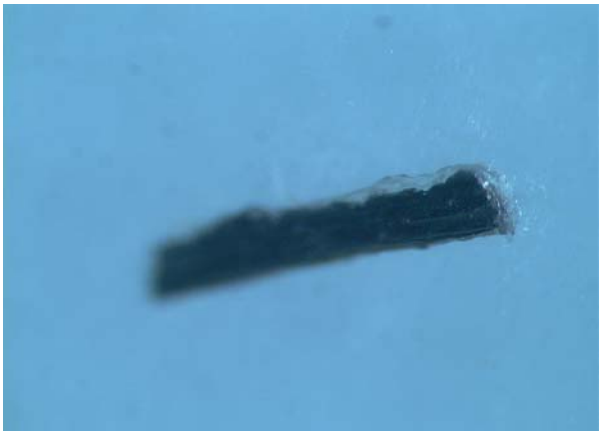

Figure 5.9: Piece of steel embedded in polyethylene (magnification x 40)

Another defect detected visually was an acetabular cup with severe plastic flow visible round the rim of the cup together with cracks running radially from the area of plastic flow. This is shown in Figures 5.10 and 5.11. The cause of this plastic flow is discussed later. In Figure 5.11, a vernier is held against the “flowed” material to indicate the extent of flow that had taken place.

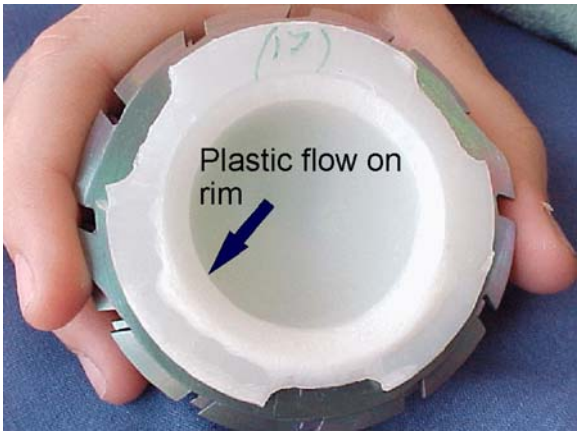


Figure 5.10: Plastic flow on the rim of cup

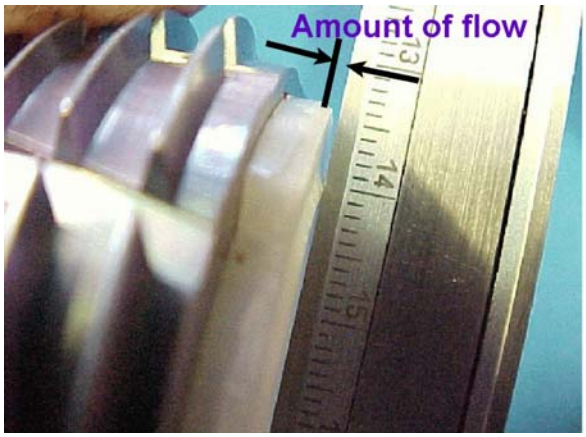


Figure 5.11: Amount of plastic flow

In virtually all of the cups, a whitish deposit was found inside the cup on the bearing area. Owing to the transparent nature of this deposit, it was very difficult to photograph. However, in one of the cups, the deposit was so thick that it was possible to collect and study it using an electron microscope. The deposit was found to be sodium chloride, which was probably deposited after washing the wound and the retrieved component in theatre during revision surgery. (The result of the electron microscope investigation is attached in Annexure B.) This deposit has no influence on the failure analysis of this investigation and will be ignored. Figure 5.12 shows the acetabular cup with the white deposit collected. Also visible in this cup is a slight brown discolouration towards the rim of the cup. The brown discolouration was also

investigated further using an electron microscope. In paragraph 5.6 it will be shown that this is not a discolouration but a deposit on the inside of the cups.


Figure 5.12: White deposits on inside of cup and brown discolouring

Based on the visual inspection, it is clear that different modes of in-vivo failure were identified in the 47 acetabular cups investigated. Although there were other causes of failure (for example misalignment during surgery and poor bone stock resulting in early loosening of the cup), the majority of these cups had failed mechanically due to excessive wear and/or creep. The wear debris found on the inside of these cups suggested that the material has been forcefully removed from the bearing area under pressure and was then deposited outside the bearing area.

## 5.4 Inspection making use of dye penetrant

The retrieved cups have many surface defects as described earlier. To be able to investigate the extent of the damage and debris deposits in the cup, it was decided to make use of a liquid dye penetrant to colour the defects. The penetrant used was Chemserve Systems Ardrox 996P. The procedure used was to clean the cups making use of Chemserve Systems Ardrox 9PR551 and then to spray the cup with the penetrant. The penetrant was allowed to penetrate the defects for 30 minutes. The excess was then wiped off and the cup was cleaned, using Ardrox 9PR551.

By making use of this technique, all the visual observations made in paragraph 5.2 were confirmed. The material extruded from the bearing contact surface as well as debris removed from the bearing surface during operation can be seen in Figure 5.13.

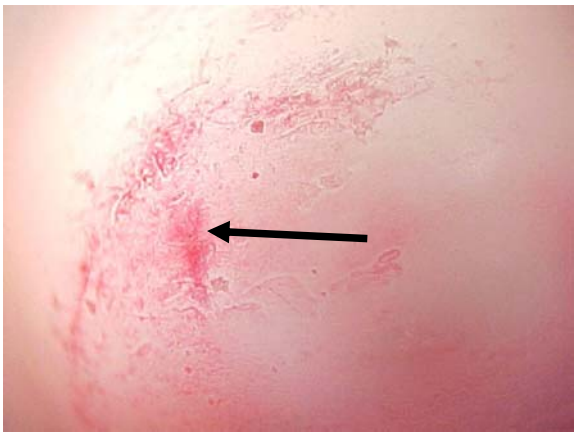

Figure 5.13: Deposited debris, resulting flow pattern and adhesion wear

The cup that had shown signs of plastic flow, Figures 5.10 and 5.11, was sectioned before treatment with the liquid dye penetrant. In Figure 5.14, the damage to the rim of the cup can be seen. With the dye penetrant test, it is clear that the material was subjected to conditions of plastic flow and had totally parted with the base material. What is interesting is that the flow had occurred over almost 80% of the rim circumference and not only in the high pressure area.

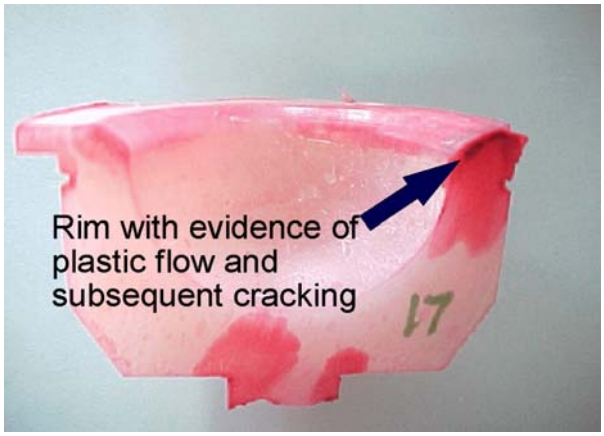


Figure 5.14: The rim of cup showing plastic flow on circumference of rim

Another feature of the plastic flow that became evident during the dye penetrant tests was that although the running surface looked polished, debris was deposited over the total bearing area. This deposited debris is visible in Figure 5.13. This led to the conclusion that the bearing surface is in actual fact not smooth but “pockmarked” due to debris deposited and then flattened and pressed into the bearing surface. The deposited wear debris is not evenly spread over the bearing surface as can be seen in Figures 5.13 and 5.15. Areas with higher concentrations of wear debris are found. These areas are investigated using a stereoscope, as discussed later.

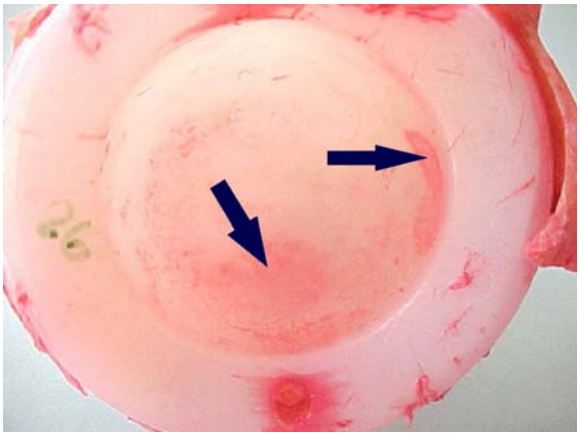

Figure 5.15: A cup with areas of higher concentration of debris

Another defect became clear when the acetabular cups were treated with the dye penetrant spray, namely areas of adhesion wear that had taken place. An acetabular cup with these areas clearly visible is shown in Figure 5.16 with a schematic layout of the positioning of this adhesion wear shown in Figure 5.17. This defect is also investigated further making use of the stereoscope as well as the electron microscope.

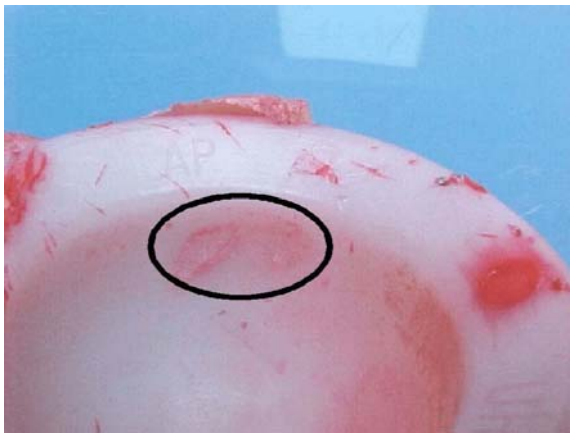

Figure 5.16: Close-up of the area of adhesion wear

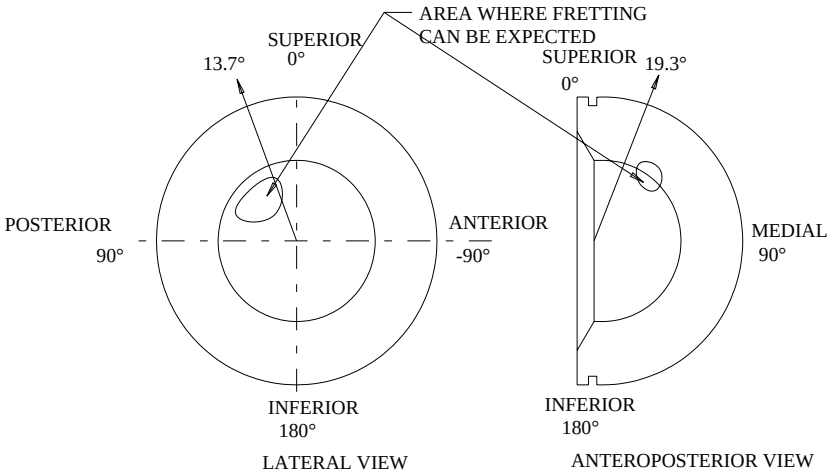


Figure 5.17: Schematic layout to indicate position of adhesion wear mark

At the position indicated in Figure 5.17, the contact stress of an implant is the highest. Adhesion wear is most likely to occur at this point where there is a combination of the different actions. The extension and flexion movement of the leg under load will force the lubricant from the bearing surface, while the abduction/adduction rotation and flexion movements of the leg will provide the energy input to cause adhesion wear or extrusion of material.

## 5.5 Investigation making use of stereoscope

Based on the investigations of paragraph 5.3 and 5.4, it became evident that more attention had to be paid to certain areas in the acetabular cups. The cups were examined using a Nikon stereoscope, equipped with a digital camera. It must be noted that in this investigation some parts of the photographs will be out of focus, because of the curvature of the cups.

The first cup investigated was the cup that had fractured (Figure 4.1). During the visual inspection and dye penetrant tests serious surface defects were visible as can be seen from Figure 5.6. When these defects were magnified, they turned out to be small craters formed when material was ripped from the base material. (See Figures 5.18 to 5.21.)

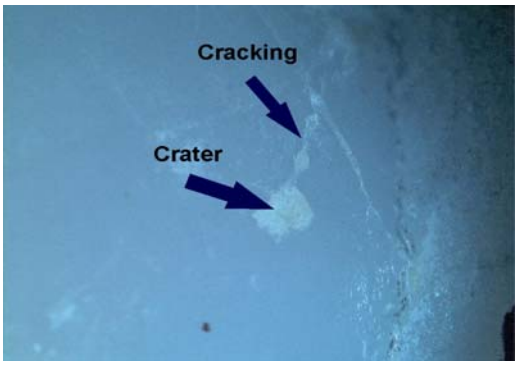


Figure 5.18: Magnification (x 10) of defect before treatment with dye penetrant

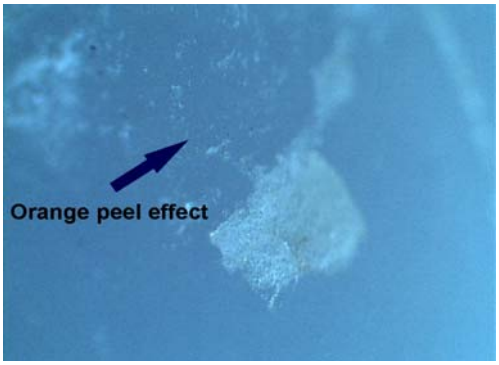


Figure 5.19: Magnification (x 20) of defect before treatment with dye penetrant

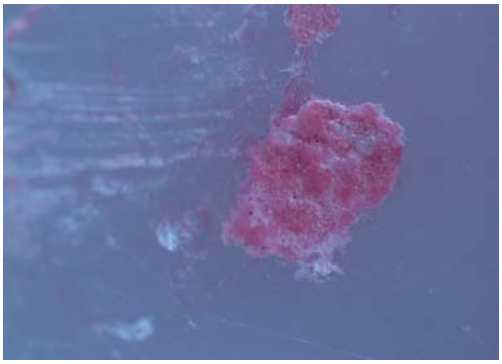

Figure 5.20: Magnification(x 20) of defect after treatment with dye penetrant

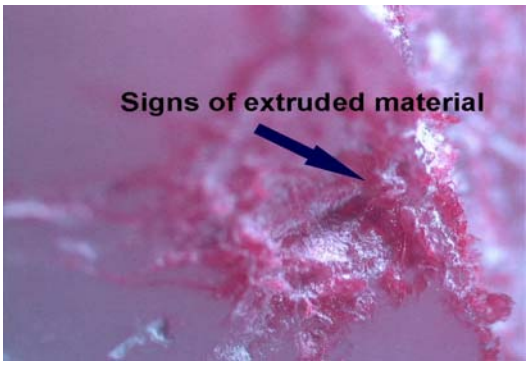


Figure 5.21: Magnification (x 40) of second crater after treatment with dye penetrant

The cracks seen in Figure 5.6 are now clearly visible in Figure 5.18. It is believed that the final fracture occurred after the cracks that had propagated from these defects (Figure 5.21) had extended beyond the critical crack length for this material. Also visible in Figure 5.19 are indications of the orange peel effect, as discussed earlier. Visible in Figure 5.21, is material that was extruded or forced out leaving the crater as indicated by the arrow.

If this material transfer takes place without evidence of high temperatures on the surface where the particles were removed or if the particles show no signs of having been extruded, the process will be referred to as adhesion wear. It is obvious that it will not always be possible to clearly distinguish between the two modes of failure, i.e. adhesion wear or extrusion. The starting point is, however, the same namely lack of lubrication and raised temperature (Hutchings 1992). Adhesion wear will occur when the movement of the femoral

ball in the acetabular cup is too small or too slow to cause sufficient heat build up to cause extrusion and/or plastic deformation.

The second failure that was investigated was the cup with material that flowed along the rim of the cup as shown in Figure 5.10. From the stereoscope photographs (Figures 5.22 and 5.23), it is clear that the material that flowed showed signs of separation from the base material. In this case the mass of the patient was approximately 70 kg. If it is assumed that the 32 mm diameter head made full contact, then the maximum pressure on the material is only approximately 1 MPa. This type of defect was found to be common in all of the specific type of acetabular cups retrieved.

The rest of the investigation concentrated on the wear debris found on the inside of the cups as well as the “pockmarked” bearing surface.

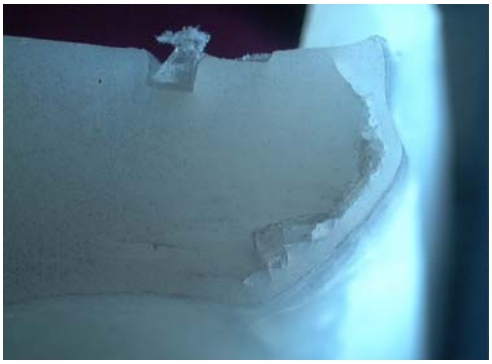

Figure 5.22: Magnification (x 10) of defect on rim of cup

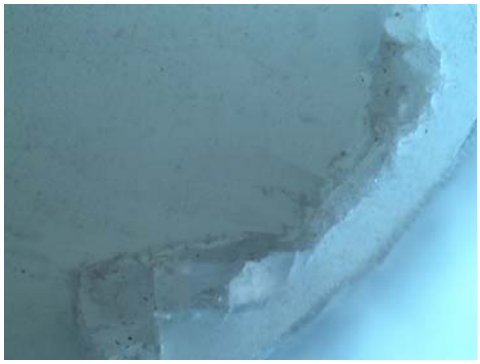

Figure 5.23: Magnification (x 20) of defect on rim of cup

As described in paragraphs 5.2 and 5.3, wear debris is normally seen just outside the bearing surface. Photographs as shown in Figures 5.24 through 5.27 were taken to show what the debris typically looks like.

Figure 5.24: Magnification (x 10). From this photograph the white irregular shape of material deposited is clearly visible

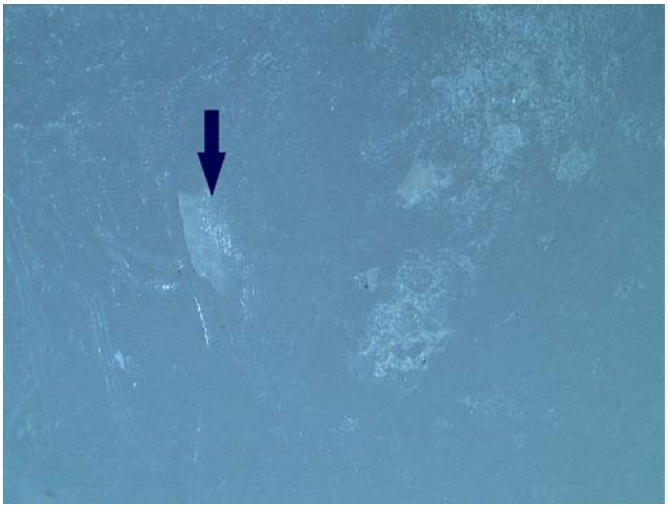

Figure 5.25: Magnification (x 20). The arrow points to a droplet of material which was either extruded from the bearing surface or was flattened after being ripped out of the surface

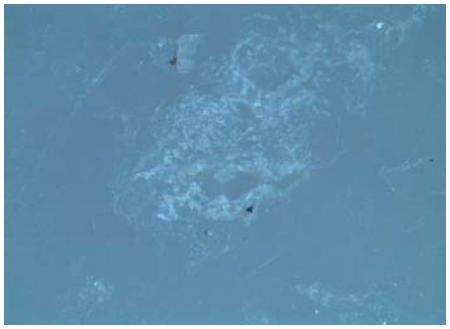

Figure 5.26: Magnification (x 20). The photograph shows softened/extruded debris with what looks like craters in between. Note the irregular shape of the deposit after being flattened by the ball.

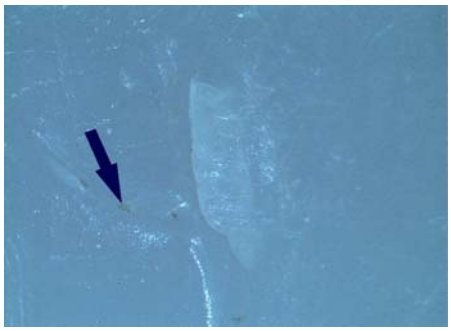

Figure 5.27a: Magnification (x 40): The results from Figure 5.25 are investigated further. It can be seen that the white piece of material appears not to have been totally removed from the base material, as there are no sharp edges on one side.

The indication is that material was extruded from the bearing surface. Some brown discolouring/deposit (indicated by arrow) can be seen in the grooves where material flowed over it. The schematic layout in Figure 5.27b shows a cross section of the described surface phenomenon.

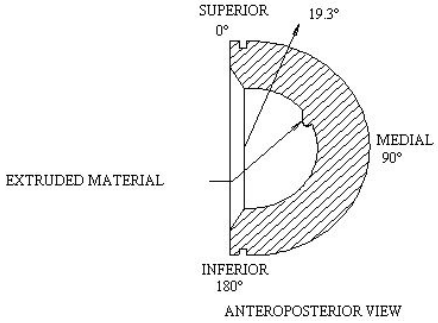


Figure 5.27b: Schematic of material extruded from the bearing surface

A further investigation was conducted into what looked like debris deposited on the bearing surface as shown in Figure 5.15. Under close examination with the stereoscope, it was found that the material was not deposited in these areas but that a skin or surface layer of the material was actually ripped off (see Figures 5.28 and 5.29). The machining marks are still partly visible. The extruded edges are also visible. Owing to the hardness and smoothness of the femoral head, these sheared off and flattened particles came loose, as was also found during the experimental tests. The debris showed up as a whitish deposit (see Figure 5.24).

Borne out by this study, is the resemblance between the wear pattern and the "butterfly" stress pattern as calculated and described by Wang et al. (1997) and Bennet et al. (1996), and shown in Figure 5.28.

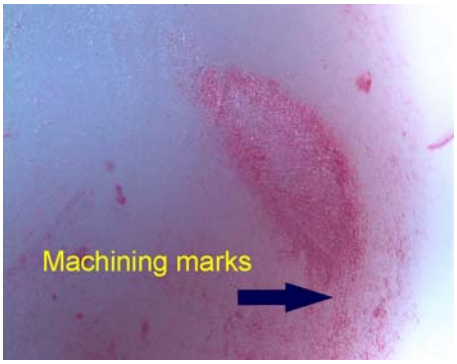


Figure 5.28: Magnification (x 20) of wear area on bearing surface

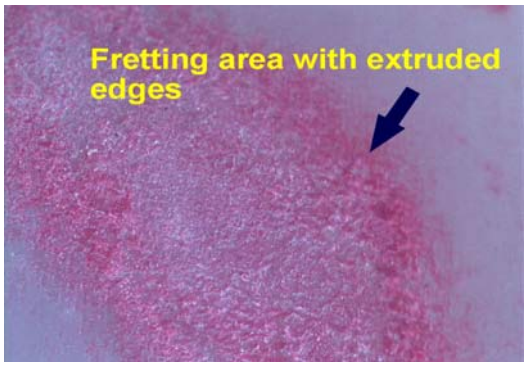


Figure 5.29: Magnification (x 40) of wear on bearing surface area

## 5.6 Electron microscope investigation

In some of the retrieved cups, a brown discolouration was visible, as noted in paragraph 5.2. What is very noticeable from the retrieved samples was that this discolouration again occurred just outside the boundary line of the bearing surface. The brownish discolouration was found attached to the polyethylene and could easily be scratched off. When investigated under a stereoscope no further detail could be detected.

The brown discolouring in the retrieved acetabular cups was then investigated under an electron microscope. This is shown in Figure 5.30. Under smaller magnification, the brown discolouring appears as tiles that are laid down on the polyethylene, while under higher magnification the structure of the brown discolouring is typically that of a protein, as shown in Figure 5.31.

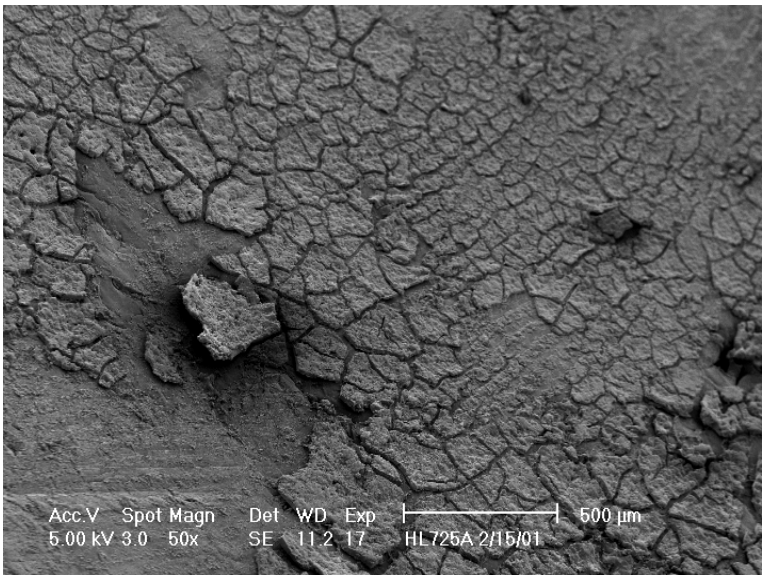


Figure 5.30: Electron microscope investigation of a brown layer on inside of cup (magnification x 50)

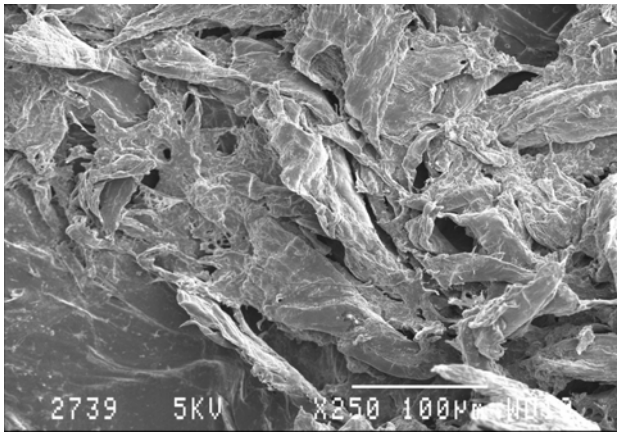


Figure 5.31: Electron microscope investigation of the brown layer on inside of the cup (magnification x 250)

As a first step in eliminating polyethylene as the observed texture, two samples were prepared of which one was deformed under compression, for investigation under the electron microscope (see Figures 5.32 and 5.33).

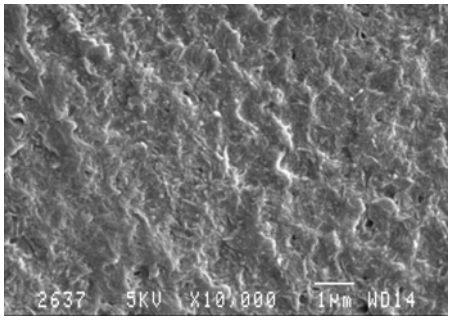


Figure 5.32: Electron microscope image of virgin UHMWPE sample (magnification x 10 000)

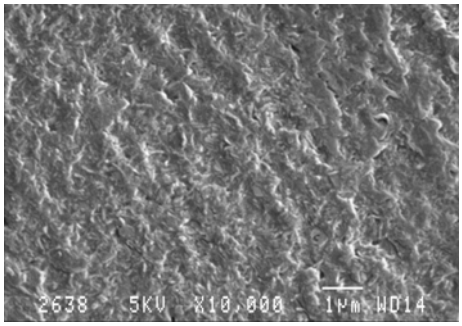


Figure 5.33: An electron microscope image of deformed UHMWPE (magnification x 10 000)

If the images in Figures 5.32 and 5.33 are compared, no difference can be seen between the virgin and deformed material, even under a magnification of 10000. The structure of the brown discolouring is totally different from that of the virgin or deformed UHMWPE and therefore the composition of the brown layer will have to be determined. (See paragraph 5.6.) The rest of the photographs for the electron microscope investigation into the brown discolouring can be seen in Annexure C and the photographs investigating the structure of UHMWPE can be seen in Annexure D.

To allow for smooth operation from the first day after implantation, the acetabular component is manufactured to allow for a maximum clearance of 0.5 mm on the diameter of the femoral ball. The allowance for the fit together with the angle at which the load is transferred into the joint results in an off-centre wear pattern as shown in Figure 5.34.

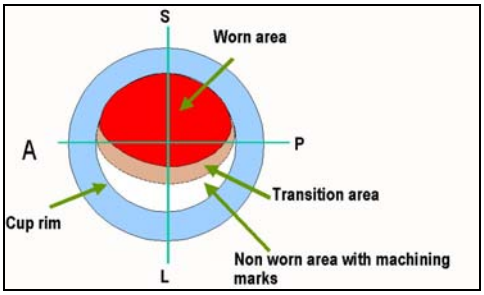


Figure 5.34: Anatomical cup orientation with position of worn area

The surface finish specified for manufacturing of the cups is 0.8µm. The result is a gramophone finish in the cup. This can clearly be seen in Figure 5.35 and with a larger magnification in Figure 5.36. This finish is independent of whether the cup is crosslinked or not, as the crosslinking is done as the final step in the manufacturing.

These machining marks with the accompanying polyethylene debris attached to them are now subjected to a fatigue loading when the joint is in operation. This dynamic loading causes a varying shearing action on the polyethylene, resulting

in the separation of the particles. A typical particle separated from the base material can be seen in Figure 5.37.

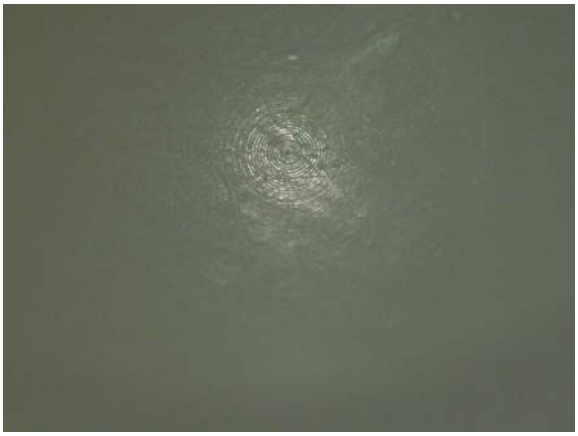

Figure 5.35: Machining marks visible in acetabular cup

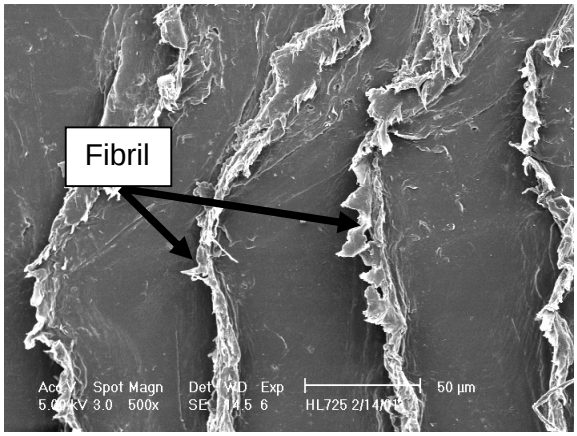


Figure 5.36: Machining marks on inside of cup (magnification x 500)

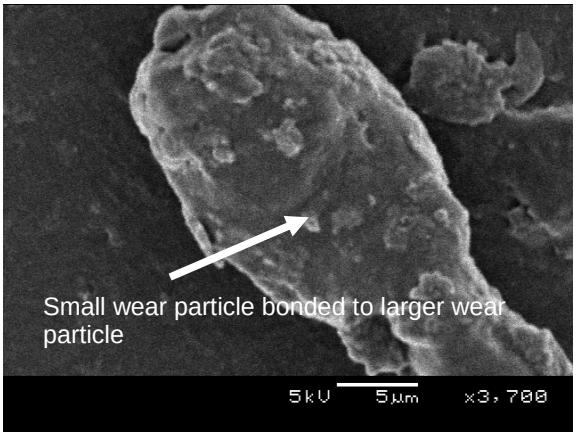


Figure 5.37: Wear particle entrapped in cup (magnification x 3 700)

These particles ripped from the base material, result in abrasion wear as can be seen in Figures 5.38 and 5.39.

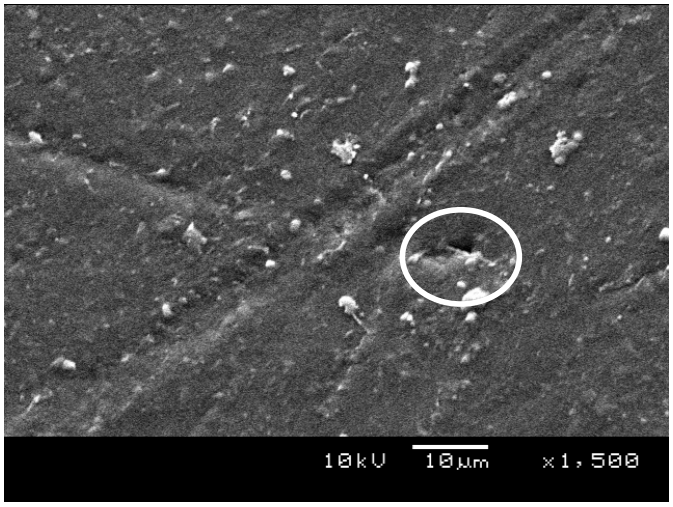


Figure 5.38: Surface of acetabular cup with scratches due to third-body wear (magnification x 1 500)

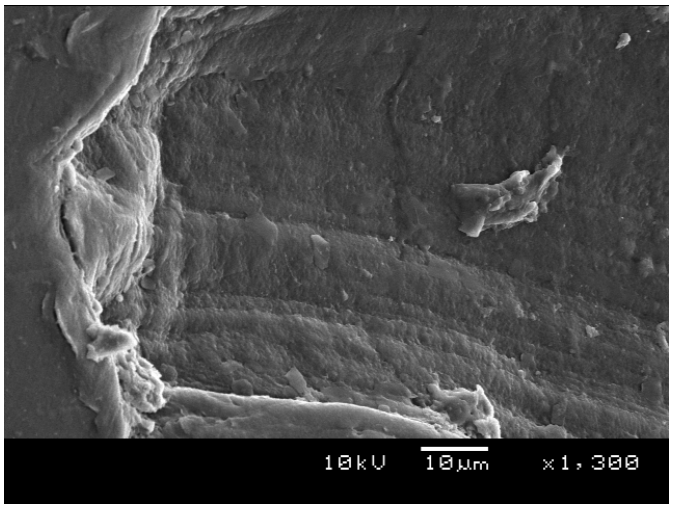


Figure 5.39: Abrasion wear on acetabular cup (magnification x 1 300)

To ensure that the scratches, as can be seen in Figure 5.38, were not a result of PMMA cement entering the bearing area, an electron microscope study with back scatter analysis was performed. In doing this analysis, the base material (UHMWPE) is compared with the particle lodged in the base material (encircled in Figure 5.38) at the end of the scratch to see if the particle is the same or if the

particle is from a different source. The result of this back scatter analysis can be seen in Figure 5.40.

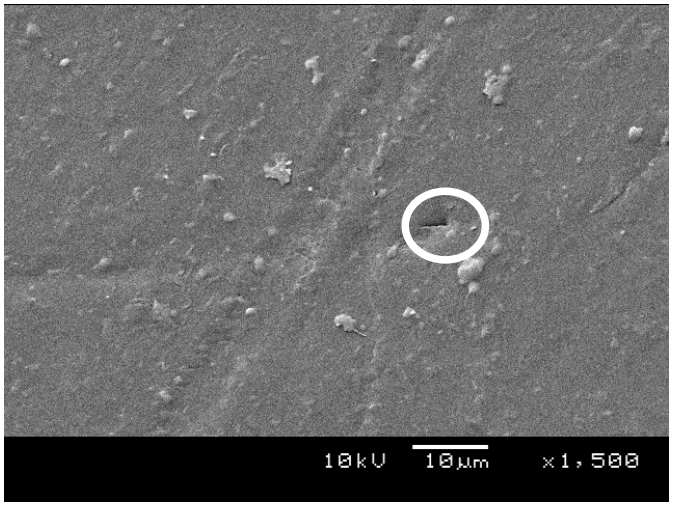


Figure 5.40: Back scatter analysis on wear particle lodged at end of abrasion wear in acetabular cup (magnification x 1 500)

From the back scatter analysis, as presented in Figure 5.40, in conjunction with a stereoscope investigation it can be concluded that the particle responsible for the abrasion wear as shown in Figures 5.38 and 5.39 was indeed an UHMWPE particle that was dislodged from the bearing area as foreign particles are now showing up in the abrasion area. In the area encircled in Figure 5.40, a cavity is also exposed penetrating into the acetabular cup. This type of cavity can create a stress raiser which can lead to early fracture of the acetabular cup.

A further analysis was done making use of the electron microscope. In Figure 5.41 an acetabular cup is shown with defects similar to the adhesion wear defects shown in Figures 5.28 and 5.29. The aim of this analysis was to gain a better understanding of the detail inside these adhesion wear areas.

Figure 5.41: Adhesion wear area in acetabular cup

The area as indicated in Figure 5.41 was cut out and gold-plated to be analysed in the electron microscope. The result of this analysis can be seen in Figures 5.42 and 5.43.

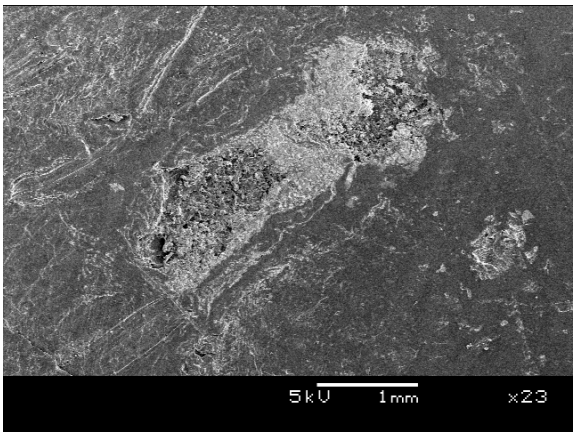


Figure 5.42: Electron microscope photograph of adhesion wear in acetabular cup (magnification x 23)

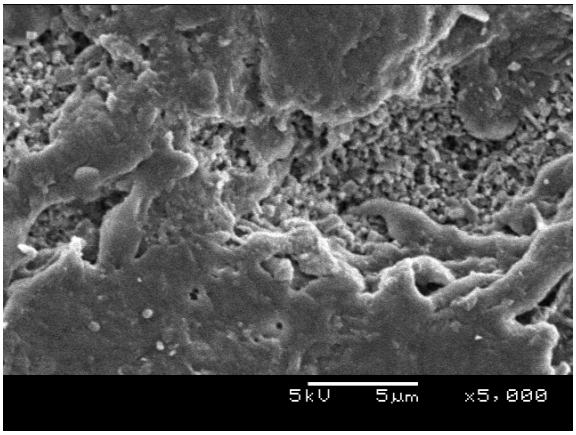


Figure 5.43: Adhesion wear area under higher magnification (magnification x 5 000)

From the data as presented in Figures 5.42 and 5.43, it is clear that the top layer of the material was ripped off by adhesion to the femoral head exposing the deeper part of the UHMWPE in the acetabular cup.

A second cup with a similar adhesion defect (visually) was also prepared for analysis in the electron microscope. The basic adhesion wear can be seen in Figure 5.44 with a higher magnification shown in Figure 5.45. The black markings on the picture are placed there to enable quicker detection of the defect under the electron microscope.

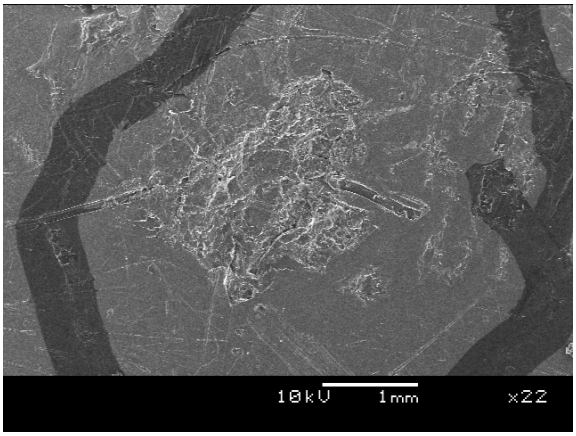


Figure 5.44: Adhesion wear defect under electron microscope (magnification x 22)

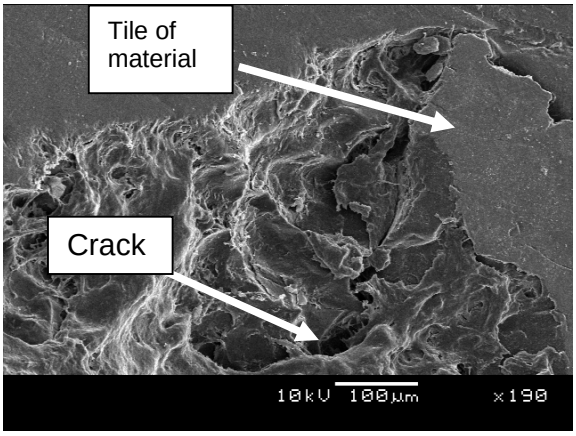


Figure 5.45: Adhesion wear under higher magnification (magnification x 190)

In the top right-hand corner of adhesion wear defect as presented in Figure 5.45 again it is clear that the top surface of the bearing area has been ripped off by adhering to the femoral head exposing the deeper part of the UHMWPE. It

would appear that the area was exposed by ripped-of tiles of UHMWPE. A tile at the verge of being dislodged is shown in Figure 5.45. Also visible in Figure 5.45 is the start of a deep crack propagating into the base of the acetabular cup. This crack will likewise create a stress raiser that may lead to early fracture of the acetabular cup.

During this investigation, areas where plastic flow of the base material had occurred were also exposed, as can be seen in Figures 5.46 and 5.47.

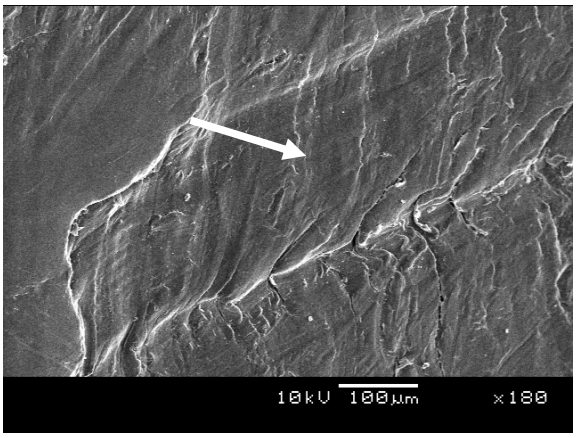


Figure 5.46: Acetabular cup with visible plastic flow on bearing area (magnification x 180)

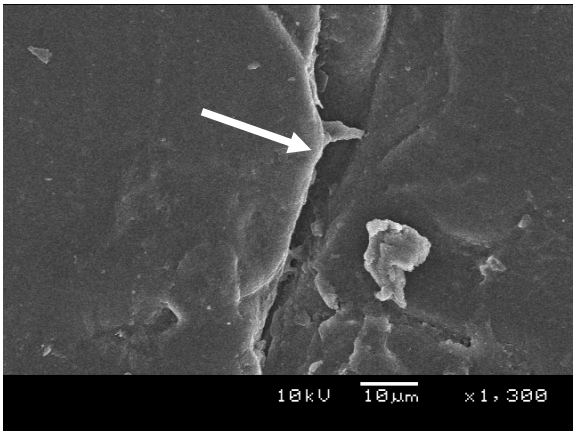


Figure 5.47: Plastic flow on bearing area under higher magnification (magnification x 1300)

The remainder of the pictures from the electron microscope analysis into the micro wear of the acetabular cup can be seen in Annexure E.

## 5.7 Electrophoresis

After reviewing the results of the electron microscope investigation it was decided to confirm the presence of proteins in the cup.

### 5.7.1 Method

Freshly retrieved cups were prepared by washing them with distilled water and then extracting the residue with an SDS-PAGE sample buffer, which is both a detergent and reducing agent for proteins. (http://www.ehime-u.ac.jp/~manabet/act01eng.htm; Rybicki & Purves, 1996). The samples were prepared within one hour after removal from the patients. During the preparation of the samples, it was already clear that there were proteins present as the SDS-PAGE buffer was cleaning off the brown discolouration. The samples dissolved with the SDS-PAGE buffer were then analysed by means of electrophoresis. (This work as well as the mass-spectrometric analysis was done by Mr Ben Mans of the Department of Biochemistry, University of Pretoria.)

### 5.7.2 Results

A sample of the results obtained for samples from the different acetabular cups, can be seen in Figure 5.48. Column 1 defines the markers to indicate the molar mass of the proteins. Column 2 is the analysis of a sample of synovial fluid retrieved from a patient. From the analysis of the fluid, it can be seen that there is a concentration of protein at 67 kDa as well as at 30 and 14 kDa. From literature (http://www.ehime-u.ac.jp/~manabet/act01eng.htm; Rybicki & Purves, 1996), it is found that the protein with a mass of 67 kDa is human serum albumen (HSA). Columns 3 to 6 give the results of the samples taken from a cup retrieved from a 72-year-old male patient eight years after implantation. This prosthesis was fitted with a 28 mm zirconium femoral head. Column 7 is a separator. Columns 8 to 12 represent the results obtained for a cup retrieved from a 42-year-old male

patient 4 years after implantation. This prosthesis was fitted with a 32 mm alumina head. From the results in Figure 5.48, it is clear that in both cases there is a presence of HSA, although the presence is not as marked as in the synovial fluid. A possible explanation for this is that the mechanism of lubrication in the cup is boundary lubrication and therefore the deposits detected were accumulated over a period of time.

From the relevant literature, it has been found that the denaturation temperature for HSA is between 333 and 343 K (60 - 70°C) (Sulkowska, 1997). The denaturation pressure for HSA at 25°C is 100 MPa. At a load of 4 000 N and with the femoral ball protruding 0.1 mm into the polyethylene the pressure on the contact surface is about 19.3 MPa, which is only 20% of the denaturation pressure. It is not clear what the relationship between temperature and pressure is when considering denaturation. This will have to be investigated in follow-up studies.

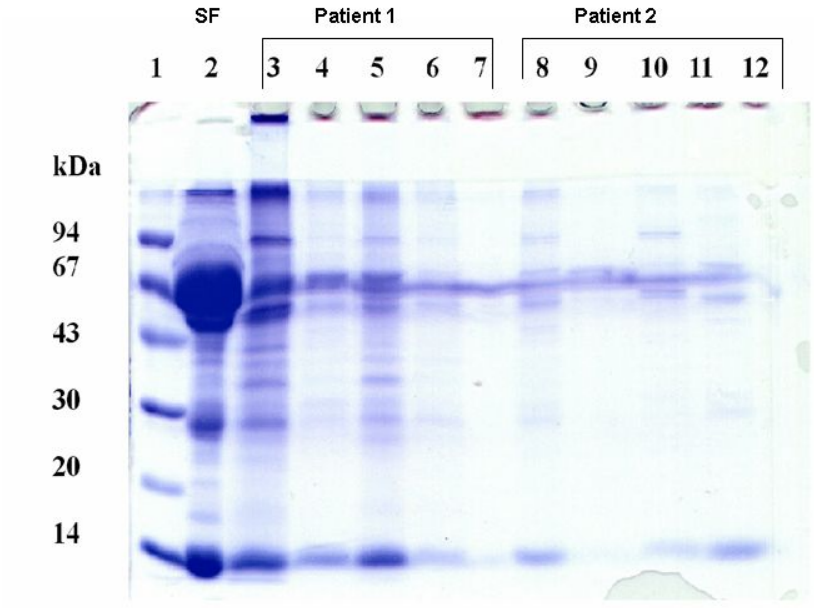


Figure 5.48: Electrophoresis analysis of synovial fluid and retrieved proteins from acetabular cups

The rest of the results can be found in Annexure F. The results indicate that proteins were deposited on the inside of the cups. Owing to deposited proteins, the coefficient of friction between the femoral head and the acetabular cup will probably increase, depending the percentage deposited proteins, resulting in more heat being released. Existing research has found that deposited proteins alone do not provide sufficient lubrication (Wang et al., 1998). These deposited proteins could possibly cause third body wear.

## 5.8 Mass-spectrometric analysis

Although it was not the aim of this study to determine the exact proteins deposited on the inside of the cups, it was still decided to do a mass-spectrometric analysis just to make sure that the brown discolouring that is visible is indeed protein-based.

### 5.8.1 Method

Mass-spectrometric analyses are done as follows:

1. A protein consists of a string of amino acids, coupled together in a chain with a specific sequence, for example:
   $NH_2$-A-N-D-C-P-E-R-G-T-Y-V-K-L-M-N-E-G-V-C-D-D-Y-E-K-CO-OH
   The left-hand side is called the N-terminal side while the right-hand side is called the C-terminal side (there is a free carboxyl acid group).
2. The above chain will have a specific mass which is determined as the sum of the masses of the different amino acids.
3. A specific enzyme is used to split proteins on a particular amino acid. The enzyme used during this test is tripsyn and it cleaves to the string on the C-terminal side of arginine (R) and lysine (K) that are both being positively charged amino acids.
4. If the protein, with an arrangement as in 1, is digested with tripsyn, fragments of each with their own unique mass will be formed, for example:
   a. $NH_2$A-N-D-C-P-E-R-COOH Mr~660 Da

b. $NH_2$-G-T-Y-V-K Mr~440 Da

c. $NH_2$-L-M-N-E-G-V-C-T-D-D-Y-E-K-COOH Mr~1430Da

5. Mass-spectrometric analysis only determines the masses of the generated peptides and with this example three peaks can be expected on positions 440, 660 and 1430.

6. Because each protein has a unique amino acid arrangement, it will result in unique fragments. Because tripsyn is also a protein, it can be digested into a specific fragment, and therefore a control experiment must be done.

### 5.8.2 Results

Five samples from the SDS-PAGE analysis were taken and put through the mass-spectrometric analysis. The result of one of the samples is shown in Figure 5.49. The rest of the results can be found in Annexure G. Two mass-spectrometric tests were done on each of the samples, explaining the first two lines on the graph. A control test was done for the tripsyn, as explained above. The tripsyn is represented by the third line (green) on the graph. In Figure 5.49, the tripsyn line must be subtracted from the two lines above. The presence of amino acid fragments (after subtraction) forming proteins can be seen. What is also clear from the five different graphs is that the protein deposits vary from patient to patient.

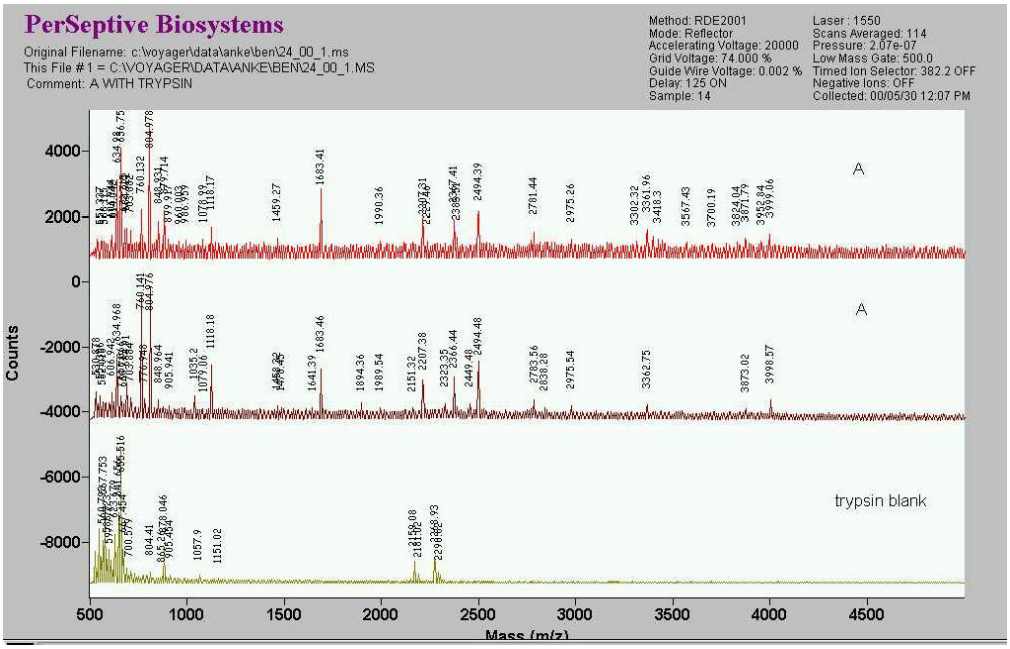


Figure 5.49: Mass-spectrometric analysis of a synovial fluid sample.

## 5.9 Analysis of wear particles from human tissue

The wear particles retrieved from tissue surrounding the prosthesis in-vivo, provided useful information regarding the mechanism causing the wear debris.

### 5.9.1 Method used

Ten prostheses were retrieved during revision surgery. Care was taken not to wash the retrievals during surgery. The main aim was to retrieve any loose wear particles attached to the retrieved implants. The retrievals were prepared in the laboratory by washing them down with distilled water. The water and all residues were captured in a beaker. The mixture of water and residue was filtered through a 0.45 μm filter. Throughout the literature (Claus et al., 2001; Dumbleton et al., 2002; Foguet et al., 2003), reference is made to wear particles of sub micron size leading to severe osteolysis. (See Chapter 2.) The filter size was chosen to ensure that wear particles larger than 0.5 μm will be isolated.

Tissue retrieved during the same surgical procedure was dissolved using caustic soda. The solution was left for a minimum of four hours to allow segregation to take place. The light polyethylene wear particles will float on top of the solution. The top layer of the solution was decanted and passed through the 0.45µm filters to isolate the wear debris.

The biggest challenge during this investigation was to see the wear debris under the microscope, as the filters are white and the wear particles are transparent, therefore it was difficult to see the wear particles on the filter material. A decision was taken to spray the filter material with dye penetrant. The penetrant will penetrate the filter material, colouring it pink. The wear debris is not porous and thus the penetrant will hardly have an effect on the wear particles.

### 5.9.2 Results

The microscope revealed particles with extruded edges, namely particles that became sufficiently plastic to allow extrusion of fibre-like particles from the base material under the prevailing pressure. The retrieved particles are shown in Figures 5.51 to 5.54.

The formation of the wavy edges can be compared to defects found in the extrusion of aluminium. (See Figure 5.50.) The temperature of the thinner material drops at a faster rate than the temperature of the material in the middle. When the material in the middle shrinks during the cooling-off process, the thinner material on the outside that has already cooled off is put under compression causing wavy edges.

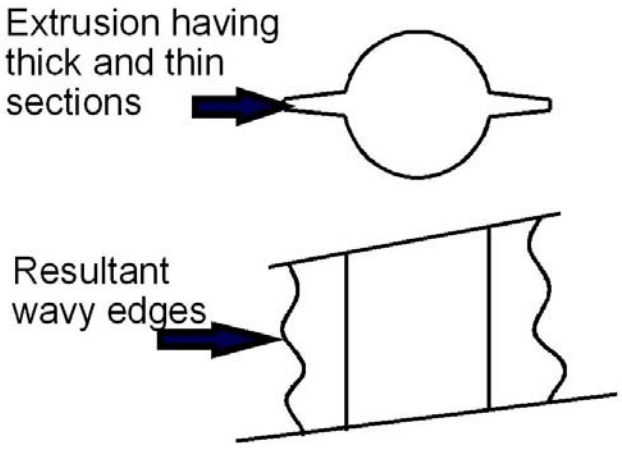


Figure 5.50: Schematic explanation of formation of jagged/wavy edges during extrusion

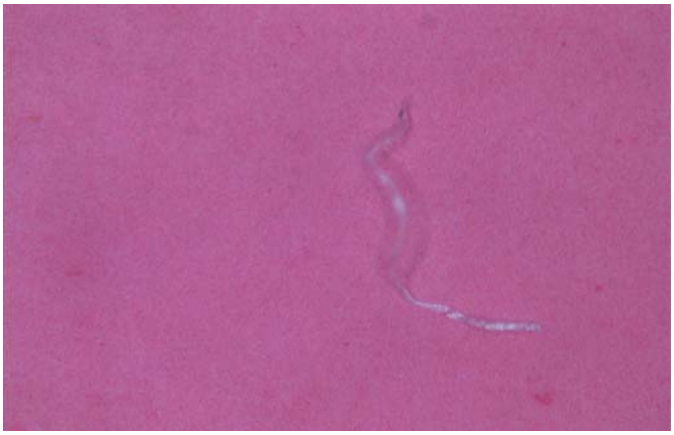

Figure 5.51: Particles retrieved from tissue (magnification x 40)

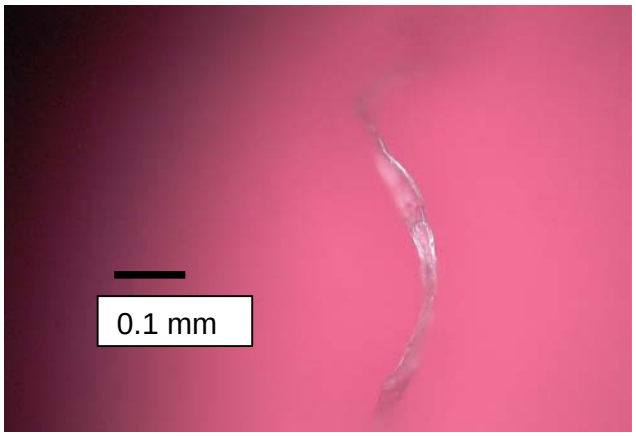


Figure 5.52: Retrieved particle (magnification x 100)

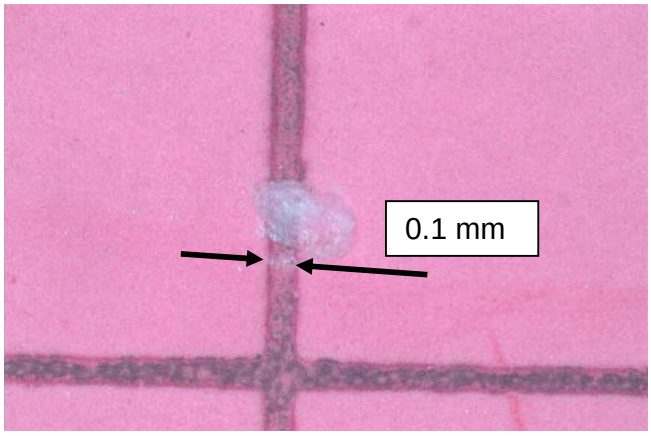


Figure 5.53: Retrieved particle (magnification x 40)

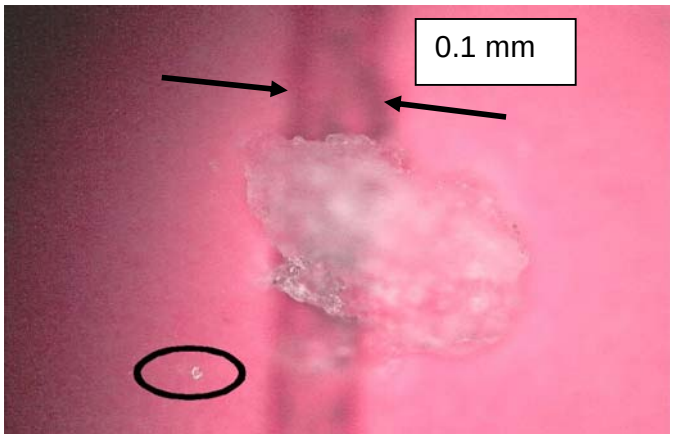


Figure 5.54: Retrieved particle (magnification x 100)

It should be noted that although particles smaller than 1 μm are also visible, the particles shown in the above Figures are quite large. The large particle in Figure 5.54 is approximately 0.3 mm long. The small particles look like droplets rather than products of normal wear. One of these droplets can be seen (encircled) in Figure 5.54.

The extruded whisker shown in Figure 5.52 is almost 0.6 mm long. The full whisker is not shown in the picture as it curves up and down on the filter paper and is therefore difficult to get in focus.

In the work done by Schmalzried et al. *(*1997) and Maloney et al. (1995), different techniques were used to retrieve wear particles from tissue. The

emphasis in these studies is to quantify the amount and size distribution of wear debris released. This was done in an attempt to determine the amount of third-body wear present in the joints. Photographs were taken of the debris. Although the photographs were taken of debris smaller than 1μm, the shape of the debris is exactly the same as found in the present study.

# CHAPTER 6
# FAILURE ANALYSIS OF RETRIEVED ACETABULAR COMPONENTS

## 6.1 Introduction

Detailed failure analysis of retrieved acetabular components to determine the root cause of failure provides the designer with invaluable information regarding the input to a new design of an acetabular cup.

In Chapter 5 the observations regarding 47 retrievals and the defects found were described. Various techniques were used to identify these defects and to determine the extent of the defects found. In this chapter, the cause of the failures present is discussed while the experimental verification of the stated postulate (paragraph 6.6) follows in Chapter 7.

## 6.2 Cracks in acetabular components

During the retrieval study various acetabular components with cracks in the base material were identified. The cracks appear in various locations within the cup, but the cracks fall into one of the following two categories, namely:

a. Cracks on the rim of the cup
b. Cracks inside the bearing area.

The failure analysis of the two different categories is dealt with separately.

### 6.2.1 Cracks on the rim of the cup

Various metal back acetabular components fitted with UHMWPE liners where cracks were visible on the rim of the cup were retrieved as shown in Figure 6.1. Apart from the cracks on the rim of the cup, delamination in

the area where the rim meets up with the body of the cup was also visible. This delamination varied from small localised areas to a single retrieved cup where this delamination was on the complete circumference of the cup. A cross section of a cup with this delamination visible is shown in Figure 6.2

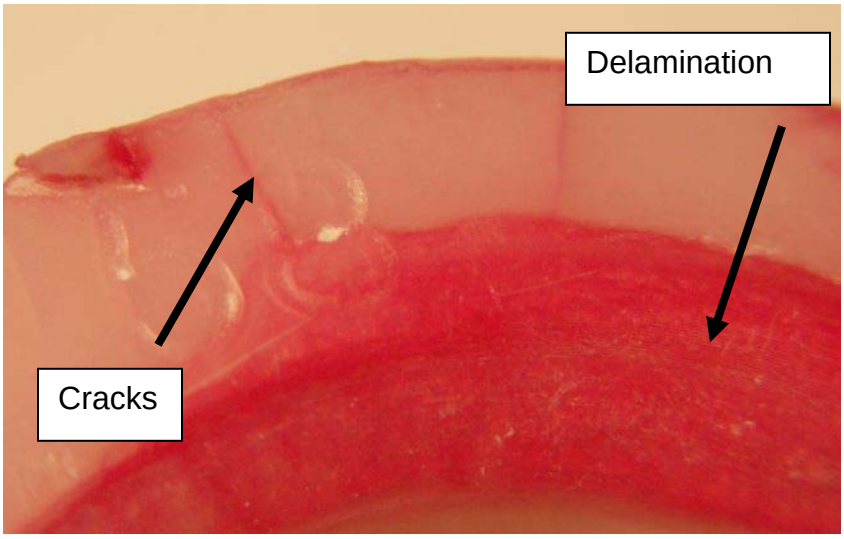


Figure 6.1: Metal back acetabular cup with cracks and delamination on rim of cup

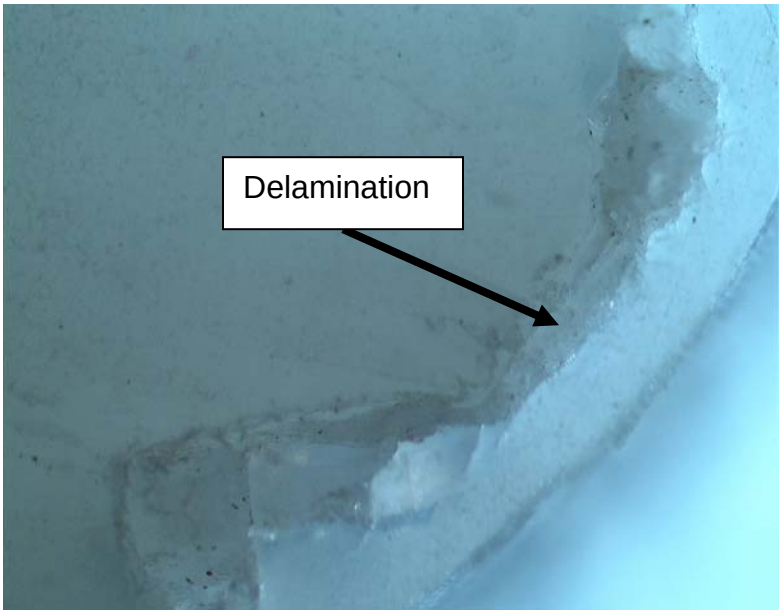


Figure 6.2: Cross section of acetabular cup showing delamination on the rim of the cup (magnification x 20)

This failure of cracks and accompanying delamination on the rim of the cup were only seen in metal back cups and also only in the metal back cups from one specific manufacturer. On closer inspection, it was noted that the UHMWPE liner does not fit snugly into the metal backing allowing the resultant forces in the hip joint to be transmitted into the pelvis via the rim of the UHMWPE liner only. This principle is schematically shown in Figure 6.3.

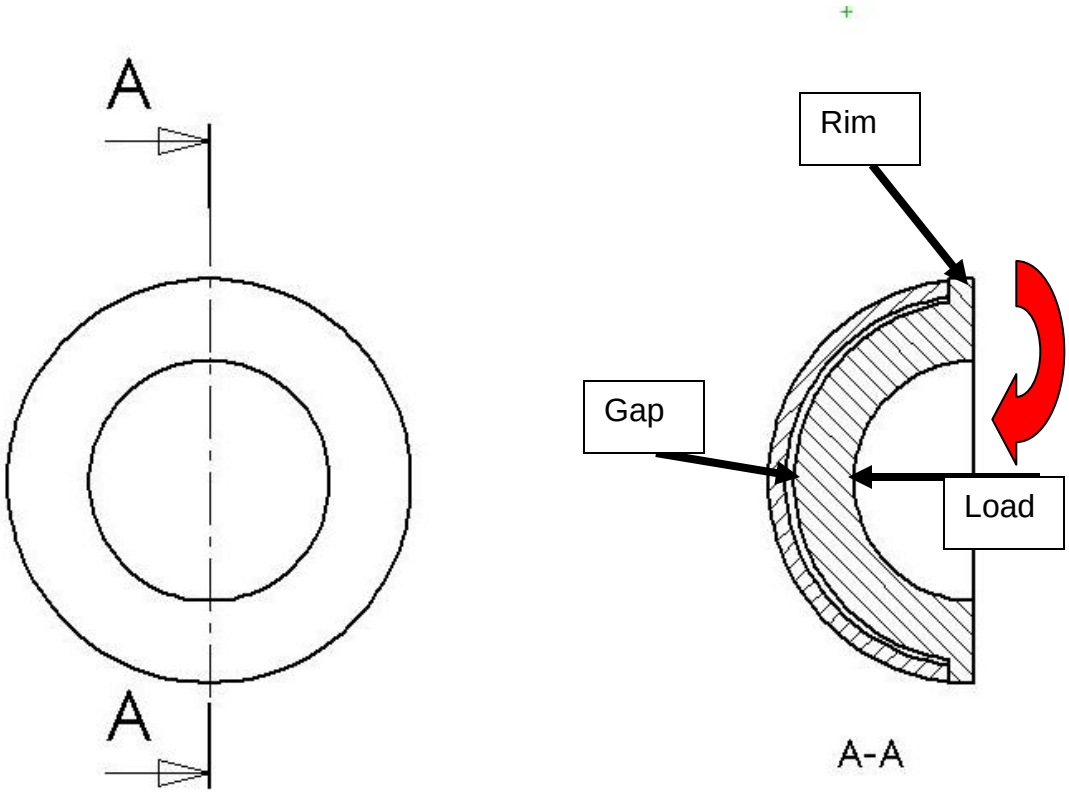


Figure 6.3: Schematic layout of UHMWPE liner not fitting snugly into metal backing

As can be seen from Figure 6.3, there is a small gap between the UHMWPE liner and the metal backing. The load coming into the bearing area will now deform the cup resulting in a bending moment with the corresponding bending stress in the rim of the cup. As the patient is walking, this load will vary according to the load profiles defined in Chapter

2 (Paul, 1976; Bergmann et al., 1993; ISO 14242-1, 2002), resulting in a dynamic load input into the rim of the UHMWPE that can lead to the fatigue failure that is manifested in the form of cracks and the delamination of the rim interface.

From the data presented, it can be accepted that this failure is due to an error either during the design or during the manufacturing process of the metal backing or the UHMWPE liner. As this defect is not a result of the wear mechanism active in-vivo, this defect will not be investigated further.

### 6.2.2 Cracks inside the bearing area

Cracks inside the bearing area can lead to the catastrophic failure of an acetabular component as can be seen in Figure 6.4.

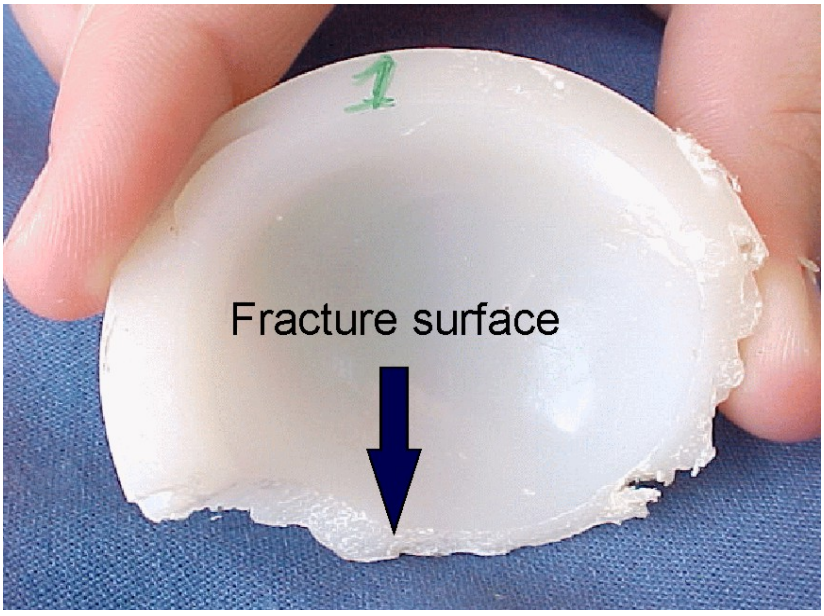


Figure 6.4: Acetabular component after catastrophic failure

From the data presented in Chapter 5 it is evident that cracks in the bearing area are fairly common as can be seen in Figure 6.5. On closer examination, making use of dye penetrant spray and the use of an electron microscope, the origin of these cracks can be established. The cracks originate in areas where severe adhesion wear has taken place. A

crack starting from an area of adhesion wear can be seen in the electron microscope picture as presented in Figure 6.6.

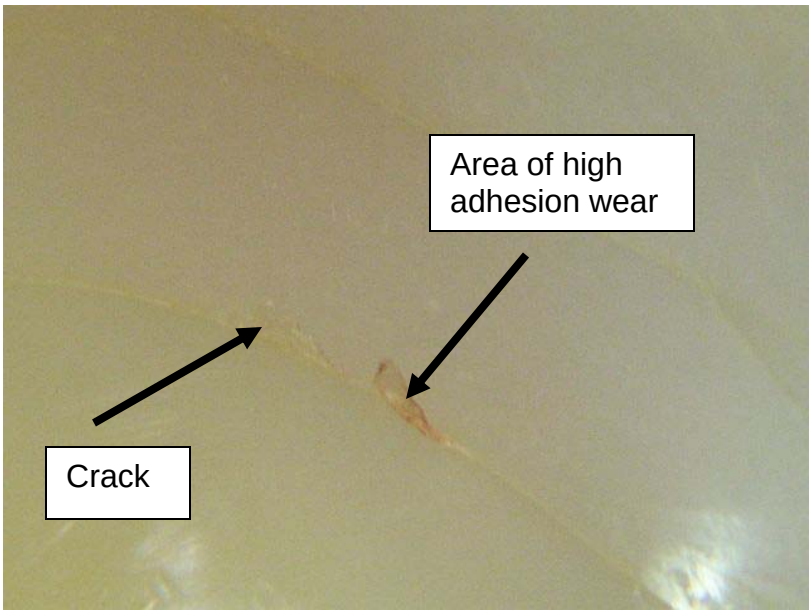


Figure 6.5: Crack on inside of acetabular cup

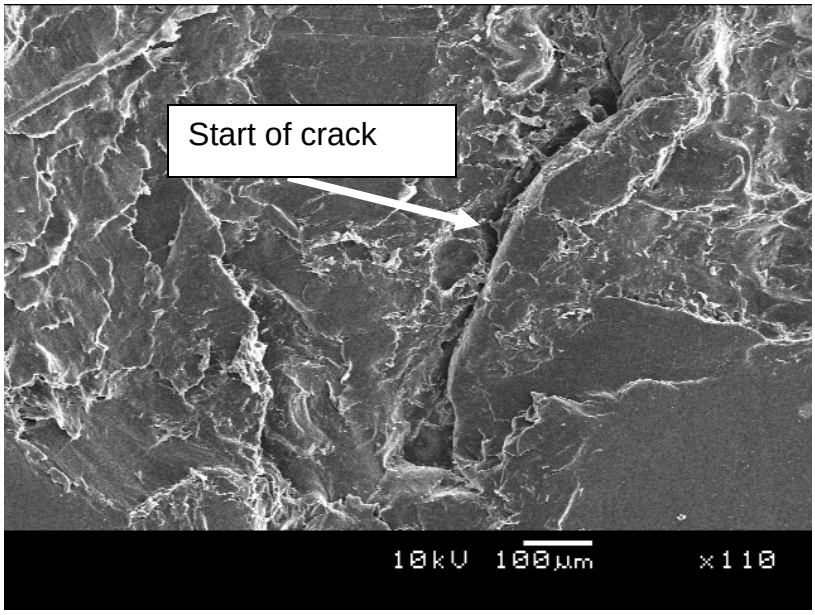


Figure 6.6: Electron microscope analysis of adhesion wear area (magnification x 110)

Under the electron microscope (Figure 6.6), it became clear that as the top layer of the material is being ripped away from the base material by adhering to the femoral head, craters are formed giving

rise to areas with high stress concentrations. A crater under the surface after the removal of the top layer of material can be seen in Figure 6.7. Under the dynamic loading conditions, these stress raisers will lead to the formation of long cracks, which can lead to catastrophic failures of the acetabular component.

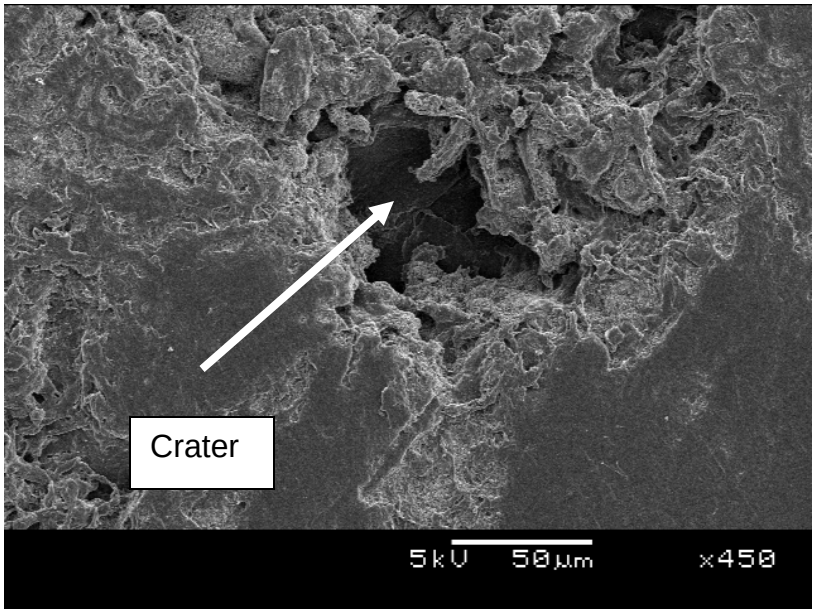


Figure 6.7: Crater under the surface after adhesion wear (magnification x 450)

From the data presented it is clear that the root cause for the formation of the cracks on the bearing area is the uneven removal of the surface of the bearing area by means of adhesion wear. This uneven removal will result in stress raisers in the form of craters which under the continuous dynamic loading will result in the formation of cracks.

It can be concluded that the cracks on the bearing surface are secondary to the formation of areas of uneven material as a result of adhesion wear. The formation of these areas is investigated further and will be discussed in paragraph 6.5.

## 6.3 Scratches

The scratches found on the bearing surface of the retrieved acetabular cups can again be classified into two categories namely:

a. Scratches caused by third-body wear particles

b. Scratches formed by normal UHMWPE wear products.

The failure analysis to establish the root cause for the formation of the scratches will be dealt with separately.

### 6.3.1 Scratches caused by third-body wear

The entering of foreign particles into the bearing is not that uncommon. These particles normally originate from the PMMA cement with which the implant is fixated. An acetabular cup with severe signs of third-body wear is shown in Figure 6.8. In this specific case glass ionomer cement was used for the fixation of the implant. This type of cement is no longer in use and has been replaced with PMMA cement.

Figure 6.8: Acetabular cup with severe scratches on inside

This type of defect is not a direct result of the active wear mechanism in the acetabular cup and is therefore not investigated further.

### 6.3.2 Scratches formed by normal UHMWPE wear products

In all the acetabular components retrieved, scratches as a result of the normal wear products floating around in the bearing area can be seen. The majority of these scratches are too small to see visually and it can only be seen under a magnifying glass. Throughout the literature reference is made to multidirectional fine scratches (Jasty et al., 1997; Schmalzried et al., 1999; Haraguchi et al., 2001), which are not easily visible to the naked eye. An acetabular cup with multidirectional fine scratches under a magnification of 20X can be seen in Figure 6.9. (Note that the machining marks are also visible in the Figure.)

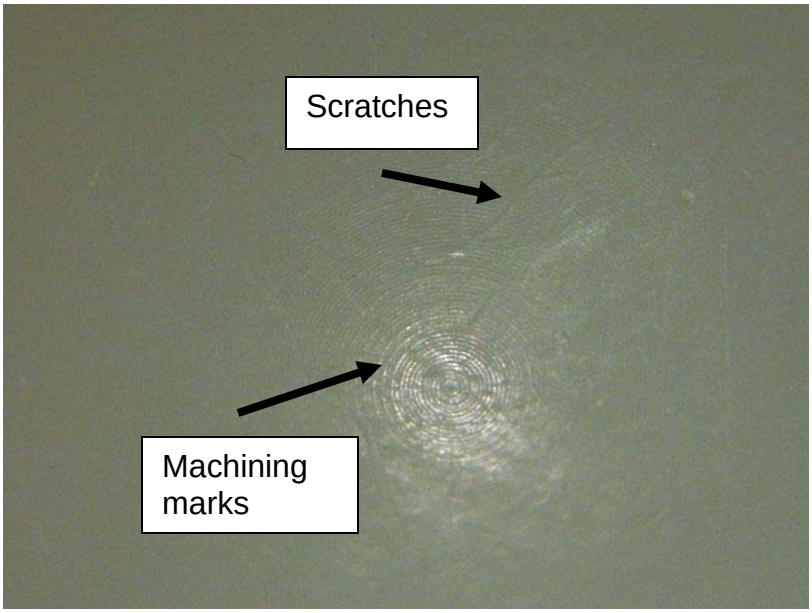


Figure 6.9: Acetabular cup with multidirectional fine scratches and with machining marks still visible (magnification x 20)

Scratches visible to the naked eye are also seen in some of the retrieved acetabular cups. When inspecting the acetabular components with a magnifying glass, treating it with dye penetrant spray and investigating under an electron microscope, the size and magnitude of these scratches become evident. The first impression is that this type of scratch must be the result of a third-body particle floating around in the bearing area. An acetabular cup with this type of scratch is shown in Figure 6.10.

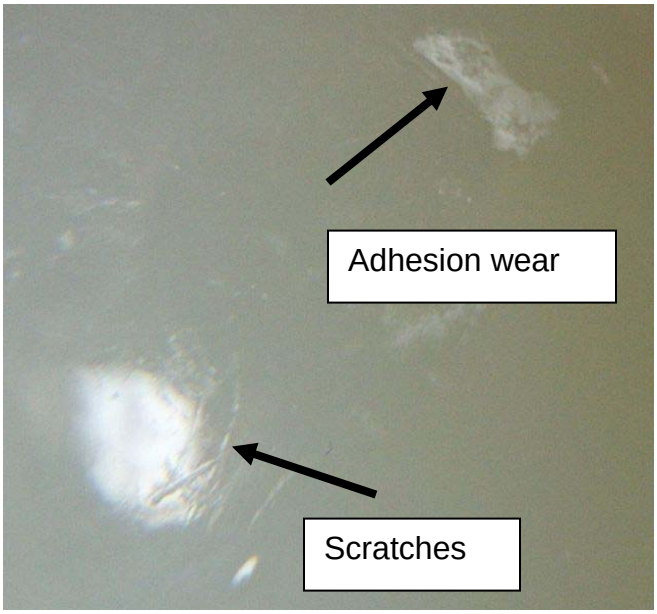


Figure 6.10: Bearing area with signs of large scratches and area with adhesion wear

Under the electron microscope, it is clear that these scratches are not fine, multidirectional scratches, but are scratches that had been formed by debris floating around in the joint. The scratches as indicated in Figure 6.10 under higher magnification in the electron microscope can be seen in Figure 6.11. The scratches have been encircled to facilitate the finding of scratches under the electron microscope. In the area of the scratches, a number of white dots are visible, which would appear as if they are pieces of PMMA cement that had entered the bearing area causing the resulting damage. In Figure 6.12, the path of one of these particles can be seen under higher magnification with the end clearly visible where the particle came to a standstill. The final path of the particle is visible in Figure 6.13 clearly showing the ploughing marks of the particle as it was destroying the bearing surface.

To eliminate PMMA as a third-body wear particle creating the scratch, a back scatter analysis was performed to establish the presence of any

foreign particle at the end of the scratch. The back scatter analysis is shown in Figure 6.14.

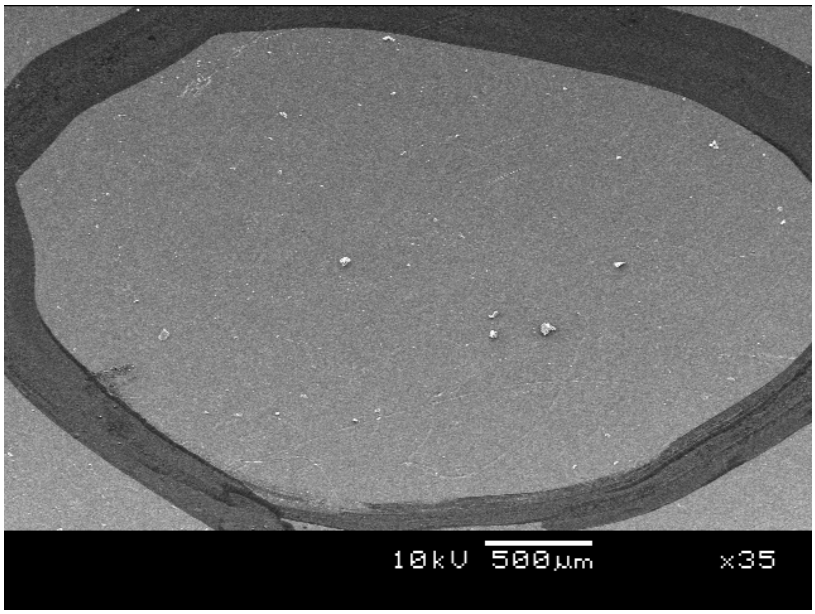


Figure 6.11: Scratches on bearing surface with white particles visible (magnification x 35)

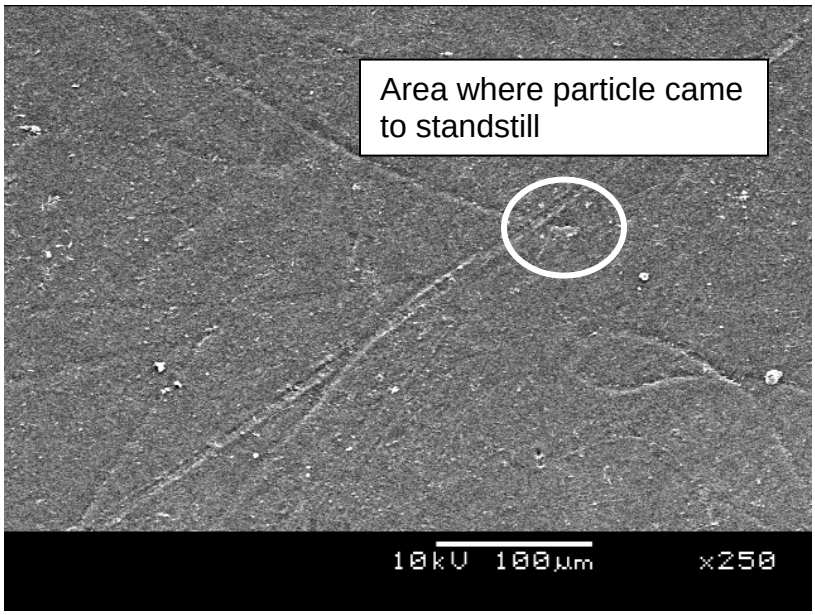


Figure 6.12: Scratch mark on bearing surface (magnification x 250)

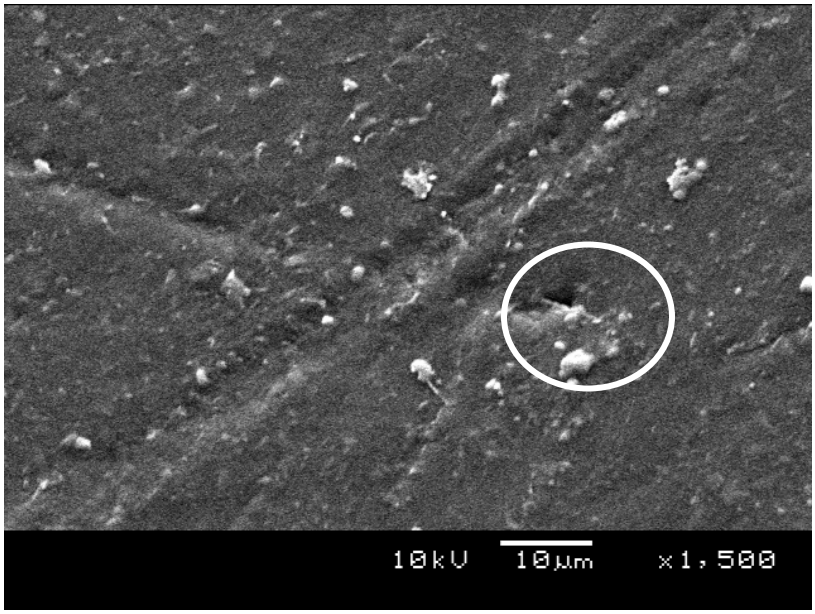


Figure 6.13: Final position of particle causing damage to bearing surface (magnification x 1 500)

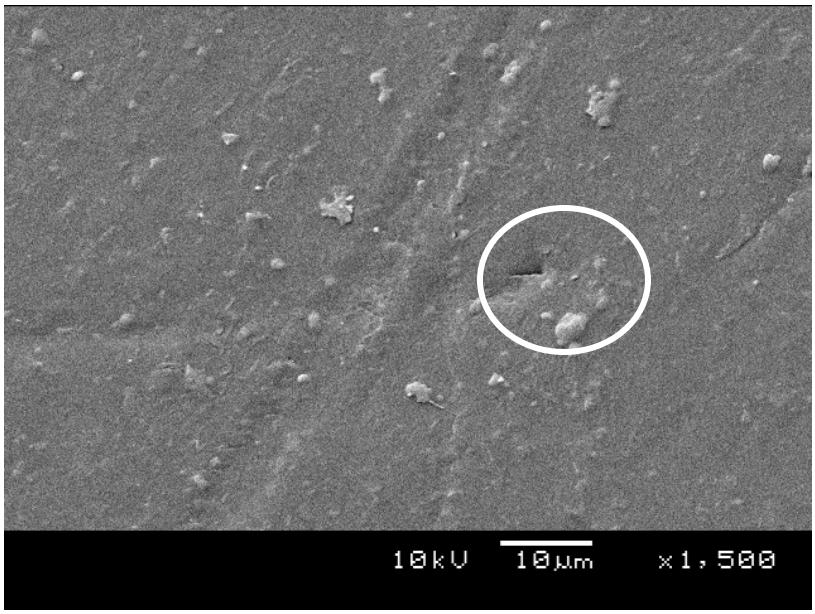


Figure 6.14: Electron microscope back scatter analysis of scratch (magnification x 1 500)

As the areas encircled in Figures 6.13 and 6.14 are compared, it is clear that there is no foreign particle present that could have caused the damage as seen. There is even wear debris trapped around the ploughing mark that is the same as the base material, UHMWPE.

A further analysis was done on another spot in the same acetabular cup as shown in Figure 6.15. This analysis was done closer to the area of adhesion wear. The main scratch can be seen in Figure 6.15 with the final damage enlarged in Figure 6.16.

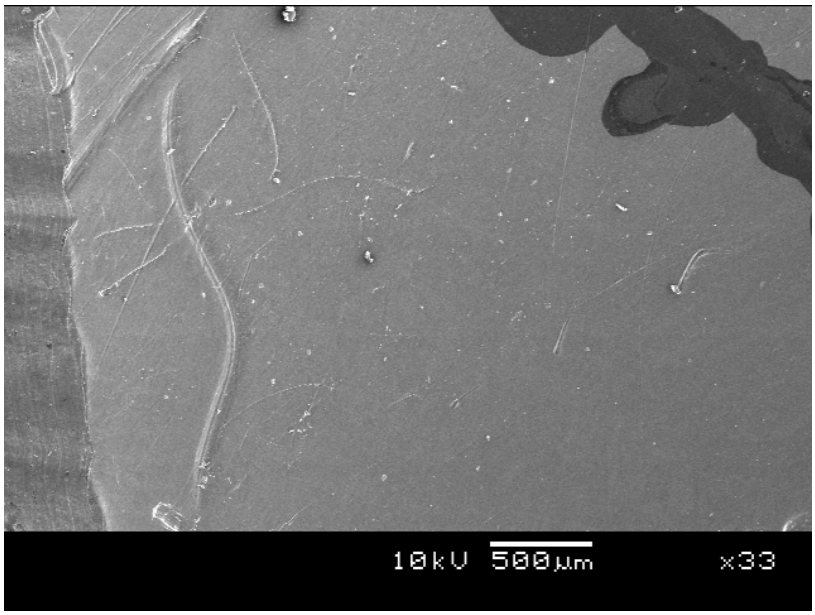


Figure 6.15: Scratch on bearing surface (magnification x 33)

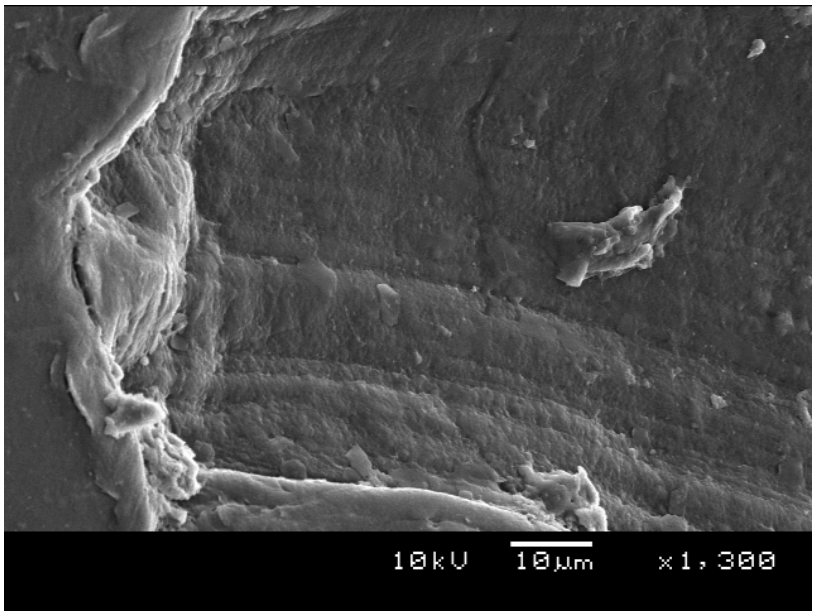


Figure 6.16: End of scratch on bearing surface (magnification x 1 300)

In both these scratch marks, the damage was not caused by a foreign body, but by a wear particle generated during the in-vivo use of the

implant. The conclusion can be drawn that no foreign body is present in the wear scar. When the damage to the acetabular cup is compared to the wear debris retrieved from tissue surrounding the joint, the resemblance is clear. Typical debris retrieved from the same patient can be seen in Figures 6.17 and 6.18.

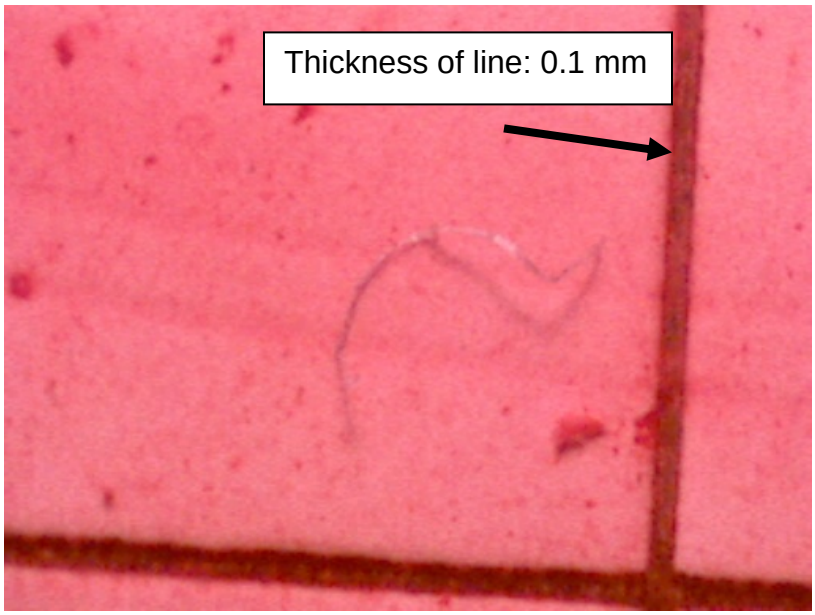


Figure 6.17: Whisker-like debris retrieved from patient (magnification x 20)

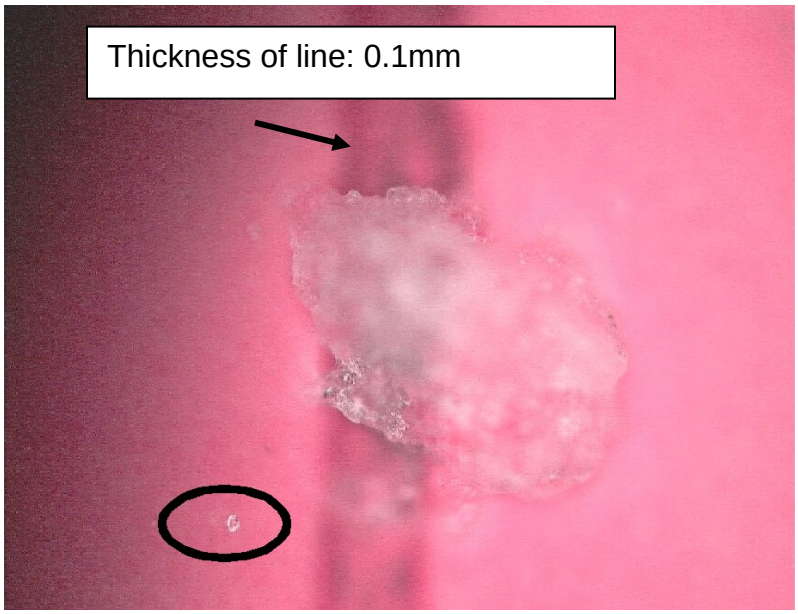


Figure 6.18: Debris retrieved from patient (magnification x 40)

The shape and the appearance of these items of debris suggest that both the whiskers and the droplets were formed under excessive heat conditions. From the literature survey, it was clear that for UHMWPE temperatures above 40ºC should be avoided, with short time (seconds) peak temperatures of 80ºC given by the manufacturers as the absolute maximum (Engineering Material Handbook 1987; Material data sheet, UHMWPE Poli HiSolidur 1999).

If the data obtained from the electrophoresis and mass-spectrometric analysis (Chapter 5) of the brown discolouration on the inside of the acetabular cups is taken into account, it can be concluded that during the in-vivo service of these implants temperatures of at least 60ºC were generated. It must be accepted that these high temperatures will only be generated in localised areas where the asperities due to machining are the highest. The complete acetabular cup will not be at this elevated temperature.

During the experimental phase of this study it has been proven that the type of damage as explained in this paragraph, with the accompanying wear debris, can only be generated if enough heat is applied under the prevailing pressure during walking to allow the extrusion of the whisker-like debris or the adhesion of particles to the femoral head.

## 6.4 Plastic flow

In the observations discussed in Chapter 5, areas of material that had plastically flowed under the prevailing pressure were identified. An acetabular cup with the type of plastic flow mentioned is shown in Figure 6.19. Under higher magnification, making use of the electron microscope, a number of these areas of plastic flow were identified. (See Figures 6.20 and 6.21.)

If the higher creep data at elevated temperatures (Chapter 3) together with the analysis of the brown discolouration is taken into account with the resulting conclusion of localised elevated temperatures, it is clear that the only way this type of plastic flow can occur is that the material at elevated temperatures is squeezed out of the high pressure area to an area of lower pressure.

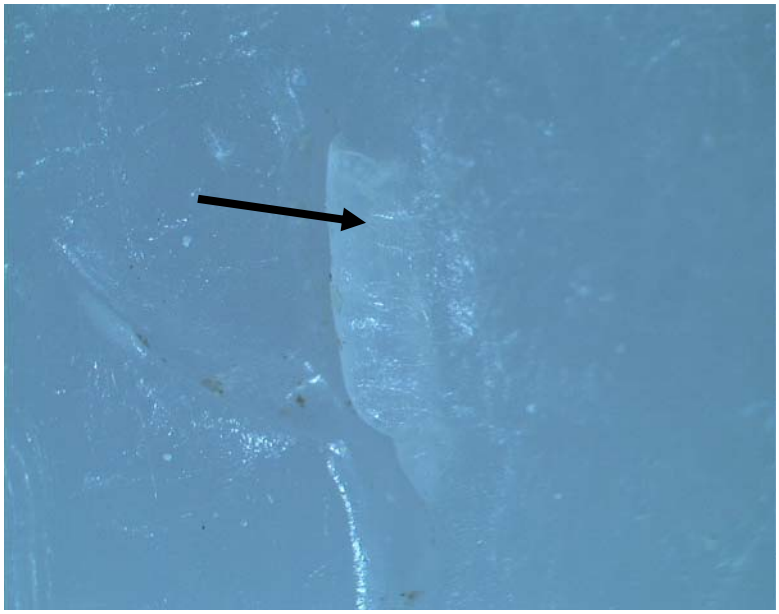

Figure 6.19: Plastic flow of material visible in cup (magnification x 10)

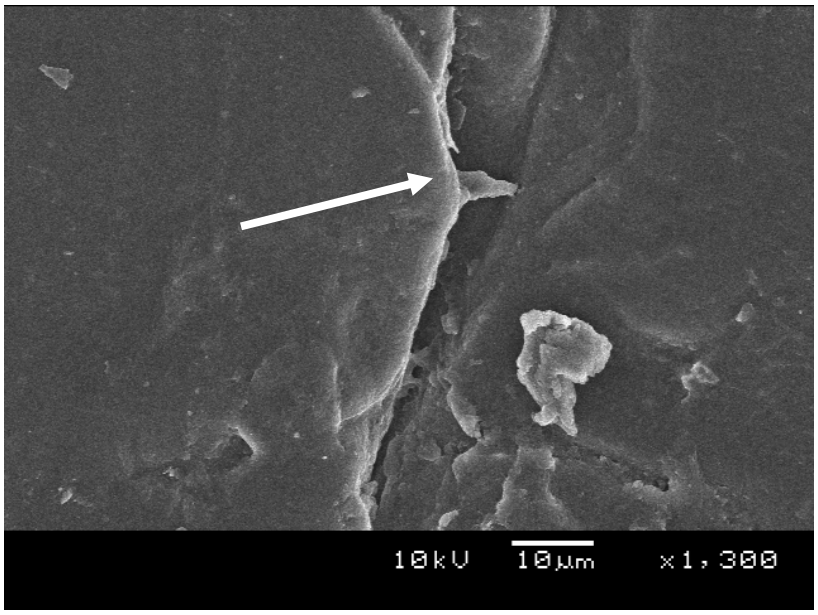


Figure 6.20: Plastic flow in acetabular cup (magnification x 1 300)

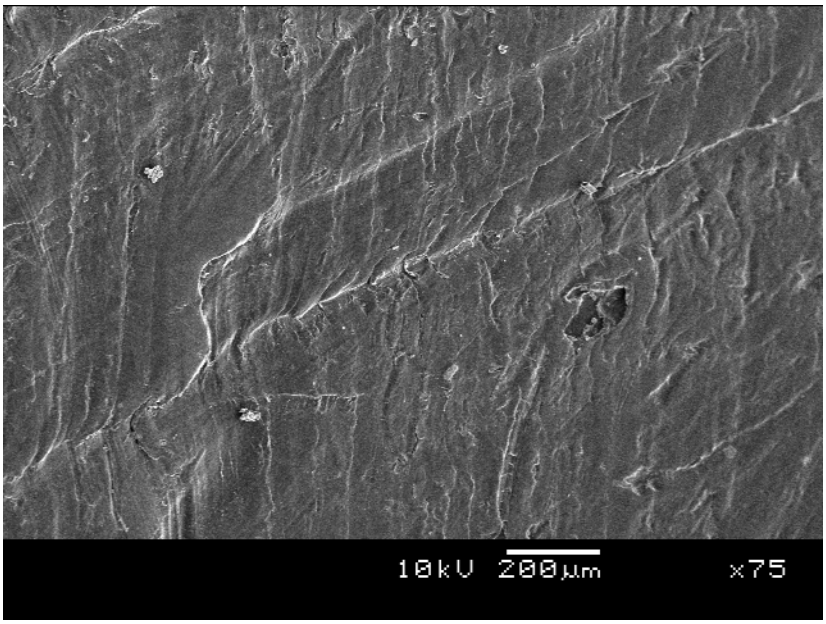


Figure 6.21: Area with plastic flow lines visible (magnification x 75)

During the experimental phase of this study, plastic flow similar to the plastic flow shown in Figures 6.19 to 6.21 was generated in the laboratory. It is shown that the only way to simulate this type of plastic flow under the equivalent prevailing pressure is at an elevated temperature.

## 6.5 Adhesion wear

In the observations done in this chapter, areas of adhesion wear were identified. These areas were first identified during the visual examination of the retrieved components as shown in Figure 6.22. When the components were treated with dye penetrant spray, these affected areas became clearly visible, as shown in Figure 6.23. The areas were characterised by a typical butterfly shape as described by Wang et al. (1997), where the surface of the bearing area seemed to be broken up. In some of the cups, the machining marks are also still visible under higher magnification, as shown in Figure 6.24. The edges of these areas are very rough and this is indicative of the temperature under which the removal of the material took place.

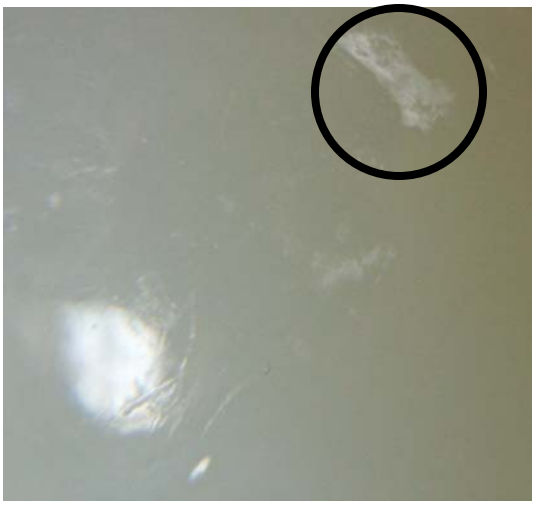

Figure 6.22: Visible adhesion wear in acetabular cup

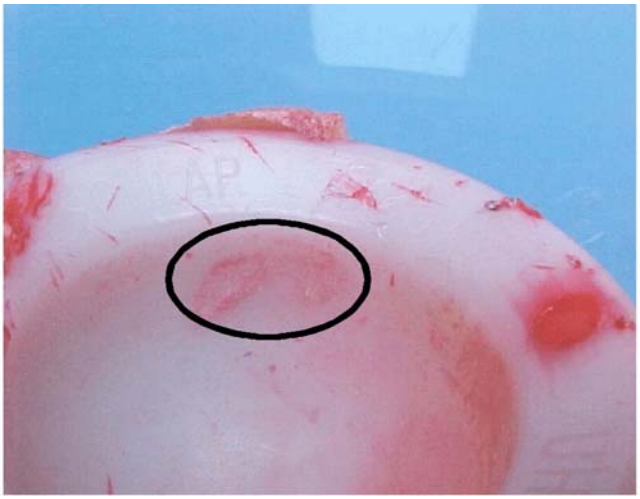

Figure 6.23: Butterfly wear pattern on inside of acetabular cup

Figure 6.24: Area with adhesion wear (magnification x 40)

The area with adhesion wear, as indicated in Figure 6.21, was then further investigated making use of the electron microscope. From the data obtained from the electron microscope, as presented in Chapter 5, it is evident that in this area adhesion of the material to the femoral head took place. The surface of the bearing was subsequently ripped, exposing the deeper part of the base material as is shown in Figure 6.25.

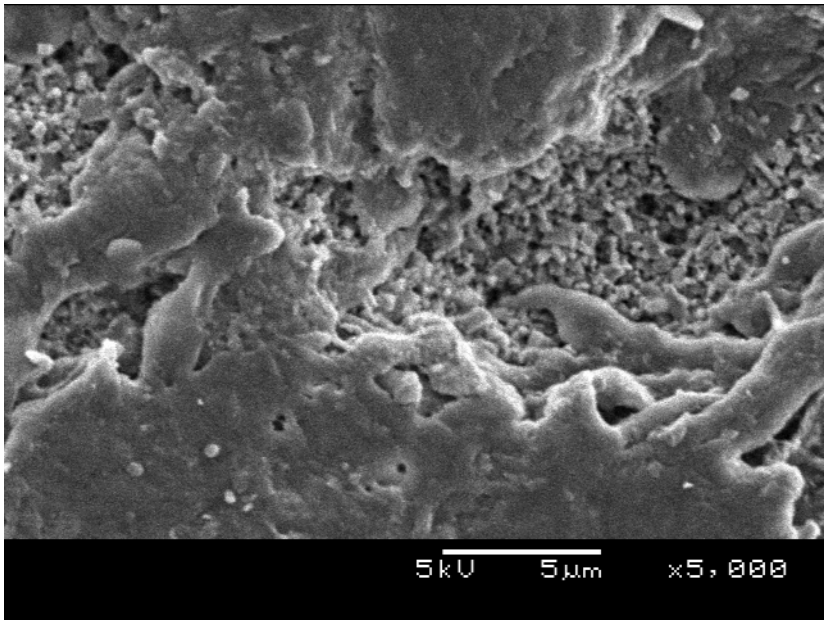


Figure 6.25: Area with adhesion wear exposing the base material of the acetabular cup (magnification x 5 000)

The typical particle that was dislodged from the bearing area is shown in Figure 6.26. This is also the type of particle that can result in the scratches, as shown in Figures 6.15 and 6.16. Examining the particle closely in Figure 6.26 actually reveals a number of smaller particles that were dislodged and is now adhering to the outer part of the bigger particle. The rest of the pictures can be seen in Annexure E. It must be noted that although the particle shown in Figure 6.26 was worked out of the high-pressure high-temperature area of the bearing, it was again attached to the base material when the pressure and temperature dropped sufficiently.

.

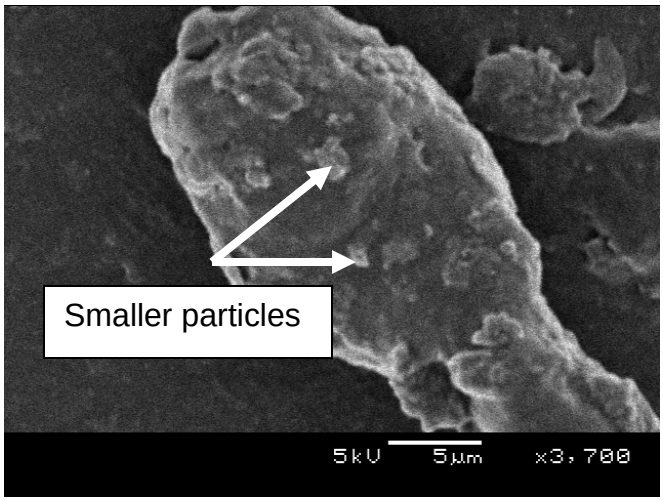


Figure 6.26: Wear particle with smaller particles attached to it (magnification x 3 700)

The mechanism for the formation of this type of particle can therefore be described as a snowball effect where the smaller particles, which were sufficiently softened by the prevailing head and pressure, adhere to the bigger particle as this was rolling or skidding along on the inside of the acetabular bearing.

A second type of adhesion wear was identified where the surface layer of the acetabular bearing is ripped off in what looks like tile-shaped wear debris, as shown in Figure 6.27.

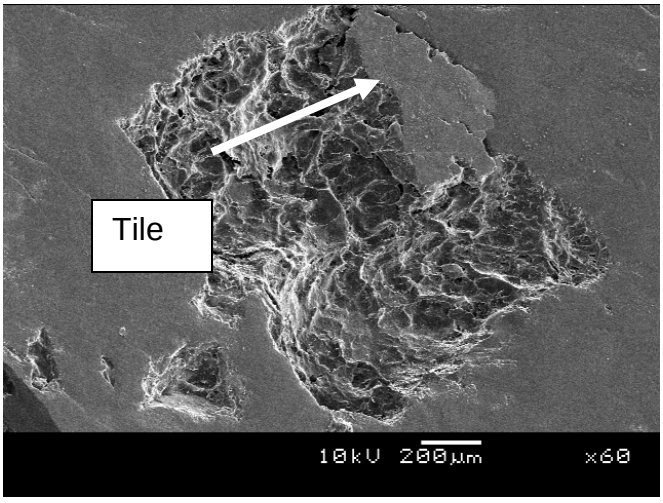


Figure 6.27: Area with adhesion wear (magnification x 60)

If the defect as shown in Figure 6.27 is investigated further under higher magnification, it appears that the tile, as shown in Figure 6.28, is almost completely loose and is only attached at the one corner. The moment this tile is dislodged, it will be wear debris that floats around in the joint area.

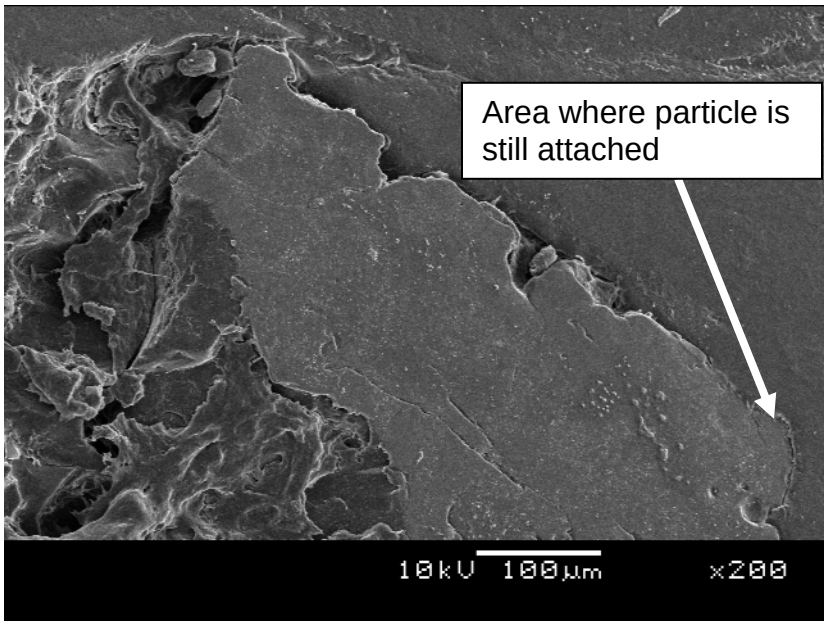


Figure 6.28: Adhesion particle about to be broken out (magnification x 200)

During the experimental phase (Chapter 7), this type of failure will be simulated in the laboratory, showing that the root cause for failure is due to excessive heat build-up on the bearing surface giving rise to adhesion of the surface layer to the femoral head.

## 6.6 Postulate for mechanical failure of acetabular cups

The shape of the particles as well as the shape of the small craters with the resulting scratches and plastic flow observed can readily be explained as follows: If the bearing load plus the rate of movement is not too high, the temperature will be relatively low and excellent bearing life will be obtained. The heat input into the bearing is determined by the product of load and speed (PxV) (Hutchings, 1992). If the PV value increases the

surface temperature at the point of highest loading increases accordingly. As the temperature goes up, adhesion between the femoral ball and the socket increases with a resultant higher heat input in the high-stress area. (See Figure 6.29(A).) A point is reached where the material has softened sufficiently and the adhesion has increased to the point where the bearing material is dragged along by the ball, in a similar manner to a wear particle being dragged along by a shaft in a rotating plain bearing couple. This leaves behind a crater, with the displaced material trapped between the cooler edges of the crater and the femoral head. Loading will flatten the material removed (see Figure 6.29 (B)) into a wafer with irregular edges as shown by the retrieved particles in Figures 6.26 and 6.28. If, on the other hand, a scratch exists under the wafer, there will be a tendency to extrude material along the scratch as a fibre or whisker as shown in Figure 6.17. It should be noted that the pressure in the wafer of removed material will be very high as the wafer will, in effect, be forced between the ball and the cup, effectively raising the ball relative to the cup with the load being mainly supported by the wafer. (Note that the flattened wafer can be forced into the bearing surface.) The particles will with time migrate through the bearing to the surrounding tissue.

A further aspect to consider is that after a crater has been formed, the edges of the crater will be bearing the highest load, as shown in Figure 6.29(C). The process described above will be repeated during the dynamic loading, with the result that the crater will grow in size and in depth, as is commonly observed in retrieved acetabular cups.

The rate of particle migration is expected to be very slow, because of the slow oscillating movement of the femoral head. It can also be seen from the experimental results (Chapter 7) that the coefficient of friction of the bearing as a whole is not affected by the presence of loose bits of bearing (UHMWPE) material on the bearing face. The difference in the coefficient

of friction was too small to measure with the existing techniques. The process described above must therefore not be regarded as rapid and catastrophic but rather as slow and eventually catastrophic. This is a slow process that is largely activated by high PV incidents.

Inadequate lubrication will accelerate the build-up of heat and therefore will accelerate the wear process. It is shown in the experimental work done on lubrication of the hip joint (Chapter 8), that the average lubricating capabilities of the synovial fluid retrieved from ten patients do not meet the standards of a basic lubricant. This lack of lubrication will definitely result in accelerated heat built-up on the bearing surface with the consequential damage as shown in Chapters 5 and 6.

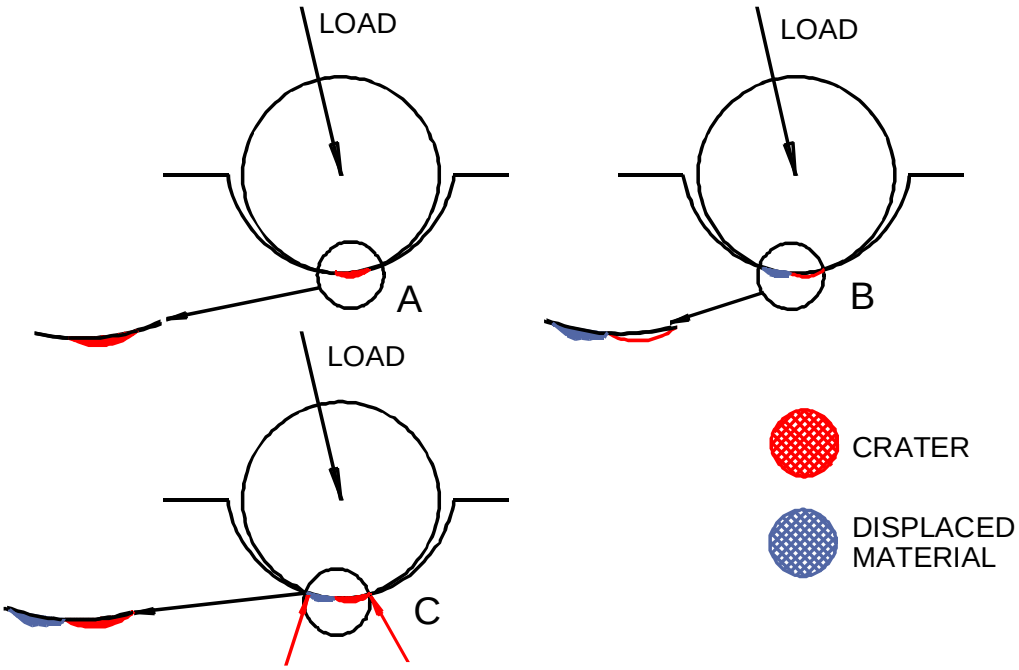


Figure 6.29: Steps in wear debris formation in acetabular cup

# CHAPTER 7

# EXPERIMENTAL VERIFICATION

## 7.1 Simulator studies

### 7.1.1 Introduction

The literature study (Chapter 2) and also the results of Chapters 4, 5 and 6, indicate that acetabular cups fail principally because of excessive wear. This wear can be classified according to different modes of failure. Various simulator wear studies have been completed by McKellop et al. (2000) and Clarke et al. (1996), during which wear rates were recorded. Some temperature recordings were also made to try to quantify the temperature in the joint. From the literature available, the finding is that the typical average wear of hip implants is approximately 35 $mm^3$ per year or 3.5 $mm^3$ per 100 000 cycles (Sychterz et al., 1996; Jasty et al., 1997; Buford & Goswani, 2004). (See paragraph 2.6, page 35.) However, simulator studies reported on in the literature surveyed make use of a common experimental technique, in that the cups were removed at regular intervals (500 000 cycles) during the tests to measure the wear rates and to clean the acetabular cups and holders. This practice is in accordance with ISO 14242-1 (2002).

Using the technique to remove the acetabular cup after every 500 000 cycles to determine the amount of wear creates three basic problems which are:

a. The wear debris formed during the test, in the joint, is gradually washed out with every cleaning cycle. Although the surface defect is still present, the effect is that the test is restarted with new lubricating fluid and that the cumulative damage due to the generated debris, if any, cannot be accounted for. It was shown in paragraph 6.2.2 that severe scratches became the result of

wear debris floating around in the joint area.

b. The material has an inherent plastic memory (Engineering Material Handbook, 1987). When the cup is removed from the simulator, it allows restoration within the plastic limit of the material. As indicated in Chapter 3, it was found that the creep of the UHMWPE should not be ignored. If the cups are removed from the simulator, the effect of cumulative creep is to some extent compromised.

c. The greatest problem with the technique of removing the acetabular cup to determine the mass loss is that the generated wear pattern in the acetabular cup cannot be aligned after disassembly. The net result of this is that every time the system is reassembled a new test is started.

McKellop et al. (2000) report temperatures as high as 90°C on the bearing surface in simulator testing. The bearing couple used was zirconium for the femoral head and UHMWPE for the acetabular cup. As the temperature was measured inside the zirconium femoral head, it should be remembered that the heat transfer coefficient of zirconium is so low that it can be regarded as a super isolator (k = 0.0152 $W/m^2K$). The measured temperature was then extrapolated by means of a finite element analysis to a temperature below the surface of the ultra-high molecular weight polyethylene (UHMWPE). This is not a true reflection of the highest obtained temperature on the contact surface. Owing to the difference in heat transfer coefficients, the heat flux through the UHMWPE is much higher than through the zirconium. The temperature in localised areas can rise as high as 90°C to 100°C, but the average temperature on the bearing surface will not reach these values, otherwise the bearing will collapse.

To provide answers to the abovementioned aspects, a five poster hip

simulator was built in which acetabular cups could be mounted and tested.

The main aim of the experimental verification during the course of this study was:

a. To deal with the deficiencies in the ISO procedure (ISO 14242-1 (2002)) and
b. to determine the effect of localised heat build-up on the bearing surface.

### 7.1.2 Design of a simulator

Simulators described in the literature, as discussed in Chapter 2, paragraph 2.10, are all hydraulically actuated with obvious advantages in flexibility, but with a high cost factor. It was decided to design a simulator where load is applied mechanically. A swing-over arm provides the necessary movement. The final concept decided upon can be seen in Figure 7.1. The basic layout of the machine is shown in Figures 7.2a and 7.2b. The basic principle is that the swing-over-arm has a length of 1 000 mm while the stem onto which the ball is mounted has a length (radius) of 300 mm. This means that when the swing arm moves through an angle $\theta$ by means of the crank, the stem moves through an angle of +30° and -30°. As the stem moves through the zero position, the cup is depressed 28 mm. The springs (Figure 7.4) on which the cups rest were designed to deliver a resisting force of 1500 N at 30° and 4000 N at 0°. This is representative of the forces on the hip during walking and corresponds to a walking speed of 6 km/h as measured by Bergmann et al. (1993). (See Figure 7.3.)

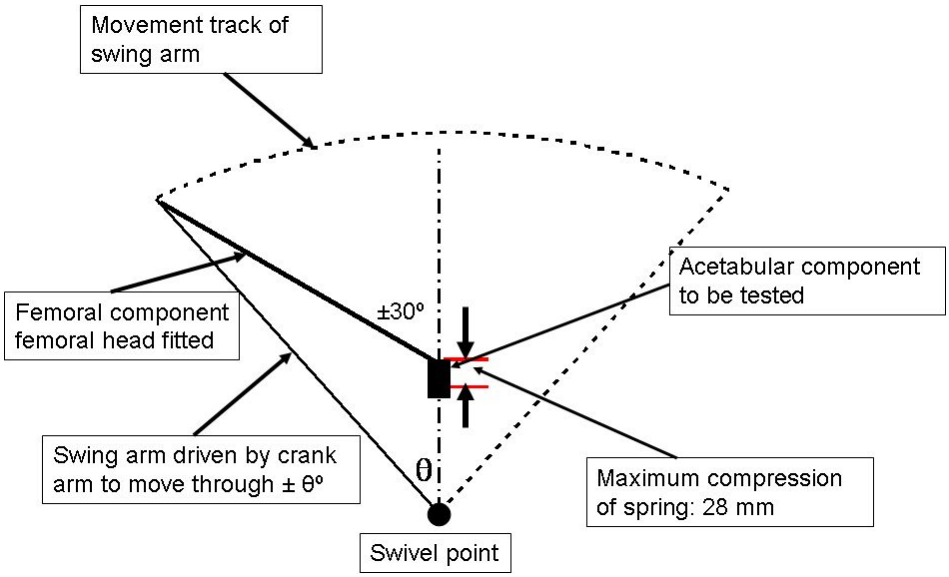


Figure 7.1: Concept for simulator movement

Figure 7.4 shows the achieved movement. The recorded force data was obtained from strain gauges mounted on the neck of the femoral stems. (See Figure 7.9.) These strain gauges were also used to set up the simulator, and to monitor the movement of the machine and determine the limits as to when to stop the machine if something should fail. A limit value of ± 5% of the applied load was decided upon. The stiffness value used in the design of the spring was 105 kN/m.

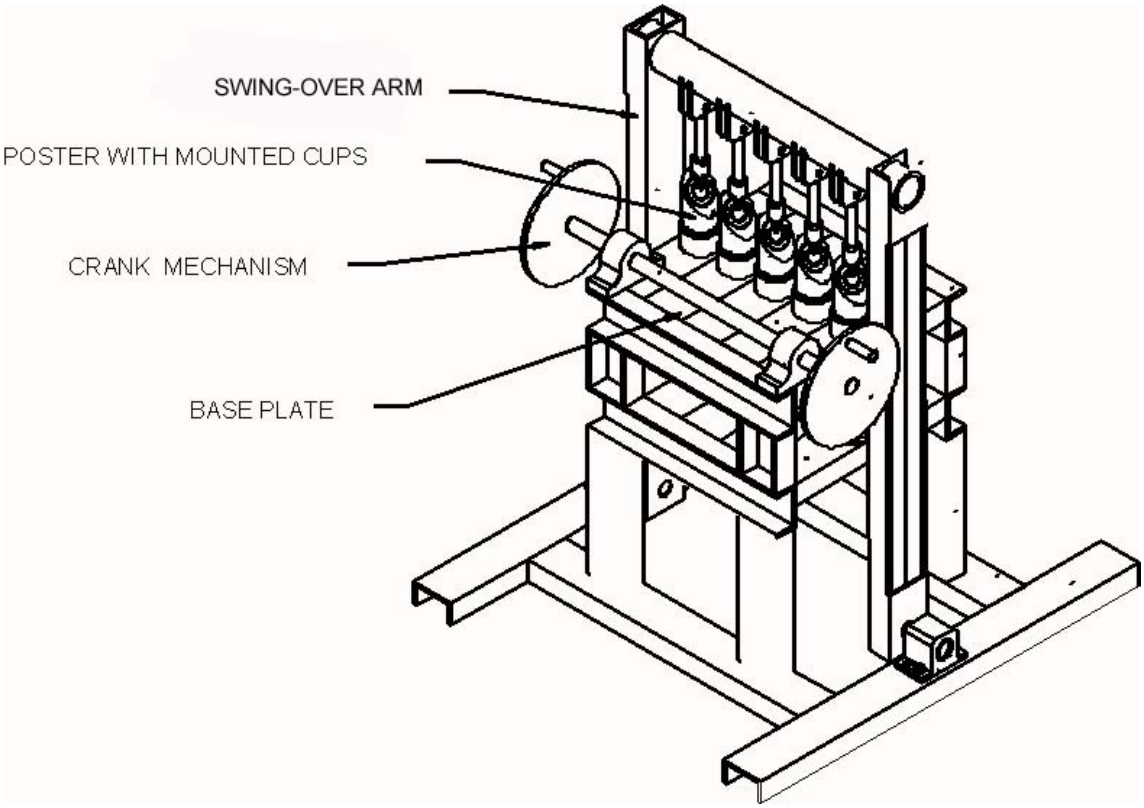


Figure 7.2a: Schematic layout of the simulator

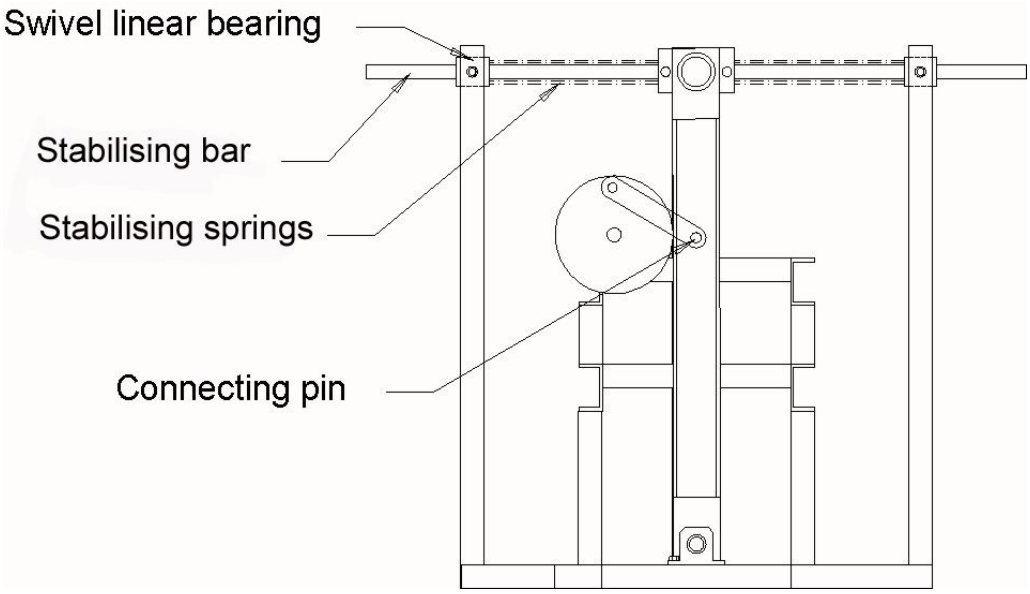


Figure 7.2b: Schematic layout of the simulator: Side view

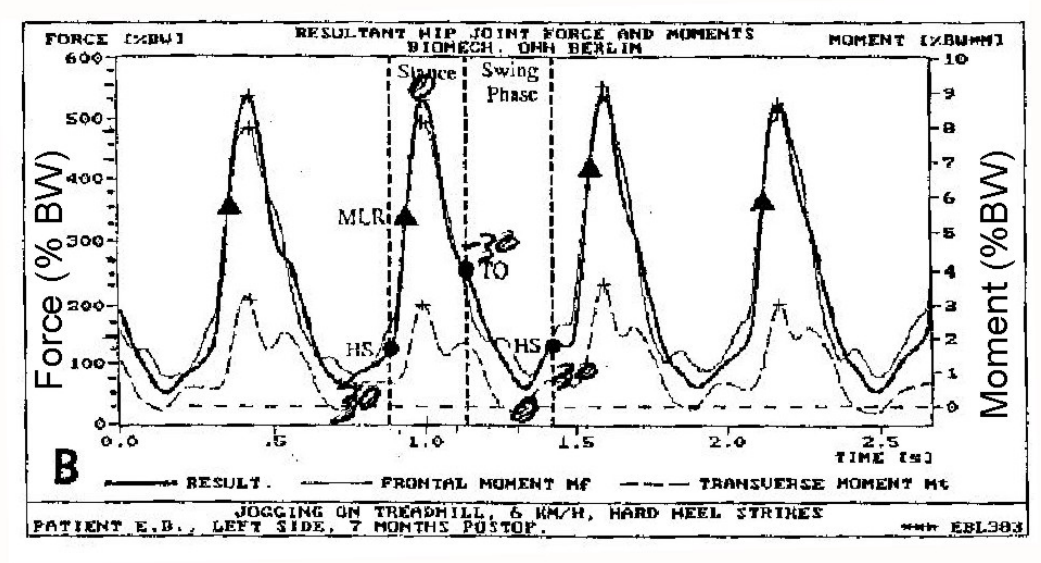


Figure 7.3: Hip movement as measured by Bergmann et al. (1993)

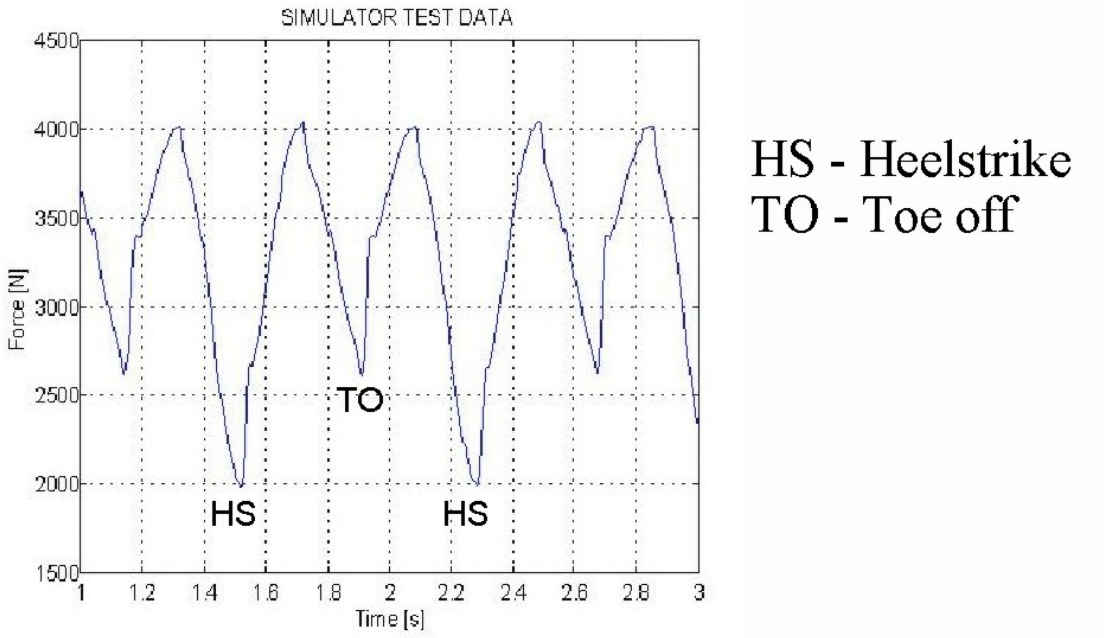


Figure 7.4: Recorded force/time graph of the simulator

The springs were manufactured and then calibrated to achieve the required stiffness for each spring. In the design of the simulator, provision

was made for an adjusting plate (Figure 7.5) on which the springs are mounted. The purpose of these plates is to permit final adjustment after assembly to ensure an exact and equal loading on each post. Top dead centre is taken as the zero point. The swing-over arm is driven with an electric motor via a crank mechanism as shown in Figure 7.2. Also shown are the stabiliser bars mounted at the side, fitted with two springs on two corners to smooth out the high accelerations at the end of each cycle. (See Figure 7.6 for a photograph of the stabilising spring assembly.)

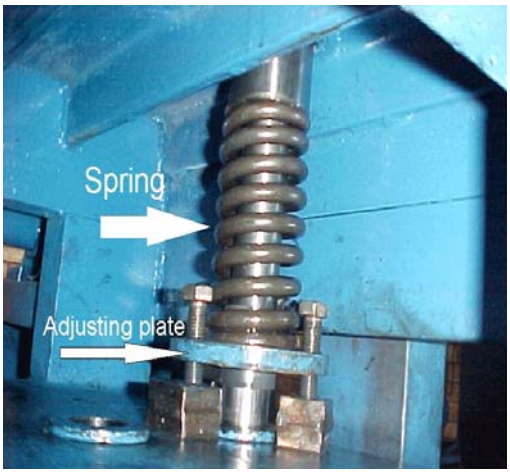


Figure 7.5: Loading spring with adjusting plate


Figure 7.6: Assembly of stabilising springs

A model of the dynamic response of the simulator was prepared. The purpose of this model was to determine the size of the stabilising springs mounted on the corners. The model was used to determine the resultant force on the pin connecting the connecting rod to the swing arm. Figure 7.7 is a graphical presentation of the effect of the stabilising springs. The stiffness finally determined was 20 kN/m. (See Figures 7.2b and 7.6 for the position of these springs.)

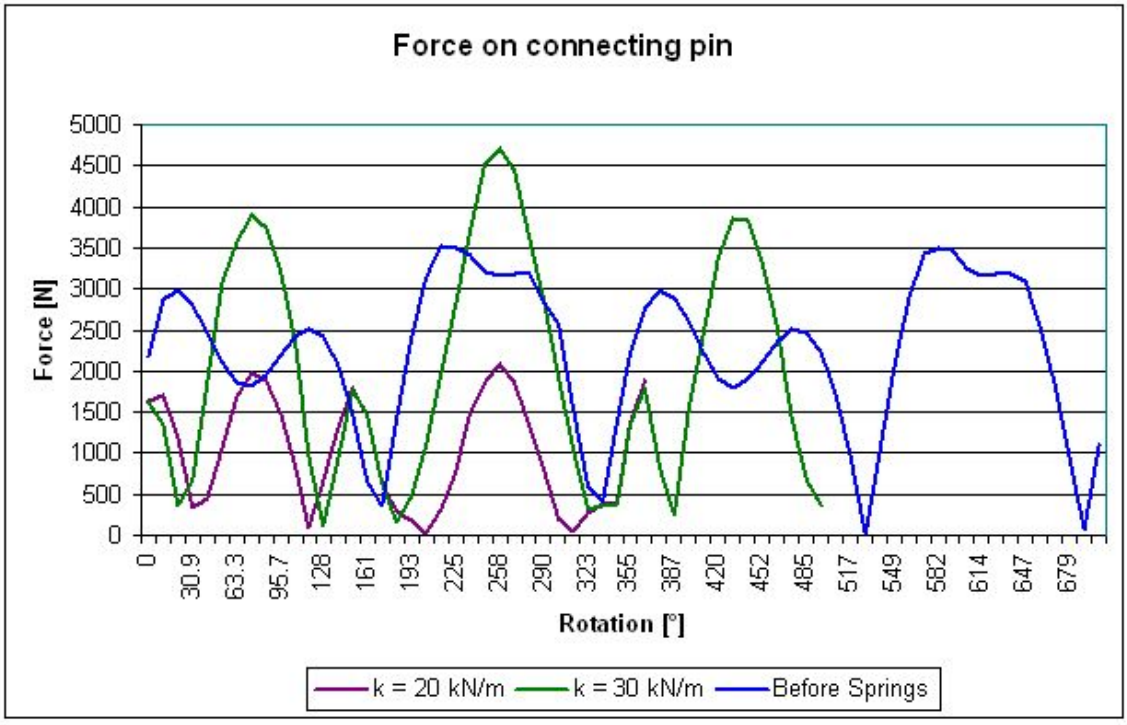


Figure 7.7: Graphical presentation of the forces on the connecting pin

The design of the simulator also makes provision for 5° adduction/abduction rotation.

The femoral head is connected to the swing-over arm with rod ends in which the ±5° movement can be achieved. The rotation of the femoral stem is mechanically activated at the end of each cycle by a deep groove ball bearing connected to the stem, stopping against an adjustable stopper. This rotation simulates adduction/abduction rotation at heel strike and toe-off. The detail is shown in Figure 7.8.

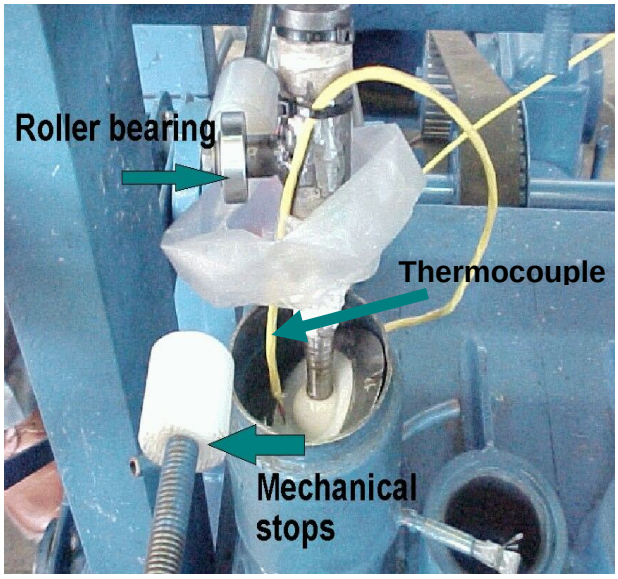


Figure 7.8: Mechanical stops to achieve ±5º abduction/adduction rotation

The steel backing of the post is mounted inside a container. Water is circulated through the jacket of the container to maintain the temperature of the lubrication fluid at 37.5°C. The temperature in each post is monitored by means of a thermocouple, as can be seen in Figure 7.8. Detail of the strain gauges as well as the detail of the cup mounted in the post is shown in Figures 7.9 and 7.10.

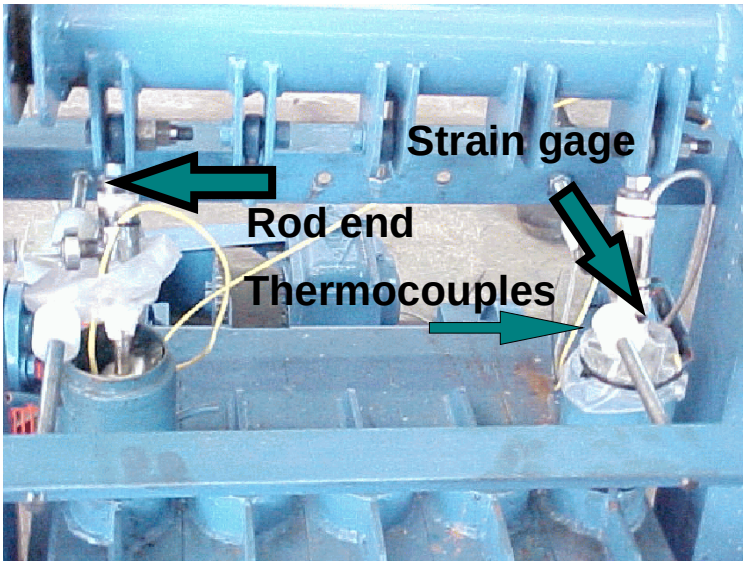


Figure 7.9: Two cups in position showing the thermocouples and strain gages

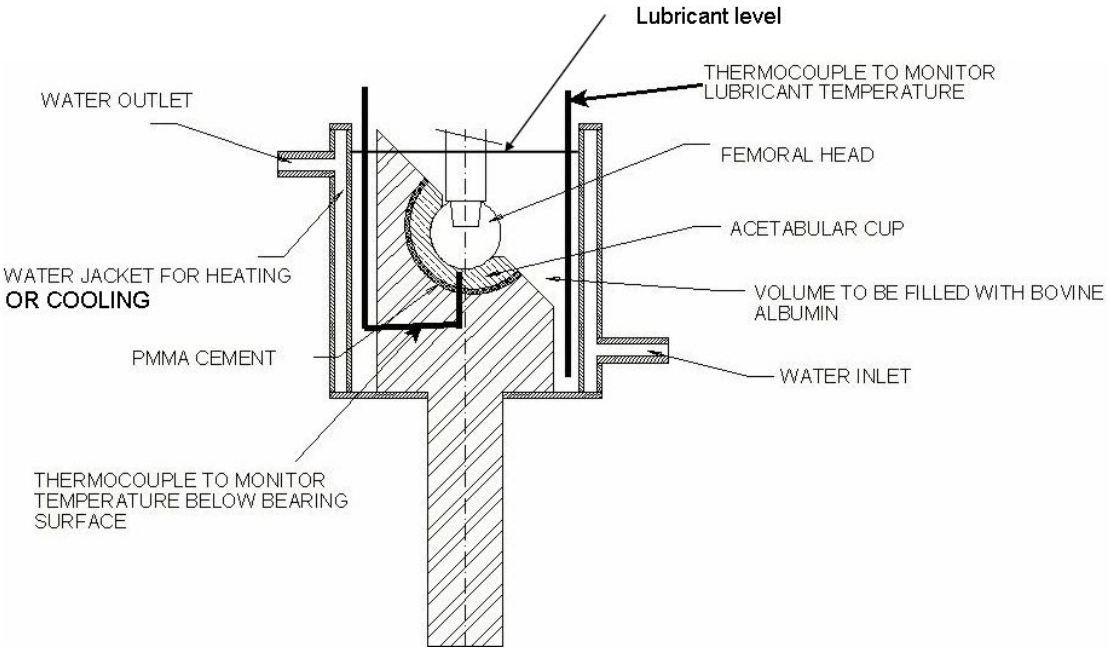


Figure 7.10: Detail of the acetabular cup in the test station

## 7.2 Overview of test work to be carried out

During the experimental phase of this study, a number of tests were conducted to establish the effect of overheating between the ceramic femoral head and the UHMWPE acetabular cup.

The first tests were done in the hip simulator as described in paragraph 7.1. The main aim of these tests was to establish whether the differences in the wear debris formed under the following test conditions could be detected:

a. When the simulator was running with lubricant.
b. When the simulator was running without lubricant.

In both cases, the wear debris generated was collected and compared. The temperature rise in the acetabular cup was also monitored to establish the rise in temperature against time.

Throughout the experimental phase, the control test performed was to compare the debris generated during the laboratory experiment with the debris retrieved from tissue surrounding the joint in-vivo, as this is the only way to calibrate the tests and to establish the effect of the various parameters. The design and test parameters were altered continuously until similar debris resulted.

The second set of experiments was conducted to establish what temperature was required to generate the type of wear debris as retrieved from the tissue surrounding the joint in-vivo. Two tests were designed to determine the temperature at which the debris formation starts namely:

a. Test to generate wear particles by generating frictional heat on the bearing surface between the ceramic femoral head and the UHMWPE test piece.
b. Test to generate wear particles by heating a ceramic femoral head externally and then ploughing it through the test piece.

The third set of tests was designed to determine the coefficient of friction between

a ceramic femoral head and an UHMWPE acetabular cup. As friction is the main component generating heat in-vivo, it was necessary to determine the correlation between the theoretical values and the actual values as measured in an acetabular cup. The tests were performed under the following conditions:

a. Dry
b. Dry with wear debris on the surface
c. At an elevated temperature of approximately 60ºC.

## 7.3 Test with lubrication – test 1(a)

### 7.3.1 Test protocol

The simulator is operated at 1.5 Hz, similar to the simulator of McKellop et al. (1997, 2000), Wang et al. (1996) and as defined in ISO 14242-1, (2002). This corresponds to 90 cycles per minute or the equivalent of approximately 90 metres in one minute. The lubricating fluid used for the current study was 0.9% NaCl solution. The reason for using NaCl as a lubricant is that the lubricant as prescribed by ISO 14242-1, (2002) namely a 25 ± 2% calf serum solution with a minimum protein mass of 17 g/l, must be changed after every 500 000 cycles as it decomposes. Although NaCl is not a good lubricant, it will provide accelerated results, especially in view of the fact that no long-term tests were planned, but merely the determination of the rise in temperature and the nature of the particles generated. At a rate of 1.5 Hz, a life cycle test of 20 years will take approximately three months to complete.

Continuous temperature readings (Figure 7.9) were taken in and around the cup to establish the temperature of the UHMWPE just below the wear surface. (See Figure 7.9.) The loading in each femoral component was also monitored to ensure that the machine remains within the determined specification. (See Figure 7.11.)

Samples of the lubricating fluid (0.9% NaCl) were taken at every 250 000 cycles. The fluid was filtered through a 0.45µm filter. These are the same

filters that were used to extract the wear debris from the tissue surrounding the joint in-vivo and retrieved during revision surgery. The filtered fluid was returned to the test station.

Figure 7.11: Test-recording equipment

### 7.3.2 Test results

Temperatures of up to 65°C were measured in the bottom of the cup within 15 minutes of operation where after the temperature stabilised at 65°C. The lubricating fluid in the chamber was kept at a constant temperature of 37.5°C. As described, the first sample was taken after only 250 000 cycles and the lubricating fluid was filtered through a 0.45µm filter. The same technique, as described in Chapter 5, was used, in other words colouring of the filter paper enabled the wear particles to become visible against the coloured filter paper and allowed them to be studied under a microscope. In Figure 7.12, two wear particles can be seen at 40 times magnification.

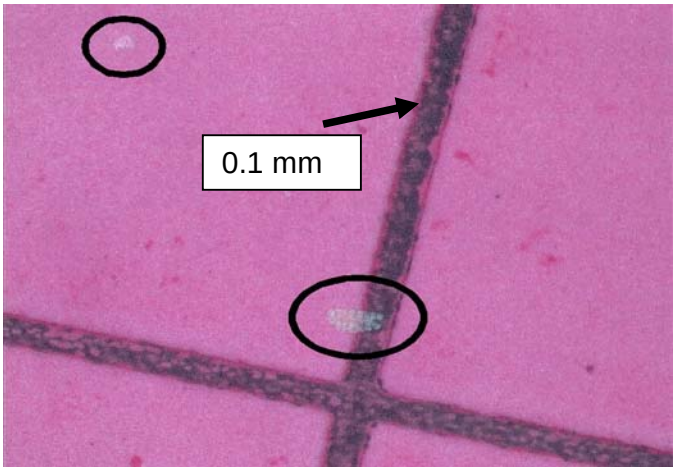


Figure 7.12: Wear particles on filter material (magnification x 40)

In Figure 7.13, the larger particle is shown under a magnification of 100 times. From this photograph (see the enclosed CD for better clarity), the extruded edges are clearly visible. The shape of the wear particle indicates that the temperature at localised spots rises sufficiently to allow the particle to be transferred or to be extruded. The same particle but under 900 x magnification is shown in Figure 7.14.

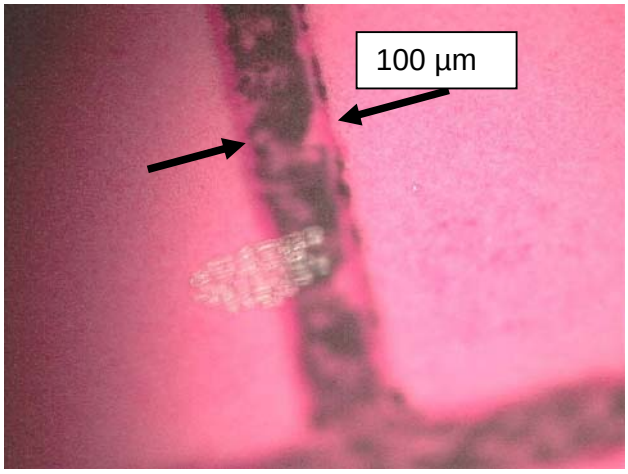


Figure 7.13: Wear particle retrieved from simulator (magnification x 100)

Figure 7.14: Retrieved wear particle from simulator (magnification x 900)

In total, four samples were drawn through the test of 1 000 000 cycles, all with the same shape and size of wear debris.

## 7.4 Test without lubricant – test 1(b)

### 7.4.1 Test protocol

The same test protocol as for the UHMWPE acetabular cup, with lubricant, was used. The test was done without any lubricant to obtain accelerated wear and to establish the shape of the wear particles generated. The purpose was to obtain particles generated under the most extreme conditions and then to study their shape, and the damage caused to the bearing surface. It was expected that under these extreme conditions the acetabular cups would fail very quickly and therefore no temperature recordings were made. Another problem is that the failure due to overheating is localised, which makes it almost impossible to measure in the current test configuration. It was decided that the rise in temperature would be determined later on with a different test configuration. (These results are presented in paragraph 7.3.)

### 7.4.2 Test results

Failure occurred after about 10 minutes, at 90 Hz, when strands of plastic were forced out from the bearing surface in the acetabular cup. The

surface, after failure, can be seen in Figures 7.15 and 7.16.

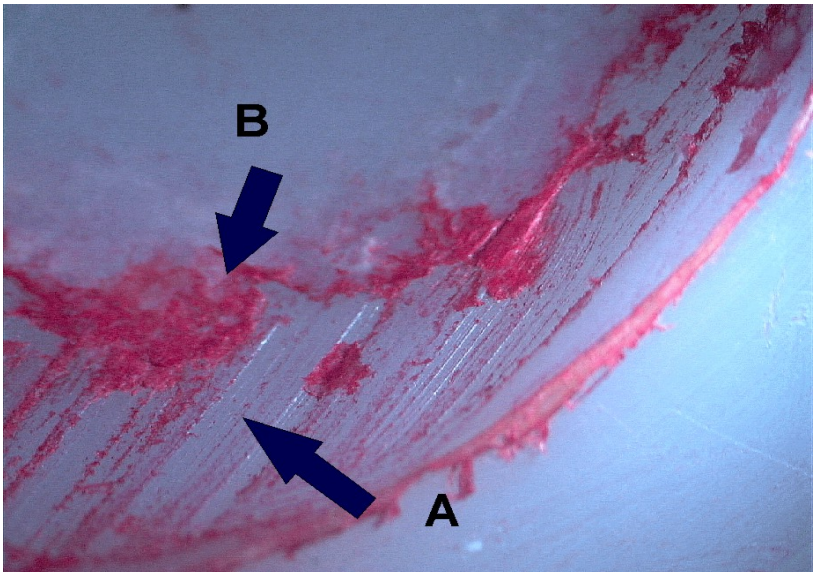


Figure 7.15: Wear surface on the inside of the cup (magnification x 10)

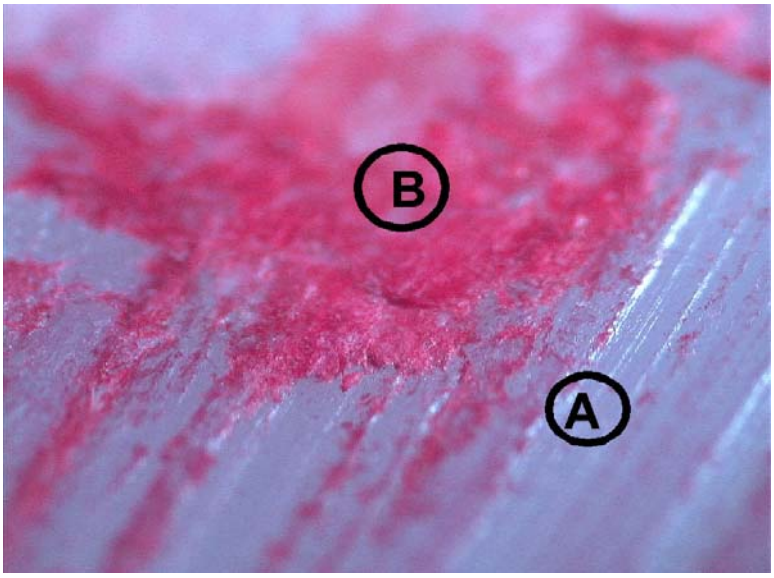


Figure 7.16: Wear on inside of a cup (magnification x 20)

On close examination of the wear surface, the following two aspects are

visible:

a. An area is visible where it appears as if the material was torn out of the base material, leaving what looks like scratch marks. (See A in Figure 7.15 and enlarged in Figure 7.16 also marked by an A)

b. On the edge of the high-wear area, extrusions are visible. This is marked with a B in Figure 7.15 and enlarged in Figure 7.16.

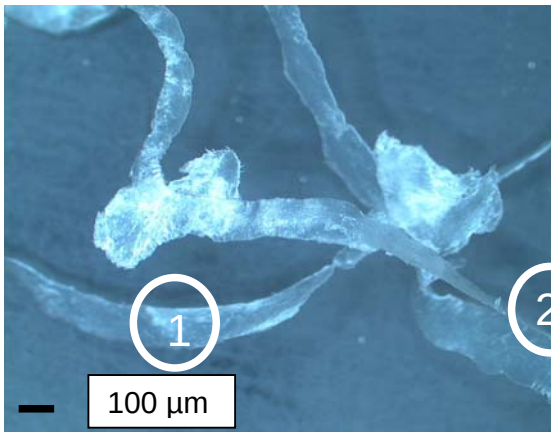


Figure 7.17: Wear debris retrieved from an acetabular cup on simulator (magnification x 20)

c. If one looks closely at the retrieved wear debris, Figures 7.17, 7.18 and 7.19, signs of waviness on the edges are visible, suggesting formation at an elevated temperature. The extruded whiskers, as described in paragraph 5.8.2, are also visible.

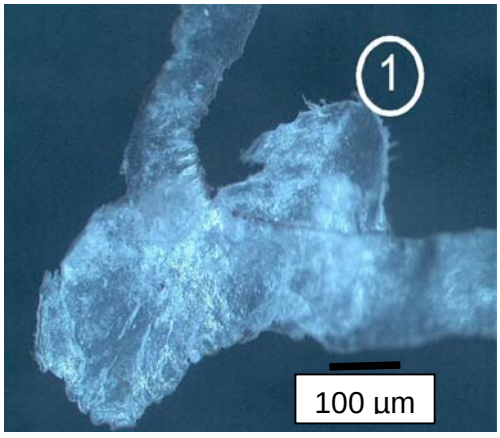


Figure 7.18: Wear debris retrieved from an unlubricated acetabular cup in a hip simulator (magnification x 40)

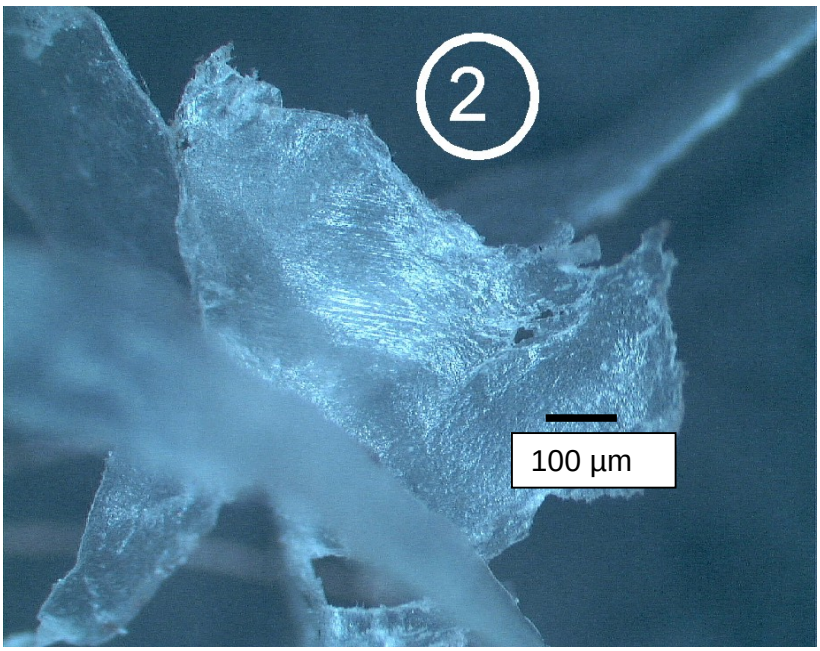


Figure 7.19: Wear debris retrieved from an unlubricated acetabular cup in a hip simulator (magnification x 40)

## 7.5 Test to generate wear particles by generating frictional heat on the bearing surface – test 2(a)

### 7.5.1 Purpose of the test

Various wear particles were retrieved throughout the course of this study whether from fresh retrievals from patients or from tests done on the hip simulator in the laboratory. All of the retrieved debris showed signs of extrusion. The temperature at which failure had occurred was still unknown. Therefore, this experiment was performed to enable manufacturing of wear debris and to determine the temperature at which the debris started forming.

### 7.5.2 Test protocol

A very simple test was designed to try to manufacture wear debris similar to that found in the tissue retrieved during revision surgery. A ceramic

femoral ball was mounted on a steel stem. The combination was then pressed against a block of UHMWPE in a milling machine. The basic layout is shown in Figure 7.20. The femoral ball was rotated at high speed (2 900 rpm) allowing frictional heat to be generated on the bearing surface between the ceramic and the UHMWPE test piece. The test was monitored and when the first wear debris started to appear the ball was quickly removed from the bearing surface and the temperature was immediately measured using a laser-guided infrared thermometer. The advantage of the infrared thermometer is that temperatures can be measured instantaneously and, at the distance used, the object diameter of the temperature reading is about 0.4 mm in diameter.

The wear debris generated was collected for further analysis.

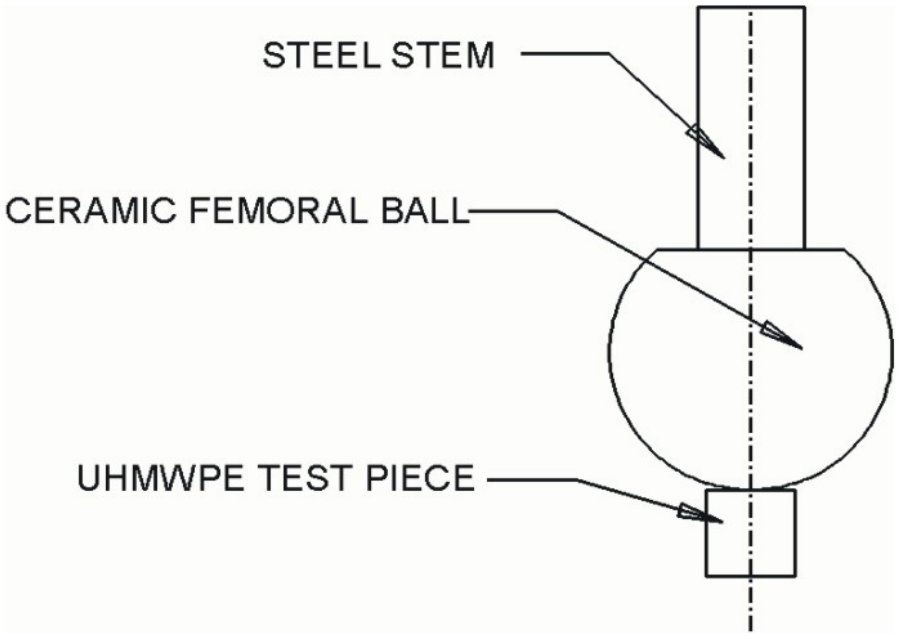


Figure 7.20: Test layout to manufacture wear particles with frictional heat

### 7.5.3 Test results

A temperature of 105°C was measured on the surface of the UHMWPE test piece at the onset of debris formation. The resulting damage on the UHMWPE test piece can be seen in Figures 7.21 and 7.22.

In Figure 7.23, the wear debris adhering to the ceramic femoral ball is also visible. The extruded edges, as presented earlier, are also visible on the debris that had formed during the test.

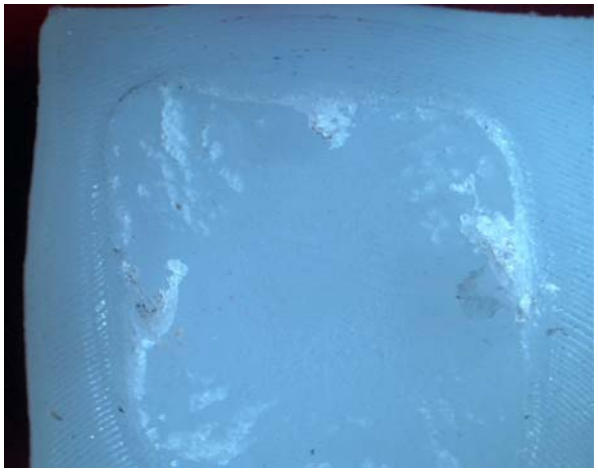

Figure 7.21: Area of damage on a test piece

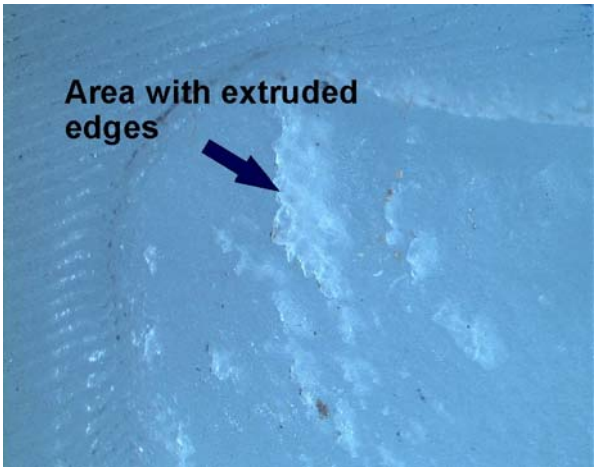


Figure 7.22: Surface damage on UHMWPE test piece (magnification x 20)

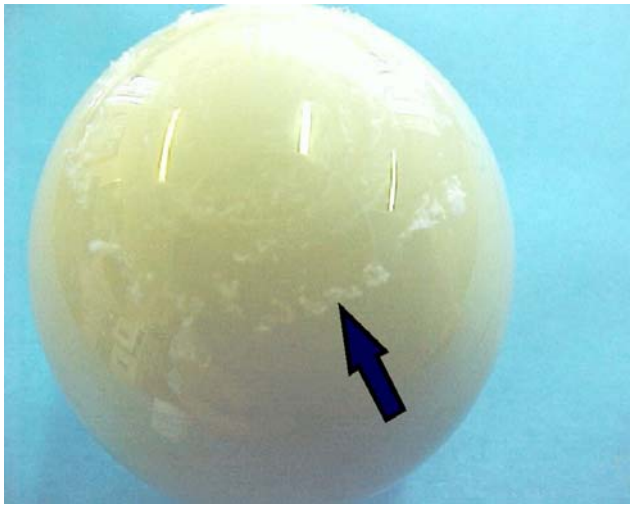

Figure 7.23: Wear debris adhering to femoral ball — indicated with an arrow

The wear debris was retrieved and then examined under a microscope. The same colouring procedure was used as described earlier to see the debris on the filter paper. The resulting debris is presented in Figures 7.24 and 7.25.

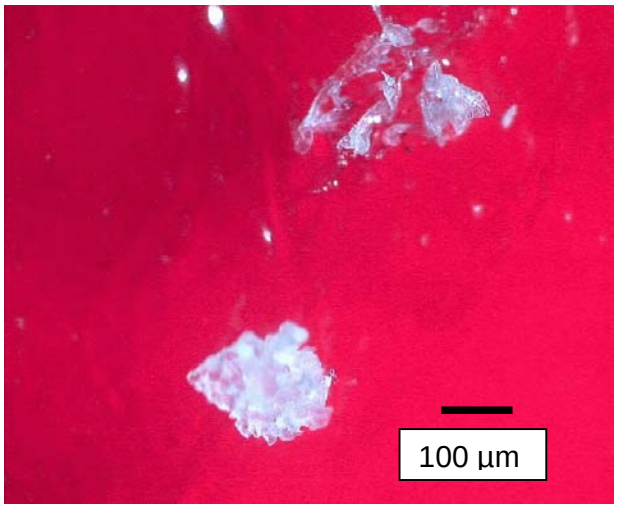


Figure 7.24: Wear debris generated by frictional heat at a measured temperature of 105°C (magnification x 40)

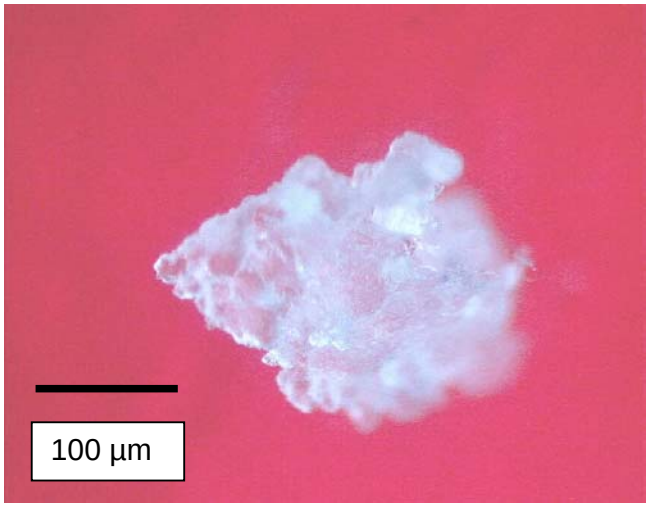


Figure 7.25: Wear particle at higher magnification (magnification x 100)

The particle shows evidence that it heated up sufficiently to adhere to the ceramic femoral head and to be ripped from the base material.

In this investigation, a laser-guided infrared thermometer was used to measure the surface temperature in known hot spot areas. It would, however, be a mistake to assume that the microscopic hot spots can be picked up by the instrument. To explain the principle of uneven surface asperities, a very brief summary of surface action is given here as the phenomenon is well documented in text books on bearing materials (Hutchings, 1992).

Despite the best surface preparation, all surfaces have remaining waviness or surface roughness. When two surfaces are moved relative to each other, as shown in Figure 7.26, the peaks collide and deform. In the case of a well-prepared acetabular cup, the surface peaks are in the order of 2 to 4 µm, compared to a human hair typically having a thickness of 50 µm. The surface peaks that collide are where the biggest temperature rise due to friction is going to take place, although it is almost impossible to measure the exact temperature rise, as already stated.

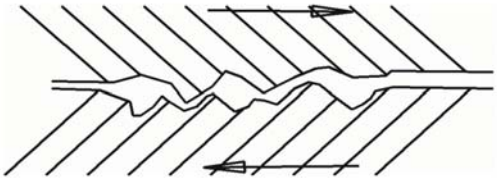

Figure 7.26: Schematic layout of surface roughness

The laser-guided infrared thermometer used in this investigation has an object diameter of only 0.4 mm at the distance used. Although this object diameter is much better than that which can be achieved by thermocouples, this spans approximately 200 surface peaks. The best that can therefore be achieved is to measure the average temperature of a known hot spot.

## 7.6 Test to generate wear particles by externally heating up a femoral head – test 2(b)

### 7.6.1 Purpose of the test

The purpose of the test was to generate wear debris under conditions where the ceramic femoral head was preheated to a specific temperature. This enabled the generation of wear debris between the ceramic femoral head and the UHMWPE test piece as verification for the debris generated by means of frictional heating.

### 7.6.2 Test protocol

The test set-up designed and built for the frictional heating test was again used (Figure 7.20). The ceramic femoral ball was preheated to temperatures of 70, 80, 90 and 100°C, respectively, to enable verification of the temperature measurement at which debris formation started during the frictional heating test. After heating the femoral ball, the machine was set into motion allowing the heated femoral ball to penetrate the material. The femoral ball was rotated at only 50 rpm to virtually eliminate heat generated by friction.

### 7.6.3 Test results

At 100°C, the surface of the test piece again showed evidence of the femoral head adhering to the UHMWPE and then ripping out and extruding particles from the base material. This phenomenon was not expected at 90°C or lower in this short duration test, as the temperatures measured during the frictional heating test were above 100ºC. (See Figures 7.27 and 7.28 for the damage on the UHMWPE surface and Figure 7.29 showing the wear particles adhering to the femoral ball.)

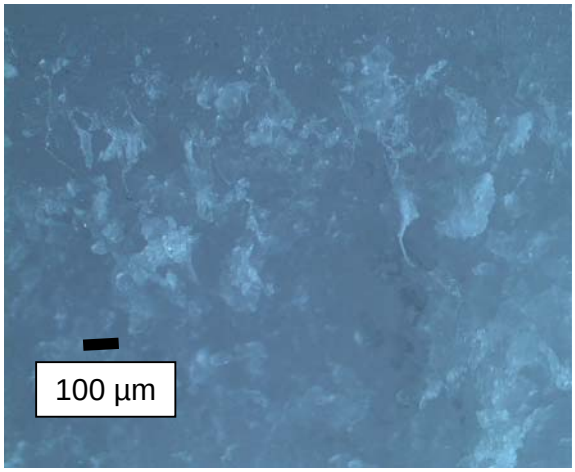


Figure 7.27: Surface of a test piece after damage by preheated femoral head (magnification x 10)

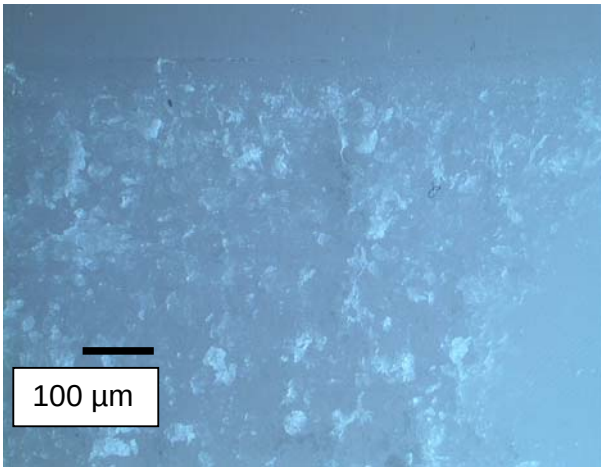


Figure 7.28: Damage surface of UHMWPE test piece (magnification x 20)

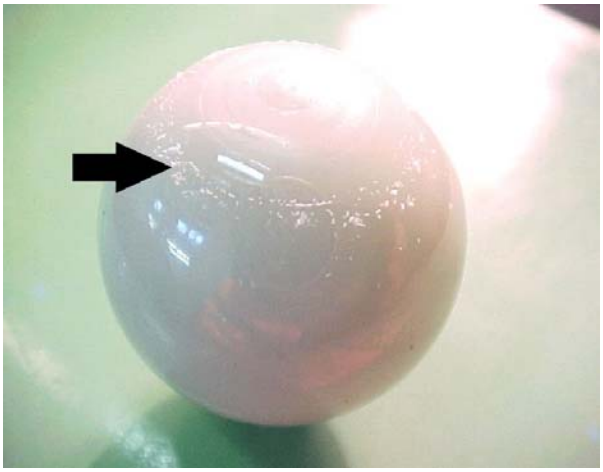

Figure 7.29: Wear particles adhering to femoral ball — indicated with an arrow

The wear debris was again collected for further analysis under the microscope making use of the same technique as described in Chapter 5. (The findings can be seen in Figures 7.30 to 7.32.)

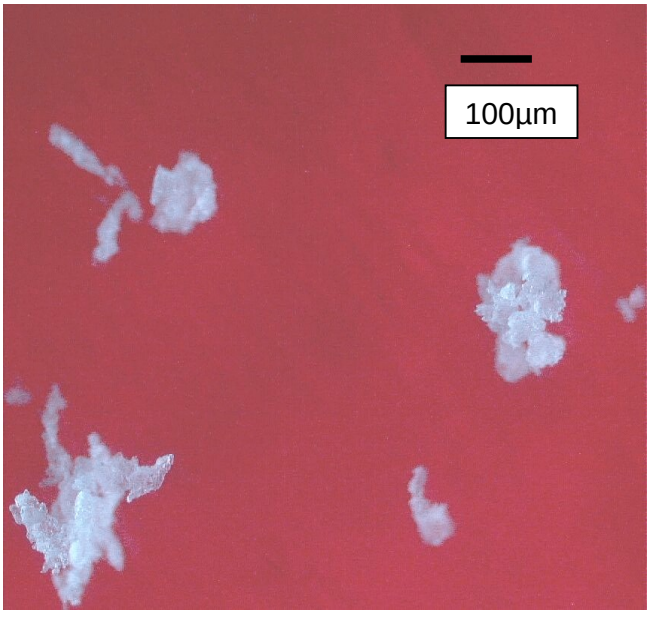


Figure 7.30: Retrieved wear debris from preheated ball test. Ball temperature 100°C (magnification x 20)

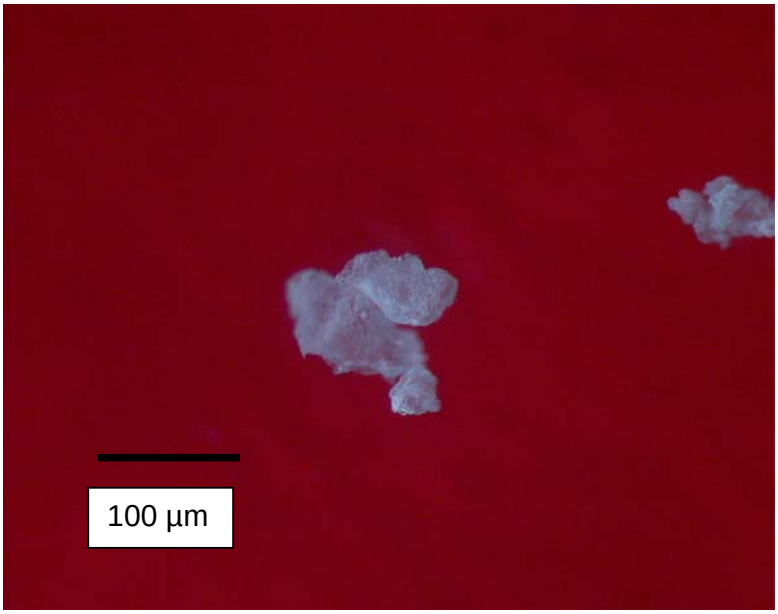


Figure 7.31: Wear particles retrieved from externally heated femoral head at temperature of 100°C (magnification x 40)

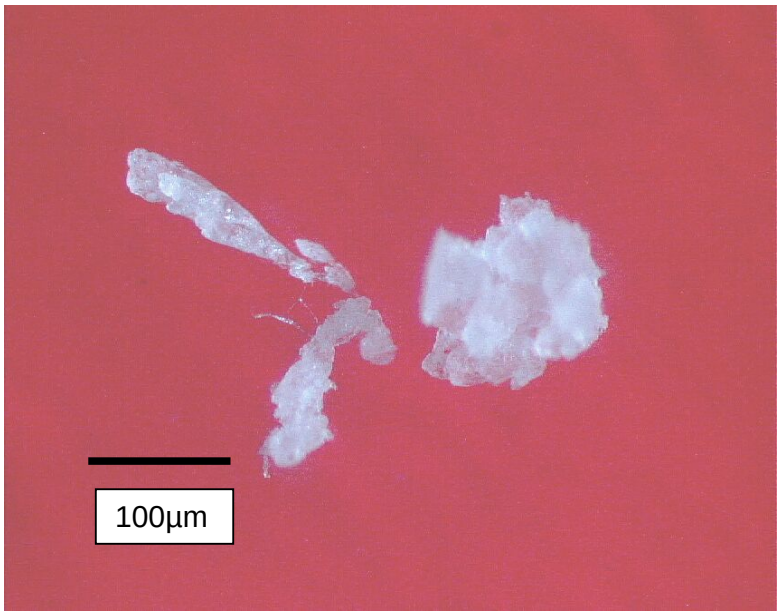


Figure 7.32: Wear particles retrieved from externally heated femoral head at a temperature of 100°C (magnification x 40)

## 7.7 Test to determine the coefficient of friction on the inside of an acetabular cup – test 3

### 7.7.1 Purpose of the test

The purpose of the test was to gain an indication of the coefficient of friction between a zirconium femoral ball and the acetabular cup under various conditions. These values are needed to explain the influence of the coefficient of friction on the heat generated in-vivo.

### 7.7.2 Test protocol

A very simple test was designed to determine the static coefficient of friction between a zirconium femoral head and the acetabular component as shown in Figure 7.33. The femoral head was mounted inside the cup with a weight at the bottom to accomplish the loading. The experiment was designed in such a way that only the friction between the femoral ball and the acetabular cup is measured. This was achieved by having the weight applied to the femoral head going through the centre of the femoral head and thereby the system could be balanced without external fixation that could influence the results.

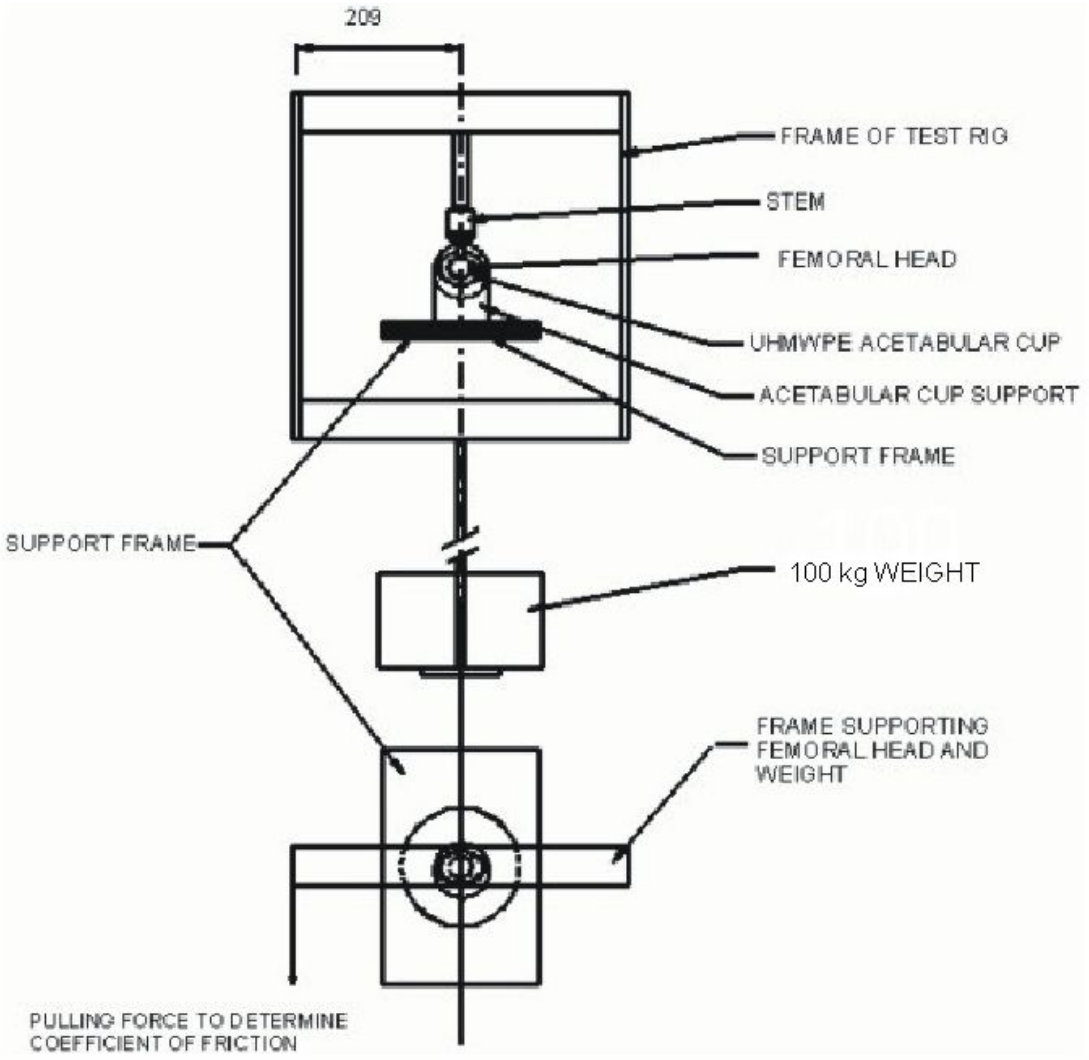


Figure 7.33: Test set up for determining coefficient of friction between ceramic femoral head and UHMWPE acetabular cup

The experiment was repeated a number of times to gain an indication of the coefficient of friction for the following conditions:

a. Dry.

b. Dry with wear debris on the bearing surface.

c. Lubricated with one drop of water on the bearing surface.
d. At a temperature of approximately 60°C. Owing to the fact that the UHMWPE was preheated, the temperature was limited to 60°C to prevent the bearing from collapsing.

The wear debris generated during the previous two tests (frictional heating between femoral head and UHMWPE test piece and the external heating of the femoral head) was placed on the bearing surface to simulate the wear debris generated over a period of time in-vivo.

To determine the static coefficient of friction, the force needed to cause the test rig to move was measured. The force was applied over a pulley system to cause the minimum deflection of the system. Small weights were suspended on the rope attached to the frame providing the input force, enabling the calculation of the coefficient of friction. (See Table 7.1 for the different weights as measured.) A dial gauge was used to indicate the point at which the static friction was overcome.

### 7.7.3 Test results

Table 7.1: Values for masses needed to cause movement

| Condition | Mass (gram) |
|---|---|
| Dry | 405 |
| Dry with wear debris on bearing surface | 385 |
| Lubricated with one drop of water on the bearing surface | 306 |
| At a temperature of approximately 60°C | 505 |

To calculate the coefficient of friction, a mean friction radius of 7 mm was assumed as is shown in Figure 7.34. In this case, a 28 mm femoral head

was used. This friction radius is determined by the tolerances during manufacturing.

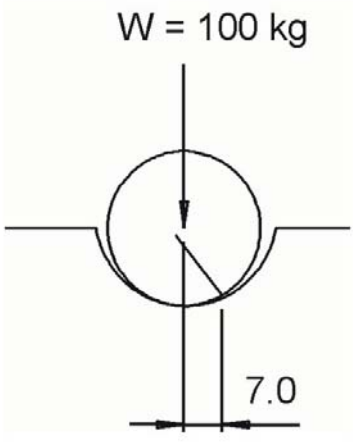


Figure 7.34: Data used for the calculation of coefficient of friction

With a moment arm of 209 mm (Figure 7.33) and a given load, the coefficient of friction was calculated as follows:

$$F.r = \mu.W.r$$

$$\mu = \frac{F.r}{W.r} = \frac{0.405x0.209}{100x0.007} = 0.12$$

If this result is compared with the data found in the relevant literature, (Chapter 2), a value of 0.1 - 0.22 is given for a polished steel ball on UHMWPE with a ceramic/UHMWPE couple having a coefficient of friction of approximately 0.01–0.03. (http://www.utahhipandknee.com/history.htm).

(The results of the estimated coefficients of friction are shown in Table 7.2.)

Table 7.2: Values for estimated coefficient of friction under various conditions

| Condition | Coefficient of friction determined experimentally | Values from literature (Engineering materials Handbook, 1987) |
|---|---|---|
| Dry | 0.12 | 0.1 - 0.22 |
| Dry with wear debris on bearing surface | 0.115 | ---------- |
| Lubricated with one drop of water on the bearing surface | 0.09 | 0.05-0.1 |
| At a temperature of approximately 60°C (Dry) | 0.15 | ---------- |

From the data, as presented in Table 7.2, it can be seen that wear debris accumulated on the bearing surface has virtually no effect on the coefficient of friction. What is interesting is the 25% increase in the coefficient of friction at the elevated temperature of 60ºC. Lubrication in the form of water caused an almost 30% decrease in the friction coefficient.

## 7.8 Conclusion of experimental results

### 7.8.1 Simulator study

The simulator studies were conducted with the following aims:

a. To get an indication of the temperature below the bearing surface in the acetabular cup while in operation.

b. To generate wear debris and to compare the shape of the wear debris

to the shape of the debris retrieved from scar tissue surrounding the joint in-vivo.

The tests were performed with and without lubrication to enable an accelerated test.

#### 7.8.1.1 Temperature in acetabular cup

The temperature in the cup was measured by inserting a thermocouple approximately 0.5 mm just below the bearing surface of the acetabular cup. It must be accepted that the thermocouple will not be able to measure the temperature on the surface peaks, as explained in paragraph 7.5.3. The temperature reported will be an average value over a larger area of approximately 3 mm as the diameter of the thermocouples is 1 mm.

The temperature recorded after 15 minutes of continuous operation, with 0.9% NaCl as lubricant, was 60ºC. The temperature fluctuated, but stabilised between 60º and 65ºC. The temperature measured during the current study actually correlates very well with the values reported by McKellop et al. (2000), although in the test done by the McKellop group, the thermocouple was inserted in the ceramic femoral head and not in the UHMWPE acetabular cup. In the study done by the McKellop group, the measured temperature was extrapolated to the surface and a value of 90ºC was reported.

The test without any lubrication failure of the acetabular cups, as shown in Figures 7.15 and 7.16, happened so quickly that no temperature readings were possible.

#### 7.8.1.2 Wear debris retrieved from simulator

During the simulator test, with lubrication, wear debris was retrieved every 250 000 cycles without stripping the assembly. A sample of the lubricant was retrieved and filtered through 0.4 µm filters before investigating the

filter paper under a microscope to determine the shape and size of the wear debris. The procedure for retrieving the debris and investigating the filter paper under the microscope is the same as discussed in Chapter 5.

An example of the wear debris retrieved from the simulator is shown in Figure 7.35.

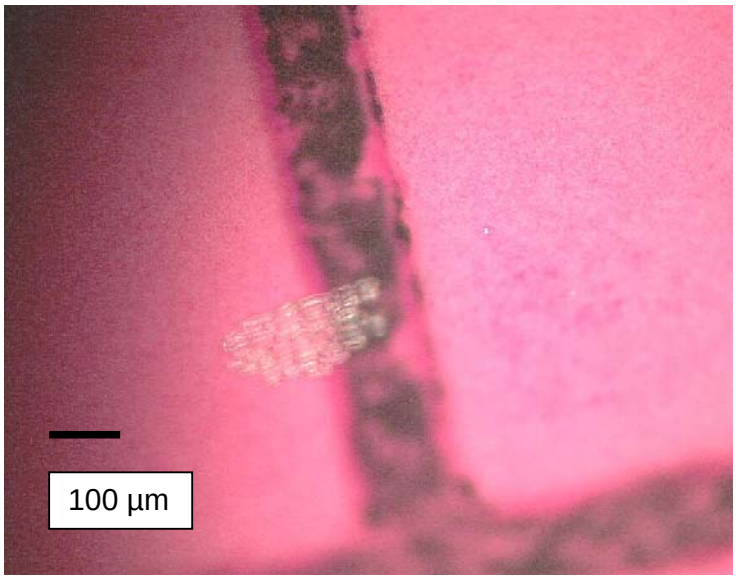


Figure 7.35: Wear debris retrieved from simulator (magnification x 100)

If the wear debris in Figure 7.35 is compared with wear debris retrieved from the scar tissue, as shown in Figure 7.36, as well as the particle still attached to the acetabular cup as shown in Figure 7.37, a similarity in shape and size between the different debris is visible.

All the debris retrieved from simulator and tissue, showed signs of the bumpy surface where the particles were ripped from the base material after adhering to the femoral head. This failure is only possible if the localised temperature in the acetabular cup is high enough for the material to be sufficiently softened to enable the adhesion of the UHMWPE to the femoral head with the consequent ripping of the material from the base material. The temperatures measured during the current study showed

that localised temperatures in excess of 60ºC have been achieved resulting in the damage as explained in Chapters 5 and 6 and verified in Chapter 7.

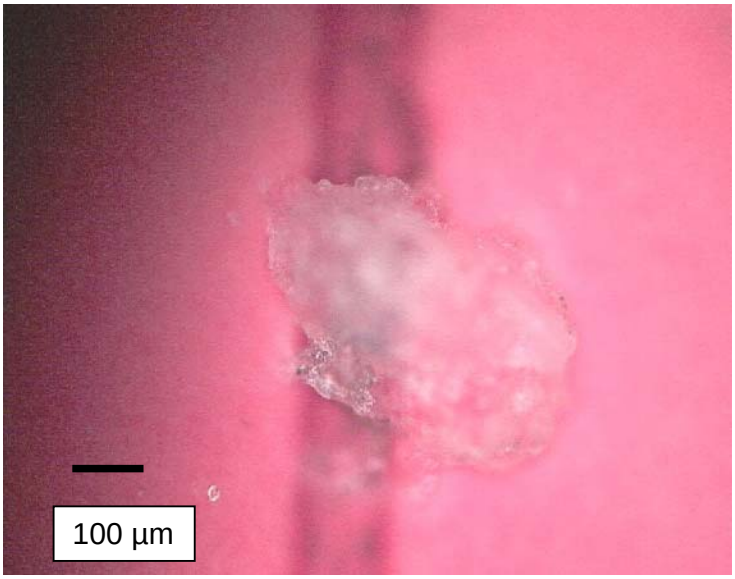


Figure 7.36: UHMWPE wear debris retrieved from scar tissue (magnification x 100)

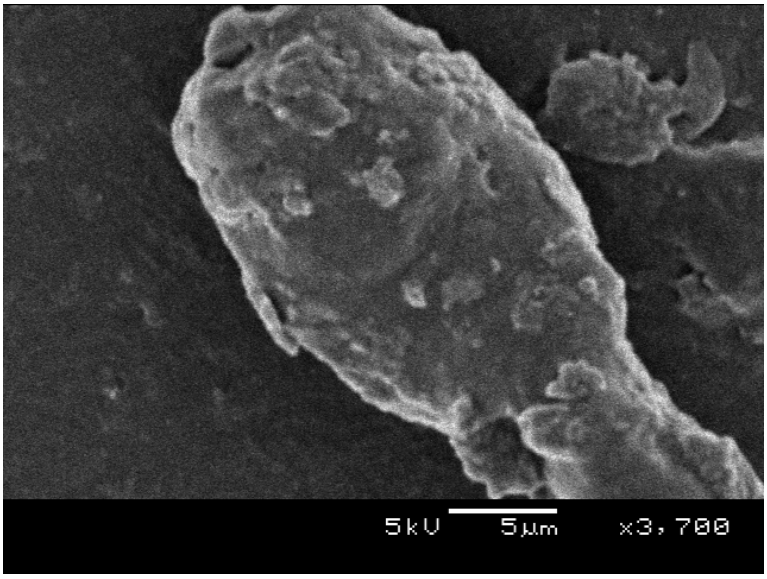


Figure 7.37: UHMWPE wear particle still attached to base material (magnification x 3 700)

The same procedure can now be followed in comparing the wear debris retrieved from the simulator test that had run without lubrication, as shown in Figure 7.38, to the debris retrieved from the scar tissue shown in Figure 7.39.

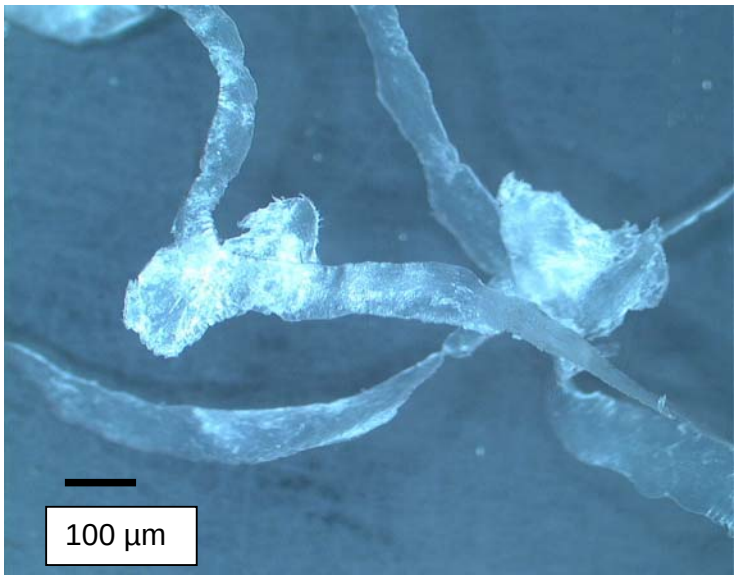


Figure 7.38: UHMWPE wear debris retrieved from simulator running without lubrication (magnification x 20)

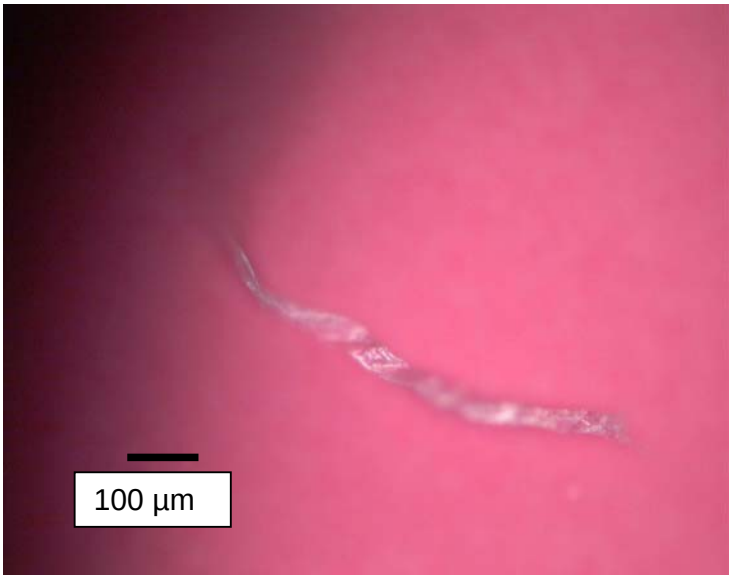


Figure 7.39: UHMWPE wear debris retrieved from scar tissue (magnification x 100)

If the debris in Figures 7.38 and 7.39 is compared again the similarities are clear, although the debris retrieved from the simulator is much bigger. (See paragraph 7.4.)

All of the retrieved debris showed signs of extruded edges. It is proof that the extruded edges are indicative of overheating on the interface between the ceramic femoral head and the UHMWPE acetabular cups. The indication in both the wear debris retrieved from the scar tissue and the debris generated in the simulator is that the material was heated sufficiently to be softened to such an extent that the material was extruded under the prevailing pressure.

### 7.8.2 Simulating of wear debris formation in laboratory

A test set-up was designed and built to simulate the formation of the type of wear debris retrieved from the scar tissue. The aim of this part of the experimental work was to establish a more accurate temperature at which the wear debris starts to form. Two tests were conducted namely:

a. The formation of wear debris by generating heat between the femoral head and the UHMWPE test piece by means of friction.
b. Preheating the femoral head to a predetermined temperature and the running of the femoral head through the UHMWPE test piece generating wear debris.

The wear debris generated during both of these tests was fairly similar, as can be seen in Figures 7.40 and 7.41. In both tests, the temperature generated and the preheated temperature required to form the type of wear debris as shown were in excess of 90ºC. The similarity between the wear debris generated and the debris retrieved from the scar tissue is also remarkable. A particle retrieved from the scar tissue is shown in Figure 7.42. Both pieces of material ripped from the base material after adhering to the femoral head are

visible, as well as whiskers of material that were extruded under the prevailing heat and pressure. Also visible in these test results is the plastic flow of the material as described in Chapters 5 and 6. The plastic flow on the test piece can be seen in Figure 7.22.

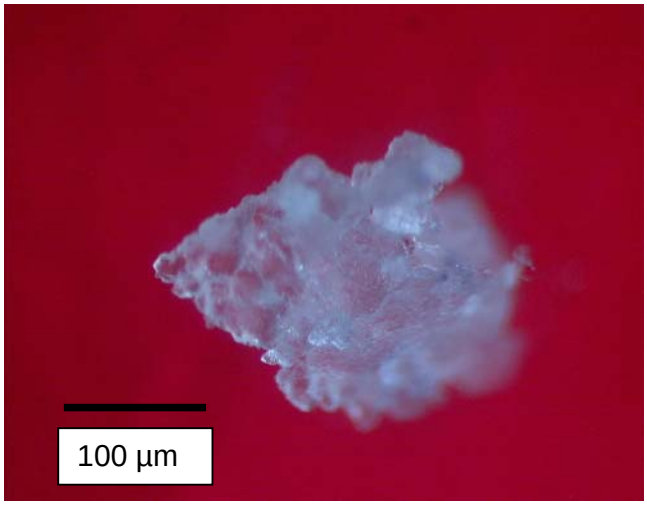


Figure 7.40: UHMWPE wear particle generated by means of frictional heating (magnification x 100)

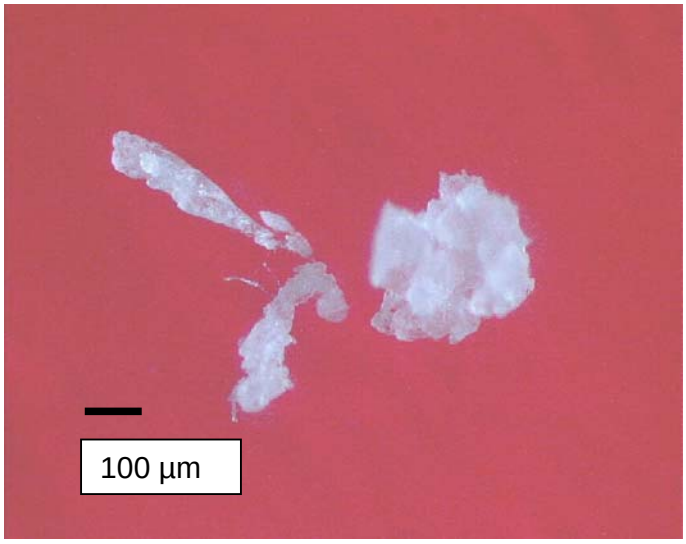


Figure 7.41: UHMWPE wear debris generated by preheating the femoral head (magnification x 40)

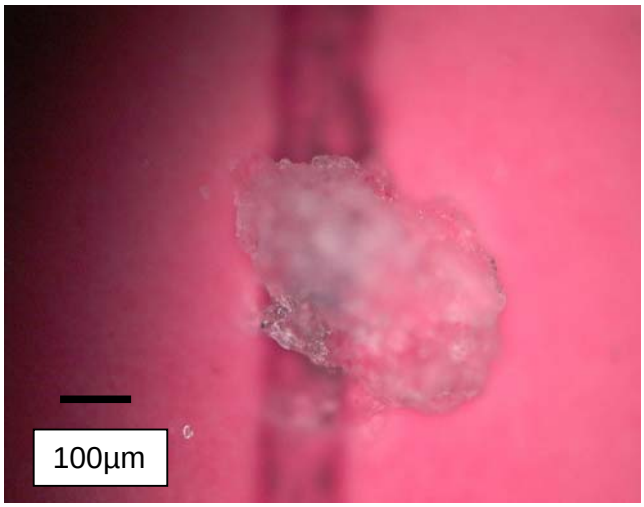


Figure 7.42: UHMWPE wear debris retrieved from scar tissue (magnification x 100)

If the data as presented is examined, it is clear that two mechanisms are responsible for the formation of the UHMWPE wear debris as shown in Chapters 5, 6 and 7. The three mechanisms are as follows:

a. The material is locally heated to a point where the material becomes sufficiently softened to adhere to the femoral head with the result that a piece of material gets ripped from the base material. The result is the typical adhesion wear marks visible in the acetabular cups as shown in Chapters 5 and 6. The cracks seen in the acetabular cups are secondary to the formation of the patches of adhesion wear resulting in stress raisers.

b. The material is locally heated to a point where the material becomes sufficiently softened to be extruded under the prevailing pressure and temperature forming whisker-like wear debris as shown. The areas where extrusion of the material had taken place will also present as scratches, similar to the scratches caused by third-body wear particles.

c. The material was sufficiently softened in localised areas by elevated temperatures to result in the plastic flow of sections of the bearing surface.

## 7.9 Lubrication of the hip joint

The lubrication of any bearing couple is very important as the lubrication has basically three functions (Hutchings, 1992). The three functions associated with lubrication are:

a. To keep the different bearing surfaces apart.

b. To act as surface contaminant to prevent peaks from welding to each other.

c. To cool down the contact surface between the two load-carrying components.

As the three aspects of lubrication and the lubricating characteristics of the synovial fluid are such an unexplored area, Chapter 8 is devoted to a study of the lubrication of the joint and to establish the lubricating characteristics of synovial fluid.

# CHAPTER 8

# LUBRICATION OF THE HIP JOINT

## 8.1 Introduction

Synovial fluid is found in a healthy natural synovial joint. Typical synovial joints are the hip, knee and shoulder. All of these joints differ in shape and size, but the lubrication mechanisms stay the same. The basic lay-out of the synovial joint can be described as follows and is shown in Figure 8.1.

The ends of the bones are covered with articular cartilage. The whole joint is closed up in a capsule called the fibrous capsule. This capsule is lined with the synovial membrane called the synovial capsule, and is filled with a fluid called synovial fluid or synovial, meaning “like egg white” (Sokoloff, 1978). The synovial fluid inside the synovial joint appears yellowish in colour and almost has the consistency of water.

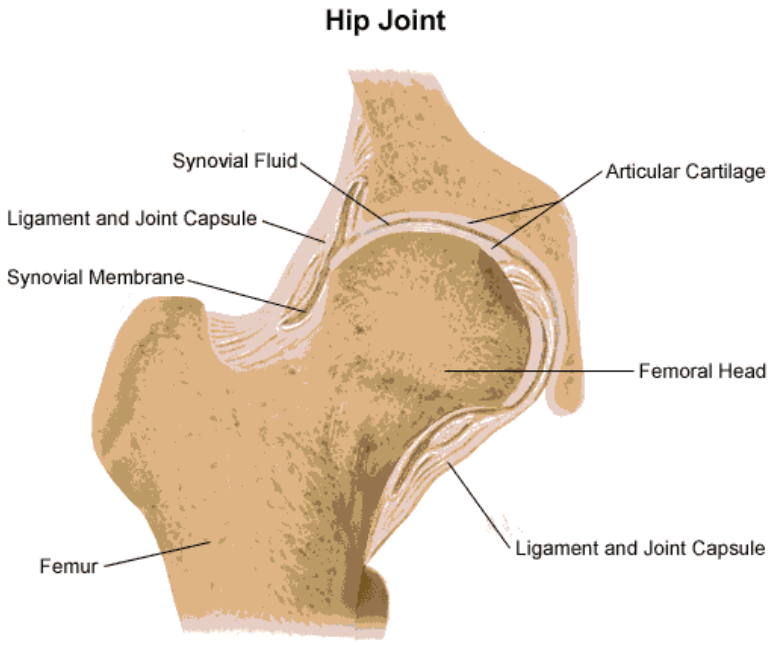


Figure 8.1: A schematic drawing of the human hip joint
(http://www.healthsystem.virginia.edu/UVAHealth/adult_arthritis/anatomy.cfm)

The synovial membrane is a thin sheet of areolar tissue as is shown in Figure 8.2. The areolar tissue is known for its richness in blood vessels and lymphatics. Its main function is that it forms a soppy tissue that lubricates and nourishes epithelial tissue in the synovial joint. It also provides strength, elasticity, support and immune system protection. (http://science.nhmccd.edu/biol/tissue/areolar.html). The synovial membrane has the ability to change the plasma into synovial fluid. By using this ability, the level and concentration of the synovial fluid can be monitored.

a. Elastin fibre
b. Collagen fibre
c. Fibroblast cell that produces the fibres
d. Matrix areas that appear empty and contain ground substance that is a gelatinous watery fluid

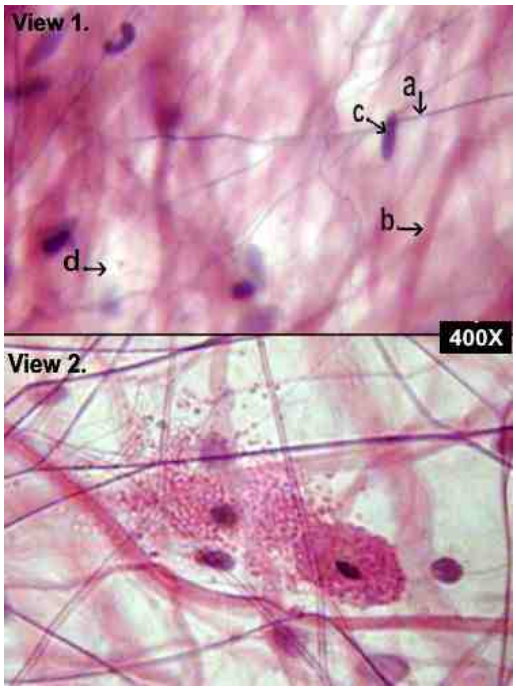


Figure 8.2: Areolar tissue (magnification x 400).
(http://science.nhmccd.edu/biol/tissue/areolar.html)

The synovial fluid, in the normal patient has two main functions namely:

a. The first function is the nutrition of the joint and especially of the articular cartilage. This is necessary, because the articular cartilage

has neither blood vessels nor lymphatics. The cartilage receives all its nourishment via the diffusion of the synovial fluid into the cartilage. Sokoloff (1978) reported that cartilage not only lives in synovial fluid, but can also grow in it. During hip replacement surgery, the cartilage is, however, removed so the function of nutrition is no longer required.

b. The second function is the lubrication of the joint. This is one of the principal interests for this research project.

From the above discussion, it can be seen that to have synovial fluid in a joint, a healthy fully functional synovial membrane is required to produce the synovial fluid. During hip replacement surgery, the synovial membrane needs to be cut to gain access to the joint. (See Figure 8.1.) It is not known as there is no reference in the available literature whether the synovial membrane can function correctly after surgery. This raises the question whether or not the fluid present in the joint after arthroplasty really is synovial fluid and whether the fluid present still has enough lubricating capabilities to support the artificial joint.

As already stated, the function of lubrication is threefold. At sufficiently high speeds, low enough surface pressure and sufficient lubricant, the surfaces can plane over each other without mechanical contact. This applies at high speeds as with motor car engine bearings. If the two surfaces do not plane over each other, mechanical contact occurs, the asperity peaks (as shown in Figure 8.3) are deformed and heat is generated. The first function is therefore to prevent contact between the two surfaces. The second function of the lubricant is to act as surface contaminant to prevent the peaks from welding together. If they are allowed to weld together or adhere sufficiently, the weaker one will be ripped out leaving a crater on one surface and a build-up on the other. The third function of the lubricant is to act as a coolant as the welding process becomes less effective at lower temperatures (Hutchings, 1992).

In metal bearings, a lack of lubrication can easily cause localised temperatures in excess of 1 000ºC, that will allow welding or even melting of the metal peaks.

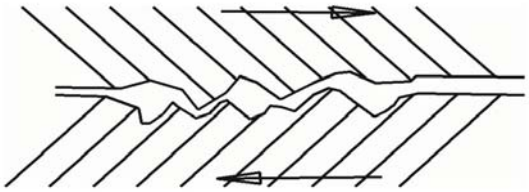

Figure 8.3: Schematic layout of surface roughness.

The main aim of this part of the research has been to establish the quality of the lubricant (synovial fluid) present in the synovial joint after total hip replacement. The lubricity of the synovial fluid is defined as the ability of the lubricant to support lubrication (Hutchings, 1992). Two parameters were used to quantify the lubricity, namely the load at failure and the average coefficient of friction over the test period. The effects of an increasing temperature were also investigated by testing at temperatures in the range of 38ºC to 60ºC.

The joint fluids of 12 patients were retrieved during revision surgery. Each sample was analysed for lubricity at 38 ºC, 50 ºC and 60 ºC.

## 8.2 Apparatus used

Lubricity testing was conducted on a linear-oscillating test machine also known as the Optimol SRV machine (ASTM D5706-97). The outcome of a lubricty test was the load (Newton) at which breakthrough of the lubricating film occurred, as well as the average coefficient of friction measured at the breakpoint. (A schematic layout of the Optimol SRV machine is shown in Figure 8.4.)

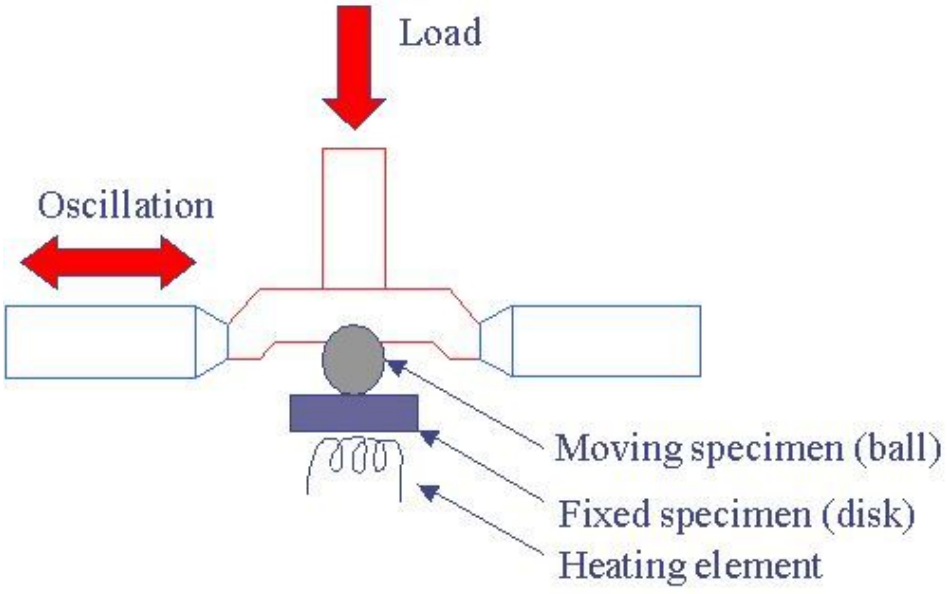


Figure 8.4: Schematic layout of the Optimol SRV machine

A specimen, known as the moving specimen, is clamped into the head of the machine; this prevents the moving specimen from rotating relative to the fixed specimen, ensuring only a sliding effect. The fixed specimen is placed on a heating element to regulate the temperature of the test sample. An oscillation motion is generated with an actuator. The frequency and stroke length of this motion can also be controlled.

It can be seen that most of the variables in this set-up can be adjusted or changed as found appropriate. It was, however, decided to use a test based on the ASTM D5606-97 standard for testing the film strength of lubricating fluids.

(The fixed specimen with the holder to contain the synovial fluid for testing is shown in Figure 8.5, with the moving specimen shown in Figure 8.6.)

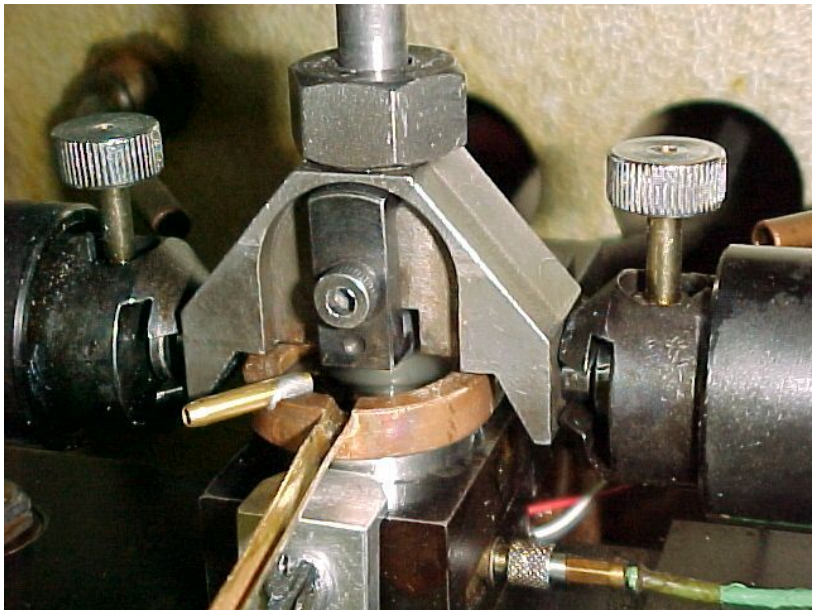

Figure 8.5: Fixed specimen in Optimol SRV machine

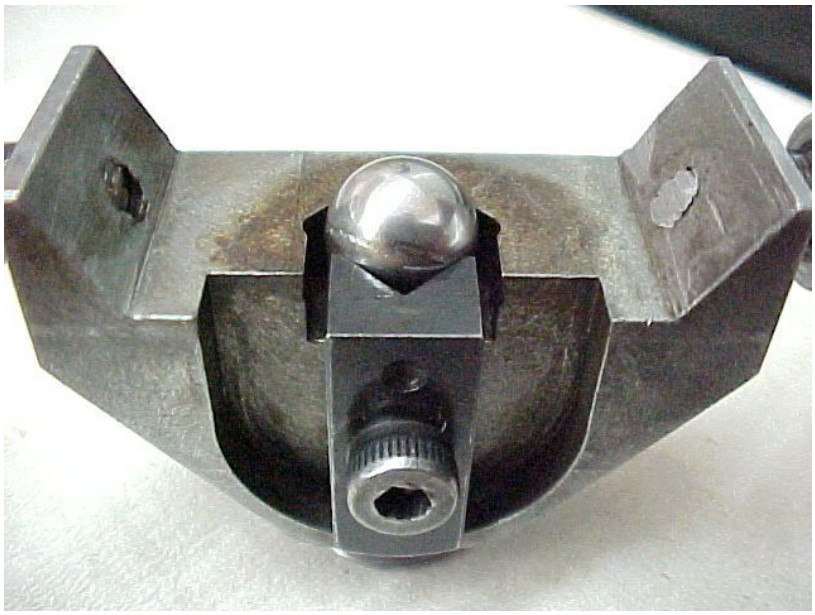

Figure 8.6: Moving specimen in Optimol SRV machine

## 8.3 Test method

The joint fluid used during this research was retrieved from the hip joints of the patients who underwent hip revision surgery. An orthopaedic surgeon did the retrieval of the joint fluid prior to the removal of the existing implant. The fluid was brought to the laboratory for testing within one hour of

retrieval from the patient. The joint fluid was then visually screened to identify the samples contaminated with blood. These samples were then excluded from the study. In total, six samples were excluded from this study. The retrieved synovial fluid was then centrifuged for five minutes at low velocity (± 1 000 g) to separate any wear particles from the retrieved fluid.

On average, volumes of between one and five millilitres of synovial fluid were retrieved per joint. The retrieved fluids were tested individually.

Three temperatures were chosen, namely 38 ºC (body temperature) 50 ºC (halfway temperature) and 60 ºC based on the temperatures measured in the simulator, (Chapter 7), and the work done by McKellop et al. (1997).

(Table 8.1 shows the test parameters used during the lubricity testing of the synovial fluid.)

Table 8.1: The test parameters used to determine the lubricity characteristics of the joint fluid

| | |
|---|---|
| Fixed specimen (Disk) | Size: Ø24 x 7.85 mm<br>Material: AISI E 52100<br>Hardness: Rockwell C 60 ± 2<br>Surface finish: $R_z$ = 0.1 – 0.15 |
| Moving specimen (Ball) | Size: Ø10 mm<br>Material: AISI E 52100<br>Hardness: Rockwell C 60 ± 2 |
| Load | A run-in load of 50N, whereafter the load is increased by 50N every minute. |
| Temperature | 38ºC, 50ºC and 60ºC |
| Oscillation | Frequency: 50 Hz<br>Stroke: 1 mm |
| Feeding mechanism | A drop of fluid was placed between the moving and fixed specimen prior to the test commencing. |

## 8.4 Test outcome

Different test set-ups on this machine can give different test outcomes. In the test specification as given in Table 8.1, the most important factor is to determine the load at failure. According to the ASTM D5606-97 method, the load at failure is defined as the load where the coefficient of friction rises by more that 0.2 over the steady state coefficient of friction, or where total seizure occurs.

A typical result of a lubricity test is shown in Figure 8.7 with all the test results attached in Annexure H.

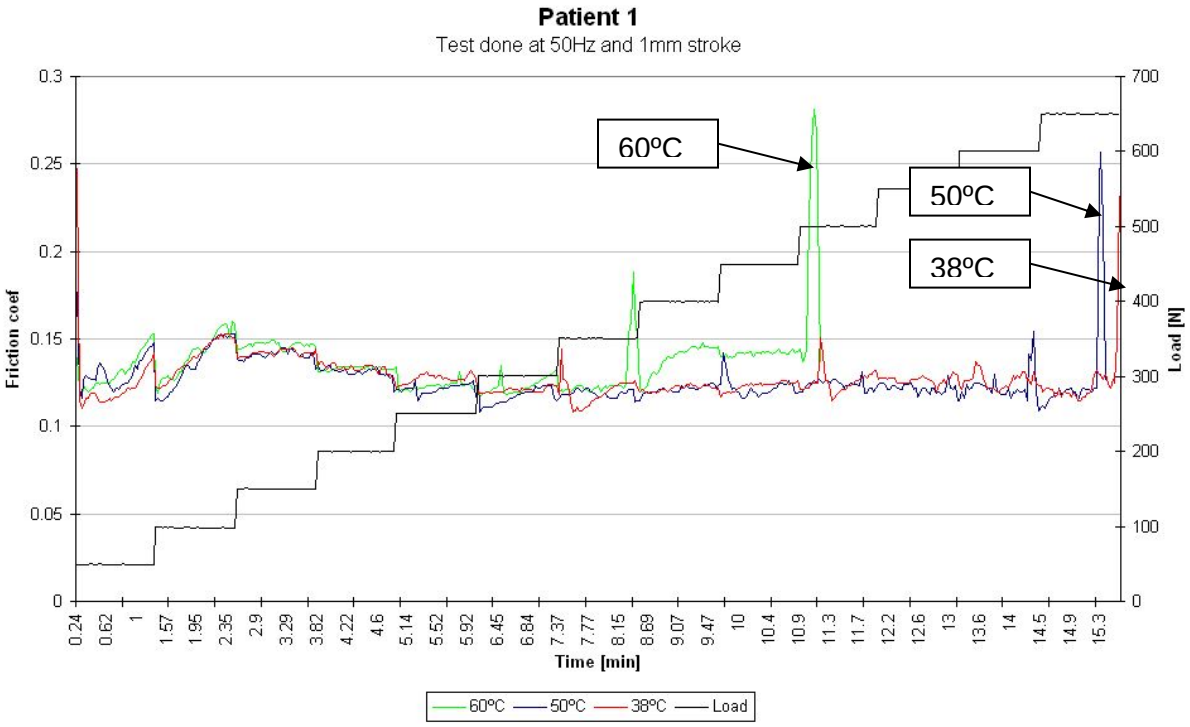


Figure 8.7: An example of a typical lubricity test result. The loads at failure are indicated on the graph

It can be seen from Figure 8.7 that the load at failure at the various temperatures was as follows:

38 º C 650 N

50 º C 650 N

60 º C 500 N.

The scar on the moving specimen (ball) can be seen in Figure 8.8 with the scar on the fixed specimen (disk) shown in Figure 8.9.

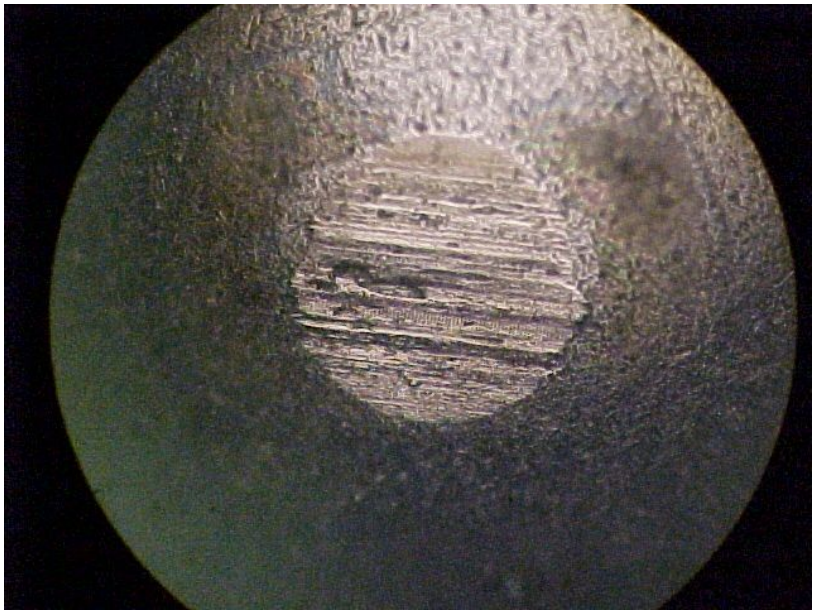

Figure 8.8: Wear scar on moving specimen (ball)

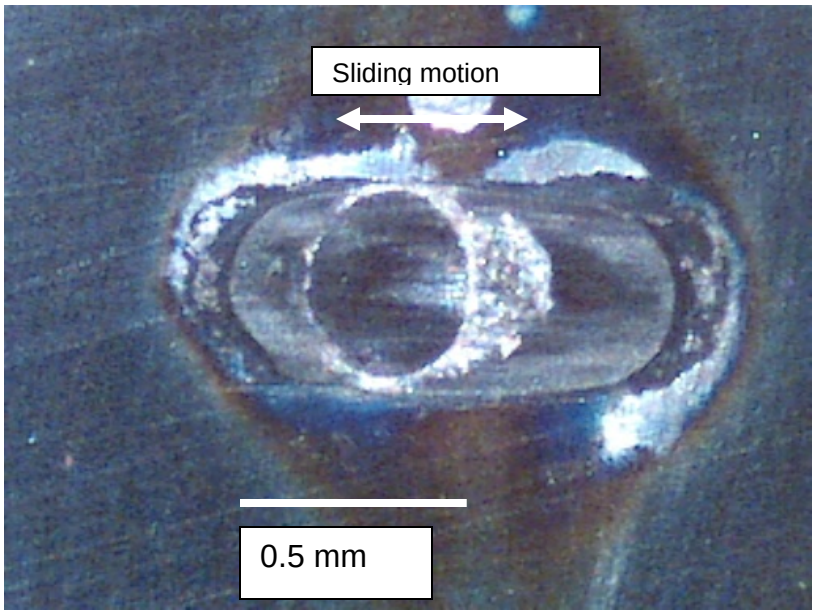


Figure 8.9: Wear scar on fixed specimen (disk) (magnification x 60)

From Figure 8.9, the visible imprint from the ball as it was cold welded to the surface and then, when disassembled, tore away. The size of the wear scar is a function of the load at which the lubricant failed.

A typical wear scar size on the ball for a load at failure of 550N is 0.65 mm in the direction of sliding motion and 0.7 mm across the direction of the sliding motion.

## 8.5 Lubricity properties of patients

The synovial fluids retrieved from a total of 12 patients were tested. The results of these tests are shown in Table 8.2 and Figure 8.10.

Table 8.2: Tests results to determine lubricity characteristics for 12 patients

| | Breakthrough load [N] | | |
|---|---|---|---|
| **Patient** | **38ºC** | **50ºC** | **60ºC** |
| 1 | 650 | 650 | 500 |
| 2 | 750 | 700 | 550 |
| 3 | 450 | 650 | 500 |
| 4 | 400 | 450 | 350 |
| 5 | 800 | 500 | 600 |
| 6 | 650 | 550 | 600 |
| 7 | 600 | 500 | 550 |
| 8 | 500 | 600 | 550 |
| 9 | 600 | 550 | 500 |
| 10 | 600 | 650 | 500 |
| 11 | 650 | 500 | 450 |
| 12 | 650 | 550 | 500 |
| Average | 608 | 571 | 513 |

From the data presented in Table 8.2, it can be seen that the average load of failure is as follows:

38 ºC: 608N with a standard deviation of 114.48N

50 ºC: 571N with a standard deviation of 78.21N

60 ºC: 513N with a standard deviation of 67.84N.

The results as presented in Figure 8.10 indicate that the lubricity of the synovial fluid decreases with increase in temperature.

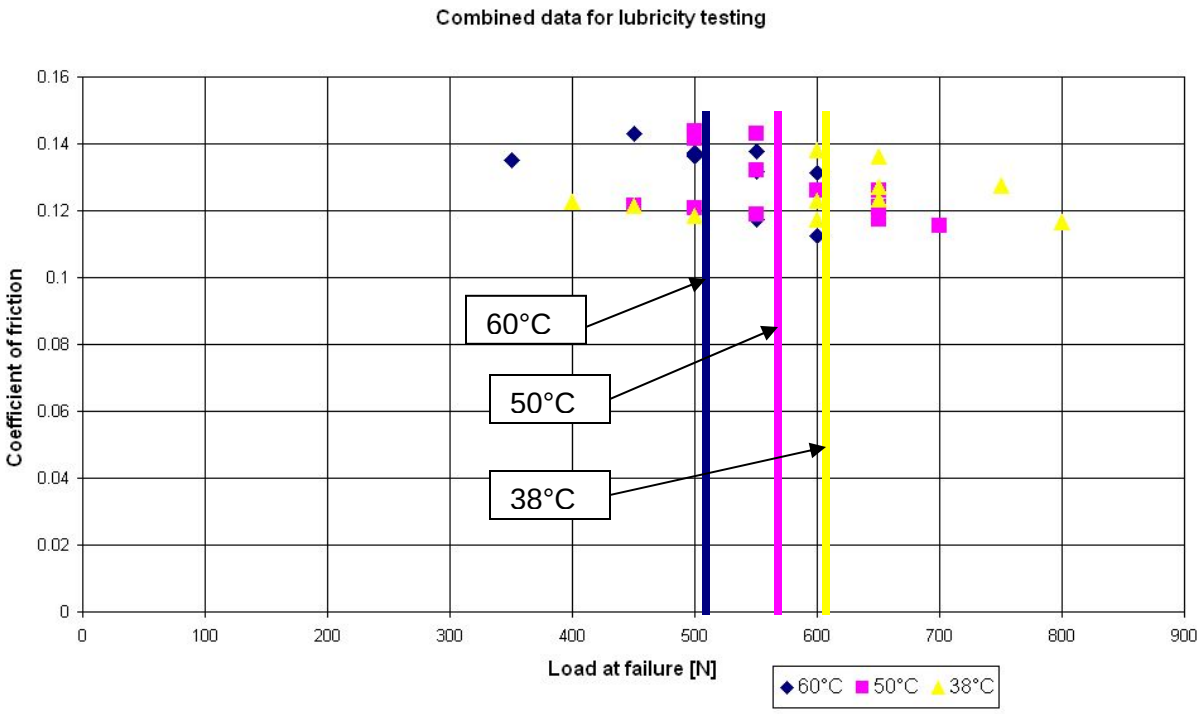


Figure 8.10: Combined lubricity data for 12 patients as tested with averages as indicated

## 8.6 Discussion

The average coefficient of friction as tested, does not differ a great deal between the three temperatures used for the lubricity testing. A small decrease can be seen in the load at failure, but if one takes into account the fact that the tests were done in 50N increments, it is realised that the difference can be neglected and can be ascribed to experimental error.

The surface defects of the acetabular components, as typically shown in Figure 8.11, Chapters 5 and 6 and in Annexure E are consistent with a lubricant with inadequate lubricity characteristics. The result of the inadequate lubrication is a heat build-up on the bearing surface between the UHMWPE acetabular cup and the ceramic femoral head resulting in the UHMWPE adhering to the femoral head and particles being ripped from the base material, as shown in Figure 8.11.

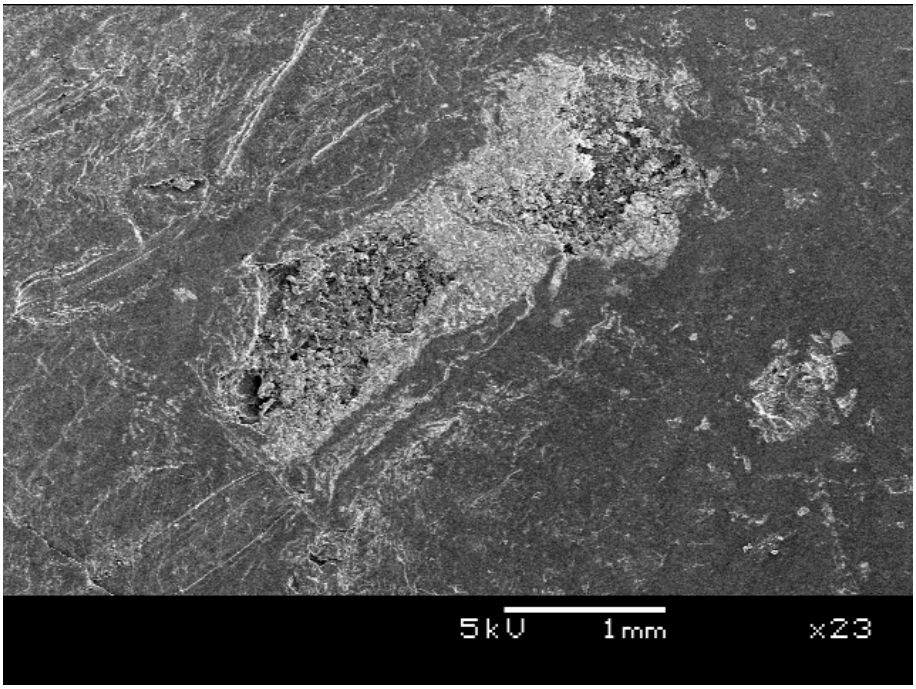


Figure 8.11: Adhesion wear on bearing surface of retrieved acetabular cup

The wear debris retrieved from the scar tissue as presented in Figures 8.12 and 8.13, as well as in Chapters 5 and 6 was also consistent of wear debris generated in a bearing where there was inadequate lubrication.

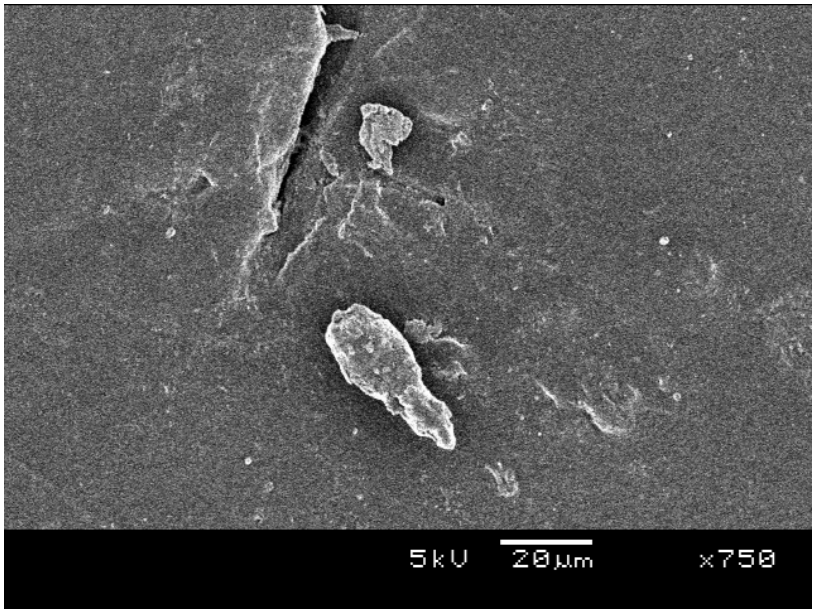


Figure 8.12: Wear particle still attached to UHMWPE acetabular cup

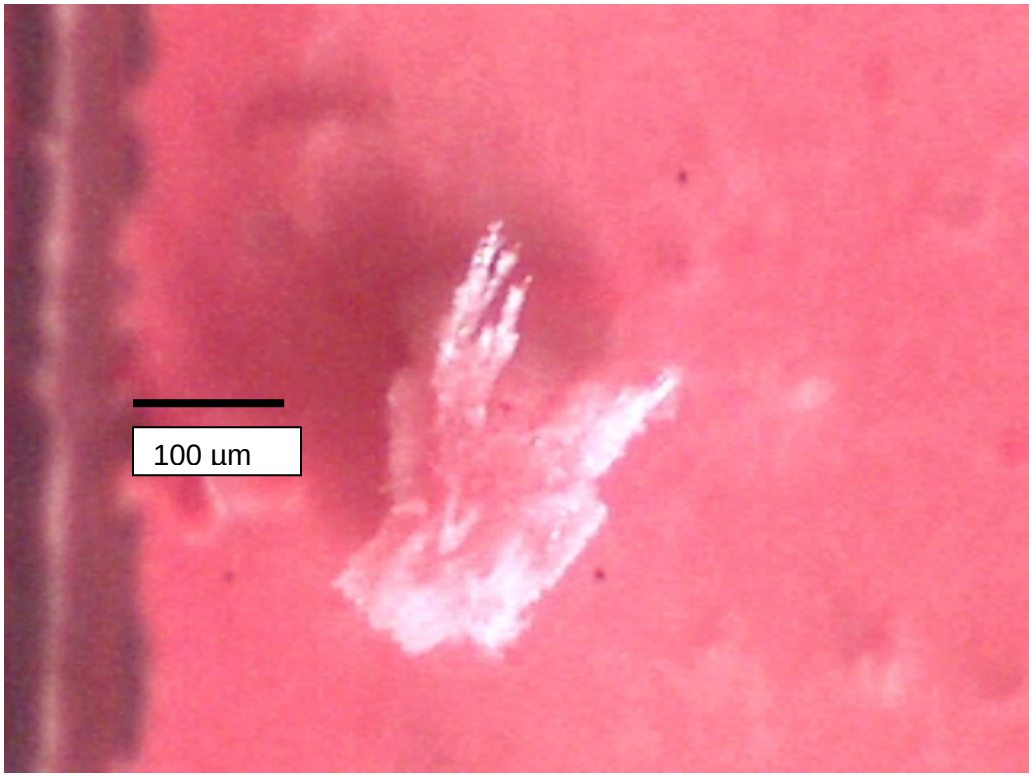


Figure 8.13: Wear debris retrieved from patient no. 5 (magnification x 200)

If the work, as presented in Chapters 5, 6 and 8 is analysed, the only conclusion that can be reached is that the main reason for mechanical failure of the UHMWPE acetabular components is overheating as a result of inadequate lubrication.

# CHAPTER 9

# CONCLUSION AND RECOMMENDATIONS

## 9.1 Conclusion

Owing to the crippling nature of arthritis, surgeons have been trying for well over a century to successfully treat this debilitating disease. Since the early 1970s when Sir John Charnley started with total hip replacement (THR) as a solution to this ever-increasing problem many different designs have been developed, but all of the designs revolved around a femoral stem, femoral head and acetabular component. Independent of the design, longevity of the implant remains a problem. The major cause of replacements, according to various hip registers (Chapter 1), is aseptic loosening due to osteolysis.

The main aim of this study has been to determine the root cause of mechanical failure of the acetabular cups and to discover the origin of the excessive amount of UHMWPE wear debris floating in the joint resulting in osteolysis.

During the study, various techniques have been used to investigate the acetabular components to try to establish the root cause for mechanical failure. These techniques include:

1. Visual inspection
2. Investigation making use of dye penetrant spray
3. Investigation under stereo microscope
4. Investigation making use of a scanning electron microscope
5. Electrophoresis
6. Mass-spectrometric analysis
7. SRV analysis of the synovial fluid.

The wear debris retrieved from the scar tissue surrounding the joint of a number of patients, were also analysed.

Apart from the obvious defects such as mechanical damage due to impingement, the main focus of this study is on the wear patches found on the inside of the acetabular components.

The wear areas presented as areas where the surface layer of the UHMWPE was ripped off by adhering to the rotating femoral head. This mechanism of failure is only possible if localised overheating takes place, which results in the material either adhering to the rotating femoral head or the material being squeezed out under the prevailing pressure. Both these mechanisms were confirmed by the wear debris retrieved from the scar tissue. This wear debris was identified as either droplets of UHMWPE or whisker-like wear products as shown in Chapters 5 and 6.

To confirm the fact that conditions with elevated temperatures exist, the brown discolouring on the inside of the acetabular cups was analysed, making use of electrophoresis, mass-spectrometric analysis and scanning electron microscope analysis. In this part of the study, it was confirmed that it was possible that the localised temperatures on the bearing surface had reached at least 60°C during in-vivo service. This temperature was confirmed by inserting a thermocouple just under the surface of an acetabular cup and then measuring the temperature while performing in-vitro testing on the hip simulator (see Chapter 7).

The wear debris as retrieved was also duplicated in the laboratory while the temperature on the surface was monitored. It was established that wear particles similar in shape and size were formed at temperatures in excess of 90 °C (see Chapter 7). At temperatures above 50 °C, the UHMWPE had shown extensive increase in creep, indicating that at these temperatures the material softens sufficiently for this type of debris to be generated (see Chapter 3).

The overheating as described can also only occur if there is a lack of lubrication in the bearing couple. The synovial fluid from 12 patients was retrieved during revision surgery. This synovial fluid was then tested on an SRV test machine to determine the lubricity characteristics of the synovial fluid as retrieved. It was discovered that the load-carrying capability of the synovial fluid did not comply with the minimum requirements for a fluid to function as a lubricant (Chapter 8). The lubricity characteristics of healthy synovial fluid were not assessed as it is very difficult to retrieve enough fluid from a healthy human being for a test.

The effect of crosslinking and irradiation was also determined on the creep characteristics of the UHMWPE. During these tests, it was determined normal irradiation as used during sterilisation has almost no effect on the creep properties. The biggest influence on the creep characteristics of the UHMWPE was obtained when the test material was crosslinked in a hydrogen atmosphere. A reduction of 82% was achieved at 60°C for crosslinked material.

The final conclusion of this study is that excessive amounts of wear debris are generated due to the localised overheating of the bearing couple as a result of insufficient lubrication. The localised heat build-up results in excessive amounts of wear debris being generated and deposited in the joint area causing osteolysis.

## 9.2 Recommendations

During the course of this study, a number of problem areas regarding the design of acetabular cups were discovered. The following recommendations are made to assist in follow-up studies in this field:

a. It has been shown that there is excessive heat build-up on the bearing surface. To enable designers to accommodate this heat build-up, a more detailed analysis to determine the material properties of UHMWPE at elevated temperatures is required. These properties include creep and impact strength, as well as creep in retained bearings as found in an acetabular cup. Another area that warrants further investigation is the influence of an alternating load on the creep behaviour of UHMWPE.

b. A better understanding of the mechanism feeding the lubrication into the joint will have to be developed. With the poor lubricity characteristics, it is vital to get enough of the lubricant into the joint to fulfil the necessary functions.

c. As indicated, the ceramic femoral heads do not have the ability to conduct heat away from the bearing surface resulting in premature failure. A suitable alternative material must be identified and tested over a substantial period of time to enable the analysis of the accumulated wear effect.

d. More conclusive comparative testing between the different materials and processes will have to be conducted. The materials that will have to be evaluated are virgin and crosslinked UHMWPE, stainless steel, chrome Cobalt, alumina and zirconium femoral heads. These tests will have to be done over a longer period than 500 000 cycles to be able to better assess the effect of third-body wear due to the wear products floating around in the joint.

e. The best alternative currently available is a crosslinked cup fitted in a metal backing, provided that the UHMWPE liner fits snugly into the metal backing. The advantage of this combination is that a thinner liner can be used resulting in better heat transfer to the surrounding bone, as well as better restraint to creep. As illustrated, the crosslinked material provides better creep resistance at elevated temperatures with the added increase in wear resistance.

f. A thorough investigation will have to be conducted to develop a lubrication model giving an even better correlation between in-vitro and in-vivo results. The size and shape of the wear debris retrieved must be used as guidance in the development of this lubrication model.

**References**

Adultdata, 1988, The handbook of adult anthropometric and strength Measurements, data for design safety, United Kingdom, Department of Trade and Industry.

ASTM D2990, see page 67, 1990, *Tensile, compressive and flexural creep and creep rupture of plastics.*

ASTM D5606-97, see page 202, 2002, Standard test method for determining extreme pressure properties of lubricating greases using high frequency, linear ossilating (SRV) machine Barbour PSM, Barton DC, Fisher J 1995, 'Influence of Contact Stress on The Wear of UHMWPE for Total Replacement Hip Prostheses', *Wear*, Vol. 181 - 183, 250 – 257.

Bajaria SH, Bellare A 1998, 'Deformation, morphology, and wear behaviour of polyethylene used in orthopaedic implants', *Medical Plastics and Biomaterials Mag.*

Bergmann G, Graichen F, Rohlmann A 1993, 'Hip loading during walking and running, measured in two patients', *J Biomech*, Vol. 26(8), 969 – 990.

Bergmann G, Kniggendorf F, Graichen F, Rohlman A 1995, 'Influence of shoes and heel strike on the loading of the hip joint', *J Biomechanics*, Vol. 28, 817 – 827.

Bennet D, Orr JF, Baker R, 1996, 'The influence of shape and sliding distance of movement loci of the femoral head on the wear of the acetabular cup', *Dep of Mech and Manufacturing Engineering,* Queens Univeristy of Belfast.

Boresi AP, Sidebottom OM 1985, *Advanced mechanics of materials*, Fourth Edition, Wiley.

Buford A, Goswani T, 2004, 'Review of wear mechanisms in hip implants: Paper I-General', *Materials & Design* Vol. 25, 385 – 393.

Bragdon CR, Jasty M, Kawate K, McGrory BJ, Elder JR, Lowenstein J, Harris WH, 1997, 'Wear of retrieved cemented polyethylene acetabula with alumina femoral heads', *J Arthro*, Vol. 2, 119 – 125.

Calonius O, Saikko V 2002, 'Slide track analysis of eight contemporary hip simulator designs'*, J Biomechanics*, Vol. 35, 1439 – 1450.

Charnley J, Halley DK 1975, 'The rate of wear in total hip replacement', *Clin Orth and Rel Res*, Vol. 112, 170 – 179.

Charnley, J. 1979, *Low friction arthroplasty of the hip - Theory and practice.* Published by Springer Verlag, Berlin, Introduction.

Claus A, Sychterz CJ, Hopper RH, Engh CA 2001, 'Pattern of osteolysis around two different cementless metal backed cups', *J Arthro,* Vol. 16(8), 177 – 182.

Clarke IC, Gustafson A. Subrata S, Campbell P 1996, 'Hip simulator ranking of polyethylene wear', *Acta Orthop Scand*, Vol. 67(2), 128 – 132.

Costa L, Bracco P 2001, 'Analysis of products diffused into UHMWPE prosthetic components in vivo*', Biometerials*, Vol. 22, 307 – 315.

Davidson JA, Gir S, Paul JP 1988, 'Heat transfer analysis of frictional heat dissipation during articulation of femoral implants', *J Biomed Mater Res*, Vol. 22(A3), 281 – 309.

Davidson D, Graves S, Batten J, Cumberland W, Fraser J, Harris J, Morgan D, Morris P, Wood D, Cooper J, Simpson S 2002, 'Australian Orthopaedic Association National joint replacement registry'. *Annual Report*, Adelaide AOA .

Davidson D, Graves S, Batten J, Cumberland W, Fraser J, Harris J, Morgan D, Morris P, Wood D, Cooper J, Simpson S 2003, 'Australian Orthopaedic Association National Joint Replacement Registry'. *Annual Report*, Adelaide AOA.

Dowson D, Taheri S, Wallbridge NC 1987, 'The role of counterface imperfections in the wear of polyethylene', *Wear*, Vol. 119, 277 – 293.

Dumbleton JH, Manley T, Avram AE 2002, 'A literature review of the association between wear rate and osteolysis in total hip arthroplasty'. *J Arthro*, Vol. 17(5), 649 – 661.

Du Plessis TA, Grobbelaar CJ, Marais F 1977, 'The improvement of polyethylene prostheses through radiation crosslinking', *Radiat Phys Chem*, Vol. 9, 647 – 652.

Eggli S, Brun S, Gerber C, Ganz R 2002, 'Comparison of polyethylene wear with femoral heads of 22 mm and 32 mm: A prospective, randomised study', *J Bone Joint Surg*, Vol. 84(B), 447 -451.

Engh CA, Bobyn JD 1985, 'Biological fixation in total hip arthroplasty', *Slack Orthopaedics*, Vol. 16.

*Engineering material handbook, Vol. 2* 1987, ASM International, 167 – 1702.

Fisher J, Chan KL, Hailey JL, Shaw D, Stone M 1995, 'Preliminary study of the effect of aging following irradiation on the wear of ultra high molecular weight polyethylene', *J Arthroplasty*, Vol. 10, 689 – 692.

Fourie EF, Burger NDL 1999, 'Ultra high molecular weight polyethylene (UHMWPE), an engineering approach', SA Bone and Joint, Vol. 9 no 3, 163 – 164.

Foguet P, Hashmi F, Lawrence T. 2003, 'Case Report: metaphyseal osteolysis around a titanium reconstruction nail', *Int J care Injured*, Vol. 34, 374 – 377.

Gold Technology no 2*, June 1990 and Workshop notes, SA Mint.*

Grobbelaar CJ, Weber FA, Spirakis K 1999, 'Clinical experience with gamma irradiation crosslinked polyethylene - A 14 to 20 year follow-up report', *SA Bone and Joint*, Vol. 9 no 3, 140 – 147.

Haraguchi K, Sugano N, Nishii, Sakai T, Yoshikawa H, Ohzona T, 2001, 'Influence of polyethylene and femoral head surface quality on wear, A retrieval study', *Int Orthopaedics*, Vol. 25, 29-34.

Havelin LI, Furnes O, Espehaug B 2003, 'The Norwegian Arthroplasty Register', *Annual Report.*

http://www.aesculap.de/ — last accessed November 2004.

http://www.centerpulse-orthopedics.com/uk/en/Home/Home — last accessed November 2004.

http://www.ceraver.fr/anglais/sommaireang.htm — last accessed November 2004.

http://www.depuy.com/ — last accessed November 2004.

http://www.geocities.com/hip_replacements/history — last accessed November 2004.

http://www.healthsystem.virginia.edu/UVAHealth/adult_arthritis/anatomy.cfm — last accessed November

http://www.principalmetals.com/glossary/odoc.htm — last accessed November 2004.

http://science.nhmccd.edu/biol/tissue/areolar.html — last accessed November 2004

http://www.thehipdoc.com/history.htm — last accessed November 2004.

http://www.uct.ac.za/microbilogy/sdspage.htm - last accessed November 2005.

http://www.utahhipandknee.com/history.htm - last accessed November 2004.

Huo MH, Cook SM 2001, 'What's new in hip arthroplasty', *J Bone Joint Surg*, 83A, number 10, 1598 – 1610.

Hutchings IM 1992 *Tribology, Friction and wear of engineering materials*, Arnold.

ISO TR 9325 1989, '*Implants for surgery - Partial and total hip joint prosthesis - Recommendations for simulators for evaluation of hip joint prosthesis'.*

ISO 12891-3, 2000, *'Retrieval and analysis of surgical implants, Part 3, Analysis of retrieved polymeric surgical implants'.*

ISO 14242-1, 2002, '*Implant for surgery - Wear of total hip joint prosthesis, Part 1: Loading and displacement parameters for wear testing machines and corresponding environmental conditions for test*' .

ISO 14242-1, 2002, *'Loading and displacement parameters for wear testing machines and corresponding environmental conditions for test'.*

Jasty M, Goetz DD, Bragdon CR. 1997, 'Wear of polyethylene acetabular components in total hip arthroplasty: An analysis of one hundred and twenty eight components retrieved at autopsy or revision operations', *J Bone and Joint Surg*, Vol. 79-A:349-358.

Kazuo Hirakawa, Thomas W Bauer 1997, 'Effect of femoral head diameter on tissue concentration of wear debris', *J Biomed Mater Res*, Vol. 36, 529 – 535.

Kesteris U, Hardinge K, Ilchmann T, Wingstrand H, 2003, 'Polyethylene wear in prosthetic hips with loose components', *J Artho*, Vol. 18, 10-15.

Klapach AS, Callaghan JJ, Goetz DD, Olejniczak JP, Richard RC 2001, 'Charnley total hip arthroplasty with use of improved cementing techniques: A minimum twenty-year follow-up study', *J Bone Joint Surg*, 83A, number 12, 1840-1848.

Kukureka SN, Chen YK, Liao P, Rao M. 1995, 'The wear mechanisms of acetal in unlubricated rolling-sliding contact', *Wear*, Vol. 185, 1 – 8.

Kummer B 1976, '*Biomechanics of the hip and knee joint, advances in artificial hip and knee joint technology*', Springer Verlag, 24 – 52.

Lee KY, Pienkowski D. 1998, 'Compressive creep characteristics of extruded ultrahigh molecular weight polyethylene', *J Biomed Mater Res*, Vol. 39, 261 – 265.

Lewis G 2001, 'Properties of crosslinked ultra high molecular weight polyethylene', *J Biomaterials*, Vol. 22, 371 – 401.

Li S, Burstein AH 1994, 'Current Concepts Review. Ultra high molecular weight polyethylene. The material and its use in total joint replacement', *J Bone and Joint Surg*, Vol. 76 A(7), 1080 – 1090.

Livermore J, Ilstrup D, Morrey B 1990, 'Effect of femoral head size on wear of the polyethylene acetabular component', *J Bone and Joint Surg*, Vol. 72A, 518 – 528.

Lu Z, McKellop H 1999, 'Potential thermal artifacts in hip joint wear simulators', *J Biomed Mater Res (appl Biomater)*, Vol. 48, 458 – 464.

Mallchau H, Herberts P, Garellick G, Söderman P, Eisler T 2000, 'Prognosis of total hip replacement, update of results and risk ratio, analysis for revision and re-revision' *Swedish National Hip Arthroplasty Register* 1979 – 2000.

Maloney W, Smith RL, Schmalzried TP, Chiba J, Huene D, Rubash H 1995, 'Isolation and characterization of wear particles generated in patients who have had failure of a hip arthroplasty without cement', *J Bone and Joint Sur*, Vol. 77(A), 1301 - 1310.

Manley MT, D'Antonio J, Capello WN, Edidin AA 2002, 'Osteolysis: A Dissease of Access to Fixation Interfaces', *Clin Orthop,* Vol. 1(405), 129 – 137.

Masaoka T, Clark IC, Yamamoto K, Tamura J, Williams PA, Good VD, Shoji H, Imakiiri A 2003, 'Validation of volumetric and linear wear measurements in UHMWPE cups - a hip simulator study', *Wear*, Vol. 254, 1 - 8, 2003.

Material data sheet, UHMWPE, Poli HiSolidur, 1999.

McCoy TH, Salvati EA, Ranawat CS, Wilson PD 1988, 'A fifteen-year follow-up study of one hundred charnley low-friction arthroplasties', *Orthop Clin North Am*, Vol. 19, 467 – 476.

McKellop H, Shen F. Lu B, Campbell P, Salovey R 1997, 'Effect of sterilization method and other modifications on the wear resistance of UHMWPE acetabular cups, in polyethylene wear in orthopaedics', *Implants Workshop, Minneapolis, Society of Biomaterials*, 20 – 31.

McKellop H, Shen F, Lu B, Campbell P, Salovey R 2000, 'Effect of sterilization method and other modifications on the wear resistance of acetabular cups made of ultra high molecular weight polyethylene: A hip simulator study', *J Bone Joint Surg*, Vol. 82(A), 1708 – 1725.

Mendenhall S 2000, 'Putting joint replacement in historical perspective - Compared to other surgeries, TJR has remained a successful and cost effective procedure', *Orthopaedics Today.*

Meng Deng R, Latour A 1998. 'Study of creep behaviour of ultra high molecular

weight polyethylene systems', *J Biomed Mater res*, Vol. 40, 214 – 223.

Moratoglu OK, Bragdon CR, O'Connor AS, Jasty M, Harris W 1999, 'A novel method of cross-linking ultra-high-molecular-weight polyethylene to improve wear, reduce oxidation, and retain mechanical properties', J of Arthoplasty, Vol 16, 2, 149 – 160

Moratoglu OK, Greenbaum BA, Bragdon CR, Jasty M, Freiberg AA, Harris WH 2004, Surface analysis of early retrieved acetabular polyethylene liners, A comparison of conventional and highly crosslinked polyethylenes, J of Arthoplasty, Vol 19, 1, 68 - 77

Norton MR, Yarlagadda R, Anderson GH 2002, 'Catastrophic failure of the elite plus total hip replacement, with a hylamer acetabulum and zirconia ceramic femoral head', *J Bone Joint Surg*, Vol. 84(B), 631 – 635.

Oakley AP, Matheson JA, Rapid 2003, 'Osteolysis after hip arthroplasty in paget's disease'*. J Artho,* Vol. 18(2), 204 – 207.

Oonishi H, Kuno M 1997, 'The optimum dose of gamma radiation-heavy dose to low wear polyethylene in total hip prostheses', *J of Mat Science in Med*, Vol. 8, 11-18.

Orishimo KF, Hopper RH, Engh CA 2003, 'Long term in-vivo wear performance of porous coated acetabular components sterilized with gamma irradiation and in air or ethylene oxide', *J Arthro*, Vol. 18, 546 – 552.

Parr, Jack E 1995, 'Effects of sterilization methods on ultra high molecular weight polyethylene (UHMWPE)*', Basic Science Conference.*

Paul JP 1976, '*Loading on normal hip and knee joints and on joint replacements, advances in artificial hip and knee joint technology'*, Springer Verlag, 53 - 70.

Pietrabissa R, Raimondi M, Martino E 1998, 'Wear of polyethylene cups in total hip arthroplasty: A parametric mathematical model', *Med Eng and Phys*, Vol. 20(3), 199 – 210.

Ries MD, Scott L 2001, 'Relationship between gravimetric wear and particle generation in hip simulators: Conventional compared with cross-linked polyethylene', *J Bone Joint Surg*, Vol. 83 (A) Suppl 2 Part 2, 116 – 122.

Rimnac CM, Klein RW, Betts F, Wright TM 1994, 'Post irradiation aging of ultra high molecular weight polyethylene', *J Bone and Joint Surg*, Vol. 76A (7), 1052 – 1056.

Robinson CM, Adams CJ 2002, 'Implant related fractures of the femur following hip fracture surgery'*, J Bone Joint Surg* Vol. 84A, Number 7, 1116 – 1122.

Rybicki E, Purves M, 1996, 'SDS Polyacrylamide gel electrophoresis (SDS-Page', *Molecular biology techniques manual,* Dept of Microbiology, University of Cape Town.

Saikko V, Ahlroos T, Calonius O, Keränen J 2001, 'Wear simulation of total hip prostheses with polyethylene against CoCr, alumina and diamond like carbon'*, Biomaterials*, Vol. 22, 1507 – 1514.

Saum KA 1994, 'Oxidation vs depth and time for polyethylene-gamma sterilized in air*', Trans ORS*, 174 – 185.

Schaldach, M, Hohmann D. 1976. '*Advances in artificial hip and knee joint technology',* Engineering in Medicine 2, Springer Verlag.

Schmalzried TP, Campbell PA, Schmitt AK, Brown IC, Amstutz HC 1997, 'Shape and dimensional characteristics of polyethylene wear particles generated in vivo by total knee replacements compared to total hip replacements', *J Biomed Mater Res*, Vol. 38, 203 -210.

Schmalzried T P, Callaghan J J 1999, 'Wear in total hip and knee replacements', *J Bone and Joint Surg*., Vol. 81-A:115-136.

Schulte KR, Callaghan JJ, Kelly SS, Johnston RC 1993, 'The outcome of charnley hip arthroplasty with cement after a minimum twenty-year followup', *J Bone Joint Surg*, Vol. 75A, Number 7, 961 – 975.

Shigley JE, Mischke CR 2003, *Mechanical engineering design - sixth metric edition,* New York, McGraw-Hill.

Smith SL, Unsworth A 2000, 'A 5 station hip simulator', *J Bone Joint Surg*, Vol. 82(B) Suppl. 2, 137-142.

Sokoloff L, 1978, 'The joints and synovial fluid Vol. 1', *Academic Press Inc*, ISBN 0 12 655101 4.

Sulkowska A, 1997, 'Temperature effect on the stability of the complexes between purine derivates and serum albumien: proton NMR study', *Journal of Molecular Structure*, Vol. 4, 410 – 411.

Sun DC, Wang A 1996, 'Effect of radiation-Induced crosslinking on creep and wear performance of ultra-high molecular weight polyethylene, American Academy of Orthopaedic Surgeons*', 1996 Annual Orthopaedic Meeting, Scientific program.*

Sychterz CJ, Moon KH, Hashimoto Y, Terefenko KM, Engh CA Jr, Bauer TW 1996, 'Wear of polyethylene cups in total hip arthroplasty: A study of specimens retrieved post mortem', *J Bone Joint Surg*, Vol. 78 (A), 1193 – 1200.

The Norwegian arthroplasty register 2003, The department of Orthopaedic Surgery, Haukeland University Hospital.

Tipper JL, Firkins PJ, Besong AA, Barbour PSM, Nevelos J, Stone MH, Ingham E, Fischer J, 2001, 'Characterisation of wear debris from UHMWPE on zirconia ceramic, metal-on-metal and alumina ceramic-on-ceramic hip prostheses generated in a physiological anatomical hip joint simulator*', Wear*, Vol. 250, 120 -128.

Trieu HH, Paxson RD 1995, 'The oxidized surface layer in shelf aged UHMWPE'*, ORS*, Vol. 758,1995.

Wang A, Sun DC, Stark C, Dumbleton JC 1995, 'Wear mechanisms of UHMWPE in total joint replacements', *Wear* 181-183, 241-249.

Wang A, Essner A, Stark C, Dumbleton JH 1996, 'Comparison of the size and morphology of UHMWPE wear debris produced by a hip joint simulator under serum and water lubricated conditions'*, Biomaterials*, Vol. 17, 865-871.

Wang A, Essner A. Polineni VK, Stark C 1997, 'Wear mechanisms and wear testing of ultra high molecular weight polyethylene in total joint replacement, in polyethylene wear in orthopaedics implants workshop'*, Minneapolis, Society of Biomaterials*, 4 – 18.

Wang A, Sun DC 1997, 'Orientation softening in the deformation and wear of ultra high molecular weight polyethylene', *Wear* 203 -204, 230-241.

Wang A, Essner A, Polineni VK, Stark C, Dumbleton JC 1998, 'Lubrication and wear of ultra high molecular weight polyethylene in total joint replacements', *Tribology International*, Vol. 31 nr 1-3, 17-33.

Wang A, Polineni VK, Stark C, Dumbleton JH 1998, 'Role of proteins and hylauronic acid in the lubrication and wear of UHMWPE acetabular cups', *24th Annual Meeting of the Society for Biomaterials, April 22-26, 1998*, San Diego, California, USA.

Wang A, Essner A, Dumbleton JH 1999, 'A biaxial line contact wear machine for the evaluation of implant bearing materials for total knee joint replacements', *Wear*, 225 -229, 701-707.

Wilkinson JM, Hamer AJ, Rogers A, Stockley I, Eastell R 2003, 'Bone mineral density and biochemical markers of bone turnover in aseptic loosening after total hip arthroplasty', *J Orth Res*, Vol. 21.

Young-Hoo, K, Kim JS, 2001, 'A comparison of polyethylene wear in hips with cobalt-chrome or zironia heads: A Prospective, randomized Study', *J Bone Joint Sur*, Vol. 83(B), 742 – 750.

Zupanc O, Antolic V, 2001, 'The assessment of contact stress in the hip joint after operative treatment for severe slipped capital femoral epiphysis', *Int Orth*, Vol. 25, 9-12.

# ANNEXURE A

## Retrieval analysis of 20 acetabular cups

## Patient 1

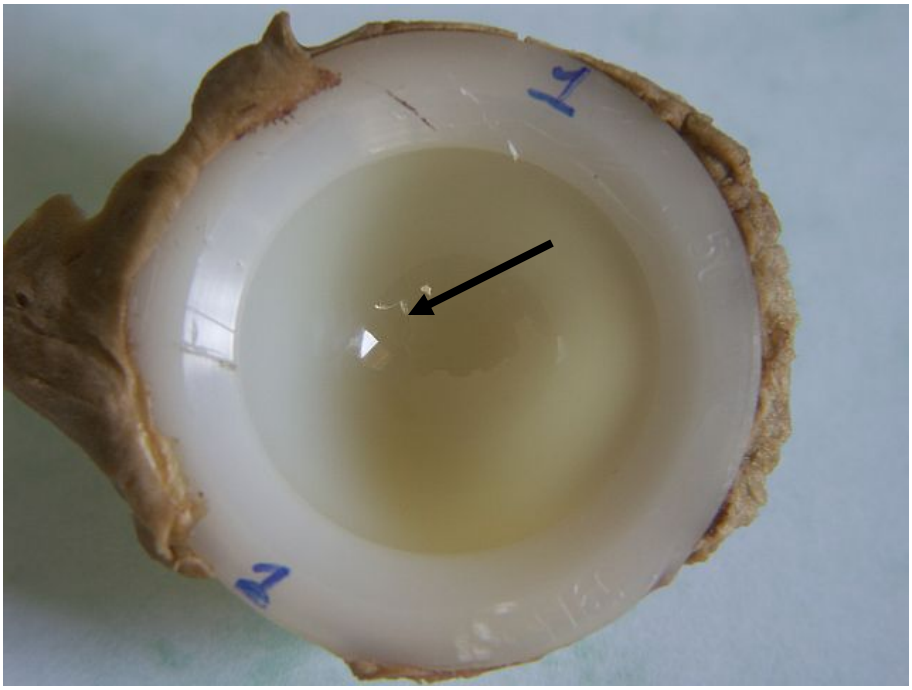

**Figure A1**

**Figure A2**

## Cup analysis: Patient 1

| | | |
|---|---|---|
| 1 | Femoral head size | 32 mm |
| 2 | Type of head | Alumina |
| 3 | Cup type | UHMWPE - Osteal |
| 4 | Crosslink | No |
| 5 | Amount of linear wear | ± 1.1 mm |
| 6 | Duration in vivo | 13 years and 7 months |
| 7 | Size of wear debris from pathologist | 10 – 30 µm |
| 8 | Visible discoloration | Yes (Figure 1) |
| 9 | Metal backing | No |
| 10 | Thickness of poly | 9 mm |
| 11 | Mechanical damage | No |
| 12 | Cracks in material | No |
| 13 | Plastic flow | No |
| 14 | Scratches | No (visually) |
| 15 | Adhesion wear | Yes |
| 16 | Wear particles embedded in base material | No |
| 17 | Flaking | No |

**Patient 2**

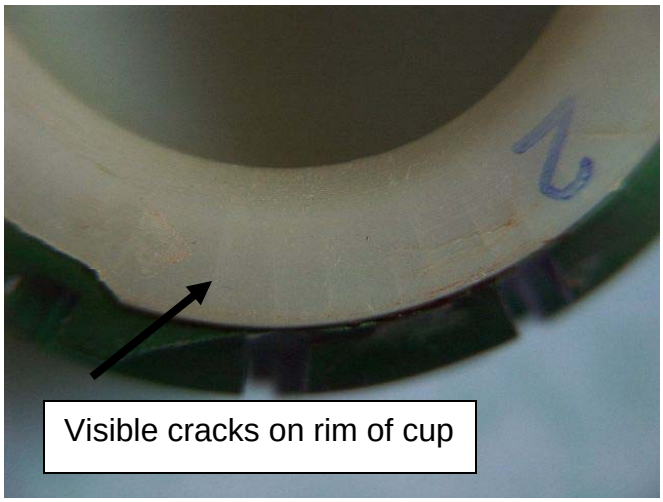


**Figure A3**

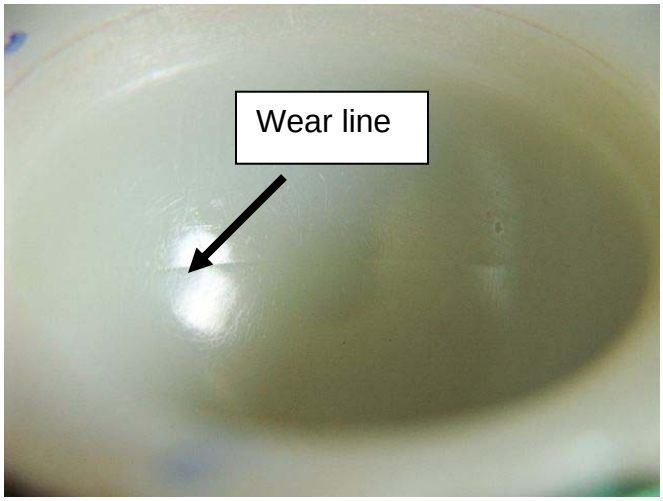


**Figure A4**

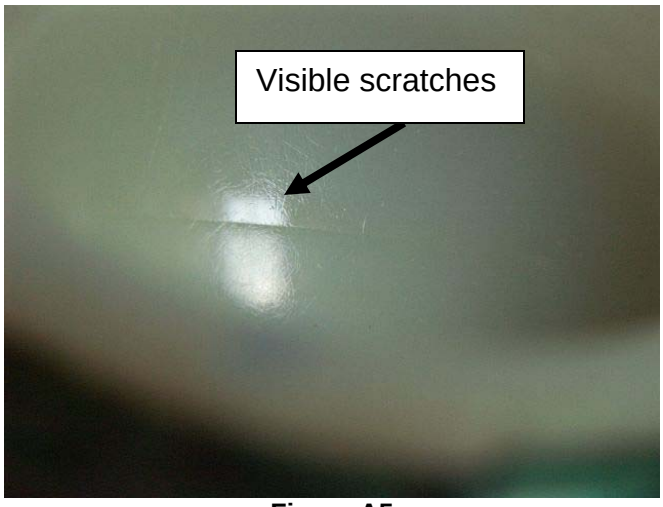


**Figure A5**

## Cup analysis: Patient 2

| | | |
|---|---|---|
| 1 | Femoral head size | 32 mm |
| 2 | Type of head | Alumina |
| 3 | Cup type | UHMWPE - Osteal |
| 4 | Crosslink | No |
| 5 | Amount of linear wear | ± 0.8 mm |
| 6 | Duration in vivo | 17 years |
| 7 | Size of wear debris from pathologist | 20 – 110 µm, avg. 40 µm |
| 8 | Visible discoloration | Yes (Figure 1) |
| 9 | Metal backing | No |
| 10 | Thickness of poly | ± 7 mm |
| 11 | Mechanical damage | Yes |
| 12 | Cracks in material | Yes |
| 13 | Plastic flow | No |
| 14 | Scratches | Yes |
| 15 | Adhesion wear | No |
| 16 | Wear particles embedded in base material | No |
| 17 | Flaking | No |

**Patient 3**

**Figure A6**

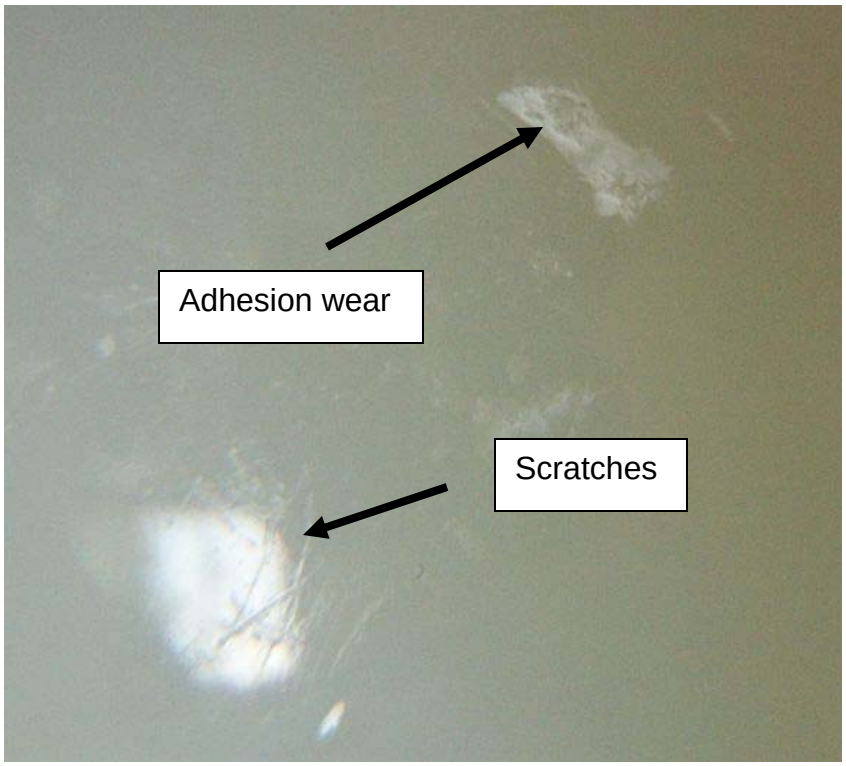


**Figure A7**

## Cup analysis: Patient 3

| | | |
|---|---|---|
| 1 | Femoral head size | 26 mm |
| 2 | Type of head | Alumina |
| 3 | Cup type | UHMWPE - Aesculab |
| 4 | Crosslink | No |
| 5 | Amount of linear wear | ± 0.4 mm |
| 6 | Duration in vivo | 6 years |
| 7 | Size of wear debris from pathologist | 10 – 50 µm |
| 8 | Visible discoloration | Yes (Figure 6) |
| 9 | Metal backing | No |
| 10 | Thickness of poly | 9 mm |
| 11 | Mechanical damage | No |
| 12 | Cracks in material | No |
| 13 | Plastic flow | No |
| 14 | Scratches | Yes |
| 15 | Adhesion wear | Yes |
| 16 | Wear particles embedded in base material | Yes |
| 17 | Flaking | No |

**Patient 4**

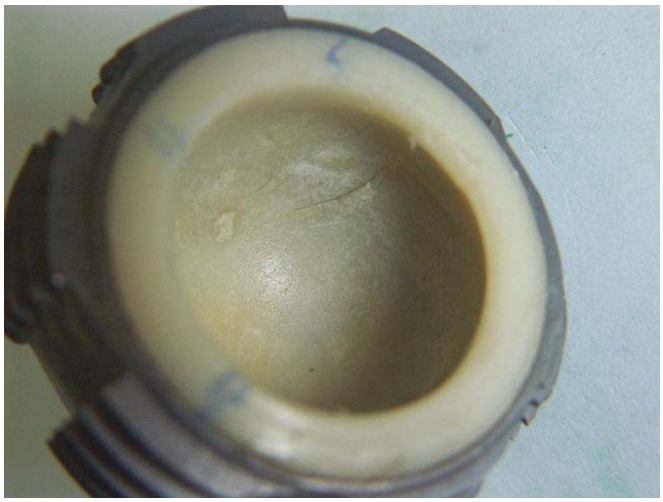

**Figure A8**

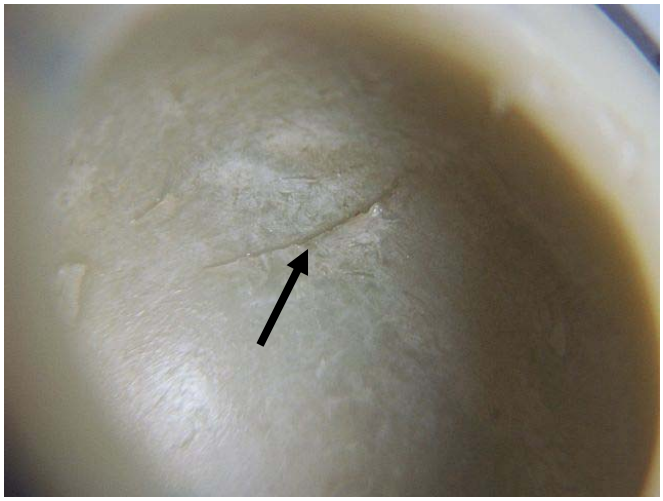

**Figure A9**

**Figure A10**

## Cup analysis: Patient 4

| | | |
|---|---|---|
| 1 | Femoral head size | 32 mm |
| 2 | Type of head | Alumina |
| 3 | Cup type | UHMWPE – ARD |
| 4 | Crosslink | No |
| 5 | Amount of linear wear | ± 4.5 mm |
| 6 | Duration in vivo | 12 years |
| 7 | Size of wear debris from pathologist | 10 – 90 µm |
| 8 | Visible discoloration | No |
| 9 | Metal backing | Yes |
| 10 | Thickness of poly | ± 5 mm |
| 11 | Mechanical damage | Yes |
| 12 | Cracks in material | Yes |
| 13 | Plastic flow | No |
| 14 | Scratches | Yes |
| 15 | Adhesion wear | Yes |
| 16 | Wear particles embedded in base material | Yes |
| 17 | Flaking | No |

**Patient 5**

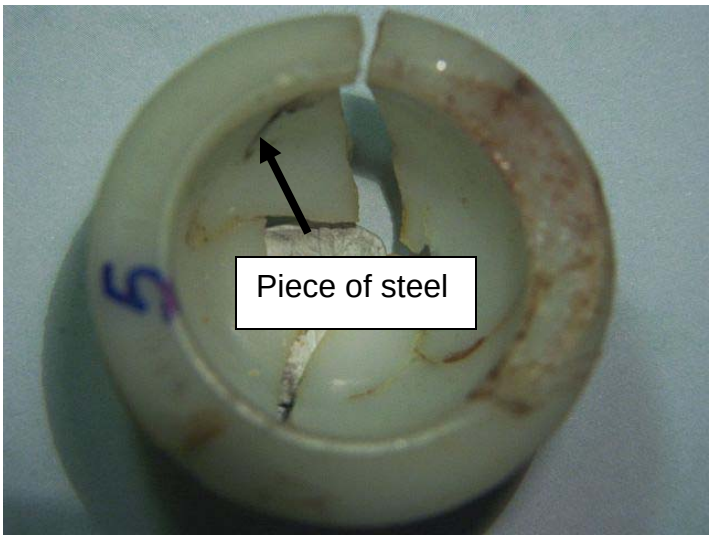


**Figure A11**

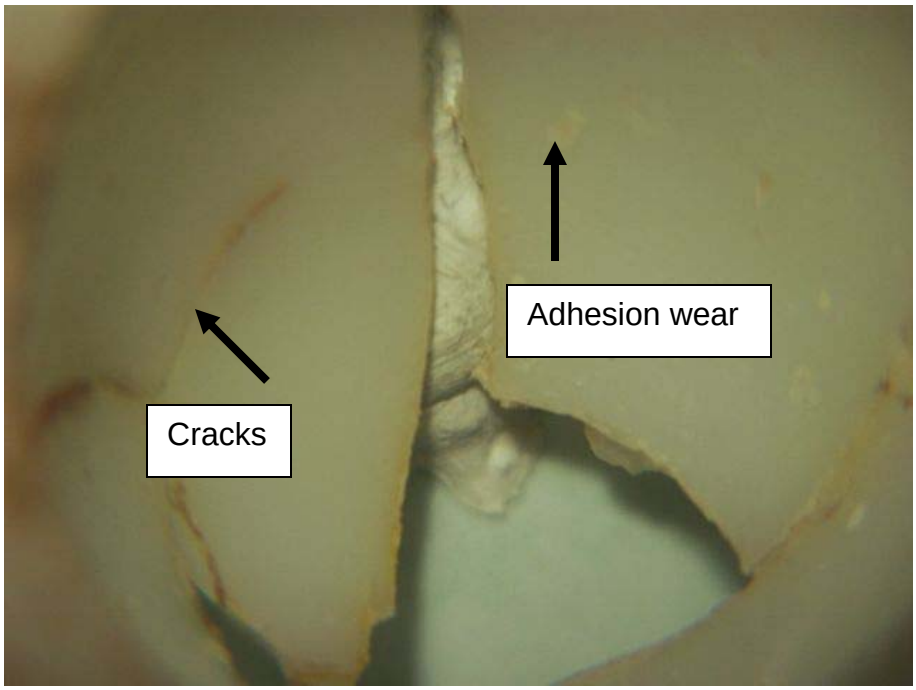


**Figure A12**

## Cup analysis: Patient 5

| | | |
|---|---|---|
| 1 | Femoral head size | 32 mm |
| 2 | Type of head | Stainless |
| 3 | Cup type | UHMWPE – ARD |
| 4 | Crosslink | No |
| 5 | Amount of linear wear | ± 5 mm |
| 6 | Duration in vivo | 9 years and 5 months |
| 7 | Size of wear debris from pathologist | 100 – 800 µm, avg. 600 µm |
| 8 | Visible discoloration | No |
| 9 | Metal backing | No |
| 10 | Thickness of poly | 7 mm |
| 11 | Mechanical damage | Yes |
| 12 | Cracks in material | Yes |
| 13 | Plastic flow | No |
| 14 | Scratches | Yes |
| 15 | Adhesion wear | Yes |
| 16 | Wear particles embedded in base material | Yes |
| 17 | Flaking | No |

**Patient 6**


**Figure A13**

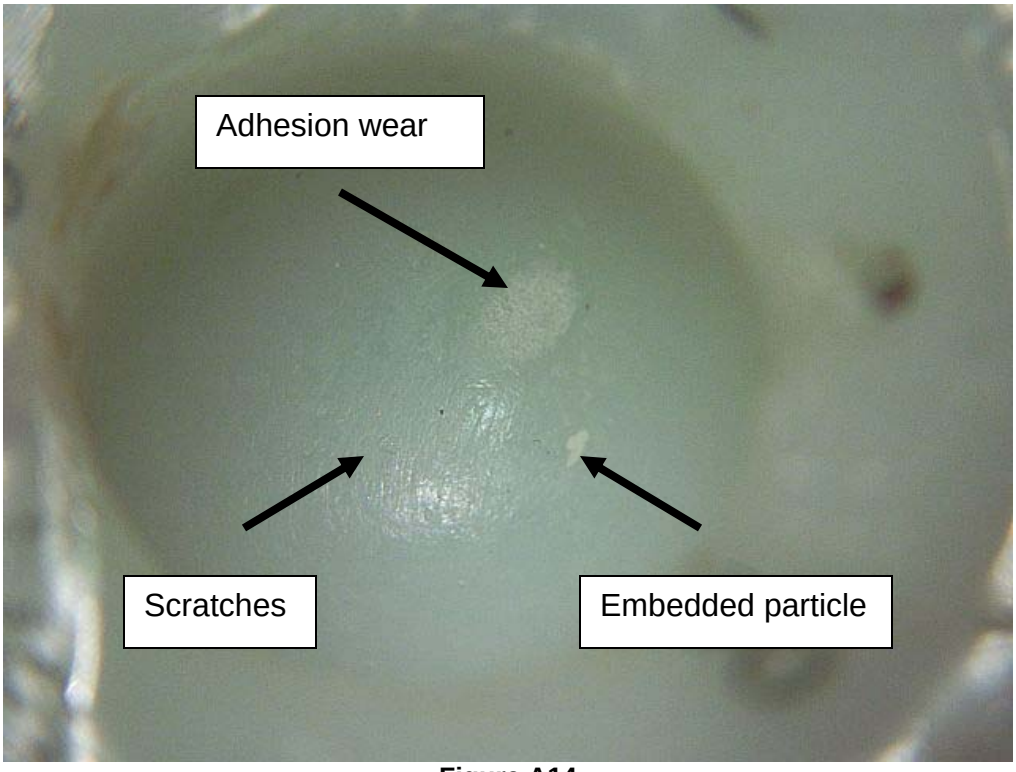


**Figure A14**

## Cup analysis: Patent 6

| | | |
|---|---|---|
| 1 | Femoral head size | 22 mm |
| 2 | Type of head | Stainless |
| 3 | Cup type | UHMWPE – Charnley |
| 4 | Crosslink | No |
| 5 | Amount of linear wear | ± 3 mm |
| 6 | Duration in vivo | 8 years |
| 7 | Size of wear debris from pathologist | 60 – 140 µm |
| 8 | Visible discoloration | No |
| 9 | Metal backing | No |
| 10 | Thickness of poly | 14 mm |
| 11 | Mechanical damage | No |
| 12 | Cracks in material | No |
| 13 | Plastic flow | No |
| 14 | Scratches | Yes (figure 14) |
| 15 | Adhesion wear | Yes (figure 14) |
| 16 | Wear particles embedded in base material | Yes (figure 14) |
| 17 | Flaking | No |

**Patient 7**

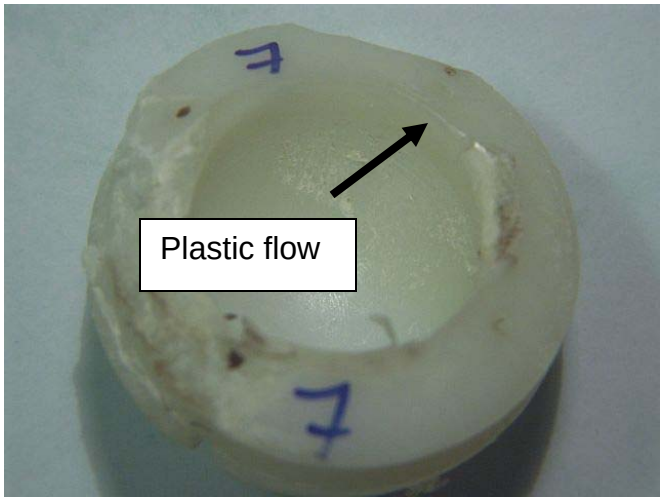


**Figure A15**

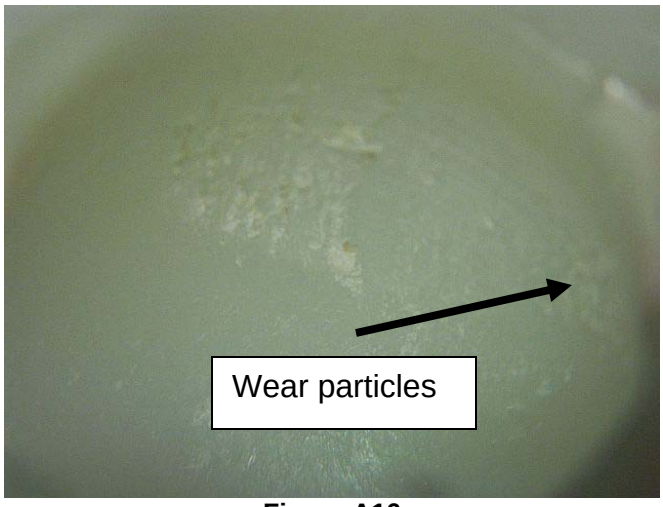


**Figure A16**

**Figure A17**

## Cup analysis: Patient 7

| | | |
|---|---|---|
| 1 | Femoral head size | 30 mm |
| 2 | Type of head | Stainless steel |
| 3 | Cup type | UHMWPE – ARD |
| 4 | Crosslink | No |
| 5 | Amount of linear wear | ± 5 mm |
| 6 | Duration in vivo | 23 years and 5 months |
| 7 | Size of wear debris from pathologist | 20 – 180 µm |
| 8 | Visible discoloration | No |
| 9 | Metal backing | No |
| 10 | Thickness of poly | 9 mm |
| 11 | Mechanical damage | Yes |
| 12 | Cracks in material | No |
| 13 | Plastic flow | Yes (figure 15) |
| 14 | Scratches | Yes (figure 16 & 17) |
| 15 | Adhesion wear | Yes (figure 16 & 17) |
| 16 | Wear particles embedded in base material | Yes (figure 16) |
| 17 | Flaking | No |

## Patient 8

**Figure A18**

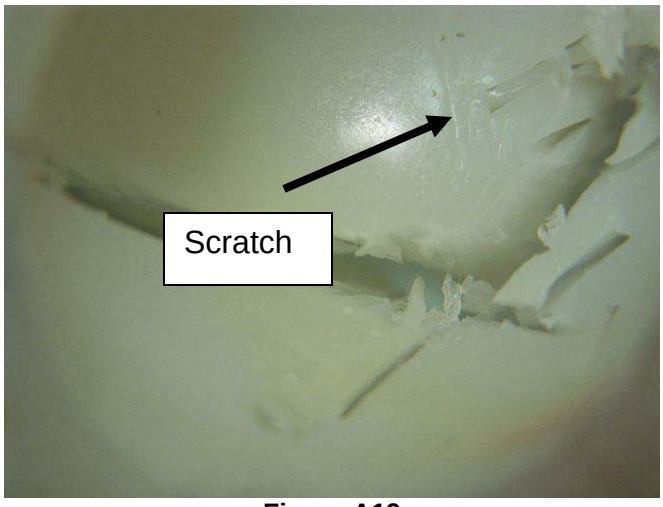


**Figure A19**

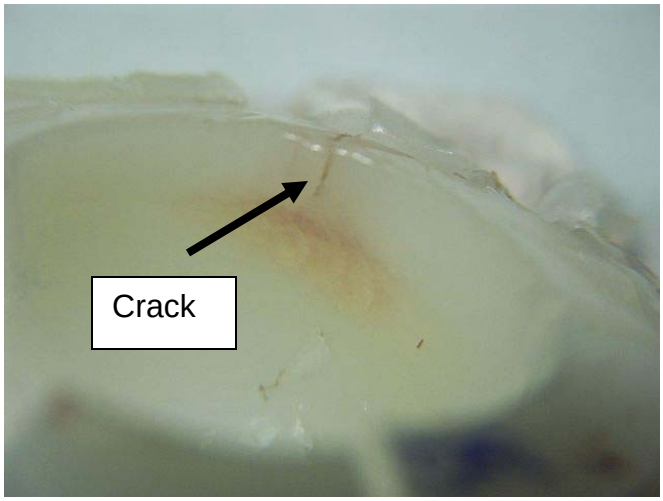


**Figure A20**

## Cup analysis: Patient 8

| | | |
|---|---|---|
| 1 | Femoral head size | 30 mm |
| 2 | Type of head | Stainless steel |
| 3 | Cup type | UHMWPE – ARD |
| 4 | Crosslink | No |
| 5 | Amount of linear wear | ± 5 mm |
| 6 | Duration in vivo | 16 years and 4 months |
| 7 | Size of wear debris from pathologist | Not known |
| 8 | Visible discoloration | Yes (Figure 18) |
| 9 | Metal backing | No |
| 10 | Thickness of poly | 9 mm |
| 11 | Mechanical damage | Yes |
| 12 | Cracks in material | Yes |
| 13 | Plastic flow | Yes |
| 14 | Scratches | Yes |
| 15 | Adhesion wear | Yes |
| 16 | Wear particles embedded in base material | Yes |
| 17 | Flaking | No |

## Patient 9

**Figure A21**

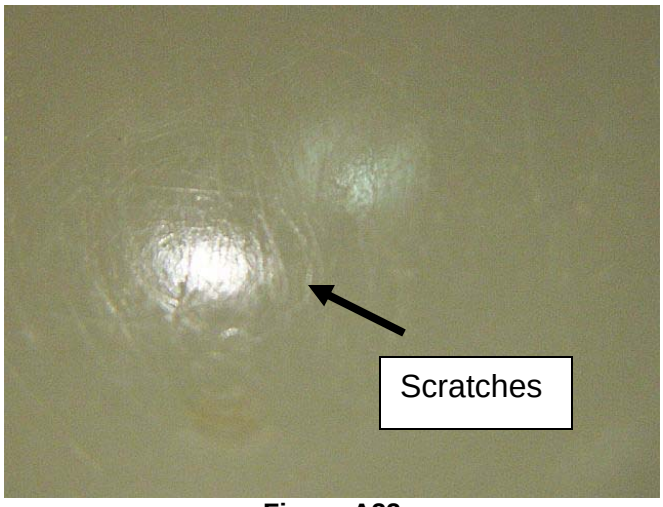


**Figure A22**

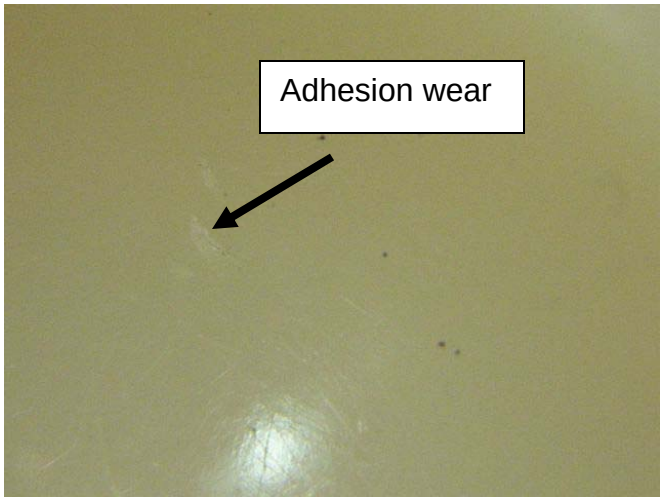


**Figure A23**

## Cup analysis: Patient 9

| | | |
|---|---|---|
| 1 | Femoral head size | 32 mm |
| 2 | Type of head | Zirconium |
| 3 | Cup type | UHMWPE – Aesculab |
| 4 | Crosslink | Yes |
| 5 | Amount of linear wear | ± 0 mm |
| 6 | Duration in vivo | 3 years and 9 months |
| 7 | Size of wear debris from pathologist | Not available |
| 8 | Visible discoloration | No |
| 9 | Metal backing | Yes |
| 10 | Thickness of poly | 19 mm |
| 11 | Mechanical damage | No |
| 12 | Cracks in material | No |
| 13 | Plastic flow | No |
| 14 | Scratches | Yes (figure 22) |
| 15 | Adhesion wear | Yes |
| 16 | Wear particles embedded in base material | No |
| 17 | Flaking | No |

## Patient 10

**Figure A24**

**Figure A25**

## Cup analysis: Patient 10

| | | |
|---|---|---|
| 1 | Femoral head size | 28 mm |
| 2 | Type of head | Alumina |
| 3 | Cup type | UHMWPE – Aesculab |
| 4 | Crosslink | Yes |
| 5 | Amount of linear wear | ± 0 mm |
| 6 | Duration in vivo | 7 Months |
| 7 | Size of wear debris from pathologist | Not available |
| 8 | Visible discoloration | No |
| 9 | Metal backing | Yes |
| 10 | Thickness of poly | 23 mm |
| 11 | Mechanical damage | No |
| 12 | Cracks in material | No |
| 13 | Plastic flow | No |
| 14 | Scratches | No |
| 15 | Adhesion wear | No |
| 16 | Wear particles embedded in base material | No |
| 17 | Flaking | No |

## Patient 11

**Figure A26**

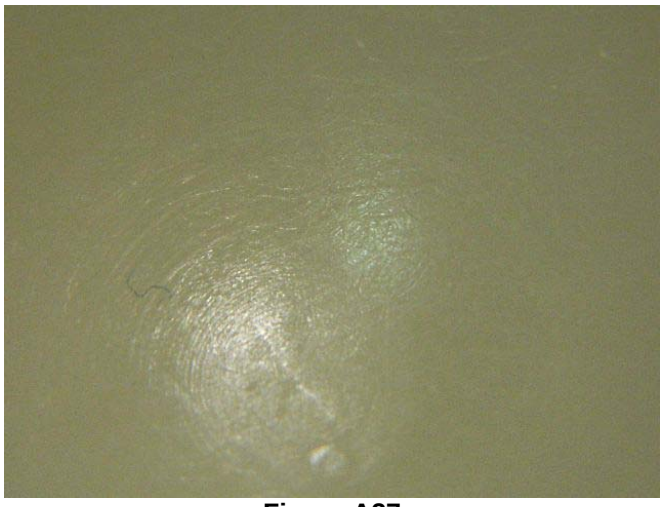

**Figure A27**

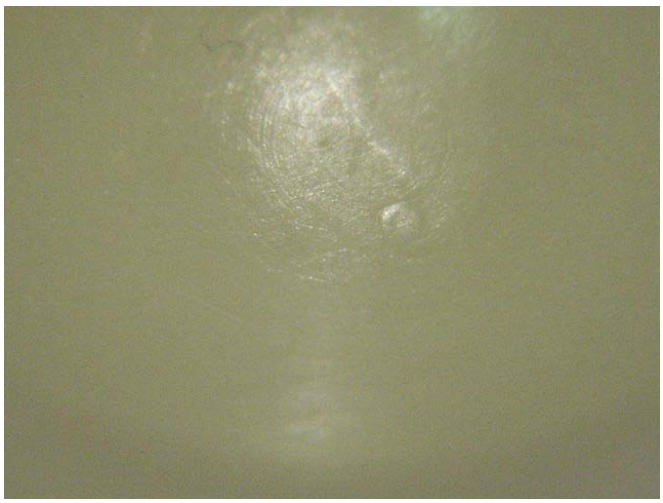

**Figure A28**

## Cup analysis: Patient 11

| | | |
|---|---|---|
| 1 | Femoral head size | 28 mm |
| 2 | Type of head | Zirconium |
| 3 | Cup type | UHMWPE – Aesculab |
| 4 | Crosslink | Yes |
| 5 | Amount of linear wear | ± 0 mm |
| 6 | Duration in vivo | 14 months |
| 7 | Size of wear debris from pathologist | 10 – 40 µm |
| 8 | Visible discoloration | No |
| 9 | Metal backing | Yes |
| 10 | Thickness of poly | 9 mm |
| 11 | Mechanical damage | No |
| 12 | Cracks in material | No |
| 13 | Plastic flow | No |
| 14 | Scratches | Yes |
| 15 | Adhesion wear | No |
| 16 | Wear particles embedded in base material | Yes |
| 17 | Flaking | No |

## Patient 12


**Figure A29**

**Figure A30**

**Figure A31**

## Cup analysis: Patient 12

| | | |
|---|---|---|
| 1 | Femoral head size | 28 mm |
| 2 | Type of head | Zirconium |
| 3 | Cup type | UHMWPE – de puy |
| 4 | Crosslink | No |
| 5 | Amount of linear wear | ± 3.5 mm |
| 6 | Duration in vivo | 10 years |
| 7 | Size of wear debris from pathologist | 20 – 80 µm |
| 8 | Visible discoloration | Yes |
| 9 | Metal backing | No |
| 10 | Thickness of poly | 9 mm |
| 11 | Mechanical damage | Yes |
| 12 | Cracks in material | Yes |
| 13 | Plastic flow | Yes |
| 14 | Scratches | Yes |
| 15 | Adhesion wear | Yes |
| 16 | Wear particles embedded in base material | No |
| 17 | Flaking | No |

**Patient 13**

**Figure A32**

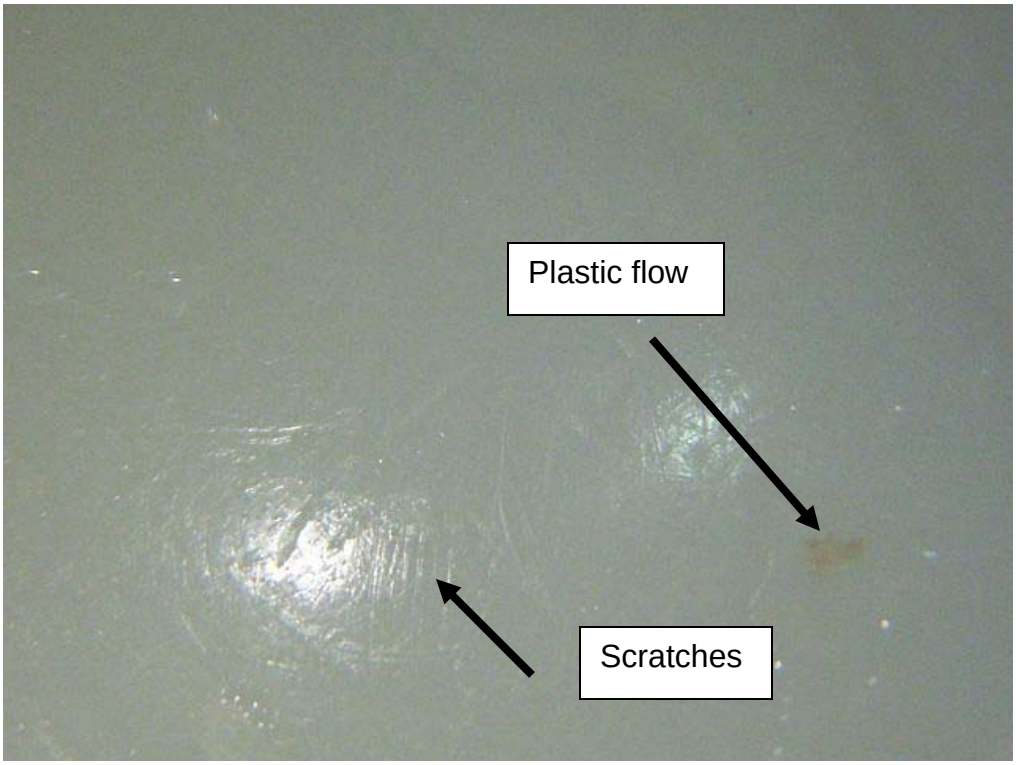


**Figure A33**

## Cup analysis: Patient 13

| | | |
|---|---|---|
| 1 | Femoral head size | 32 mm |
| 2 | Type of head | Zirconium |
| 3 | Cup type | UHMWPE – Aesculab |
| 4 | Crosslink | No |
| 5 | Amount of linear wear | ± 3.5 mm |
| 6 | Duration in vivo | 9 years and 3 months |
| 7 | Size of wear debris from pathologist | 20 – 100 µm, avg. 60 µm |
| 8 | Visible discoloration | No |
| 9 | Metal backing | No |
| 10 | Thickness of poly | 12 mm |
| 11 | Mechanical damage | No |
| 12 | Cracks in material | No |
| 13 | Plastic flow | Yes |
| 14 | Scratches | Yes |
| 15 | Adhesion wear | Yes |
| 16 | Wear particles embedded in base material | Yes |
| 17 | Flaking | No |

**Patient 14**

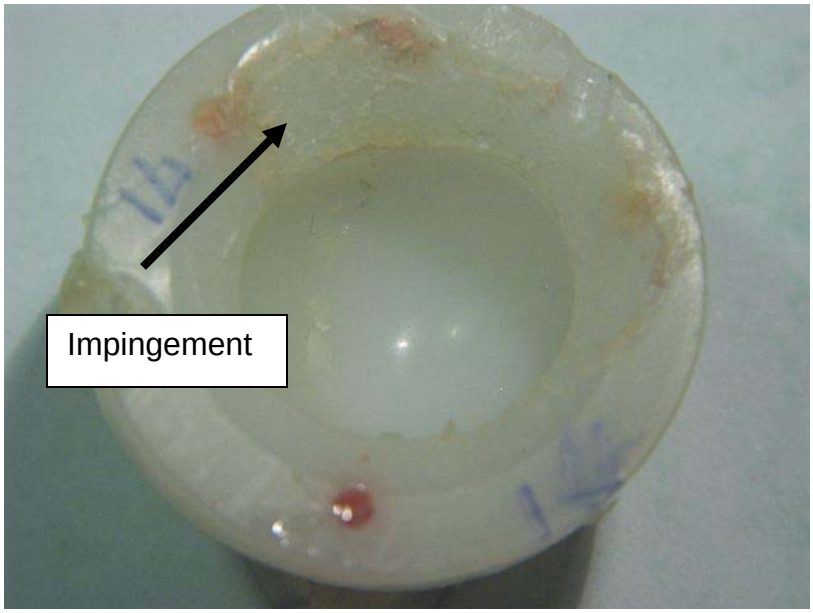


**Figure A34**

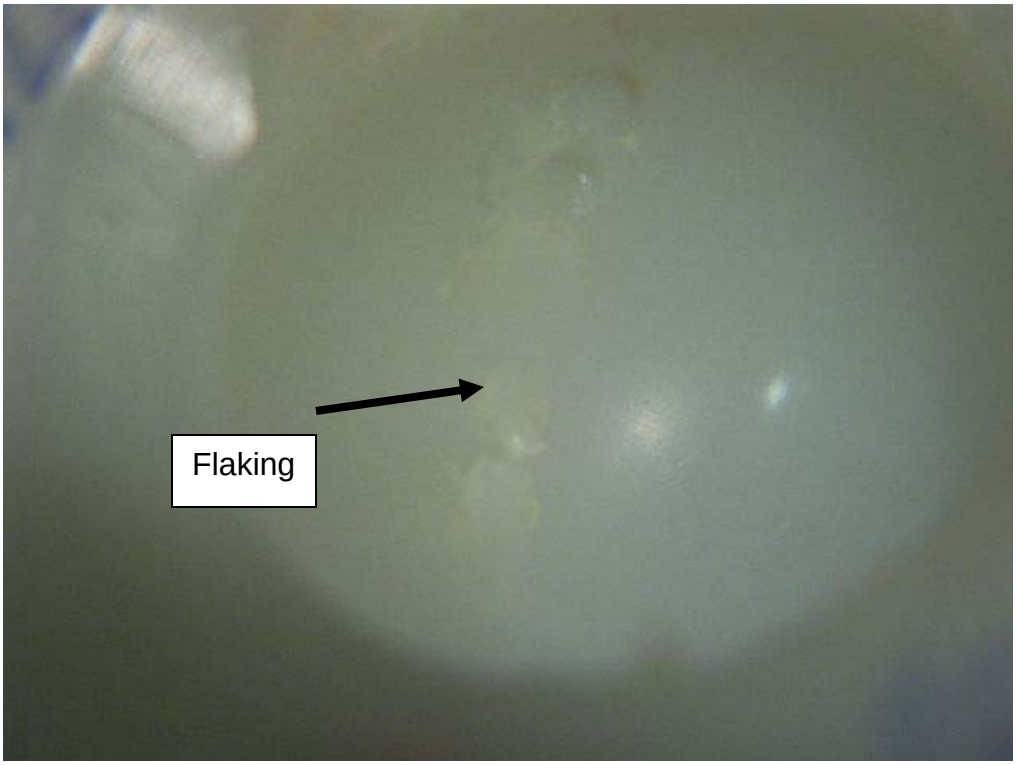


**Figure A35**

## Cup analysis: Patient 14

| | | |
|---|---|---|
| 1 | Femoral head size | 22 mm |
| 2 | Type of head | Zirconium |
| 3 | Cup type | UHMWPE – Aesculab |
| 4 | Crosslink | No |
| 5 | Amount of linear wear | ± 5 mm |
| 6 | Duration in vivo | 7 years |
| 7 | Size of wear debris from pathologist | Not available |
| 8 | Visible discoloration | Yes (Figure 34) |
| 9 | Metal backing | Yes |
| 10 | Thickness of poly | 11 mm |
| 11 | Mechanical damage | Yes (serious impingement – see figure 34) |
| 12 | Cracks in material | Yes |
| 13 | Plastic flow | No |
| 14 | Scratches | Yes |
| 15 | Adhesion wear | Yes |
| 16 | Wear particles embedded in base material | Yes |
| 17 | Flaking | Yes |

**Patient 15**

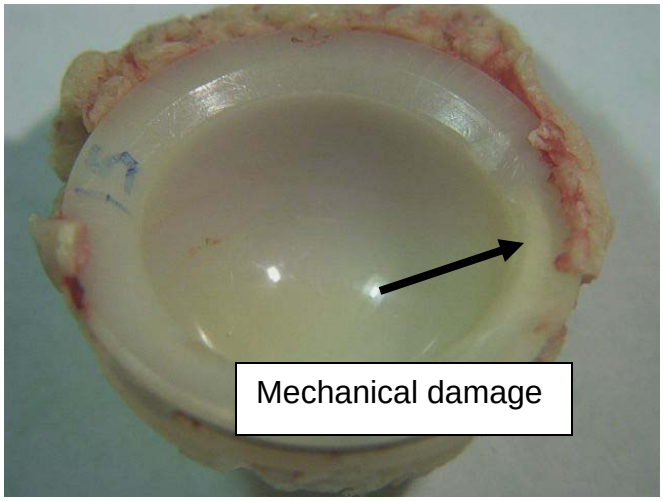


**Figure A36**

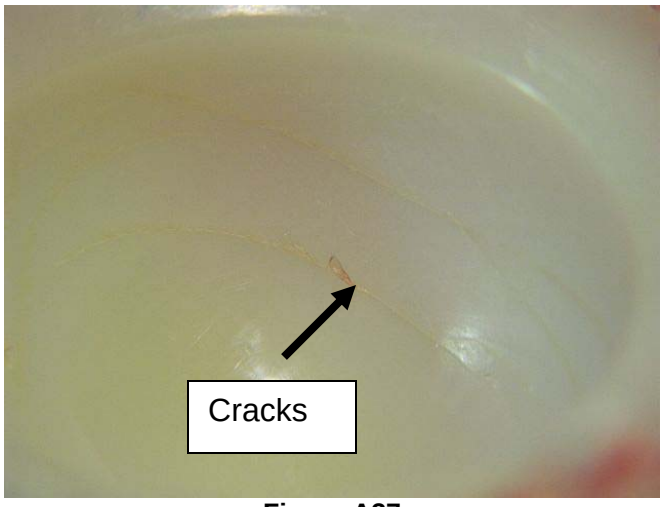


**Figure A37**

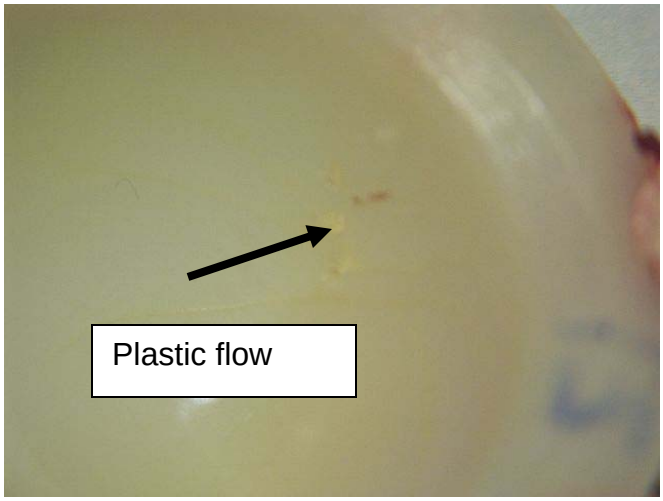


**Figure A38**

## Cup analysis: Patient 15

| | | |
|---|---|---|
| 1 | Femoral head size | 32 mm |
| 2 | Type of head | Alumina |
| 3 | Cup type | UHMWPE – Aesculab |
| 4 | Crosslink | No |
| 5 | Amount of linear wear | ± 0.2 mm |
| 6 | Duration in vivo | 15 years |
| 7 | Size of wear debris from pathologist | 20 – 140 µm, avg. 80 µm |
| 8 | Visible discoloration | Yes (Figure 36) |
| 9 | Metal backing | No |
| 10 | Thickness of poly | 7 mm |
| 11 | Mechanical damage | Yes (figure 36) |
| 12 | Cracks in material | Yes |
| 13 | Plastic flow | No |
| 14 | Scratches | Yes |
| 15 | Adhesion wear | Yes |
| 16 | Wear particles embedded in base material | Yes |
| 17 | Flaking | No |

**Patient 16**

**Figure A39**

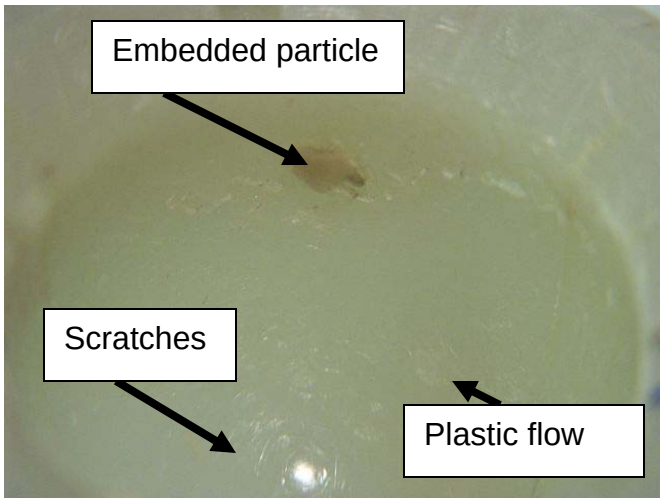


**Figure A40**

**Figure A41**

## Cup analysis: Patient 16

| | | |
|---|---|---|
| 1 | Femoral head size | 28 mm |
| 2 | Type of head | Zirconium |
| 3 | Cup type | UHMWPE – Aesculab |
| 4 | Crosslink | No |
| 5 | Amount of linear wear | ± 3.5 mm |
| 6 | Duration in vivo | 10 years |
| 7 | Size of wear debris from pathologist | 20 – 350 µm |
| 8 | Visible discoloration | Yes (Figure 39) |
| 9 | Metal backing | No |
| 10 | Thickness of poly | 11 mm |
| 11 | Mechanical damage | Yes (figure 39) |
| 12 | Cracks in material | No |
| 13 | Plastic flow | Yes |
| 14 | Scratches | Yes |
| 15 | Adhesion wear | Yes |
| 16 | Wear particles embedded in base material | Yes |
| 17 | Flaking | No |

**Patient 17**

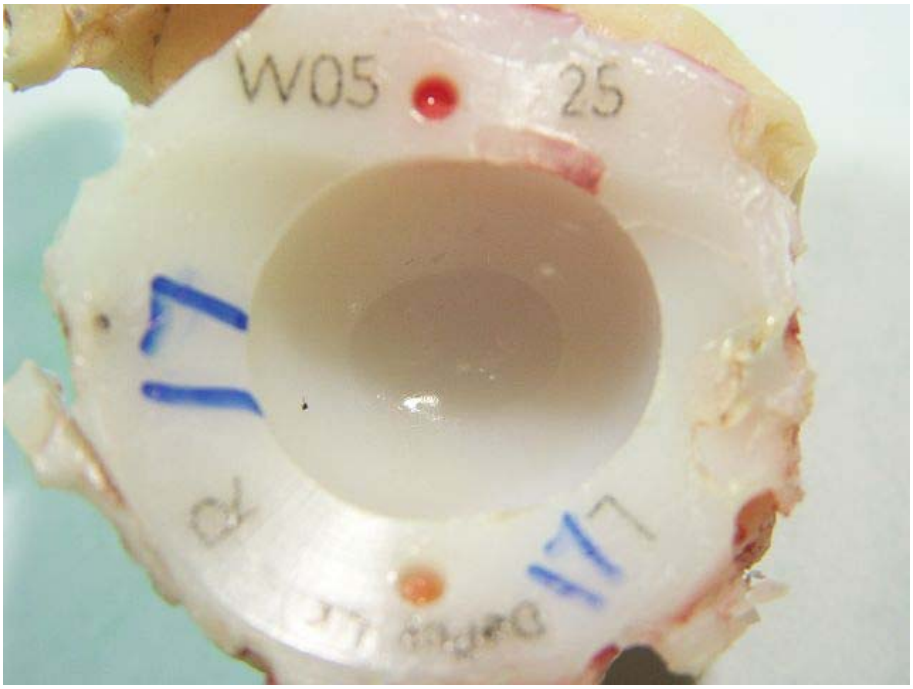


**Figure A42**

**Figure A43**

## Cup analysis: Patient 17

| | | |
|---|---|---|
| 1 | Femoral head size | 22 mm |
| 2 | Type of head | Stainless Steel |
| 3 | Cup type | UHMWPE – Charnley, de Puy |
| 4 | Crosslink | No |
| 5 | Amount of linear wear | ± 6 mm |
| 6 | Duration in vivo | 10 years and 6 months |
| 7 | Size of wear debris from pathologist | Not available |
| 8 | Visible discoloration | Yes (Figure 42) |
| 9 | Metal backing | No |
| 10 | Thickness of poly | 13 mm |
| 11 | Mechanical damage | No |
| 12 | Cracks in material | No |
| 13 | Plastic flow | No |
| 14 | Scratches | Yes |
| 15 | Adhesion wear | No |
| 16 | Wear particles embedded in base material | No |
| 17 | Flaking | No |

## Patient 18

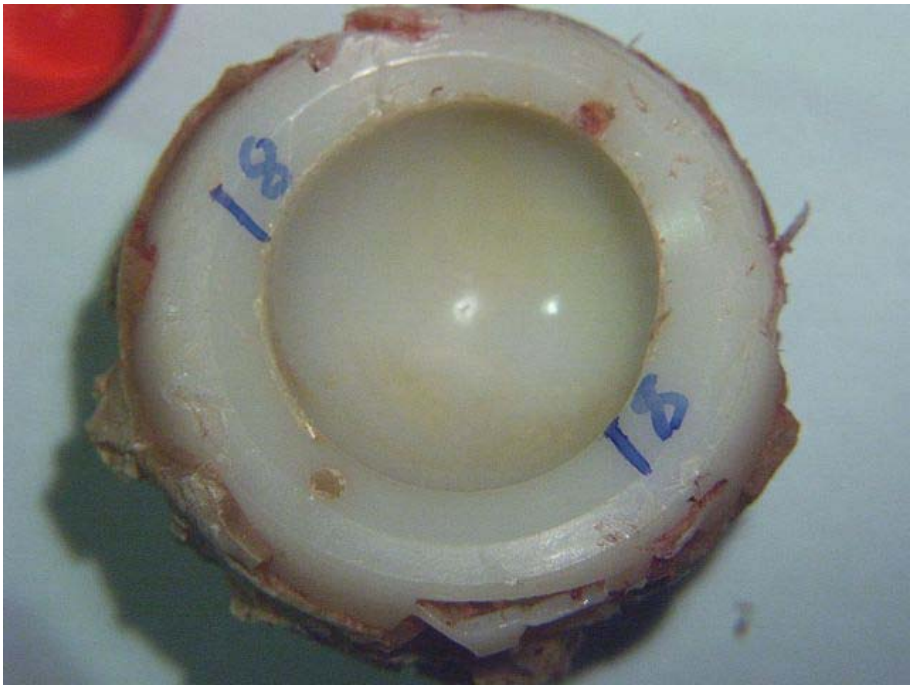


**Figure A44**

**Figure A45**

## Cup analysis: Patient 18

| | | |
|---|---|---|
| 1 | Femoral head size | 32 mm |
| 2 | Type of head | Alumina |
| 3 | Cup type | UHMWPE - Aesculab |
| 4 | Crosslink | No |
| 5 | Amount of linear wear | ± 5 mm |
| 6 | Duration in vivo | 6 years and 6 months |
| 7 | Size of wear debris from pathologist | Not available |
| 8 | Visible discoloration | Yes |
| 9 | Metal backing | No |
| 10 | Thickness of poly | 12 mm |
| 11 | Mechanical damage | Yes |
| 12 | Cracks in material | No |
| 13 | Plastic flow | No |
| 14 | Scratches | Yes |
| 15 | Adhesion wear | Yes |
| 16 | Wear particles embedded in base material | Yes |
| 17 | Flaking | No |

## Patient 19

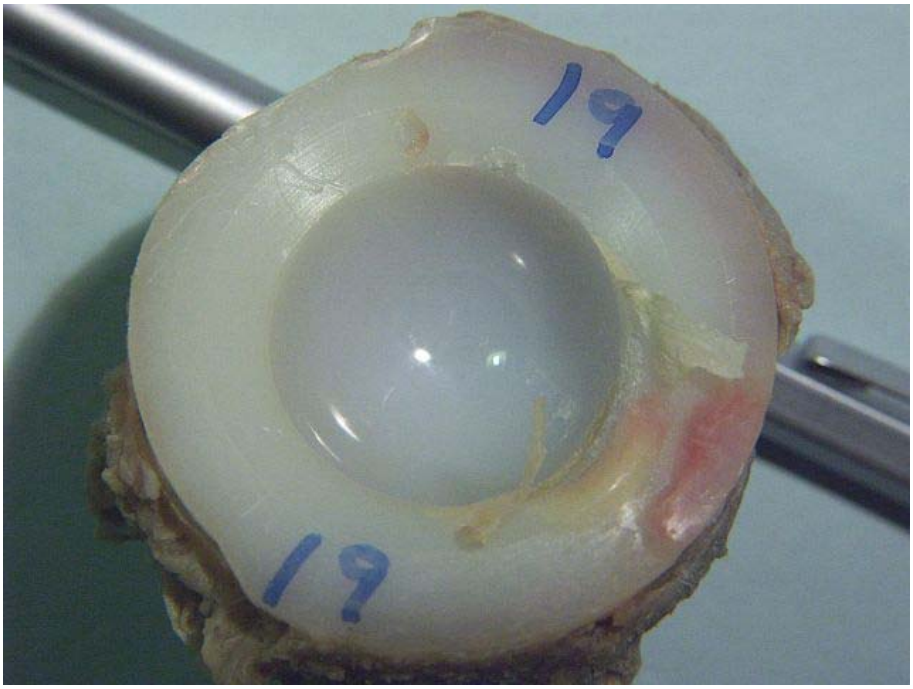


**Figure A46**

**Figure A47**

## Cup analysis: Patient 19

| | | |
|---|---|---|
| 1 | Femoral head size | 28 mm |
| 2 | Type of head | Alumina |
| 3 | Cup type | UHMWPE - BARC |
| 4 | Crosslink | No |
| 5 | Amount of linear wear | ± 2 mm |
| 6 | Duration in vivo | 15 years and 6 months |
| 7 | Size of wear debris from pathologist | Not available |
| 8 | Visible discoloration | Yes |
| 9 | Metal backing | No |
| 10 | Thickness of poly | 10 mm |
| 11 | Mechanical damage | Yes |
| 12 | Cracks in material | Yes |
| 13 | Plastic flow | Yes |
| 14 | Scratches | Yes |
| 15 | Adhesion wear | Yes |
| 16 | Wear particles embedded in base material | Yes |
| 17 | Flaking | Yes |

## Patient 20


**Figure A48**

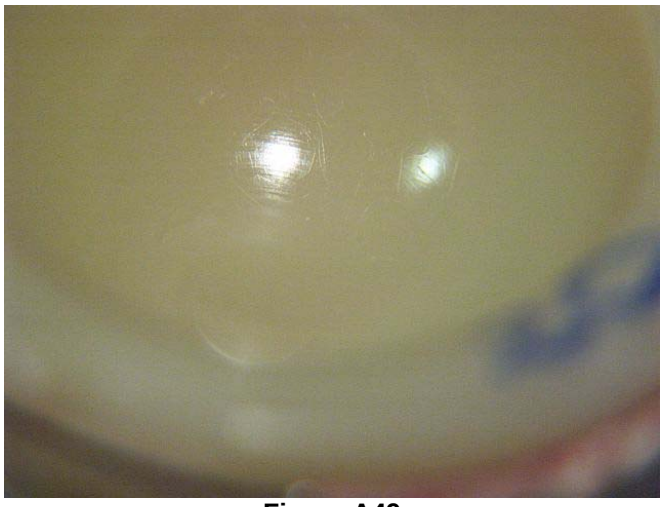

**Figure A49**

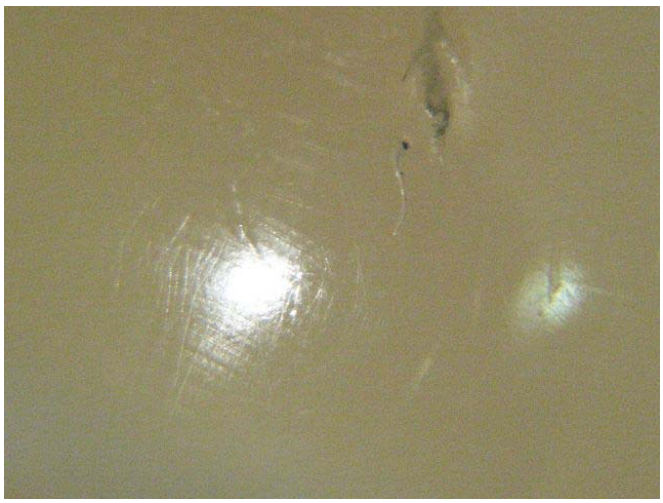

**Figure A50**

## Cup analysis: Patient 20

| | | |
|---|---|---|
| 1 | Femoral head size | 32 mm |
| 2 | Type of head | Zirconium |
| 3 | Cup type | UHMWPE - Aesculab |
| 4 | Crosslink | Yes |
| 5 | Amount of linear wear | ± 0 mm |
| 6 | Duration in vivo | 2 years and 4 months |
| 7 | Size of wear debris from pathologist | Not available |
| 8 | Visible discoloration | No |
| 9 | Metal backing | No |
| 10 | Thickness of poly | 7 mm |
| 11 | Mechanical damage | No |
| 12 | Cracks in material | No |
| 13 | Plastic flow | No |
| 14 | Scratches | Yes |
| 15 | Adhesion wear | Yes |
| 16 | Wear particles embedded in base material | No |
| 17 | Flaking | No |

# ANNEXURE B

Electron microscope analysis of white deposits in acetabular cups

Annexure B

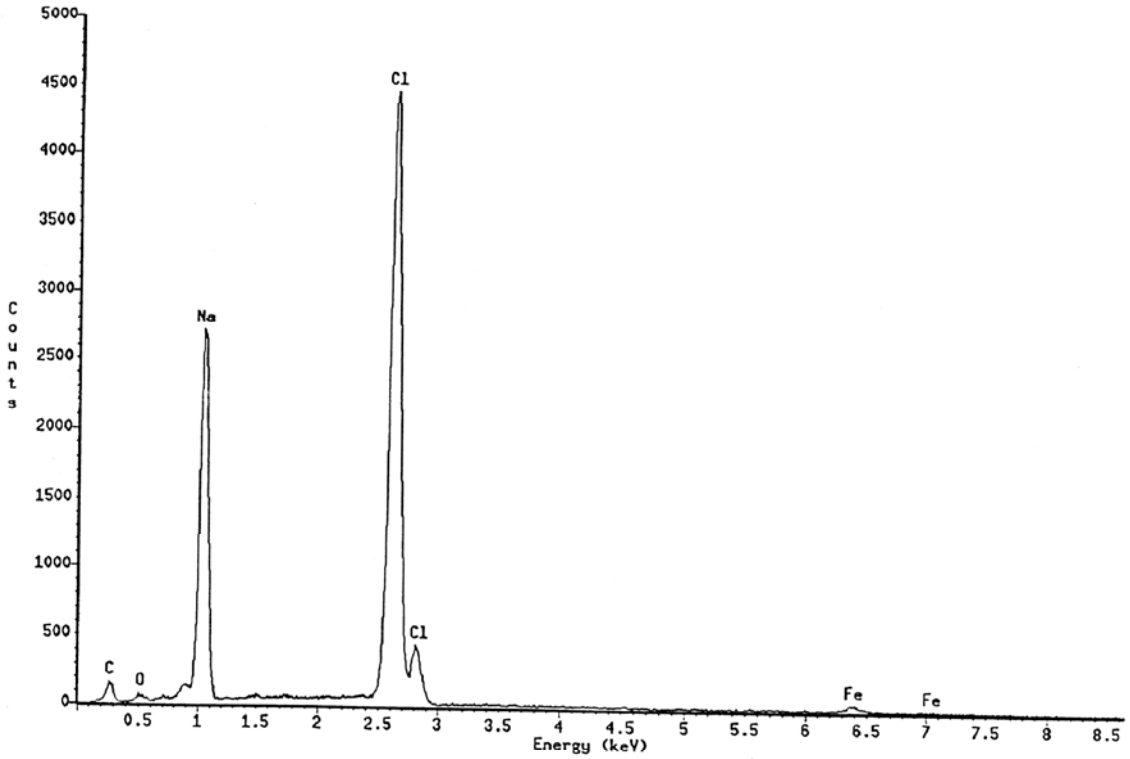


| | |
|---|---|
| Column | : JEOL5800.Pioneer |
| Take-off angle | : 35 |
| Acquisition type | : eds |
| Creation time | : 100/05/17 15:05 |
| Livetime | : 100 |
| Deadtime | : 28.089 |
| Channels | : 2048 |
| Channel width | : 10 |
| Detector type | : Silicon/Lithium |
| Window type | : norvar |
| Window thickness | : 0.3 |
| Coating material | : Al |
| Coating thickness | : 0.04 |
| Contact material | : Au |
| Contact thickness | : 0.02 |
| Crystal thickness | : 3 |

| | |
|---|---|
| Accelerating voltage | : 20 |
| Magnification | : 3500 |
| Charge | : 100 |
| Beam current | : 1 |
| Beam spot size | : 0 |
| Beam location | : 0,0 |
| Working distance | : 10 |
| Stage X | : 1.306 |
| Stage Y | : -19.637 |
| Stage Z | : 11.369 |
| Stage tilt | : 0 |
| Stage rotation | : 0 |
| Contamination material | : none |
| Contamination thickness | : 0 |

File name :

Notes:

Wed May 17 15:04:01 2000

Livetime : 15.2 Sec.
Technique: Least Squares Fit

Elements Present:
C(6), Zn(30), Cl(17)

| Energy (keV) | Intensity (counts) | Elements Present |
|---|---|---|
| 0.273 | 127 | C Ka |
| 1.044 | 5019 | Zn La1 |
| 2.626 | 8560 | Cl Ka |

# ANNEXURE C

Electron microscope investigation into Brown discolouring in acetabular cups

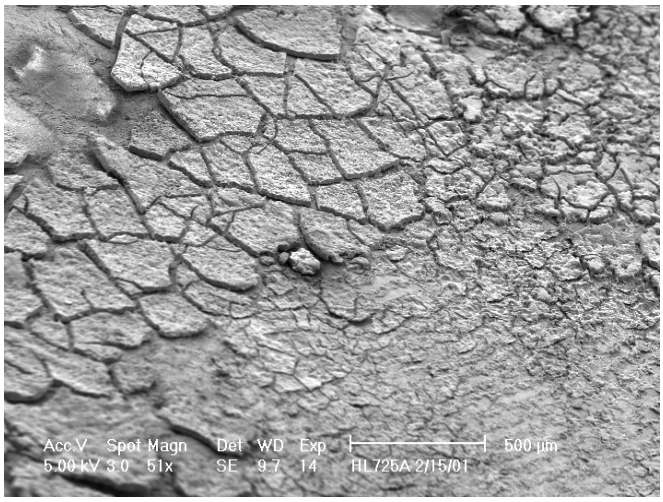


**Figure C1**

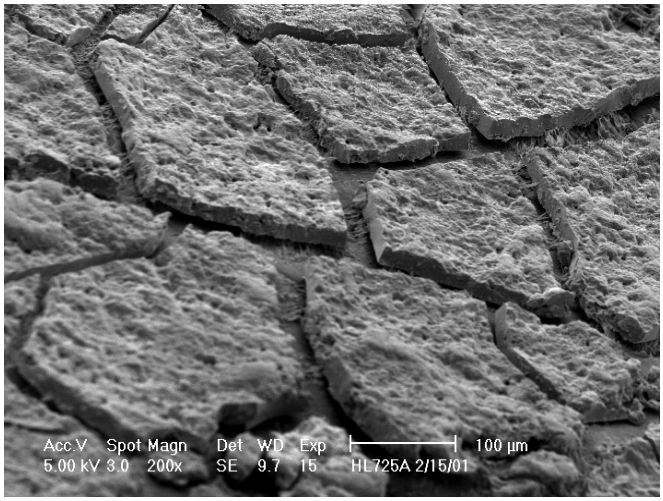


**Figure C2**

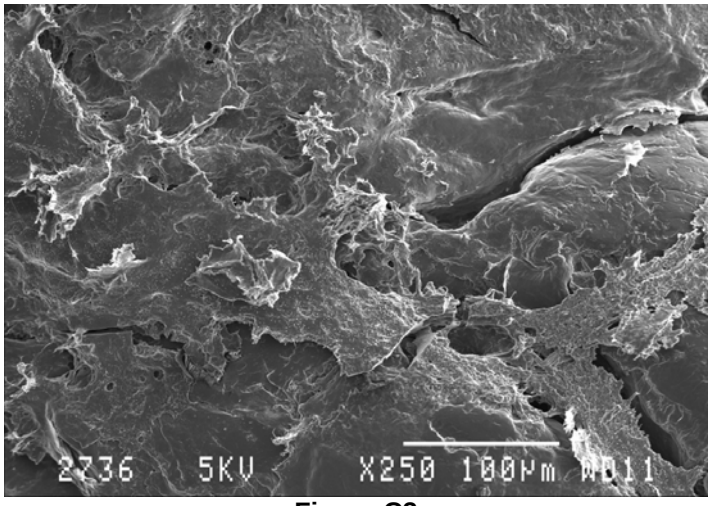


**Figure C3**

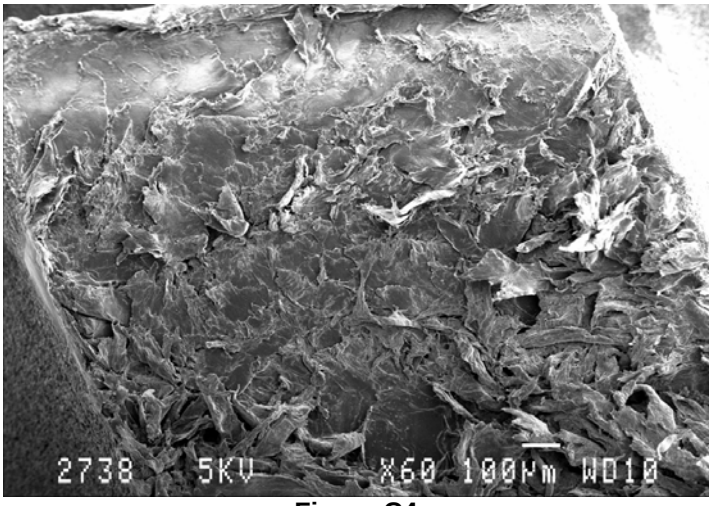


**Figure C4**

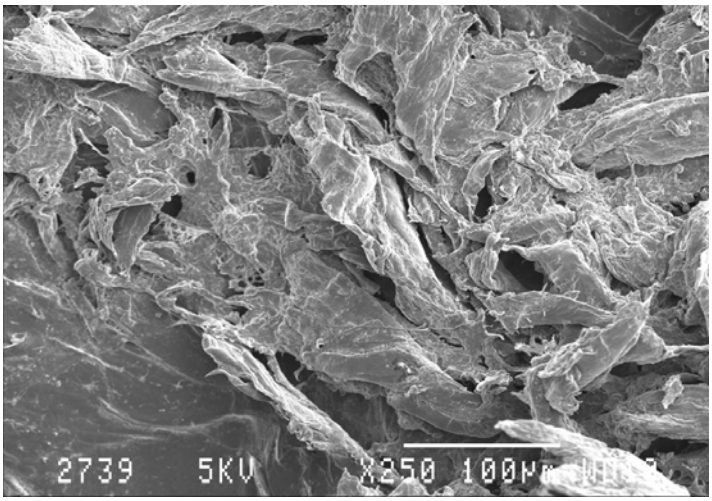


**Figure C5**

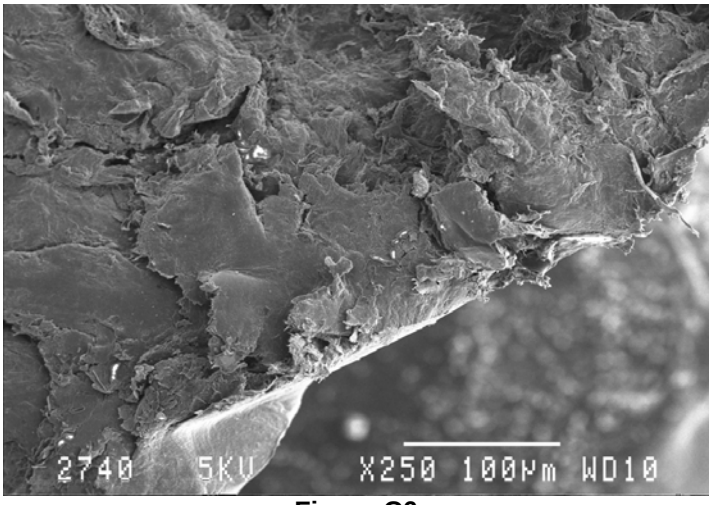


**Figure C6**

# ANNEXURE D

Electron microscope investigation into structure of UHMWPE

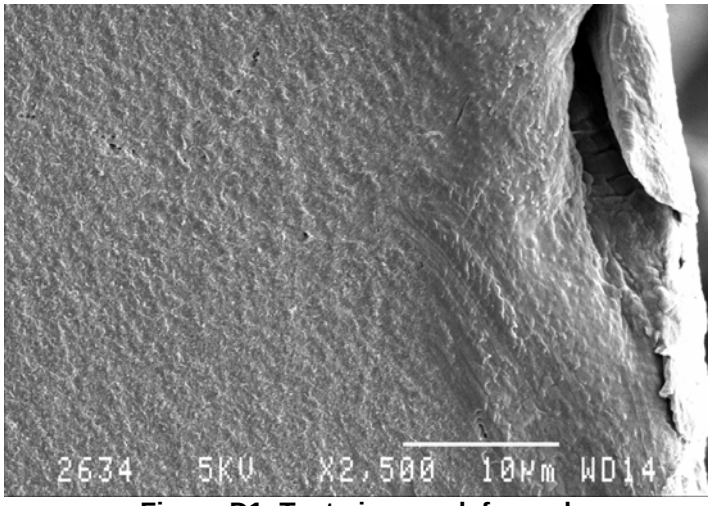


**Figure D1: Test piece undeformed**

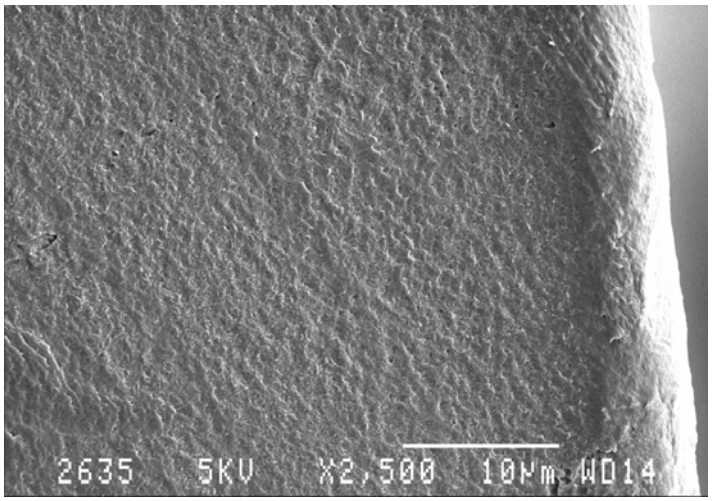


**Figure D2: Test piece undeformed**

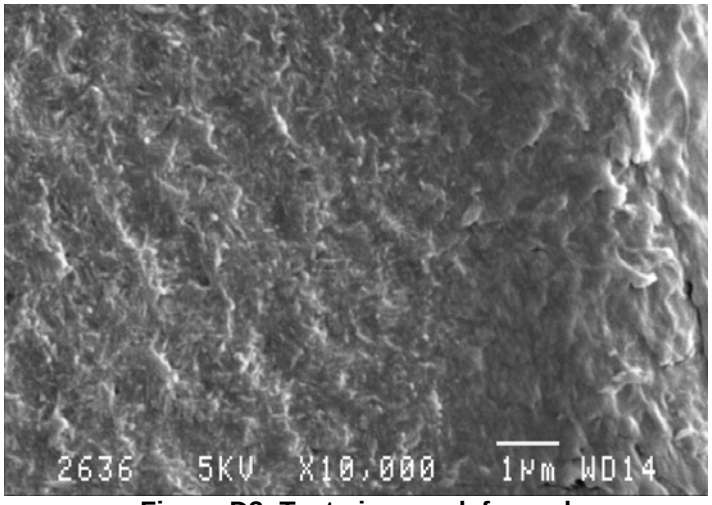


**Figure D3: Test piece undeformed**

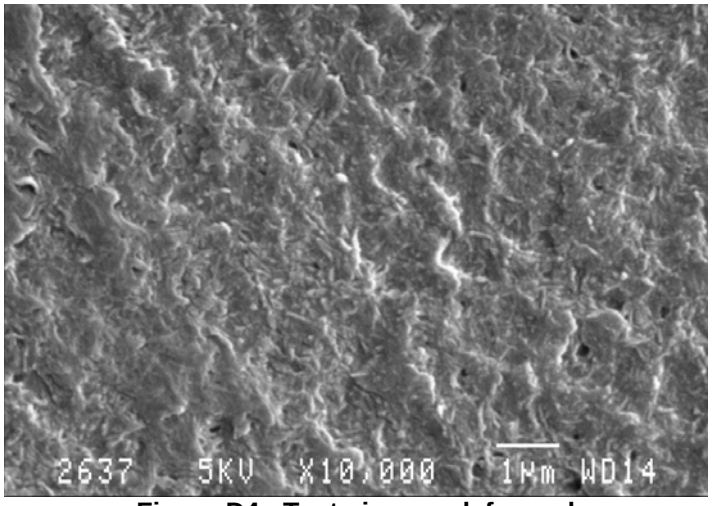


**Figure D4: Test piece undeformed**

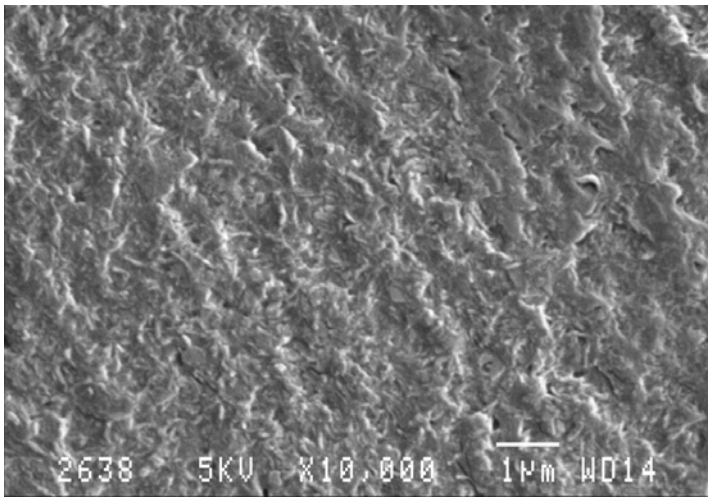


**Figure D5: Test piece deformed**

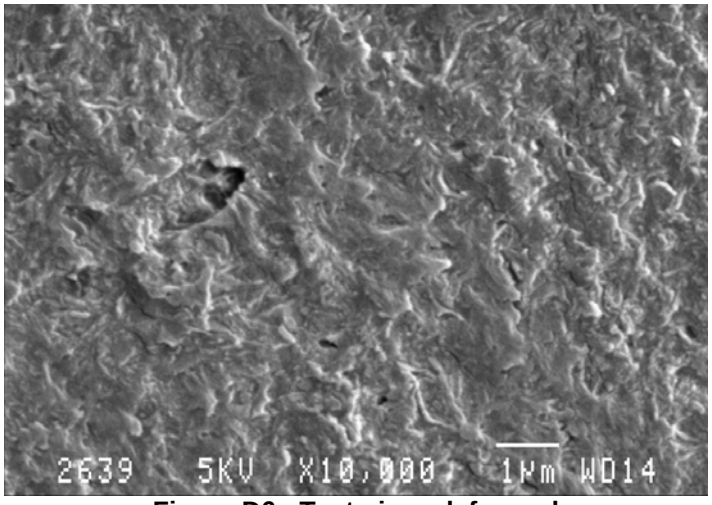


**Figure D6: Test piece deformed**

# ANNEXURE E

Electron microscope investigation into micro wear

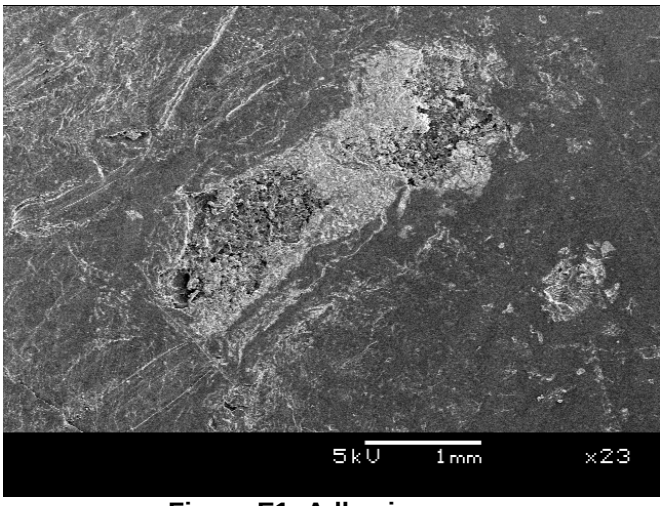


**Figure E1: Adhesion wear**

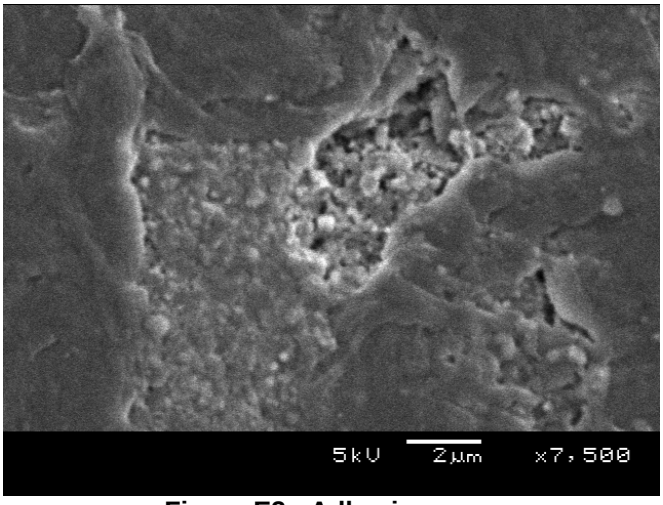


**Figure E2: Adhesion wear**

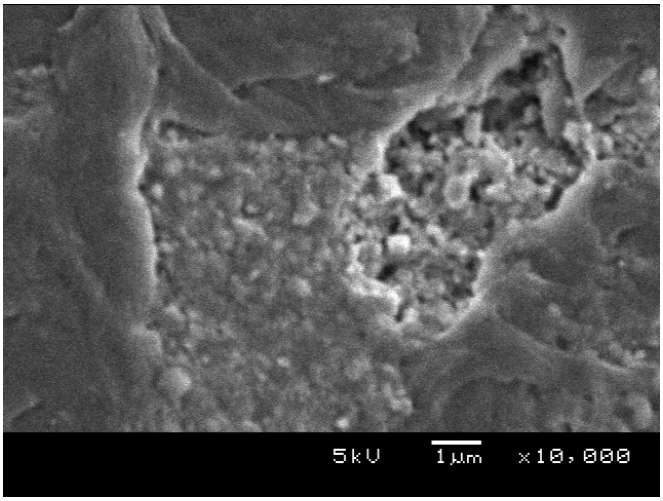


**Figure E3: Adhesion wear**

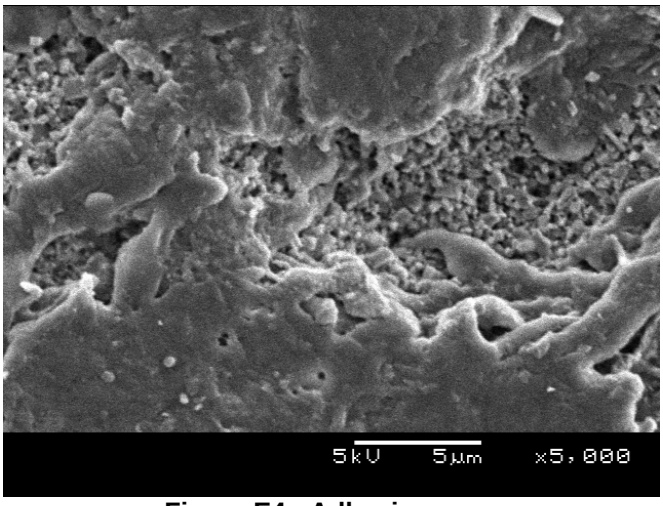


**Figure E4: Adhesion wear**

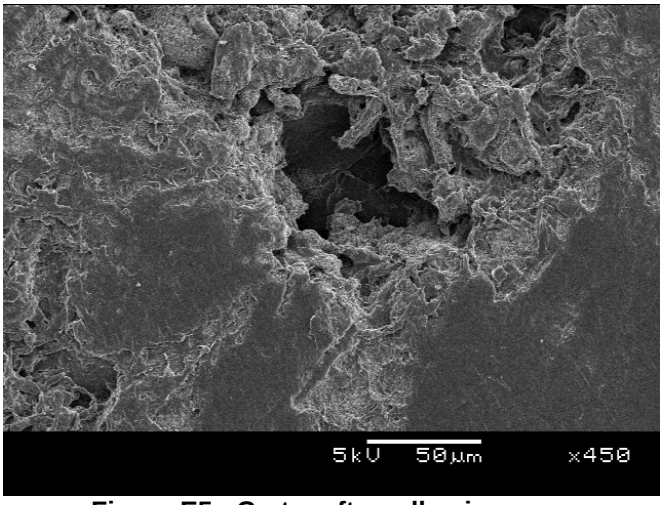


**Figure E5: Crater after adhesion wear**

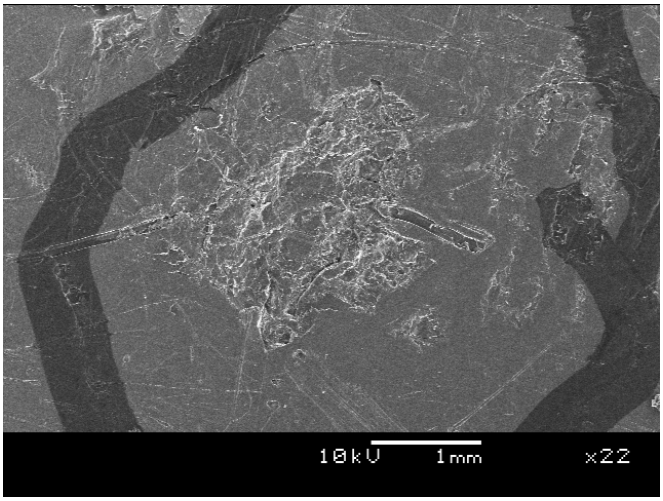


**Figure E6: Patch with adhesion wear**

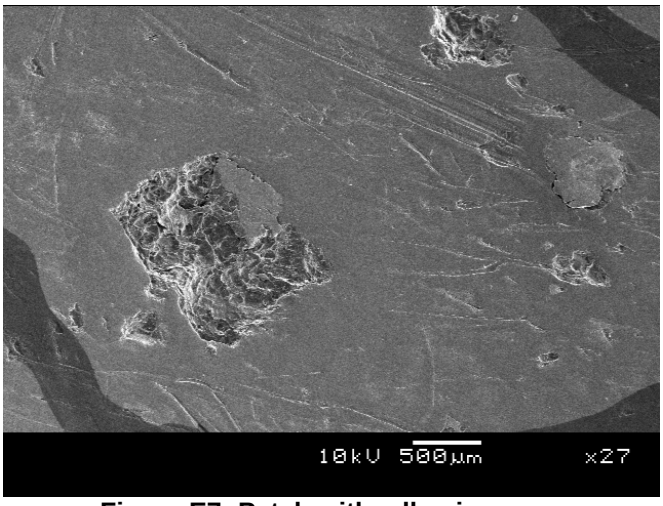


**Figure E7: Patch with adhesion wear**

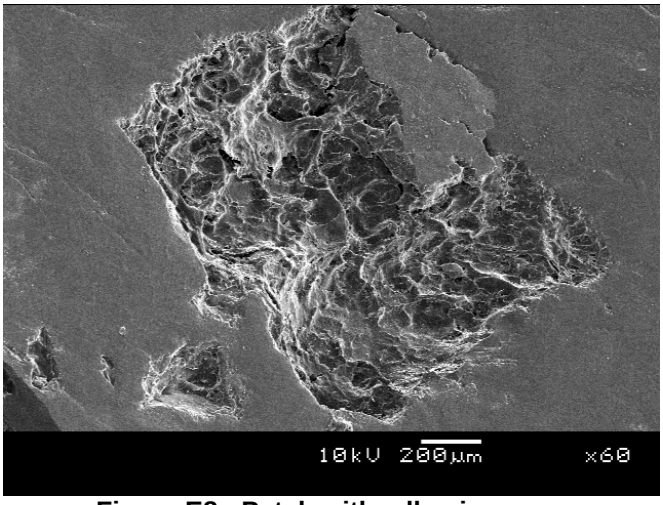


**Figure E8: Patch with adhesion wear**

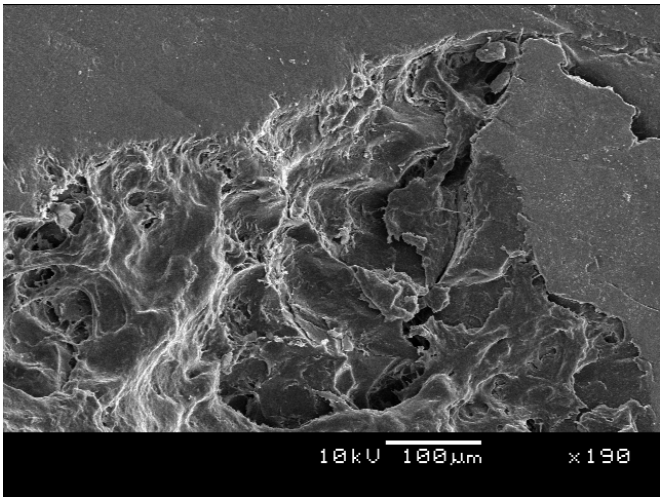


**Figure E9: Patch with adhesion wear**

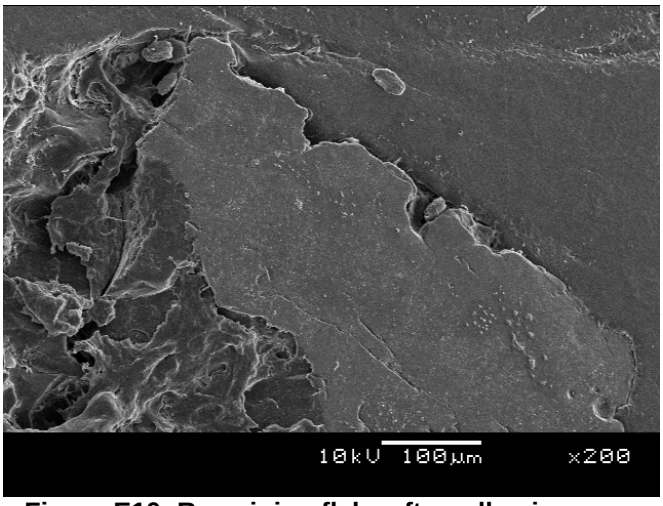


**Figure E10: Remaining flake after adhesion wear**

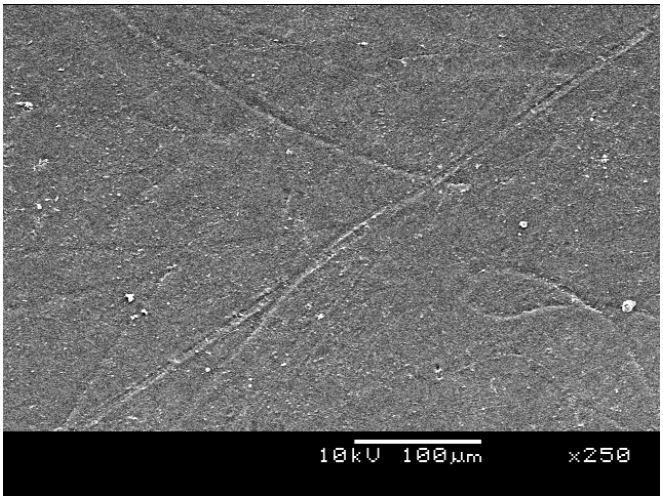


**Figure E11: Scratches on bearing surfaces**

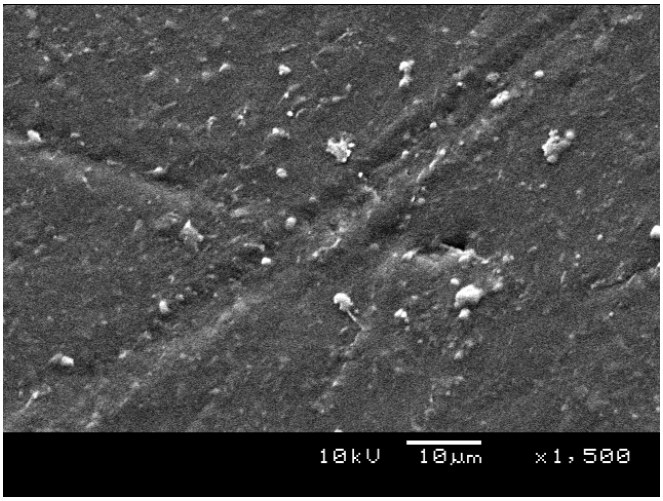


**Figure E12: Scratches on bearing surfaces**

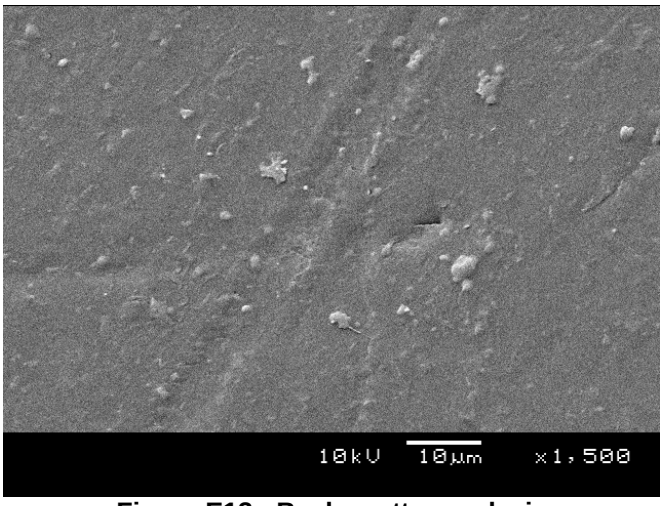


**Figure E13: Back scatter analysis**

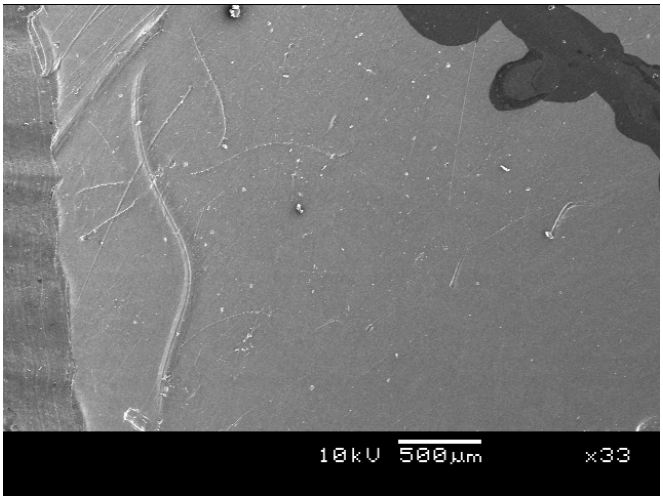


**Figure E14: Scratches on bearing surfaces**

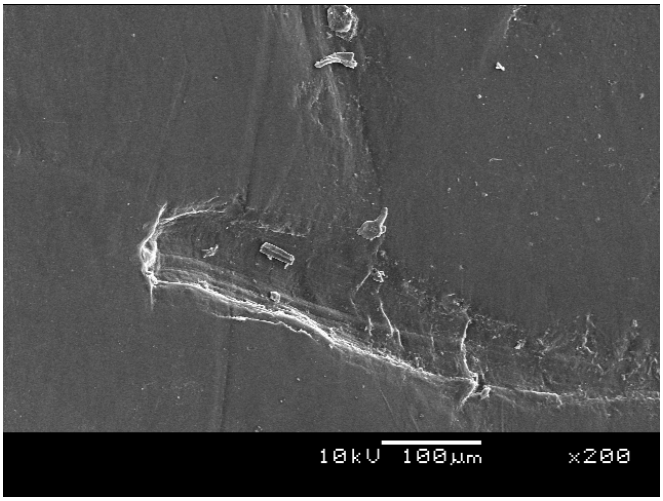


**Figure E15: Scratches on bearing surfaces**

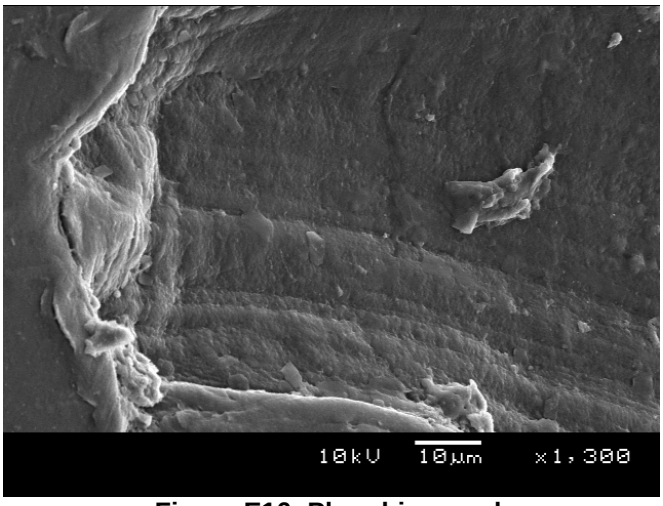


**Figure E16: Ploughing mark**

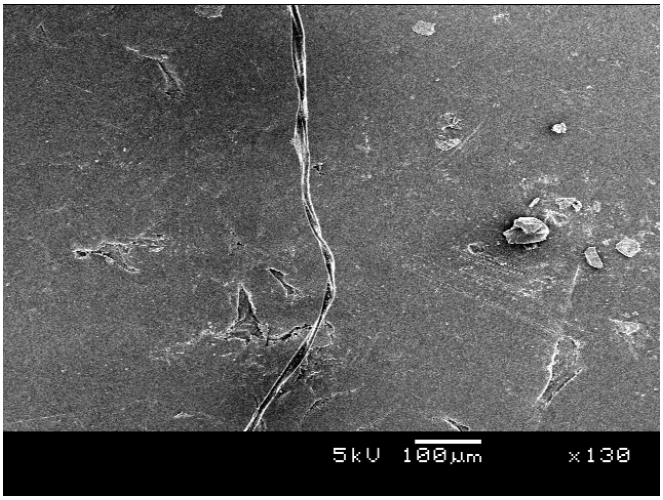


**Figure E17: Scratch on bearing surface**

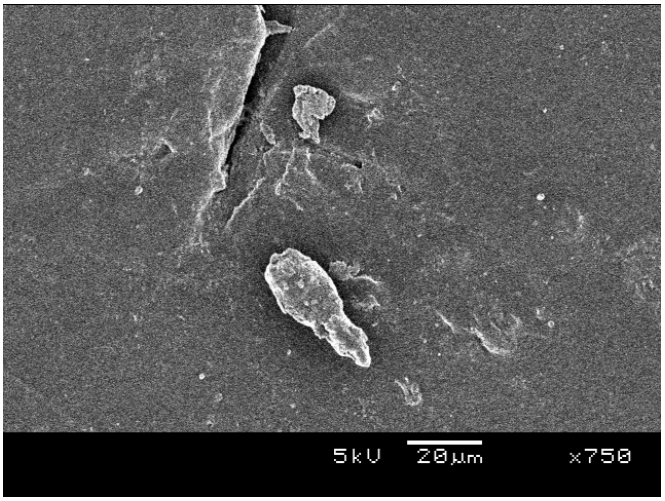


**Figure E18: Wear particle**

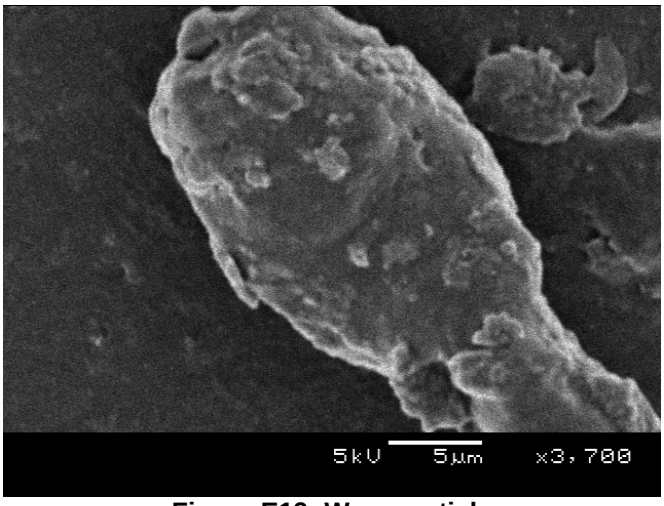


**Figure E19: Wear particle**

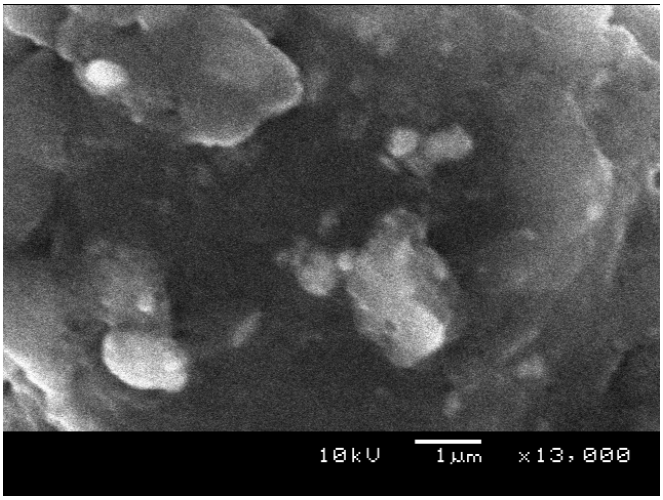


**Figure E20: Wear particle**

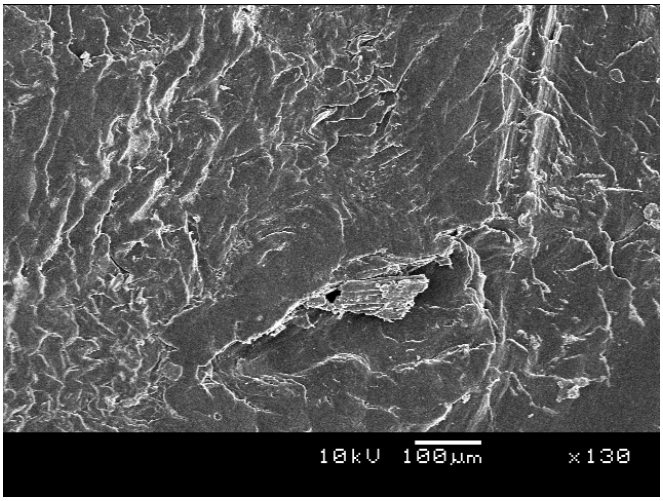


**Figure E21: Plastic flow**

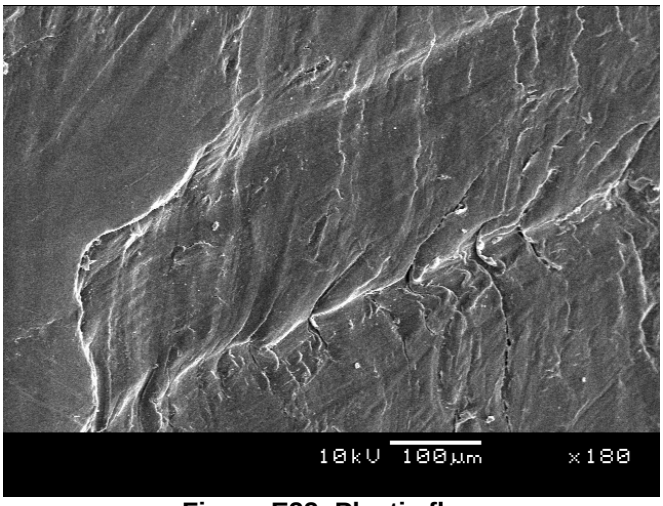


**Figure E22: Plastic flow**

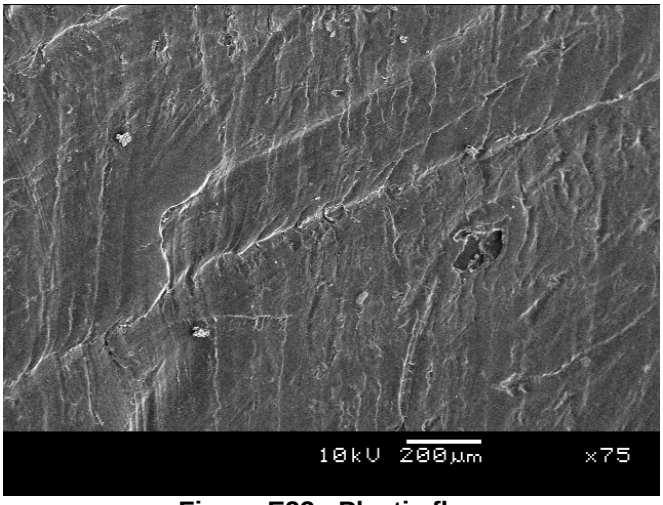


**Figure E23: Plastic flow**

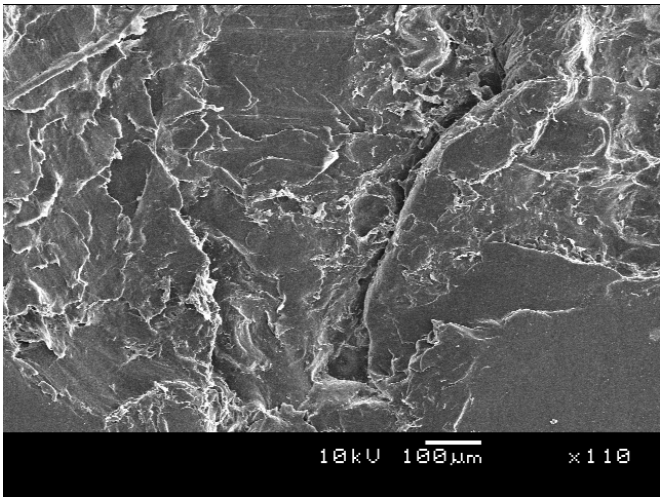


**Figure E24: Crack after adhesion wear**

# ANNEXURE F

Electrophoresis analysis of particles retrieved from brown deposit in acetabular cups and synovial fluid

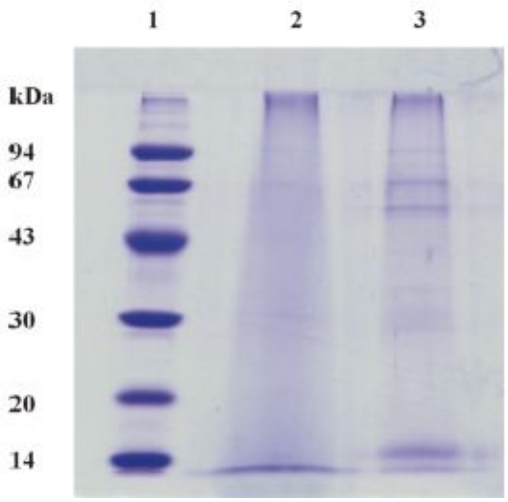


Figure F1: SDS-PAGE analysis of samples as trial study. Lane 1 is the molecular mass markers with mass indicated in kDa, on left hand side, line 2 and 3 is two different samples from different retrievals

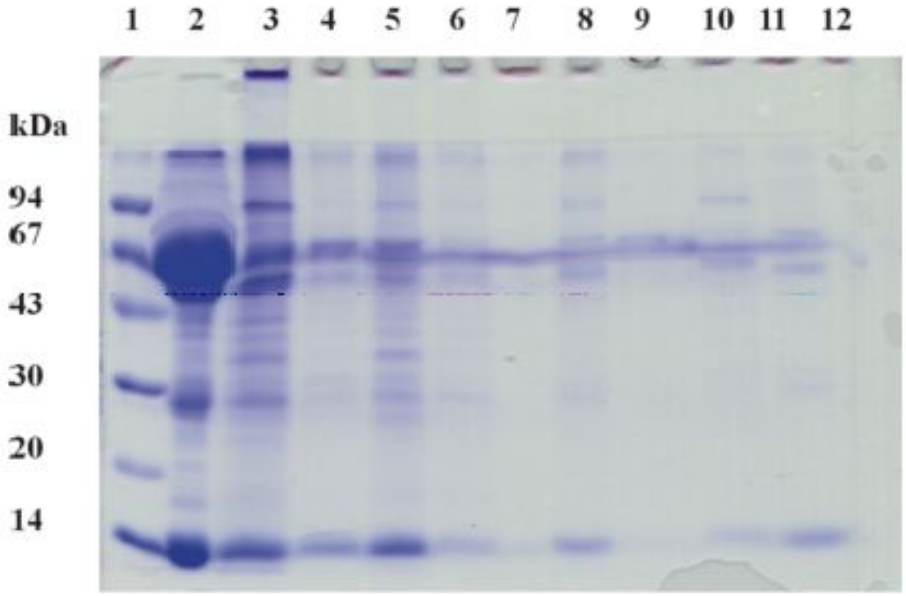


Figure F2: SDS-PAGE analysis of fresh retrievals. Lane 1 is the molecular mass indicated in kDa on left hand side. Lane 2 to 6 is a sample from a patient after 8 years in-vivo with lane 2 the synovial fluid. Lane 8 to 12 is a sample from patient after 4 years in-vivo

# ANNEXURE G

Mass spectrometric analysis of particles retrieved from brown deposit in acetabular cups and synovial fluid

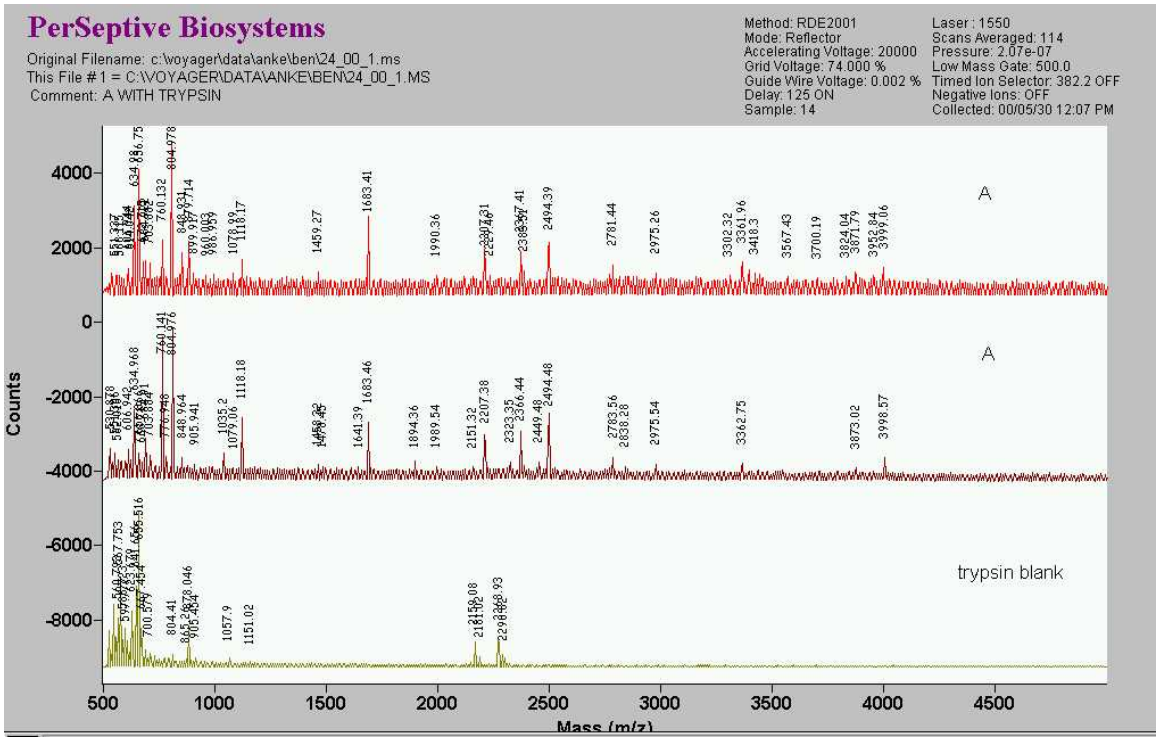


**Figure G1**

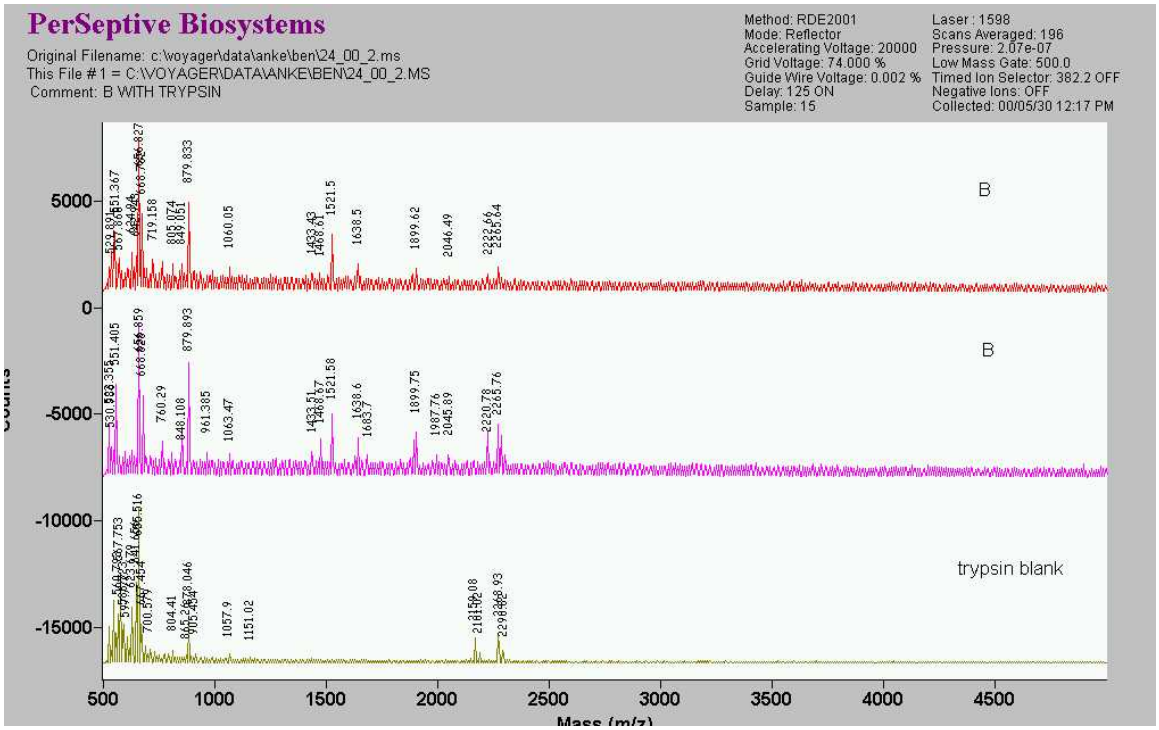


**Figure G2**

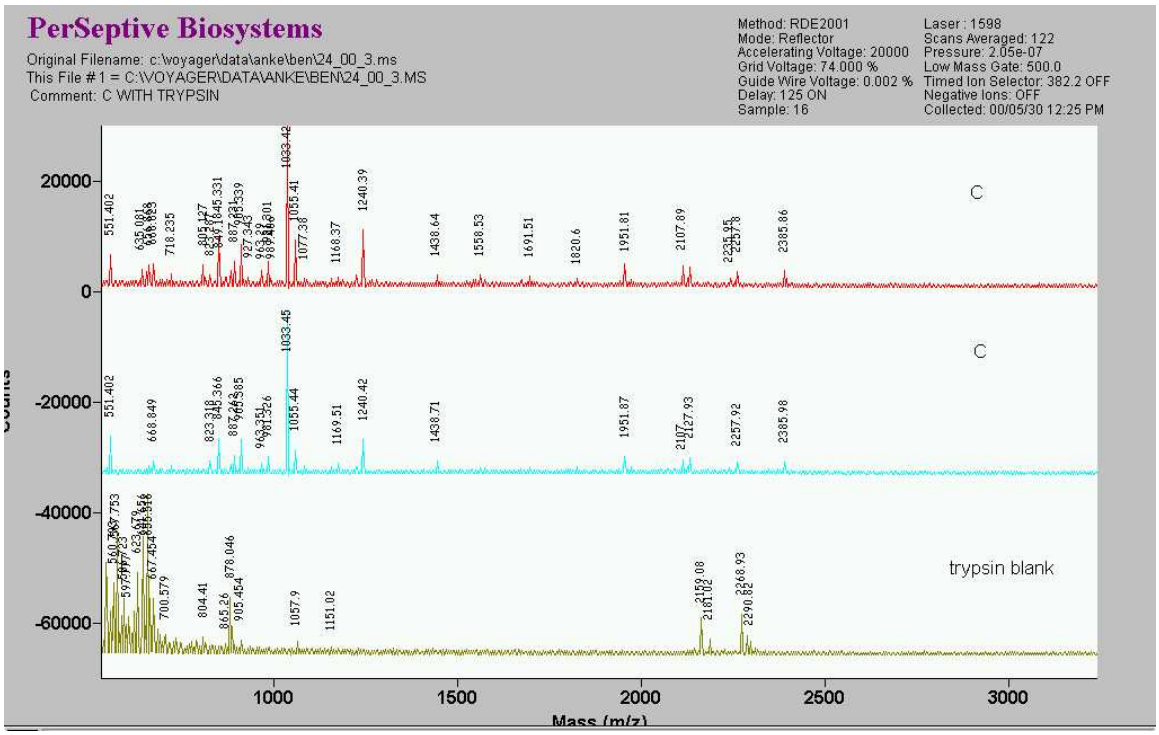


**Figure G3**

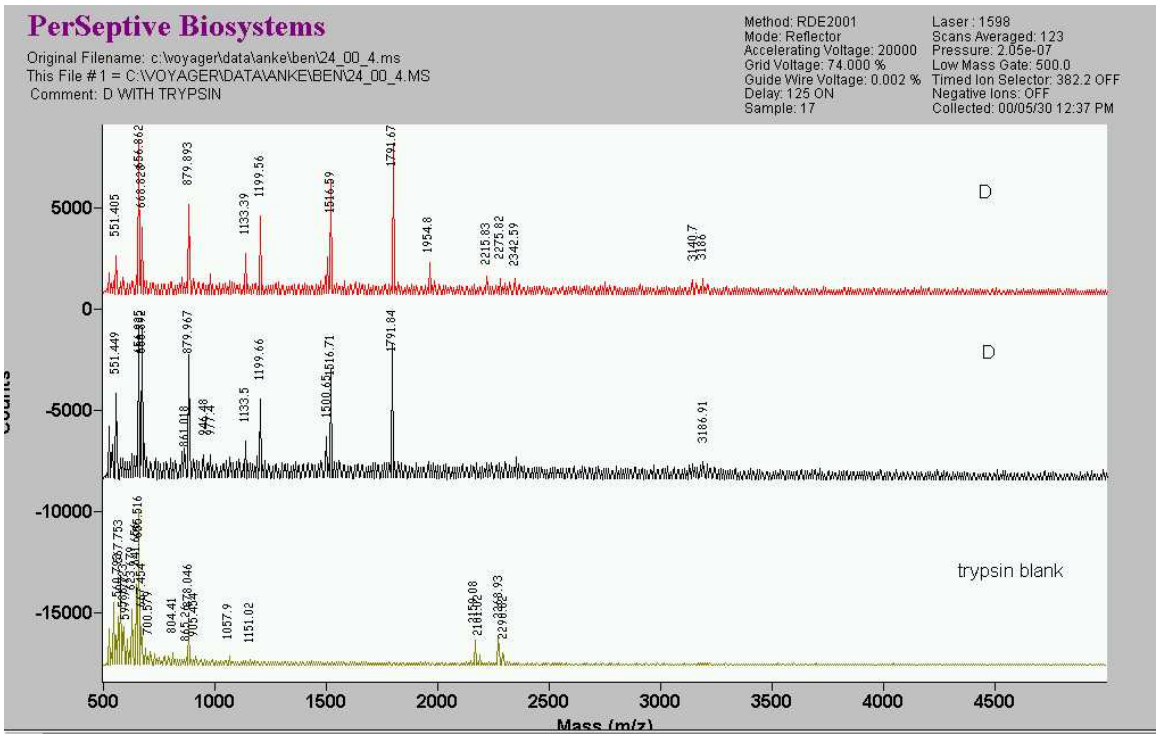


**Figure G4**

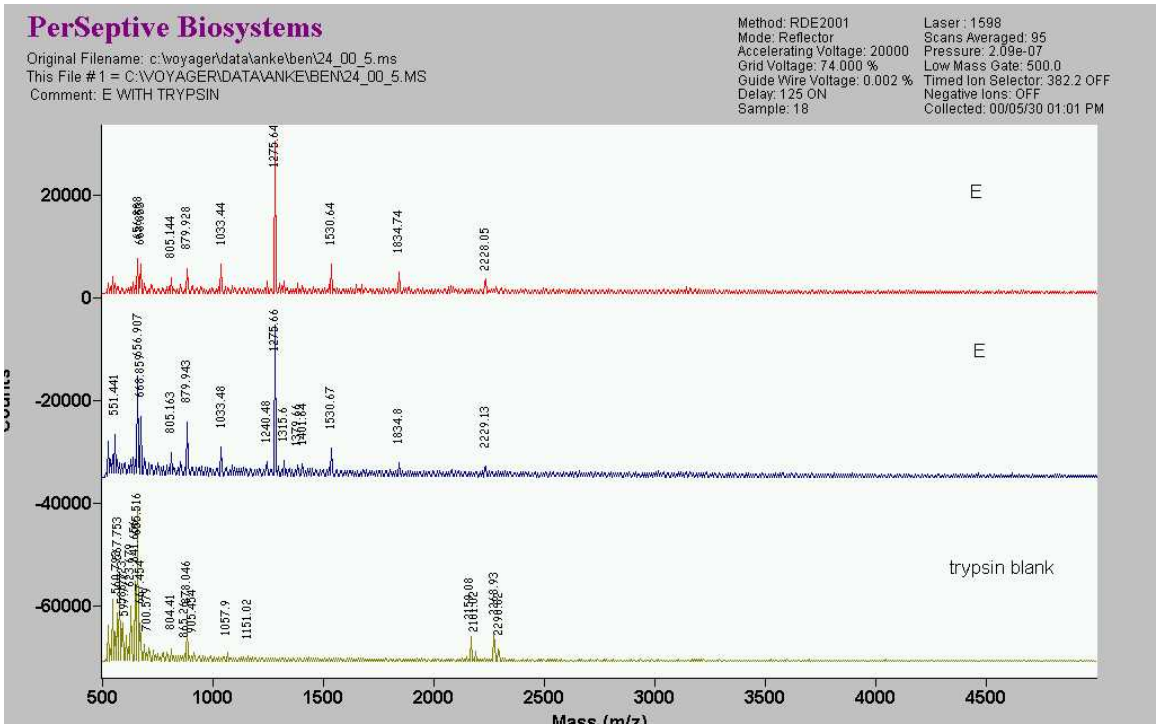
PerSeptive Biosystems
Original Filename: c:\voyager\data\anke\ben\24_00_5.ms
This File #1 = C:\VOYAGER\DATA\ANKE\BEN\24_00_5.MS
Comment: E WITH TRYPSIN
Method: RDE2001
Mode: Reflector
Accelerating Voltage: 20000
Grid Voltage: 74.000 %
Guide Wire Voltage: 0.002 %
Delay: 125 ON
Sample: 18
Laser: 1598
Scans Averaged: 95
Pressure: 2.09e-07
Low Mass Gate: 500.0
Timed Ion Selector: 382.2 OFF
Negative Ions: OFF
Collected: 00/05/30 01:01 PM
E
E
trypsin blank
20000
0
-20000
-40000
-60000
500
1000
1500
2000
2500
3000
3500
4000
4500

**Figure G5**

# ANNEXURE H

Lubricity analysis of retrieved synovial fluid

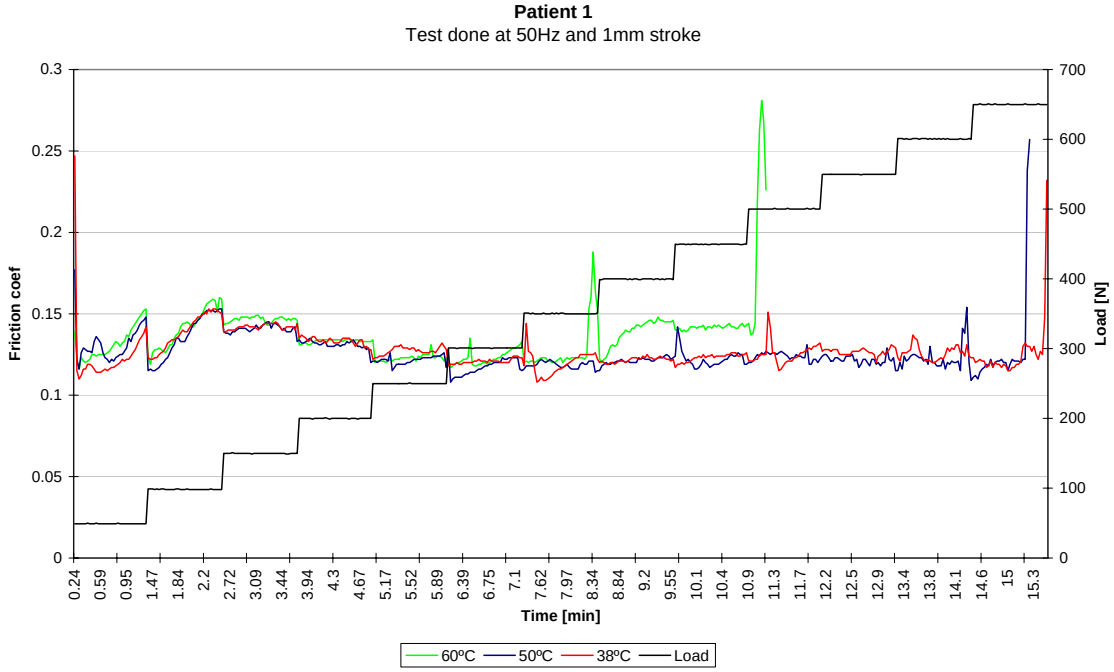


**Figure H1**

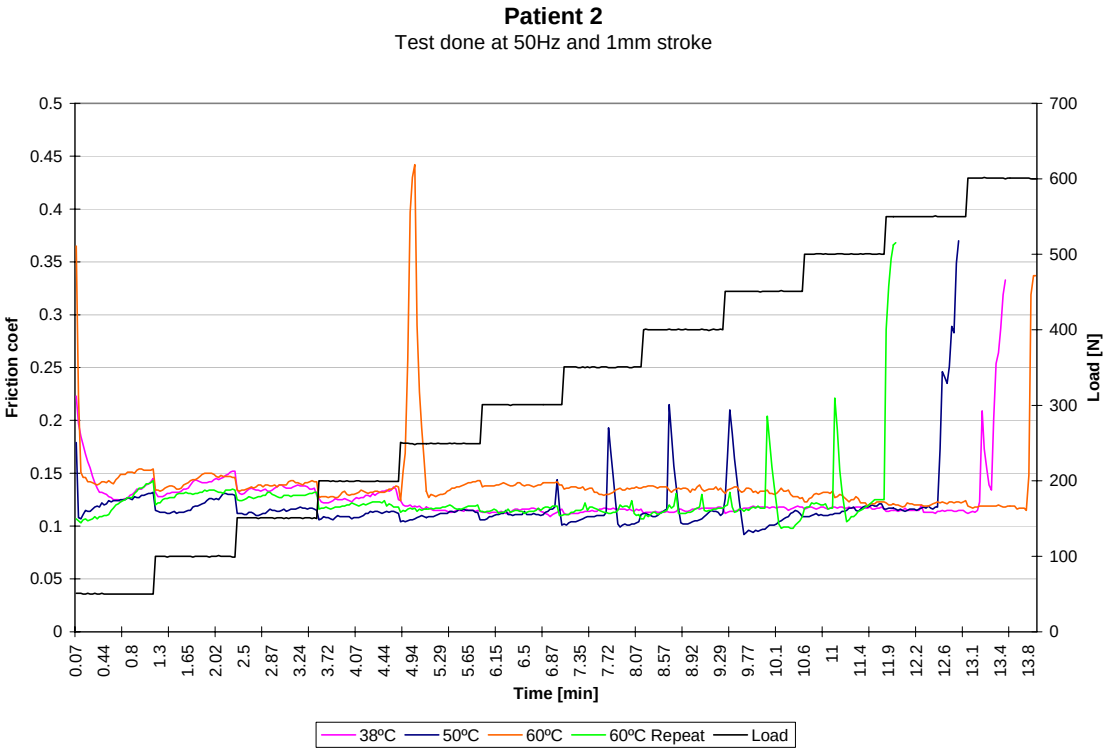


**Figure H2**

**Patient 3**
Test done at 50Hz and 1mm stroke

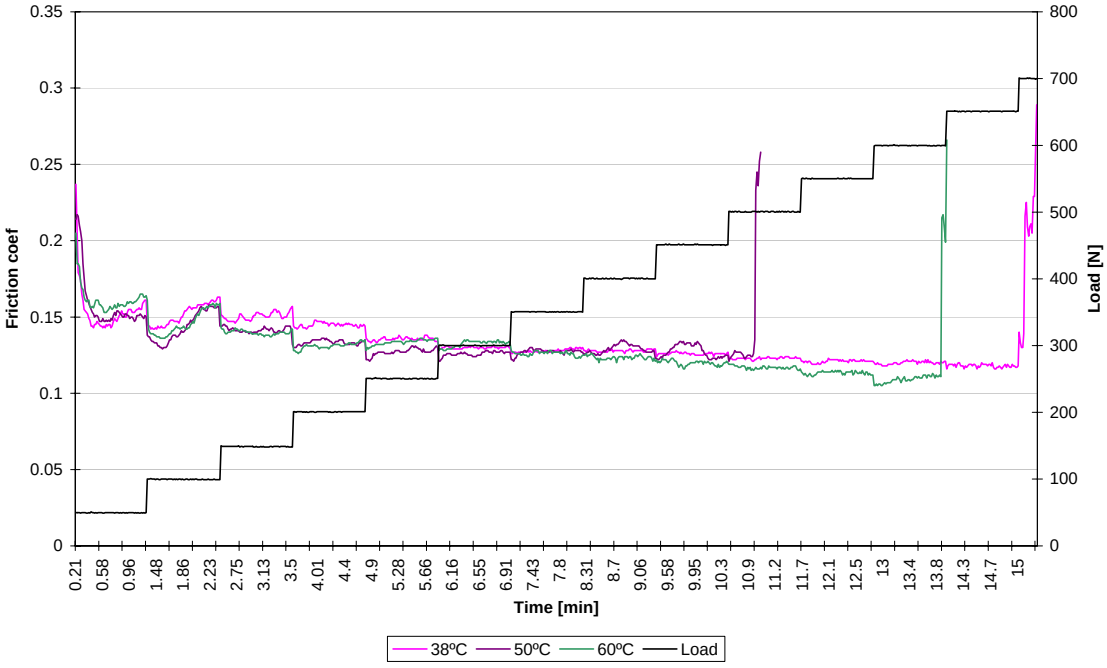


**Figure H3**

**Patient 4**
Test done at 50Hz and 1mm stroke

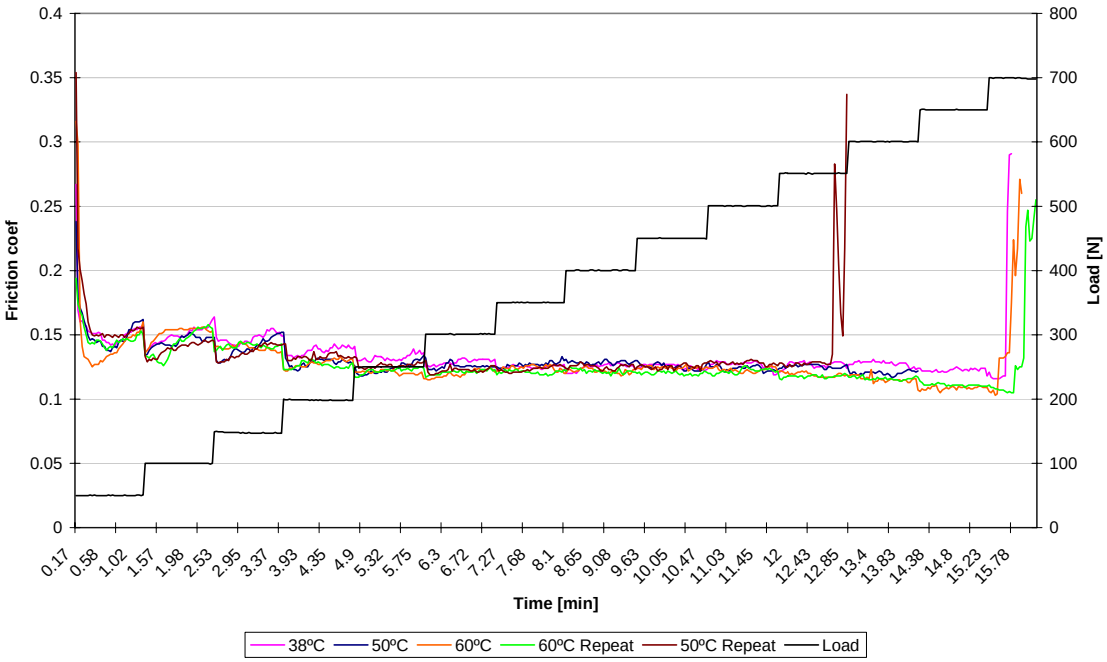


**Figure H4**

**Patient 5**
Test done at 50Hz and 1mm stroke

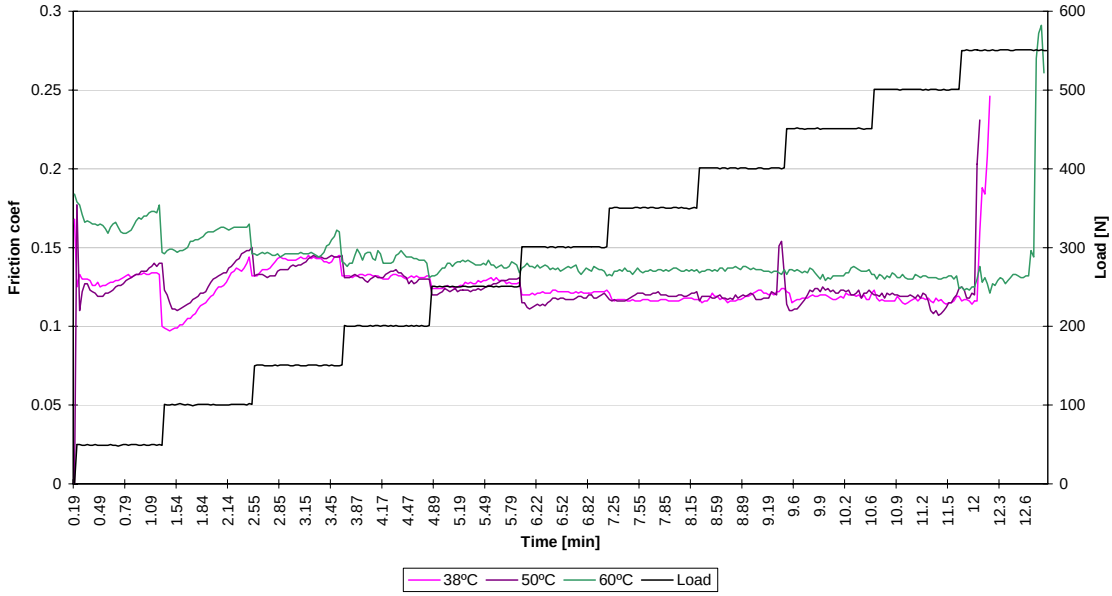


**Figure H5**

**Patient 6**
Test done at 50Hz and 1mm stroke

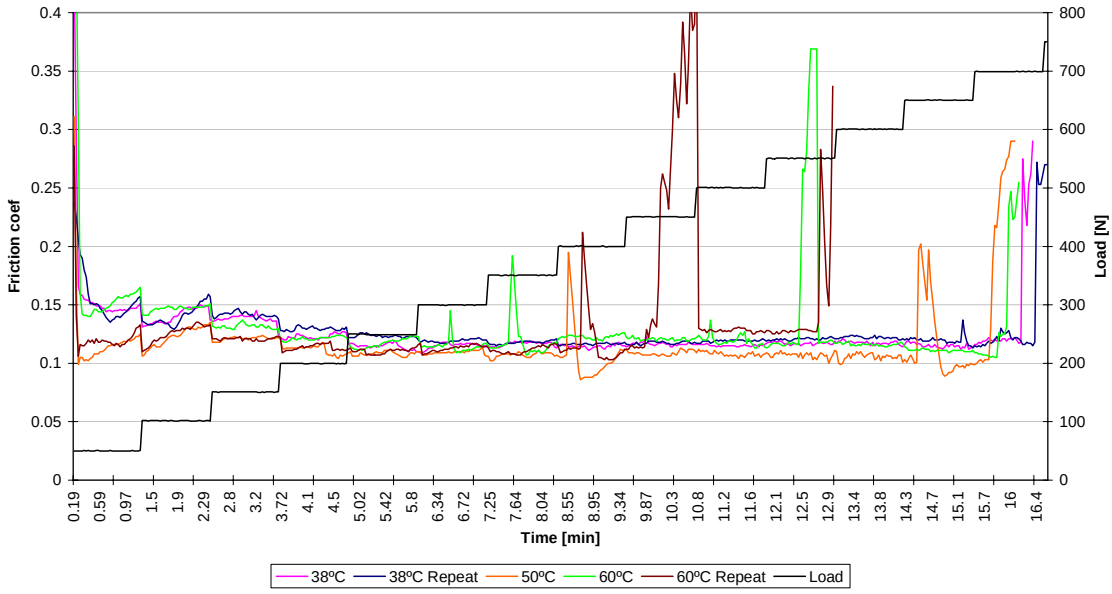


**Figure H6**

**Patient 7**
Test done at 50Hz and 1mm stroke

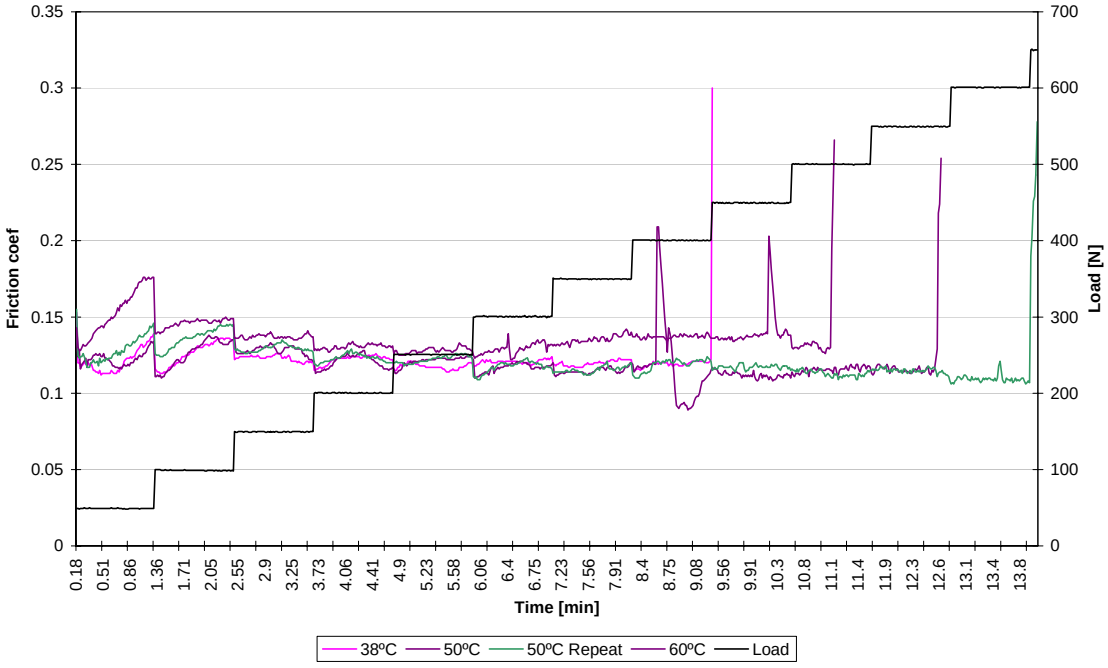


**Figure H7**

**Patient 8**
Test done at 50Hz and 1mm stroke

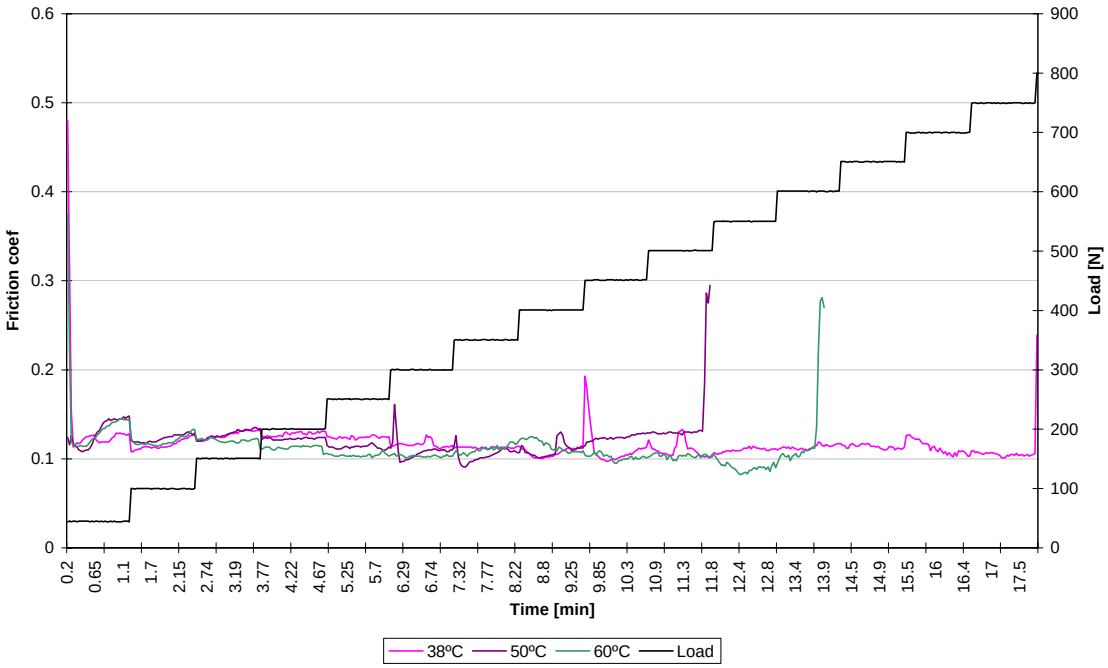


**Figure H8**

**Patient 9**
Test done at 50Hz and 1mm stroke

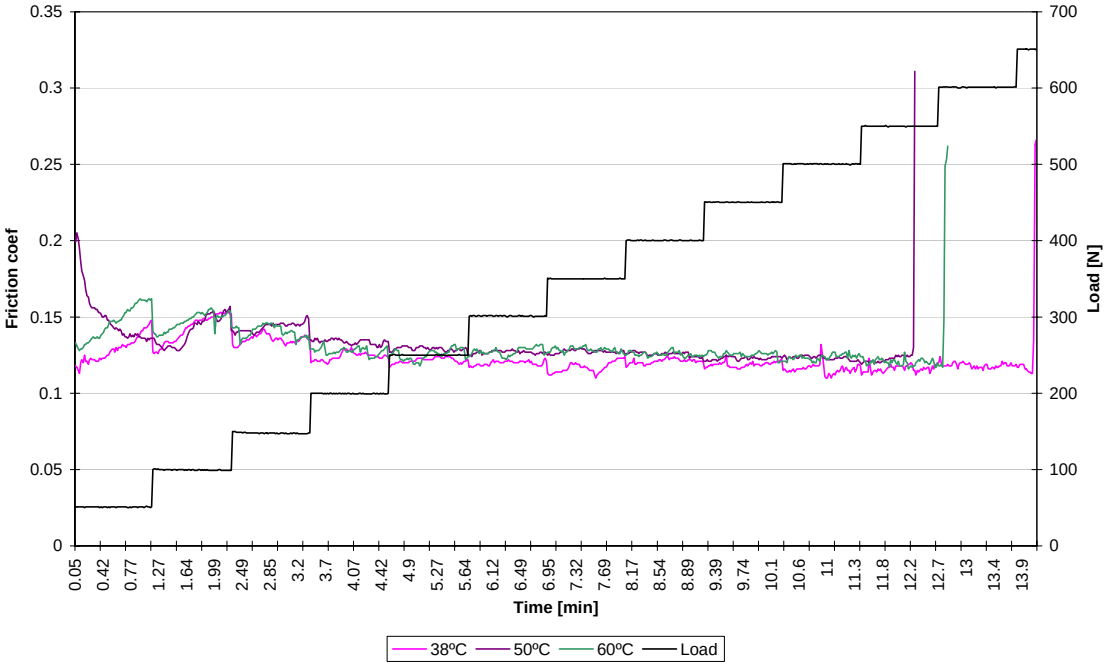


**Figure H9**

**Patient 10**
Test done at 50Hz and 1mm stroke

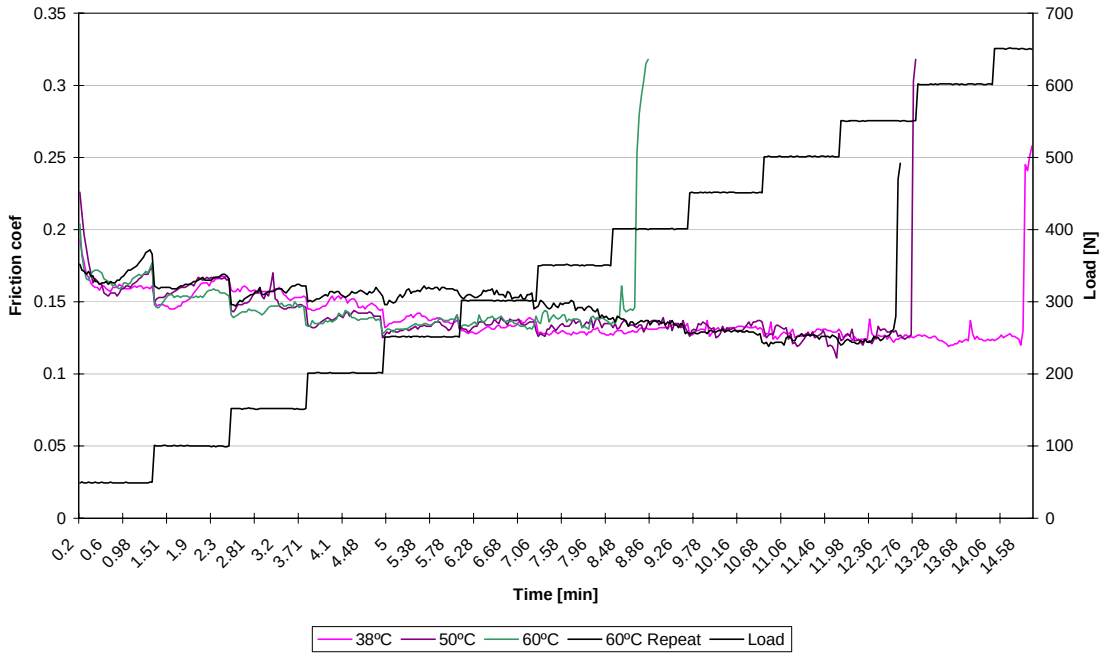


**Figure H10**

**Patient 11**
Test done at 50Hz and 1mm stroke

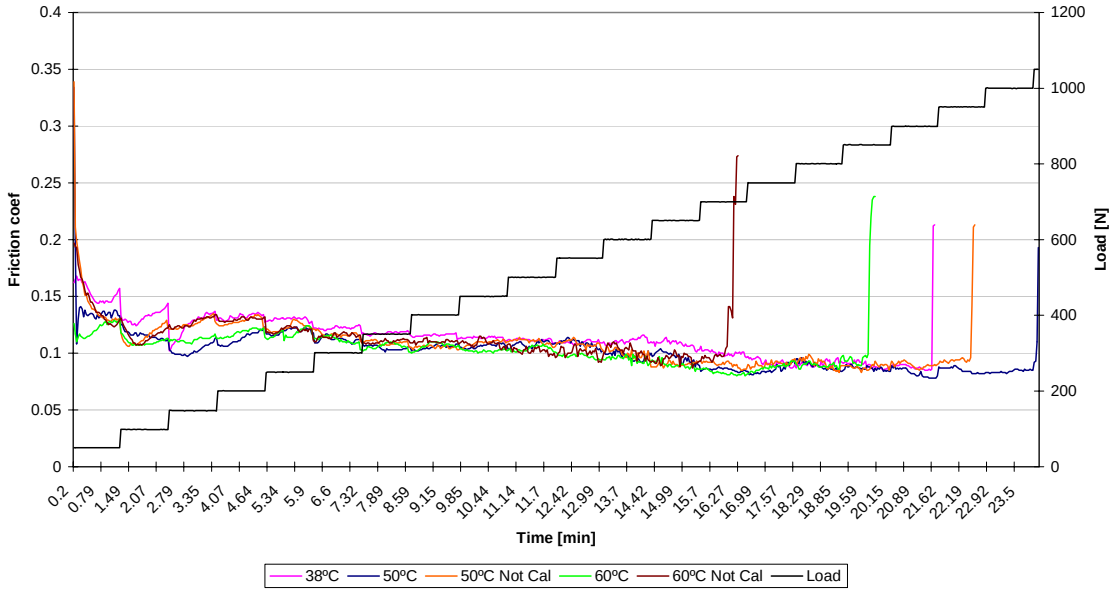


**Figure H11**

**Patient 12**
Test done at 50Hz and 1mm stroke

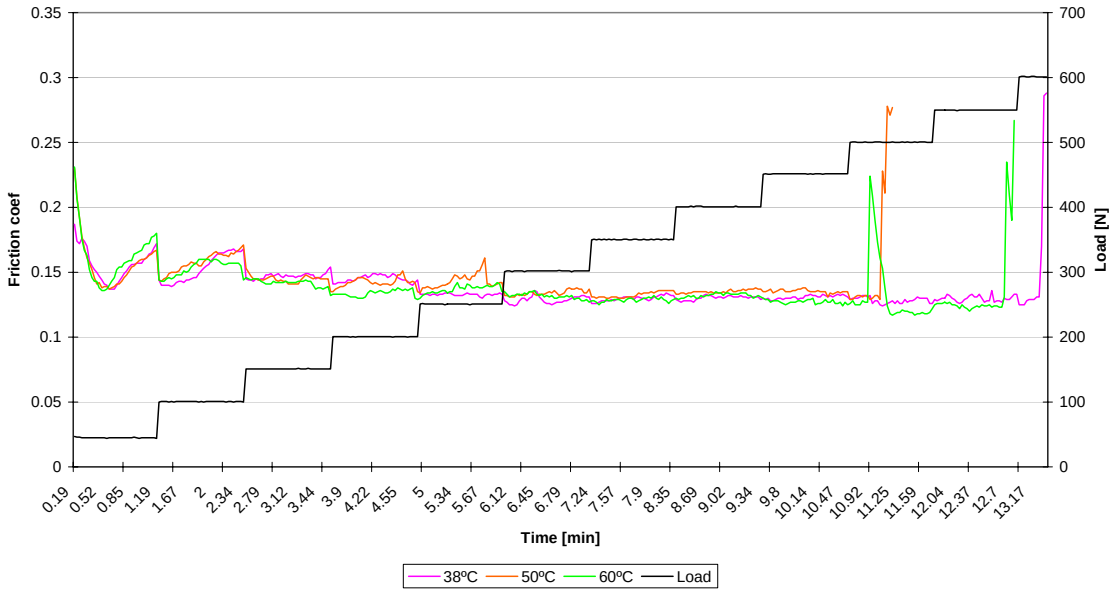


**Figure H12**